p-ISSN 1811-1165
e-ISSN 2413-2179
VOLUME 16, No. 2(32), 2019

EURASIAN PHYSICAL TECHNICAL JOURNAL

KARAGANDA STATE UNIVERSITY NAMED AFTER E.A. BUKETOV

KARAGANDA, THE REPUBLIC OF KAZAKHSTAN

EURASIAN PHYSICAL TECHNICAL JOURNAL

p - ISSN 1811-1165
e - ISSN 2413-2179

Volume 16, No. 2(32), 2019

1st issue – March, 2004

Journal Founder:

KARAGANDA STATE UNIVERSITY NAMED AFTER E.A. BUKETOV

Е.А.БӨКЕТОВ АТЫНДАҒЫ ҚАРАҒАНДЫ МЕМЛЕКЕТТІК УНИВЕРСИТЕТІ

КАРАГАНДИНСКИЙ ГОСУДАРСТВЕННЫЙ УНИВЕРСИТЕТ ИМ. Е.А.БУКЕТОВА

Contact information:

Editorial board of EPhTJ (Build. 2, room 216)
Karaganda State University
named after E.A. Buketov
Universitetskaya Str.28, Karaganda,
Kazakhstan, 100028
Subscription index: 75240
Tel: +7(7212)77-04-03
Fax: +7(7212)77-03-84
E-mail: ephtj@mail.ru

Signed to print on **25.12.2019**.
Format 60x84 1/8. Offset paper.
Volume **15.75 p.sh.** Circulation 300 copies.
Agreed price. Order No. 154.

Басуға **25.12.2019** ж. қол қойылды.
Пішімі 60×84 1/8. Офсеттік қағазы.
Көлемі **15.75** ес.-б.т. Таралымы 300 дана.
Бағасы келісім бойынша. Тапсырыс № 154**.**

Подписано к печати **25.12.2019** г.
Формат 60 × 84 1/8. Офсетная бумага.
Объем **15.75** печ.л. Тираж 300 экз.
Цена договорная. Заказ № 154.

Printed in the Publishing House
of the KarSU named after academician E.A.Buketov

академик Е.А. Бөкетов атындағы ҚарМУ
баспасының баспаханасында басылып шықты

Отпечатано в Издательстве
КарГУ имени академика Е.А.Букетова

Registered by the Ministry of Culture, Information and Public Adjustment of the Republic of Kazakhstan.
Қазақстан Республикасы мәдениет, ақпарат және қоғамдық келісім министрлігімен тіркелді
Registration Certificate No. 4382-Zh, November 7, 2003.

Eurasian Physical Technical Journal

Vol. 16, No. 2(32) **2019**

CONTENTS

Dear Authors and Readers!
Honourable colleagues!

I heartily congratulate our authors and readers with New Year 2020!

I wish you good health, happiness and creative success!

Thanks to your participation and support, as well as to our joint efforts since May 8, 2019 according decision of the Content Selection & Advisory Board the Eurasian Physical Technical Journal (Eurasian phys. tech. j.) has been inducted into Scopus in four scientific areas:

1) Energy: General Energy
2) Engineering: General Engineering
3) Materials Science: General Materials Science
4) Physics and Astronomy: General Physics and Astronomy.

Full metadata (DOI) of both issues of the Eurasian phys. tech. j., Volume 16, 2019 (No. 1(31), No. 2(32)) are available on the Scopus database website now.

As usual, the Eurasian phys. tech. j. issue presents results of studies aimed at improving the efficiency of various devices and technical processes. There are original scientific articles by scientists and researchers from different countries devoted to solving urgent problems of modern technical physics and engineering. You can see interesting results of joint research by scientists from Russia and China on the application sensor arrays to digital processing of Martian craters images made by the American satellites Mariner and Viking. Visual analysis of the processed images allows you to highlight new, previously unknown details. The research of Moscow and Minsk scientists established the optimal content of nano-structured additives in which the material with the highest microhardness is formed. The study results of photo-electro-physical characteristics in a solid film and nanowires of cobalt phthalocyanine are presented by our scientists.

Interesting scientific papers are dedicated to study of the various external influences on the structure and properties of materials, to modeling of complex processes of melting, phenomena in solid state physics and features of elementary particles, heat and mass transfer, alternative energy, wind energy, ect.

The Eurasian Physical Technical Journal offers to publish scientific articles for those who are interested in discussing and testing new scientific results at the international level.

We look forward to meeting you among the authors of our future issues.

Respectfully,
Chief Editor, Saule E. Sakipova
Kazakhstan, December, 2019

DOI 10.31489/2019No2/5-10

UDC 535.317.1 + 621.396.96

PROCESSING BY ROBUST CEPSTRAL FRACTAL - TOPOLOGICAL METHODS OF FLOWS OF OPTICAL TEXTURE IMAGES OF THE MARTIAN SURFACE

Potapov A.A.[1,2,3], Pakhomov A.A.[1], Potapov A.A. (Jr.)[1], Potapov V.A.[1]

[1]V.A. Kotelnikov IREE RAS, Moscow, Russia, potapov@cplire.ru

[2]JNU-IREE RAS Joint Laboratory of Information Techniques and Fractal Signal Processing, Jinan University, Guangzhou, China,

[3] College of Information Science and Technology, Department of Electronic Engineering, Jinan University, Guangzhou, China,

The paper presents the results of applying digital image processing methods to improve their quality and intelligibility. The method is used to process images of Martian craters made by the famous American satellites Mariner and Viking. Visual analysis of processed images allows highlighting new previously unknown details. Pictures are taken from the Internet. The developed methods are suitable for processing multichannel signals with a sensor array.

Keywords: Martian craters, multichannel signal, fractal, topology, sensor array, cepstrum, optical texture image

Introduction

The problem of improving the quality of optical images of objects obtained in the presence of distortions due to the influence of the medium of propagation and radiation remains relevant in the field of astronomy, transport and aircraft control, and, naturally, in aerospace problems (in particular, target detection and selection). We also note that in recent years, interest in such a little-studied and mysterious planet as Mars has increased noticeably in the scientific community and in the media. The possibilities of creating settlements on the surface of Mars for mining are analyzed. Similar hypotheses and programs are also discussed in the relationship of the moon. In this regard, the authors decided once again to return to the recent past, when Mars was actively explored. And using their own methods of image processing, distorted by an unknown atmosphere, the authors will try to restore in detail the most interesting parts of the planet.

1. Mathematical statement of the problem

When registering an optical image located at a considerable distance from the photo detector or camera, the distorting impact of the propagation medium of the received radiation takes place inevitably. Therefore, the general statement of the problem of processing or restoring an image frame is reduced to solving the convolution equation with two unknowns, after partial or complete elimination of the additive background [1-7]:

$$i(\vec{x}) = \int o(\vec{r})h(\vec{x}-\vec{r})d\vec{r} , \tag{1}$$

where $i(\vec{x})$ - registered image, $o(\vec{r})$ - initial unknown image of an unknown object, $h(\vec{x},\vec{r})$ - unknown impulse response of optical system which forms the image.

Proceeding to spatial spectra we get an expression:

$$I(\vec{\omega}) = O(\vec{\omega})H(\vec{\omega}) \tag{2}$$

It is clear that without the use of additional information, this problem is unsolvable. The authors used finiteness and positivity of an unknown image $o(\vec{r})$ as additional information. Also,

.

the transfer function was approximated by a Gaussian with unknown dispersion. In this case, we considered not a continuous case (2), but a discrete one - post-detector image processing. Moreover, all factors (2) are two-dimensional polynomials of finite degree. Given the features of two-dimensional discrete polynomials of finite degree and the apparatus of the Lebesgue measure, we can prove that the convolution equation in the two-dimensional discrete case is almost always (in the sense of the Lebesgue measure) uniquely solved [2, 5-7].

A practical solution to this problem even with accurate knowledge of the transfer function $H(\vec{\omega})$, where $\vec{\omega}$ are the spatial frequencies, is also a difficult task and comes down to either Wiener filtering with an unknown regularizing factor or Tikhonov regularizing filters containing, in addition to the regularizing factor, several unknown stabilizing parameters [3]. Thus, there is a need to use guaranteed and monotonously converging methods for solving the problem.

The answer to this question is given by the application of set theory and, in particular, the use of projection operators on sets of functions with given properties. In solving this problem, one can use a set of compact and a set of positive functions, since it is assumed that the images have finite sizes and represent intensity distributions. Moreover, it is obvious that these sets are closed. In general terms, the procedure for solving such ill-posed inverse problems comes down to choosing an initial estimate (image), projecting it onto a set of compact functions (taking into account boundedness in linear dimensions), projecting onto a set of positive functions (zeroing negative values), and projecting onto a set of functions with given information about the Fourier spectrum.

According to a well-known theorem from functional analysis (the point theorem), if convex sets correspond to all a priori constraints, then such a procedure converges monotonously to a single true solution [4-7]. In practice, when creating algorithms for processing, due to inevitable rounding errors, determining of image sizes, the presence of noise, etc., the restoration procedure converges in a certain neighborhood, covering the selected point and lying at the intersection of convex sets. From the point of view of image restoration when applying this approach and in the presence of noise, as a result, a set of images will be obtained that is very similar to the true one, but differing from it by small intensity fluctuations that are within the noise dispersion. The external contour of the image almost does not differ from the true one, i.e. it is restored much more accurately than the distribution of image intensity.

Returning to the original problem (2) from the point of view of the described theory, it is easy to show that the set of positive and finite functions is convex [4-7]. At the same time, the set of functions (2) with a given product of spectra is a hyperbola, i.e. non-convex and non-closed set. At first glance, it seems that projection theory is not applicable in this case. However, the described difficulty is quite surmountable if we recall the methods of cepstral processing of signals and images, which come to the transition from the complex spectra themselves to their logarithms. The Fourier spectra can be written as:

$$I(\vec{\omega}) = |I(\vec{\omega})| \;\exp\{i \arg I(\vec{\omega})\} = |I(\vec{\omega})| \;\exp\{i\varphi_I(\vec{\omega})\}.$$

Let us take logarithms from both sides of (2) and equate separately the real and imaginary parts:

$$\begin{aligned} Ln|I(\vec{\omega})| &= Ln|O(\vec{\omega})| + Ln|H(\vec{\omega})| \\ \varphi_I(\vec{\omega}) &= \varphi_O(\vec{\omega}) + \varphi_H(\vec{\omega}) \end{aligned} \quad (3)$$

Thus, it can be seen from (3) that after taking the logarithm, a set with a given product has turned into a set with a given sum. It is well known that a set with a given sum is a line, which is the limiting case of a convex set. If we introduce designation $K_I(\vec{\omega}) = Ln|I(\vec{\omega})| + i\varphi_I(\vec{\omega})$, where $K_I(\vec{\omega})$ is cepstrum of the image, then in the cepstra language, equation (2) is written as the sum:

$$K_I(\vec{\omega}) = K_O(\vec{\omega}) + K_H(\vec{\omega}). \quad (4)$$

Thus, the possibility of converting a non-convex set (2) to a convex set (4) becomes obvious. Also, the convergence of the method for solving the convolution equation using cepstral spectra or cepstral methods becomes apparent. It is worth noting that when modeling such a procedure, the authors used modified cepstra associated with the specifics of the program (FFT); while the modified cepstrum looks like:

$$K_I^M(\vec{\omega}) = Ln\{|I(\vec{\omega})| + c\}\exp i\varphi_I(\vec{\omega}), \quad c = 0.00001,$$

the constant c is caused by the uncertainty of the logarithm value for small values of the argument.

It is easy to see that for modified cepstra the linearity of the set with a given sum is preserved, i.e. convergence of the method is guaranteed. The authors approximated the unknown transfer function $H(\vec{\omega})$ by a Gaussian, as well as its impulse response, therefore this function is real and positive and does not have a complex component, which leads to acceleration of convergence.

2. Results Discussion

Let us consider typical examples. In fig. 1 - fig. 4 there are the results of processing of the Martian crater Olympus Mons. The images were taken by the Mariner spacecraft in 1976. The estimated size of the crater is 25 km in height and 500 km across.

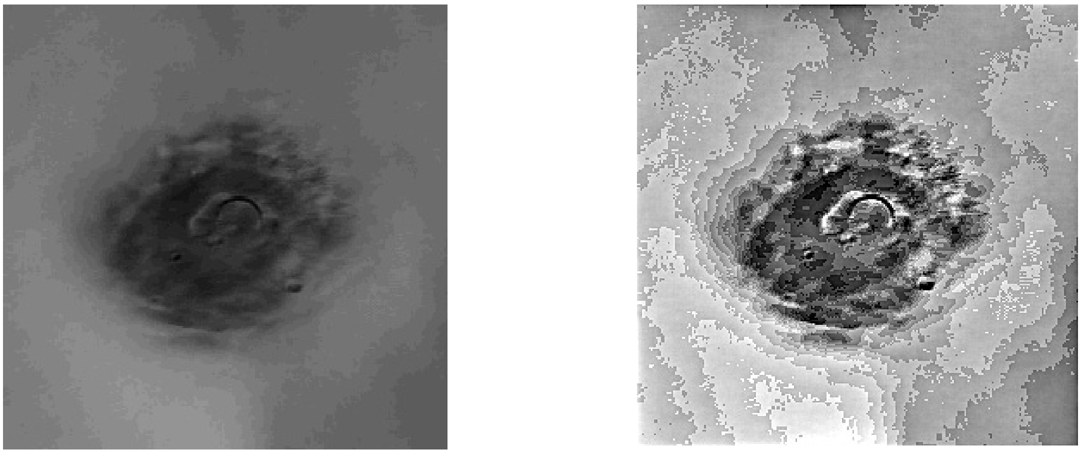

Fig.1. On the left there is the image of a fragment of the original image, on the right there is the result of processing of this fragment

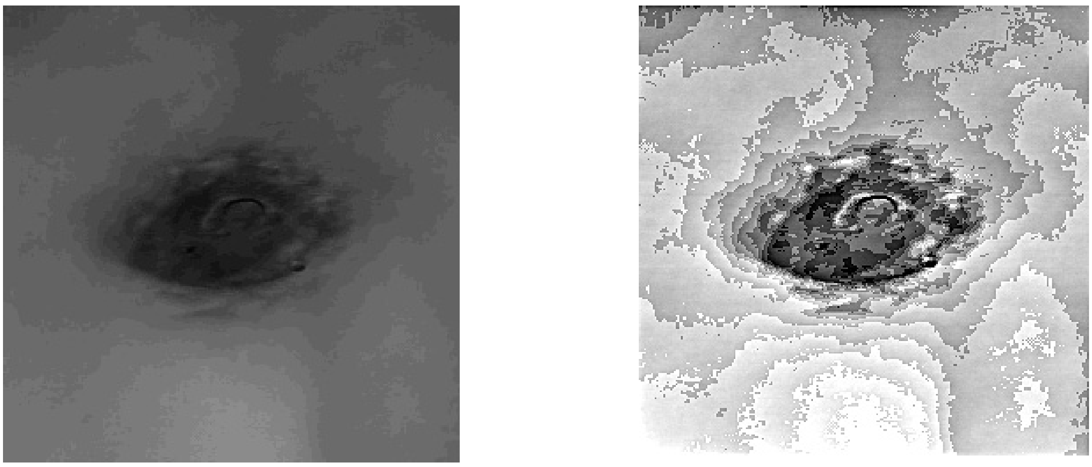

Fig.2. On the left there is the image of a fragment of the original image, on the right there is the result of processing of this fragment

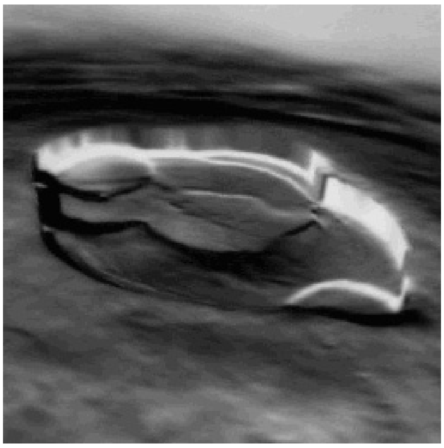
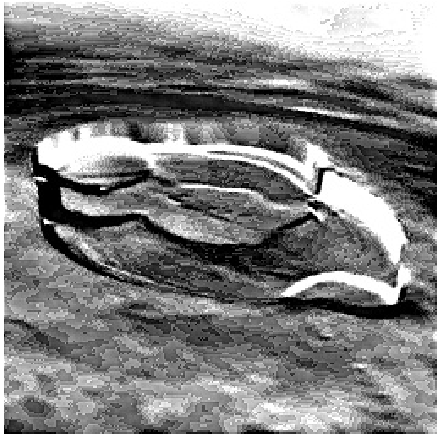

Fig. 3. On the left there is the image of a fragment of the original image, on the right there is the result of processing of this fragment

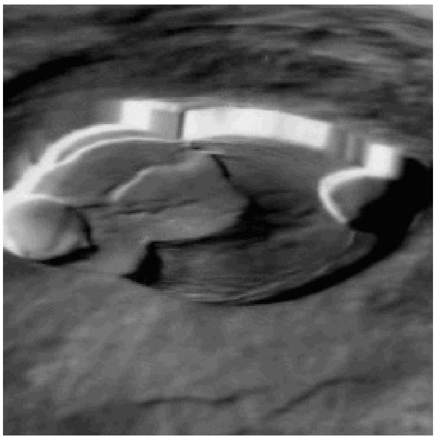
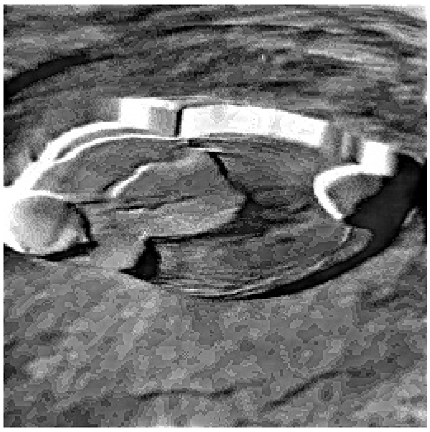

Fig. 4. On the left there is the image of a fragment of the original image, on the right there is the result of processing of this fragment

In fig. 5 - fig. 7 there are the results of processing of fragments of the Martian canyon Valles Marineris.


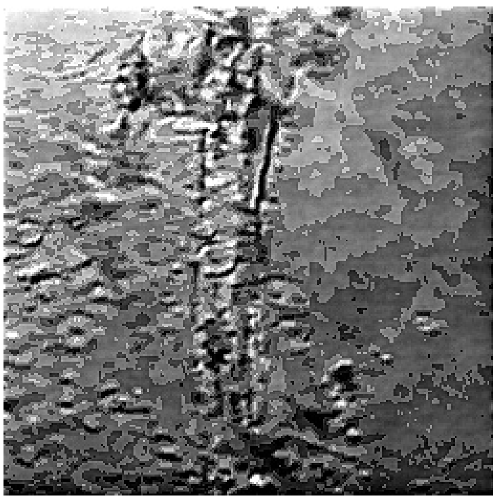

Fig.5. On the left there is the image of a fragment of the original image, on the right there is the result of processing of this fragment

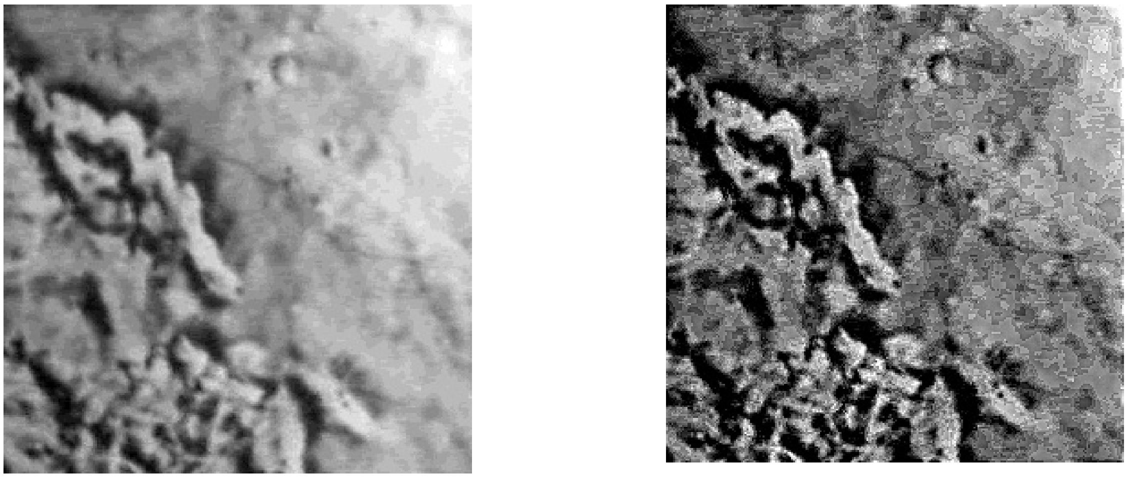

Fig.6. On the left there is the image of a fragment of the original image, on the right there is the result of processing of this fragment

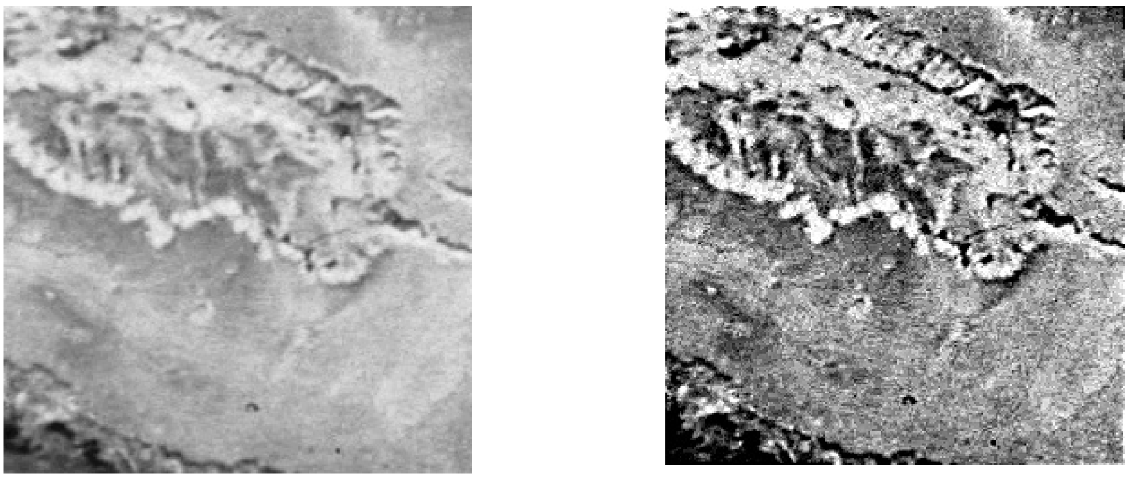

Fig.7. On the left there is the image of a fragment of the original image, on the right there is the result of processing of this fragment

Its estimated dimensions are as follows: height 10 km, length 6000 km, width 200 km. The images obtained in 1976 by the Viking apparatus.

Conclusion

As conclusions, we note that the results of processing the surface of Mars presented in this paper clearly demonstrate the effectiveness of the considered approach. The methods developed by the authors are also suitable for processing of multichannel signals by a sensor matrix system and in systems of space-time adaptive processing of multidimensional signals.

Acknowledgements

The work was partially supported by the International Scientific and Technical Center (project No. 0847.2, 2000-2005, USA), the Russian Foundation for Basic Research (RFBR projects No. 05-07-90349, 07-07-07005, 07-07-12054, 07-08 -00637, 11-07-00203, 18-08-01356-a), as well as the Leading Talents Project (project No. 00201502, 2016–2020) at Jinan University (Guangzhou, China).

REFERENCES

1 Pratt U. *Digital image processing*. Moscow, Mir, 1982. Book 1. – 312 p.; Book 2. – 480 p.

2 Troitskiy I.N., Ustinov N.D. *Statistical theory of holography*. Moscow, Radio i svyaz, 1981, 327 p. [in Russian]

3 Hayes M.H. Reconstructing of multi dimensional sequence only from amplitude or phase Fourier-spectrum. *IEEE Trans. Acoustic. Speech, Signal, Proc*. 1982, Vol. 30, No. 3, pp. 140 – 152.

4 Vasilenko G.I., Taratorin A.M. *Image restoration*. Moscow, Radio i svyaz. 1986, 304 p. [in Russian]

5 Potapov A.A., Gulyaeyev Yu.V., Nikitov S.A., Pakhomov A.A., German V.A. The latest image processing methods. Moscow, FISMATLIT, 2008, 496 p. [in Russian]

6 Potapov A.A. *Fractals in radio-physics and radiolocation*. Moscow, Logos, 2002, 664 p. [in Russian]

7 Professor Alexander Alekseyevich Potapov. Ed. by Acad. Yu. Gulyaeyev. Moscow, 2019, 256p. [in Russian]

Article accepted for publication 22.11.2019

DOI 10.31489/2019No2/11-15

UDC 621.762

STUDY OF STRUCTURE AND PROPERTIES OF SELF-FLUXING ALLOY AFTER MODIFYING WITH NANOSTRUCTURED AND MICRON-SIZED POWDERS OF CUBIC BORON NITRIDE AND HIGH PRESSURE AND HIGH TEMPERATURE TREATMENT

Senyut V.T.[1], Vityaz P.A.[2], Val`kovich I.V.[1],Kheifetz M.L.[3], Kolmakov A.G.[4]

[1] Joint Institute of Mechanical Engineering of NAS of Belarus, Minsk, Belarus, vsenyut@tut.by

[2] Presidium of the National Academy of Sciences of Belarus, Minsk, Belarus, vitiaz@presidium.bas-net.by

[3] «NPO Center» OJSC, National Academy of Sciences of Belarus, Minsk, Belarus, mlk-z@mail.ru

[4] A.A. Baykov Institute of Metallurgy and Materials Science, Russian Academy of Sciences, Moscow, Russia, agk10@bk.ru

The structural features and microhardness of sintered at high pressure and high temperature with the addition of nano- and micron-sized powders of cubic BN (cBN) self-fluxing nickel alloy PG-SR4 are studied. Based on the experiments, the modes of high pressure and high temperature treatment are established. The optimal content of the nanostructured cBN additive is determined, at which the material with the highest microhardness is formed. It is shown that the microhardness of the material with the addition of micron-sized cBN is 1.5–2 times lower than that for the samples with the same content of nanostructured cBN.

Keywords: PG-SR4 self-fluxing nickel alloy, mechanical activation, nanostructured and micron-sized cBN powders, modifying.

Introduction

Self-fluxing nickel alloys of the Ni-Cr-B-Si system are widely used in the technology of wear-resistant coatings for the restoration and hardening of tribological conjugation parts at elevated contact loads and temperatures [1].The fluxing elements boron and silicon included in the alloy contribute to lowering the melting temperature and deoxidizing the metal surface of the part with the formation of strong diffusion bonds between the coating and substrate materials during melting of the sprayed coating. For example, the coatings of powders of self-fluxing alloys deposited by a gas-flame method with reflow have high physical and mechanical characteristics: strength up to 400–500 MPa, hardness within 25–64 HRC, low friction coefficient, high wear and corrosion resistance [2, 3]. The most famous and widespread method of increasing the wear resistance of self-fluxing alloys is the development of composite materials using reinforcing additives in the form of carbides, borides, and transition metal nitrides [4]. Modifying by solid refractory compounds allows to change the structure of self-fluxing alloys effectively, contributes to its dispergation and increase the physical and mechanical properties, tribological and operational characteristics of materials based on them [5].

1. Formulation of the problem

Along with the refractory nanopowders such as Al_2O_3, SiC, TiB_2, TiC, WC, and others, single and multicarbide and oxide mechano-composites are also quite efficiently used as modifying additives for self-fluxing alloys [6, 7]. In this regard, it can be assumed that the use of cubic BN (cBN), which has high physical and mechanical properties [8], will significantly increase hardness and wear resistance and, accordingly, increase the life time of products based on self-fluxing alloys instead of traditional additives of refractory compounds. In addition, BN will serve as a source of boron, contributing to the formation of hardening phases of chromium and nickel borides in the heat treatment process.

It is known that the application of pressure during the synthesis of the materials based on cBN prevents the reverse phase transformation of cBN into a graphite-like (hexagonal) modification of BN (hBN) and provides the best combination of structural characteristics and strength parameters of the alloy [9]. The purpose of the work is to study of the structure and microhardness of samples of self-fluxing nickel alloy of the Ni-Cr-B-Si system obtained by high pressure and high temperature (HPHT) treatment, with the addition of nano- and micron powders of cubic BN.

2. The research technique.

For the manufacture of experimental samples, the powder of self-fluxing alloy PG-SR4 (GOST 21448–75) is chosen. It contains 15-18% Cr; 3.0-4.5% Si; 2.8-3.8% B; 0.6-1.0% C; no more than 5% Fe; and the rest is Ni. Two types of cBN are used as an additive: nanostructured powder with a particle size of 100–200 nm and micron-sized powder with a grain size of the main fraction within 40–60 μm. A mixture based on the PG- SR4 alloy with the addition of nano- or micron-sized cBN for HPHT treatment is obtained by mixing and mechanical activation (MA) in the attritor of the initial powders, their compacting and preliminary sintering in a protective atmosphere, dispersing the compacts to agglomerates and sieving the agglomerates into fractions. For HPHT treatment the agglomerate fraction with the size of 100–315 μm is used.

HPHT treatment of composite powders is carried out in an “anvil with a hole” high-pressure apparatus at pressures of 1.5–2.0 GPa and temperatures of 1000–1350 °C during 20 s. First, the “cold” compression of the mixture, placed in a special container made of lithographic stone, is carried out, and then the mixture is heated under pressure by direct electric current.

The studies of cross-sections of samples are performed by optical microscopy using Micro-200 metallographic microscope (Planar OJSC, Belarus). The microhardness of the samples is measured with a PMT-3 microhardness tester by Vickers diamond indenter with a load of 50 g. X-ray analysis is performed with Bruker D8 ADVANCE diffractometer in Cu-Kα radiation in an automatic recording mode.

3. Results and discussion

Figure 1 shows the appearance of the initial micron-sized and nanostructured cBN powders used as a modifying additive to prepare PG-SR4 and cBN composite powders. Composition powders in form of the agglomerates based on PG-SR4 with the addition of 2.5–10 vol. % micron-sized or nanostructured cBN have preliminary been prepared as described above.

Figure 2 shows the surface structure of the compacts made of PG-SR4 powder with the addition of nanostructured (Fig. 2 a) and micron-sized cBN (Fig. 2 b) after MA and sintering. The analysis of the surface of the compacts after sintering (Fig. 2) shows that the samples based on PG-SR 4 and nanostructured cBN has low porosity and are characterized by uniform structure. As a result of MA and sintering, nanostructured cBN is evenly distributed between particles of self-fluxing alloy and is fixed on their surface, leading to the formation of a composite powder with a cladding structure (Fig. 2 a). The compacts made of the composite powder PG-SR4 and micron-sized cBN after MA and sintering (Fig. 2b) consist of agglomerated particles of self-fluxing alloy and cBN crystals and have a much more porous and inhomogeneous dendritic type structure. Then the compacts are mechanically dispersed, and the resulting agglomerates of composite powders are sieved into fractions. As a result of the HPHT-treatment of the agglomerated composite powders with the additions of nano- and micron-sized cBN, the cylindrical samples with a diameter of 10 mm and a height of 8 mm are obtained. Then they are polished at the ends with diamond paste. In the process of preparation of the cross-sections, it is defined that the material is highly brittle, and this does not allow preparing high-quality cross-sections on them to conduct further research.

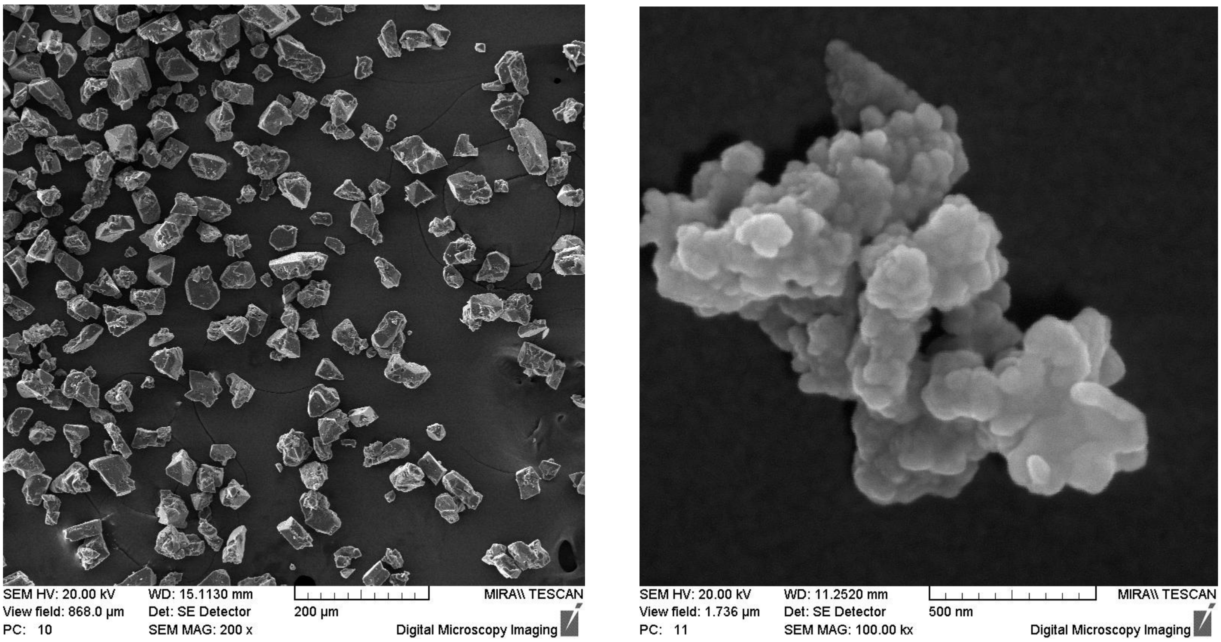

a) b)

Fig.1. Initial cBN powders used as additives: micron-sized powder (a); nanostructured powder (b).

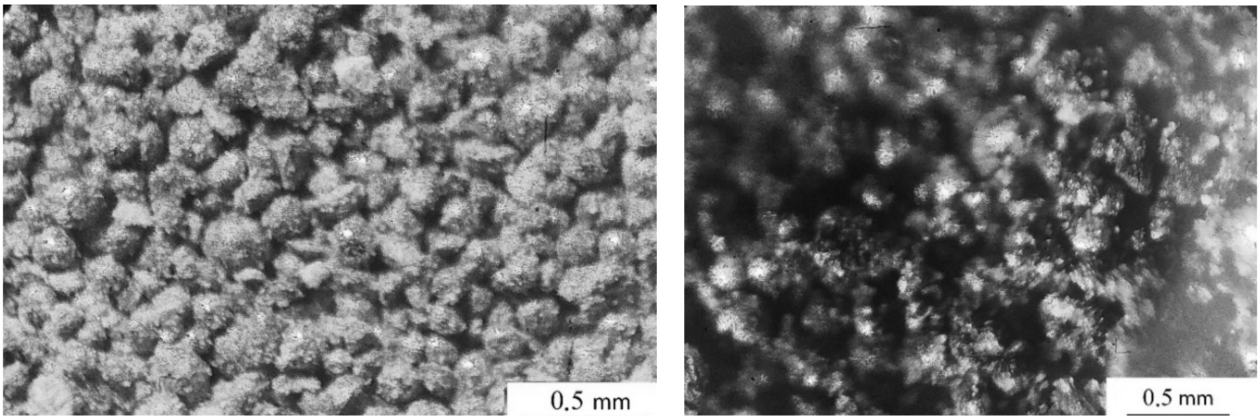

a) b)

Fig.2. The surface of the compacts based on PG-SR4 powder after MA and sintering in a protective atmosphere: PG- SR4 and nanostructured cBN (a);PG-SR4 and micron-sized cBN (b)

Therefore, in order to reduce the brittleness of the material, the powder of the initial PG-SR4 alloy of the same fraction has been additionally introduced into the mixture before the HPHT treatment. Figures 3a and 3b show the photographs of the surface of the samples based on self-fluxing alloy with the addition of nanostructured cBN after HPHT treatment. It has been established that the main structural components of the sintered material are the matrix self-fluxing alloy based on a solid solution of Cr in Ni, the chromium boride phase Cr2B, as well as BN particles, that are evenly distributed in the material. In the material obtained at temperatures up to 1200 °C, the aggregates of cBN particles are uniformly distributed in the matrix and can be clearly seen on the background of the matrix alloy in the form of point inclusions of submicron sizes and individual polyhedral particles of 5–10 μm in size (Fig. 3a) formed as a result of recrystallization of nanostructured cBN [9]. In the samples of the material obtained at temperatures above 1200 °C, boron nitride is present in the form of light particles with a size of 5–15 μm of lamellar form that is characteristic of the graphite-like phase of BN. Moreover, with increasing the temperature of the HPHT treatment, the growth of individual alloy particles above 300 μm can be marked (Fig. 3b).

.

Microhardness measurements of the samples show that for the material containing nanostructured cBN in the range of 2.5–3.5 vol. %, microhardness values are 11.8–13.7 GPa, and this is 18–32% higher than that for the samples containing no additives. An increase in concentration of nanostructured cBN promotes embrittlement of the material, and an increase in temperature leads to a decrease in microhardness due to the developing reverse phase transformation of cBN into a graphite-like modification of BN.

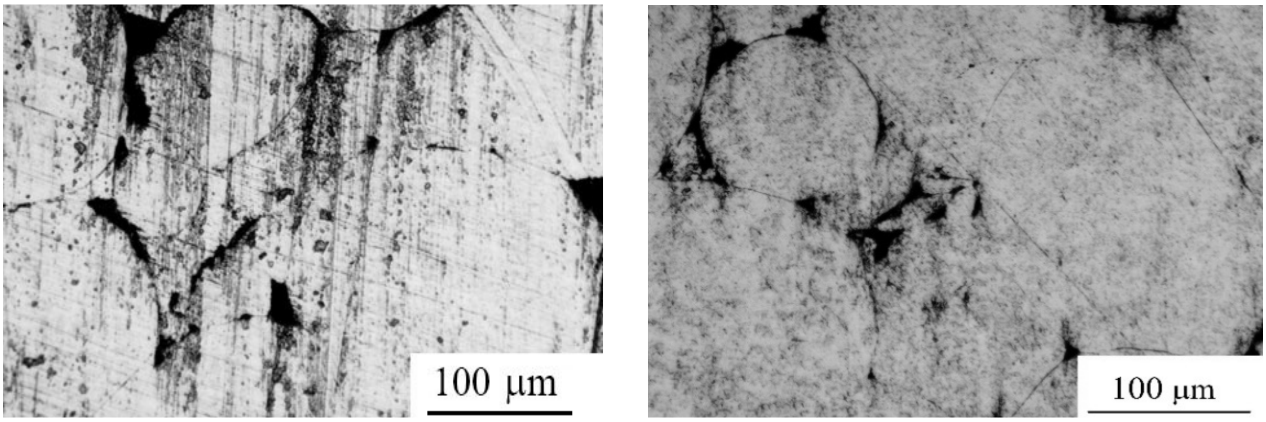

Fig.3. The surface structure of the samples based on self-fluxing alloy PG-SR4 and nanostructured cBN after the HPHT treatment: The temperature of the HPHT treatment is 1100 °C (a); 1350 °C(b)

Figure 4 shows the surface of the samples based on self-fluxing alloy with the addition of micron-sized cBN after the HPHT treatment. The analysis of the material structure shows that cBN crystals are mainly between the alloy particles (Fig. 4a). At the same time, together with the initial cBN, the material contains small fragment-type cBN crystals formed as a result of crushing of larger particles under pressure (Fig. 4b). In addition to particles of the indicated types, cBN crystals with a size of 5–8 μm of a pyramidal habit are also observed. They could be formed as a result of dissolution and crystallization of cBN from the melt under pressure (Fig. 4b). Moreover, as in the case of the use of nanostructured cBN additives, a graphite-like BN is formed in the material containing micron-sized cBN with an increase in temperature (Fig. 4c).

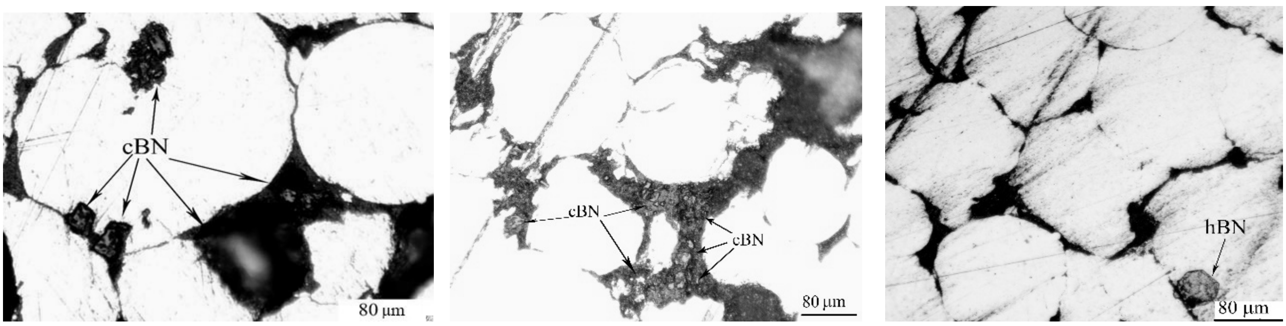

Fig.4. The surface structure of the samples based on self-fluxing alloy PG-SR4 and micron-sized cBN after the HPHT treatment: large cBN crystals along the boundaries of the alloy particles (a); small cBN crystals formed as a result of crushing and recrystallization of primary cBN crystals (b); formation of graphite-like BN(c)

The maximum microhardness of PG-SR4 samples with the addition of micron-sized powder cBN is in the range of 6.4–7.1 GPa, and this is 1.5–2 times lower than that for the material with the same content of nanostructured cBN sintered at the same parameters of the HPHT treatment.

Conclusion

The results show the promise of using of cBN nanostructured powder as a modifying additive for chromium-nickel self-fluxing alloys. It is shown that nanostructured cBN is distributed in a matrix based on self-fluxing alloy in the form of inclusions of submicron sizes and individual polyhedral particles up to 10 μm in size, while cBN micron-sized powder crystals are located between self-flux alloy particles.

In the process of HPHT treatment of the PG-SR4 alloy with the addition of cBN, the latter undergoes a number of structural and phase transformations: recrystallization of cBN, crushing of large cBN crystals, formation of secondary cBN crystals as a result of dissolution and recrystallization of the initial cBN, and the formation of a graphite-like BN.

Microhardness of the material with the addition of 2.5–3.5 vol. % of nanostructured cBN is 11.8–13.7 GPa, and this is 18–32% higher than that for the samples containing no additives of cBN. The samples with the addition of the micron-sized cBN powder are characterized by microhardness values in the range of 6.4–7.1 GPa, and this is 1.5–2 times lower than that for the material with the same content of nanostructured cBN.

Acknowledgements

The work is supported by the Belarusian Republican and Russian Foundations of Basic Research (Project code is T18R-183).

REFERENCES

1 Ilyuschenko A.Ph., Shevtsov A.I., Astashinsky V.M. et al. High-power pulse processing of thermal coatings based on a self-fluxing alloy and modified by solid high-melting compounds: research and modeling. *High Temperature Material Processes*. 2017, Vol. 21, No. 3, pp. 203–223. DOI:10.1615/HighTempMatProc.2017024942

2 Vityaz P.A., Ivashko V.S., Ilyushchenko A.F., Shevtsov A.I., Manoilo E.D. *Theory and practice of coating.* Minsk, Belarus. Science, 1998, 583 p. [in Russian]

3 Manoilo E.D., Onashchenko F.E. Gas-flame coating of self-fluxing alloys – new aspects. *Mechanical Engineer.* 2012, No. 4, pp. 6–9. [in Russian]

4 Kulik A.Ya., Borisov Yu.S., Mnukhin A.S. *Thermal spraying of composite powders.* Leningrad, Mechanical Engineering, 1985, 197 p. [in Russian]

5 Ilyushchenko A.F., Shevtsov A.I., Astashinsky V.M. et al. Investigation of the wear resistance and antifriction properties of gas-thermal coatings based on NiCrBSi alloy, modified with solid refractory compounds and pulsed high-energy impacts. *Powder metallurgy*. Minsk, 2018, No. 41. pp. 221–228. [in Russian]

6 Lyakhov N. Z., Talako T.L., Grigoryeva T.F. *Influence of mechanical activation on the processes of phase and structure formation during self-propagating high-temperature synthesis*. Novosibirsk, Parallel, 2008, 168 p. [in Russian]

7 Sobachkin A.V., Nazarov I.V., Yakovlev V.I. Morphology of coatings from multi-component, previously mechanically activated powders of SPS-composites. *Metal processing*. 2012, No 3 (56), pp. 141–144. [in Russian]

8 Golubev A.S., Kurdyumov A.V., Pilyankevich A.N. *Boron nitride. Structure, properties, production.* Kiev, Nauk. Dumka, 1987, 200 p. [in Russian]

9 Vityaz P.A., Senyut V.T., Kheifets M.L., Kolmakov A.G. Production of alumo-matrix composite material modified by nanostructured cubic boron nitride. *Proceeding of the NAS of Belarus, Phys.-Tech. Ser.* 2018, Vol. 63, No 3, pp. 271–279. DOI.org/10.29235/1561-8358-2018-63-3-271-279.

Article accepted for publication 25.10.2019

.

DOI 10.31489/2019No2/16-20

UDC 537.9

THE RESEARCH OF PHOTO-ELECTROPHYSICAL PROPERTIES OF COBALT PHTHALOCYANINE FILM

Aimukhanov A.K., Zeinidenov A.K., Ilyassov B.R., Zavgorodniy A.V., Pazyl B.M.

E.A. Buketov Karaganda State University Karaganda, Kazakhstan, alexZavgorodniy@inbox.ru

The paper presents results of a study of photo-electrophysical characteristics in a solid film and nanowires of cobalt phthalocyanine (CoPc). A solid CoPc film on a substrate with a conductive surface ITO (indium tin oxide) was obtained by thermal evaporation in vacuum. CoPc nanowires were obtained by the temperature gradient physical vapor deposition (TG-PVD). Measurements of current-voltage characteristics were carried out using a potentiostat-galvanostat P20X in the linear sweep mode. The study of transport kinetics and carrier recombination was carried out on the impedance meter P45X. A xenon lamp with radiation intensity equal to 100 mW/cm^2 was used as a solar light simulator.

***Keywords*:** cobalt phthalocyanine, solid film, nanowires, IVC, impedance spectroscopy

Introduction

Organic molecular semiconductors in the last decade have been an area of intensive research aimed at the development of various elements of organic electronics, such as field effect transistors, light emitting diodes, solar cells and memory cells. This is due to the low cost of these materials, the possibility of applying their films to flexible substrates, obtaining films of large areas, etc. Recently, among the variety of organic semiconductors, phthalocyanine complexes, which represent an extensive class of macro-heterocyclic compounds, have become very attractive. Films based on metallo-phthalocyanines have a higher conductivity than other organic compounds. Their electrical and optical properties can vary widely and depend on a number of factors. The high mobility of charge carriers and the efficiency of light energy conversion make it possible to consider metallo-phthalocyanines as promising materials for photoelectric converters [1-2].

The paper presents the results of a study of the current-voltage characteristics (IVC) of a photosensitive cell based on cobalt phthalocyanine (CoPc). The kinetics of transport and recombination of charge carriers in a solid CoPc film were studied using the impedance spectroscopy method.

1. Experimental technique

The preparation of substrates for photosensitive cells on the basis of ITO was carried out according to the method [3]. A solid film of cobalt phthalocyanine (Sigma Aldrich, 99%) ~ 75 nm thick was deposited on the surface of a substrate coated with ITO by thermal evaporation in a vacuum using a Carl Zeiss Jena HBA 120/2 installation. The deposition was carried out in a vacuum of 10^{-5}Torr at a rate of 0.5 nm/s. Growth of nanowires on the ITO surface was carried out by the temperature gradient physical vapor deposition (TG-PVD) [4].

Measurements of the current-voltage characteristics of an organic photosensitive cell were carried out using a potentiostat-galvanostat P20X in the linear sweep mode on the installation described in detail in [5]. The kinetics of transport and carrier recombination were studied on a P45X impedance meter (Elins). In both cases, the cell surface was illuminated using a 100 mW/cm^2 xenon lamp. Photovoltaic cell samples were prepared for photoelectrical measurements. They consisted of several layers: 1-glass substrate; 2-transparent conductive layer ITO (anode); 3-photoactive layer; 4-aluminum electrode (cathode). The choice of aluminum and ITO as contact layers is due to the fact that this produces the best ohmic contacts with the films and the best value of the electron output.

2. Results and discussions

The surface morphology of nanowires and the film thickness were measured using a JSPM–5400 atomic force microscope. Fig. 1 shows the surface morphology of the obtained samples. The average thickness of the solid film obtained by thermal evaporation was ~ 74 nm. The average height of the grown nanowires consisting of stacks of cobalt phthalocyanine molecules was ~ 137nm.

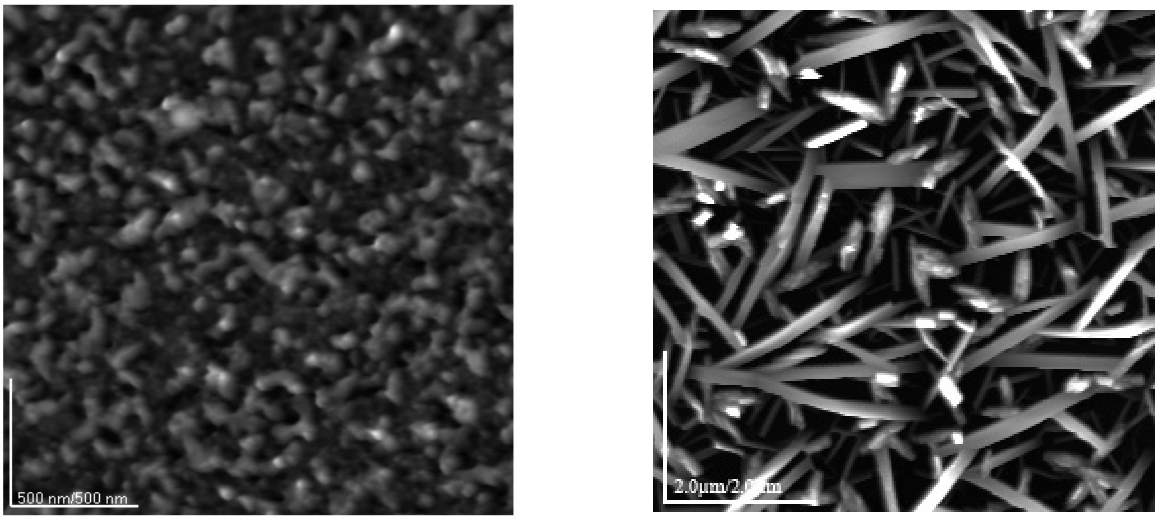

a) b)

Fig.1.AFM image of the surface of a solid film (a) and CoPc nanowires (b)

The absorption spectra of the studied samples were recorded on a CM2203 spectrophotometer (Solar). Fig. 2 (curve 1) shows the absorption spectra of cobalt phthalocyanine films obtained by thermal evaporation.

In the absorption spectra there are two very intense bands in the region of 350 nm (the Soret band or B-band), which corresponds to the mixed $\pi - \pi^*$ and $n - \pi$ transitions $a_{2u} \rightarrow {}^2e_g$and $b_{2u} \rightarrow {}^2e_g$, and the absorption band in the region 550–750 nm (Q-band), which corresponds to the $\pi - \pi^*$transition $a_{1u} \rightarrow {}^2e_g$ [11]. The absorption spectrum of CoPc film obtained by thermal evaporation (fig.2) in the Soret region has a maximum at λ=320 nm and in the Q-band there are two bands with maxima at λ=616 nm and λ=678 nm. The characteristic splitting of the absorption of nanostructures in the Q-band into two peaks is associated with the Davydov splitting [6].

In the spectrum of CoPc nanowires (Fig. 2, curve 2) the absorption band is broadened in the Soret region. The absorption band in the Q-band is also broadened, in addition, there is a bathochromic shift of the maxima in this spectral region in comparison with the film obtained by the method of thermal evaporation.

Table 1. Spectral characteristics of cobalt phthalocyanine

Sample	B-band			Q-band		
	Adsorption peak, nm	D	FWHM, nm	Adsorption peak, nm	D	FWHM, nm
Evaporated	λ=315	0.51	80	λ=616, λ=678	0.44	150
Nanowires	λ=324	0.85	125	λ=612, λ=700	0.48	225

The current-voltage characteristic of a CoPc-based photosensitive cell was determined by illuminating the sample from the ITO side with a xenon lamp in the wavelength range of 350-800 nm and a power of 100 mW/cm^2. Fig. 3 shows the IV characteristics of the samples obtained. It can be seen from Fig. 3 that the IVCs are non-linear. The values of open-circuit voltage U_{oc}, short-circuit current J_{sc}, maximum voltage and maximum current density U_{max} and J_{max}, and fill factor FF were determined according to the method [7].

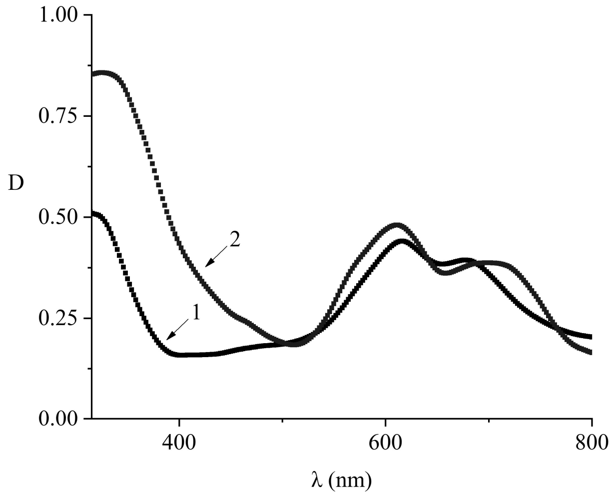

Fig.2. Absorption spectrum of CoPc:
1 – CoPc film obtained by thermal evaporation;
2 – CoPc nanowires.

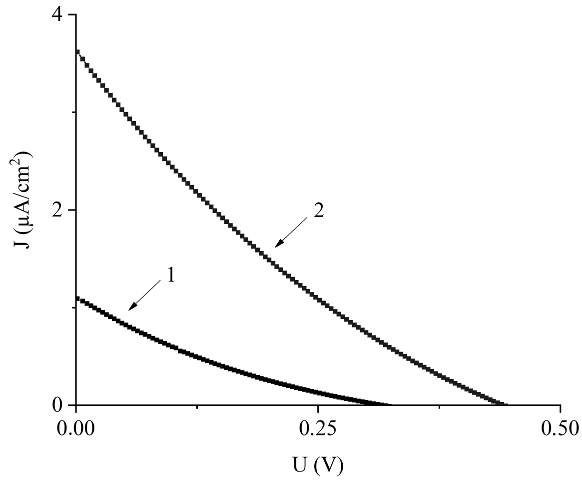

Fig.3. Comparison of current-voltage characteristics: 1 – IVC of CoPc film obtained by thermal evaporation; 2 – IVC of CoPc nanowires.

Thus, it can be concluded that the photosensitive cell based on cobalt phthalocyanine has lower values of voltage and current density compared to the photocell based on copper phthalocyanine, investigated by the authors in the paper [8]. Table 2 shows the parameters of the photoelectric characteristics of cobalt phthalocyanine nanostructures.

Table 2. Photoelectric characteristics of cobalt phthalocyanine nanostructures

Sample	U_{oc}(V)	J_{sc} (μA/cm^2)	U_{max} (V)	J_{max} (μA/cm^2)	FF
Evaporated	0.31	1.07	0.13	0.43	0.17
Nanowires	0.44	3.63	0.19	1.58	0.19

The efficiency of generation of charge carriers in a CoPc solid film obtained by thermal evaporation is low compared to nanowires. This fact is due to weak broadening of the absorption band, in contrast to nanowires. This is evidenced by the low value of the short-circuit current of the current-voltage characteristic of the cell (Figure 3, curve 1). In nanowires, CoPc molecules line up in a lamellar structure. As a result, the interaction of molecules in the unit cell increases. In this case, the broadening of the absorption bands in the Q and B ranges is more pronounced in comparison with the film obtained by thermal evaporation. Thus, this leads to an increase in the number of charge carriers in the cell (Fig. 3, curve 2).

Investigation of the mechanisms of transport and recombination of charge carriers of a cobalt phthalocyanine solid film was carried out by impedance spectroscopy. To interpret the impedance spectra, we used the equivalent circuitry of the photovoltaic cell (Fig. 4), where R1 (R_w) is the equivalent resistance of the multilayer film (R_{ITO} + R_{Al} + resistance of the photoactive layer), R2 (R_{rec}) is the resistance characterizing the recombination of localized electrons with holes.CPE1 is an element with a constant phase, which is an equivalent component of an electric circuit, modulating the behavior of the active layer, but being an imperfect capacitor.

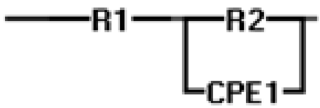

a)

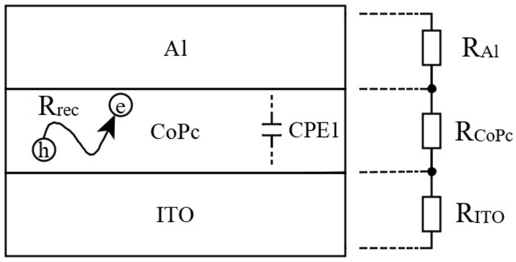

b)

Fig.4. An equivalent electrical circuit (a) and a schematic representation (b) of the photosensitive cell.

The impedance spectra in the Nyquist coordinates based on CoPc films are presented in Fig. 5. The spectra were fitted using the EIS-analyzer software package. The main electric transport properties of solar cells were calculated (Table 3), where k_{eff} is the effective recombination rate of charge carriers, and τ_{eff} is the effective electron lifetime. The analysis of impedance measurements was carried out according to the diffusion-recombination model [9].

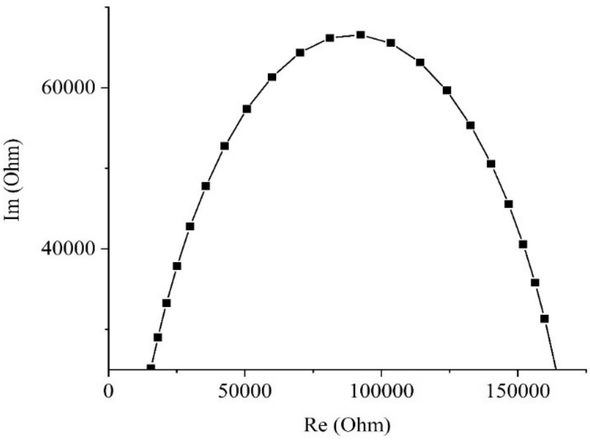

a)

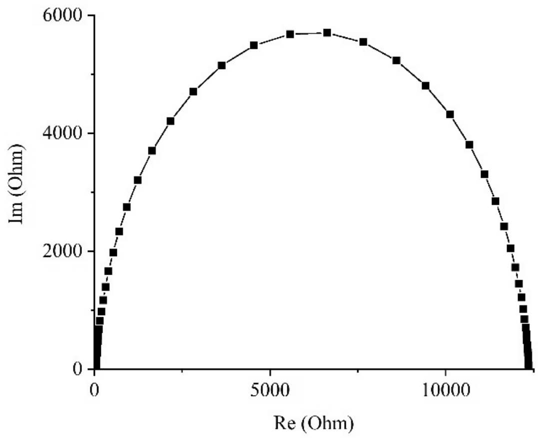

b)

Fig. 5. Impedance spectra of CoPc solid film (a) and CoPc nanowires (b)

An analysis of the impedance spectra shows that the addition of CoPc nanowires improves the conductivity of the film, which is determined by the value of R_w. Table 3 shows that, in nanowires, the effective mean free path of charge carriers (D_{eff}) is higher than the film obtained by thermal evaporation.

Table 3. Electric transport properties of CoPc cells

Sample	D_{eff}, (cm^2s^{-1})	k_{eff}, (s^{-1})	τ_{eff}, (ms)	R_k, (Ohm)	R_W, (Ohm)	C_{on}, (Ohm cms^{-1})	L,(cm)
CoPc Evaporated	4.08×10^{-8}	22.3	44.8	1.7×10^{5}	5093.4	28.1	7.4×10^{-6}
CoPc Nanowires	1.38×10^{-5}	277.8	3.6	12321	46.53	46.9	13.7×10^{-6}

.

Using the EIS – analyzer software package, R_{rec} and R_w are calculated; k_{eff} value is determined by the maximum of the hodograph arc according to the formula $\omega_{max} = k_{eff}$. The value of the effective lifetime of charge carriers τ_{eff} in the films is calculated by the formula $\tau_{eff} = \frac{1}{k_{eff}}$.

The observed effect is associated with an increase in the structuring of molecules in the film, because CoPc nanowires form a lamellar structure. A lower R_w value in cells with CoPc nanowires also suggests that nanowires contribute to better carrier transfer to the electrode. Also, the effective carrier lifetime in nanowires (τ_{eff}) is shorter. The parameter τ_{eff} determined by the method of impedance spectroscopy takes into account the time spent by charge carriers in traps. A lower value of τ_{eff} indicates a lower density of localized states in nanowires.

Conclusion

Researches have shown that in the cell based on CoPc nanowires, broadening of the B and Q bands and a shift of the maxima in the spectra are observed. The structuring of CoPc molecules with the formation of nanowires affects the value of the short-circuit current of the cell. Using the method of impedance spectroscopy, it was found that transport properties are improved in nanowires.

Acknowledgements

This work was supported by the grant of the E.A. Buketov Karaganda State University.

References

1 Vidya C., A. Hoskeri Priya, Joseph C.M. Structural and Optical Properties of Vacuum Coated and Annealed Copper Phthalocyanine (CUPC) Thin Films. *Proceedings of the 4th Intern. Conf. on Materials Processing and Characterzation (ICMPC).* Gokaraju Rangaraju Inst Engin & Technol, Hyderabad, India, 2015, pp. 1770 – 1775.

2 Keeratithiwakorn P., Songkeaw P., Onlaor K. & Tunhoo B., Structural properties of copper phthalocyanine films grown by electrophoretic deposition process. *Materials Today: Proceedings*, 2017, Issue 4, pp. 6194 – 6199.

3 Kim K., Ihm K., Kim B. Surface Property of Indium Tin Oxide (ITO) After Various Methods of Cleaning. *ACTA PHYSICA POLONICA A. Proceedings of the 4th International Congress APMAS2014*, 2015, Fethiye, Turkey, Vol. 127, No. 4, pp. 1176-1179.

4 Fangmei Liu, Jia Sun, Si Xiao et al. Controllable fabrication of copper phthalocyanine nanostructure crystals. *Nanotechnology,* 2015, 26, 22, 225601, pp. 1 – 8.

5 Zavgorodniy A.V., Aimukhanov A.K., Zeinidenov A.K., Akhatova Zh.Zh. Study of the effect of an external magnetic field on the photoelectric properties of a copper phthalocyanine film. *Bulletin of the Karaganda University. Physics Series*. 2019, No. 1 (93), pp.18 – 25.

6 El-Nahass M. M., Bahabri F.S. & Al-Harbi R. Optical Properties of Copper Phthalocyanine (CuPc) Thin Films. *Egypt. J. Sol.,*2001, Vol. 24, Issue 1, pp. 11 – 19.

7 Tiwari S., Greenham N.C. Charge mobility measurement techniques in organic semiconductors. *Optical and Quantum Electronics*, 2009, Vol. 41, Issue 2, pp. 69 – 89.

8 Zavgorodniy A.V., Aimukhanov A.K., Zeinidenov A.K., Ayubekova A.Ye. The influence of the magnetic field on the current-voltage characteristics of cupc nanostructures. *Eurasian Physical Technical Journa*l. 2019, Vol.16, No.1(31), pp.54 – 61.

9 Bisquert J., Mora-Sero I., et al. Diffusion–Recombination Impedance Model for Solar Cells with Disorder and Nonlinear Recombination. *ChemElectroChem,* 2014, Vol. 1, Issue 1, pp. 289 – 296.

Article accepted for publication 25.10.2019

DOI 10.31489/2019No2/21-25

UDC 538.1: 548

DOMAIN STRUCTURE AND MAGNETIC PROPERTIES OF TERBIUM FERRITE-GARNET IN THE VICINITY OF THE MAGNETIC COMPENSATION POINT

Sharipov M.Z., Hayitov D.E., Rizoqulov M.N., Islomov U.N., Raupova I.B.

Bukhara Engineering - Technologies Institute, 200100, Bukhara, Uzbekistan, m.z.sharipov@rambler.ru

The domain structure of a thin single crystal plate of the iron garnet $Tb_3Fe_5O_{12}$ has been investigated using the magneto-optical method in the temperature range near the magnetic compensation point of this ferrimagnet T_c = 248.6 K. It has been shown that, when the temperature of the sample approaches the magnetic compensation point, the domain width significantly increases, but remains finite at $T = T_c$. The magnetic H–T phase diagram determines the boundary between the multi domain and domain free (uniformly magnetized) states of the sample. Here the magnetic H–T phase diagram has been constructed using the data on visual observations of the transformation of the domain structure with variations in the temperature and external magnetic field.

Keywords: Ferrimagnetic, domain structure, magnetic compensation, phase diagram, domain boundary,

Introduction

Rare-earth ferrites-garnet (REFG), which include heavy RE ions, have a so-called magnetic compensation point - temperature T_c (below the Curie temperature), at which their spontaneous magnetic moment M_s vanishes. From a practical point of view, REGF with sufficiently high T_c are of interest as materials for the elemental base of magnetic microelectronics devices using the thermo-magnetic method of recording / erasing information [1, 2].

In this regard, direct visual observations of the domain structure (DS) of a thin single crystal $Tb_3Fe_5O_{12}$ terbium garnet ferrite garnet in the temperature range [3, 4], including its magnetic compensation temperature (T_c = 248,6 K [5]), were carried out, the results of which are presented below.

1. Examples and experimental technique

In our experiments, we used a $Tb_3Fe_5O_{12}$ single crystal sample in the form of a plane-parallel plate with transverse dimensions ≈ 2 × 3 mm^2 and a thickness of ≈ 100 μm, oriented so that the [111] axis makes an angle of ≈ 10^0 with the normal to its plane, and one of the axes has a smaller inclination to the plane of the sample compared with the other two (the error of the crystallographic orientation of the sample is ~ ± 2^0) [6].

It is known [7,8] that in REFG in a certain interval of the external magnetic field, the vectors $\mathbf{M}_{Fe}$ and $\mathbf{M}_R$ turn from antiparallel to parallel, i.e. a skewed magnetic phase occurs in which the angle between $\mathbf{M}_{Fe}$ and $\mathbf{M}_R$ is different from 180^0. The critical field of the beginning of the turn of the sublattice magnetic moments

$$H_\kappa \propto (M_{Fe} - M_R)H_0,$$

where H_0 is the exchange field acting between the iron and RE sublattices, whence it follows that near the magnetic compensation point $H_\kappa \to 0$, i.e. at $T \to T_c$, the scattering fields created by neighboring domains may be sufficient to start the reversal of the vectors $\mathbf{M}_{Fe}$ and $\mathbf{M}_R$. Therefore, in the general case, with normal incidence of light on the plane of the sample, the spontaneous Faraday effect in REFG can be represented as:

.

$$\theta_F = \left(a\vec{M}_{Fe}\cos\theta_1 + bM_R\cos\theta_2\right)l \ ,(1)$$

where a and b - are magneto-optical coefficients depending on the frequency of light; θ_1, θ_2 are the angles formed by the vectors $\mathbf{M}_{\mathrm{Fe}}$ and $\mathbf{M}_{\mathrm{R}}$ with a normal to the plane of the sample (in the collinear magnetic phase of the crystal $\theta_1 = \theta_2$); l - is the thickness of the sample.

In $Tb_3Fe_5O_{12}$ at $T<T_c\mathbf{M}_{\mathrm{R}} > \mathbf{M}_{\mathrm{Fe}}$, therefore, the vector $\mathbf{M}_{\mathrm{R}}$ is oriented in the direction of the external magnetic field. At $T>T_c$, the situation is the opposite — the vector $\mathbf{M}_{\mathrm{Fe}}$ is directed toward $\mathbf{H}$. Thus, at the magnetic compensation point, the vectors $\mathbf{M}_{\mathrm{Fe}}$ and $\mathbf{M}_{\mathrm{R}}$ are rotated by 180^0, which, in accordance with (1), leads to a change in the sign of the Faraday rotation angle, which can be determined by a sharp change in the color of the observed domains. Moreover, as can be seen from (1), even at ($\mathbf{M}_{\mathrm{Fe}} + \mathbf{M}_{\mathrm{R}}$) = 0 (at $T = T_c$), the Faraday Effect does not vanish, which allows us to observe the DS of the sample when the temperature passes through the point of magnetic compensation.

2. Experimental results and discussion

As observations have shown, in accordance with expectations in the entire studied temperature range of 85–295 K at H = 0, the DS of the sample formed domains in the form of light (visually red) and dark bands of approximately equal width with clearly defined boundaries [9]. In this case, an external magnetic field parallel to the middle direction of the domain walls strongly affected the domain width, transferring the sample at a certain T-dependent value of H to a homogeneous (single-domain) state, while the field oriented in the plane of the sample is perpendicular to the domain wall (DW), practically did not change the width of the domains up to the maximum intensity H = 60 Oe used in the experiment. Such a behavior of the domain structure obviously means that the vectors $\mathbf{M}_s$ in neighboring domains are antiparallel to each other and oriented along domain boundaries (i.e., 180^0 - DS is realized in the sample).

As an example in Fig.1 shows a number of photographs taken during the heating of the sample from T = 85 K (heating rate ~ 0.2 K/s), illustrating the general nature of the change in its DS depending on temperature. A series of photographs a ÷ e was obtained immediately after cooling the sample to T = 85 K; each photograph of the series shown in fig. 2 - after demagnetization of the sample at a given T in an alternating magnetic field (changing with a frequency of 50 Hz), the amplitude of which decreased from the maximum value H = 60 Oe to zero.

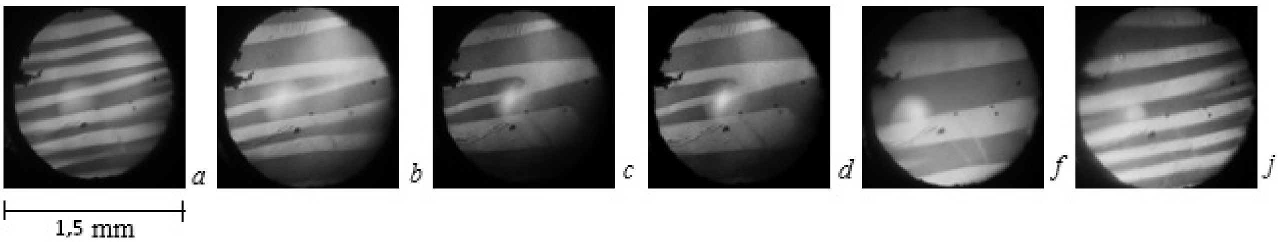

Fig. 1. Images of the domain structure of the sample obtained at different temperatures during heating: 205 (*a*), 237 (*b*), 248 (*c*), 251 (*d*), 256 (*f*) and 295 K (*j*).

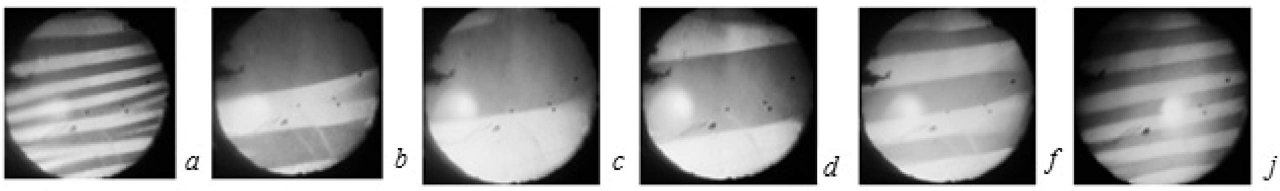

Fig. 2. Images of the "equilibrium" domain structure of the sample obtained at different temperatures during heating: 205 (*a*), 236 (*b*), 248 (*c*), 251 (*d*), 260 (*f*) and 295 K (*j*). At each temperature, the sample was demagnetized in an alternating magnetic field with amplitude decreasing to zero.

It was assumed that the demagnetization procedure allows one to obtain a domain configuration close to equilibrium at a given temperature. As a rule, after this procedure, for each value of T, 2-3 domain configurations were observed, slightly differing by the position of the domain walls, however, the average width of the domains arising from case to case remained almost constant. The temperature dependence of the average domain width of the "equilibrium" DS sample is shown in Fig. 3. Note that, when approaching the point of magnetic compensation, a deterioration in the magneto-optical contrast and a change in the color shades of images of neighboring domains were observed.

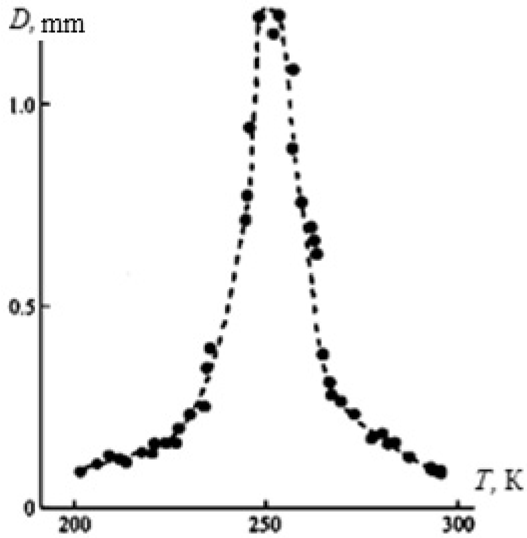

Fig. 3. Temperature dependence of the average domain width of the "equilibrium" domain structure of the sample.

The single domain state of the sample could be observed under the action of an external field **H**, which has a noticeable projection onto the direction of the domain walls. So, in a field oriented along the direction of domain walls at an angle of $\approx 10^0$ to the plane of the sample (along the assumed direction of the distinguished light axis), the single-domain state of the sample was observed near T_c at $H > 4$ Oe. In Fig. 4 shows photographs demonstrating the behavior of the DS of a sample with a change in temperature at the above orientation of the magnetizing field at $H = 5$ Oe, from which it can be seen that the single domain state of the sample occurs in a certain temperature range to the right and left of T_c. As observations showed, with an increase in H, these temperature ranges of the "single domain" gradually expanded, until at $H \approx 7$ Oe they merged into one general one. In the "single domain" region, the image of the sample has a uniform color over the entire area; when the temperature passes through the compensation point, the color of the image of the sample (in accordance with (1)) changes abruptly.

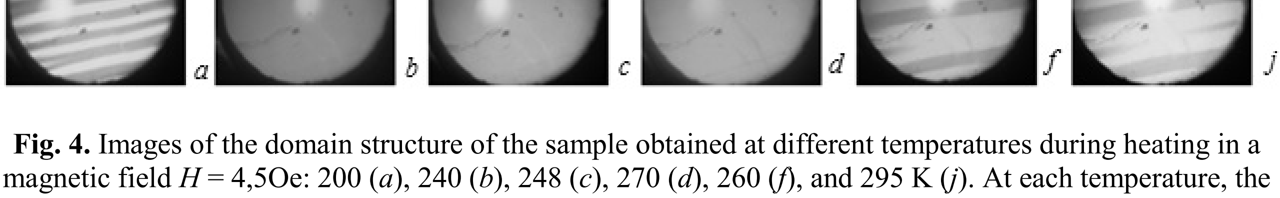

Fig. 4. Images of the domain structure of the sample obtained at different temperatures during heating in a magnetic field H = 4,5Oe: 200 (*a*), 240 (*b*), 248 (*c*), 270 (*d*), 260 (*f*), and 295 K (*j*). At each temperature, the sample was demagnetized in an alternating magnetic field with amplitude decreasing to zero. Vector **H** is parallel to O.L.N.

.

In fig. 5 shows the experimentally obtained magnetic H - T diagram that defines the boundary between multi-domain and single-domain (uniformly magnetized) states of a sample. Each point of the diagram was determined by the results of visual observations of the disappearance of domain walls in the image of the sample with a change in H and T (in the experiment, the sample was first cooled to T = 85 K, then the magnetic field of the specified strength was turned on and the process of changing the DS during heating of the sample was observed, while at each fixed temperature, the sample was subjected to a demagnetization procedure).

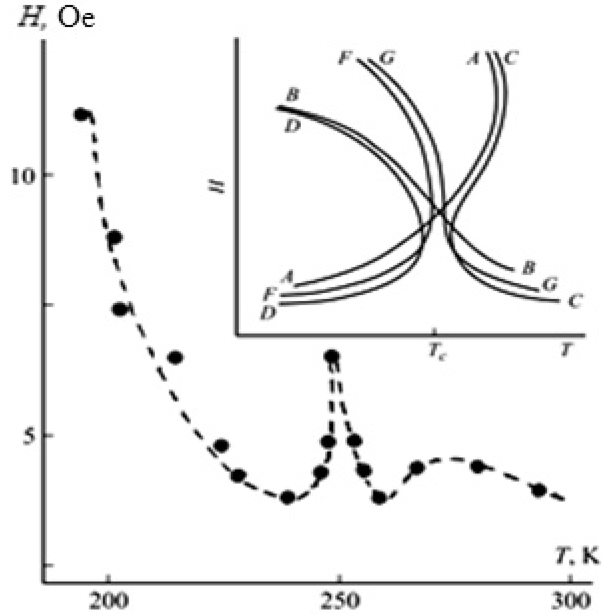

Fig. 5. Temperature dependence of the magnetic field at which the sample goes into a single domain state. The direction of the vector **H** is parallel to O.L.N. - crystallographic direction $\langle 111\rangle$. Inset: phase H – T diagram describing the magnetic state of the rare-earth phase group at **H**|| [111] [7], AA and BB are the lines of phase stability loss (φ = 0) and ($\varphi = \pi$), SS and FF are the boundaries regions of stability of states (0 <φ<π / 2, $\xi = \pi / 2, 7\pi / 6, 11\pi / 6$), DD and GG are the boundaries of the region of stability of states (π / 2 <φ<π, $\xi = \pi / 6, 5\pi / 6, 3\pi / 2$), where φ and ξ are respectively the polar and azimuthal angles of the vector $\mathbf{M}_{Fe}$ in the Cartesian coordinate system {[110], [112], [111]} (the [111] axis is the polar axis).

The $H – T$ diagram of the sample obtained in this way is in good agreement (on a qualitative level) with the magnetic phase diagram describing the magnetic state of the REFG in H || $\langle 111\rangle$ calculated in [8] (see inset of Fig. 5). From the fragment shown in the inset Fig. 5 of the phase diagram of the REFG, it can be seen that at $T \rightarrow T_c$, the angular phases of the crystal appear earlier than the magnetic moments of the iron and rare-earth sublattices are equal in magnitude. The stability loss lines of various magnetic phases of a crystal determine the boundaries of the existence of domains with the corresponding directions of magnetic moments (DS arises due to demagnetizing fields). This suggests that the experimentally observed decrease in the contrast of the image of the domains and a change in their color in the immediate vicinity of the sample temperature to $T_c$is associated with the transition of the crystal from the collinear magnetic phase to the angular one. In this case, the skew of the vectors $\mathbf{M}_{Fe}$ and $\mathbf{M}_R$ will lead to a decrease in their projection on the direction of the light propagating in the crystal, and as a result to a decrease in the magnitude of the Faraday effect (see (1)).

From fig. 1 and fig. 2, it follows that although the width of the domains at $T \rightarrow T_c$ increases significantly, nevertheless, in contrast to the results of a theoretical analysis of the DS of a plane-parallel ferrimagnet plate obtained in [10, 11], the domains in the sample do not disappear in the entire temperature range studied, i.e. e. at H = 0, the sample does not transform into a uniformly magnetized state. In addition, it follows from the theory developed in [9, 10] that, at $T \rightarrow T_c$, the maximum domain width reaches a value comparable to the plate thickness, whereas from Fig. 1 and fig. 2 shows that in our case the maximum domain width is more than 10 times the thickness of the sample.

Conclusion

Thus, the performed studies have shown that, in a plane-parallel plate of the $Tb_3Fe_5O_{12}$ garnet ferrite garnet, at H = 0, when the temperature passes through the point of magnetic compensation, the DW does not disappear. The explanation of this fact was based on the magnetic phase diagram of the REFG obtained in [8]. However, there are other possible reasons for the existence of domains in the sample near T_c — for example, defects in the crystal lattice or the presence of a noticeable entropy contribution to the thermodynamic potential of a crystal, which makes its multi-domain state energetically more favorable than a single-domain state (as is the case in collinear antiferromagnets) [12]. An unambiguous choice of the reason leading to the existence of an REFG DS at $T \rightarrow T_c$ is possible, in our opinion, if we trace the dynamics of the spatial orientation of the sublattice magnetic moments of the crystal. In particular, additional information can be obtained from a detailed analysis of the color change of domains when the temperature changes, made using a computer-based method for processing optical images.

REFERENCES

1 Rainer Waser. *Nanoelectronics and information technology. Advanced electronic materials and novel devices*. Wiley-VCH GmbH & Co. KGaA, 2003, 1001 p.

2 Shavrov V.G., Sheglov V.I. *Dinamika namagnichennosti v usloviyh izmeneniya orientachii.* Moscow, Fizmatlit, 2019, 468p. [in Russian].

3 Boidedaev S.R., Dzhuraev D.R., Sokolov B.Yu., Sharipov M.Z. Magnetooptical method of investigation of the magnetic inhomogeneity of easy-plane antiferromagnets with a weak ferro-magnetism. *Optics and Spectroscopy*, 2008, Vol. 104, No. 4, pp. 604–609.

4 Sharipov M.Z., Mirzhonova N.N., Hayitov D.E. Effect of inhomogeneous radially directed mechanical stresses on the domain structure of a $FeBO_3$ single crystal. *Eurasian Physical Technical Journal,* 2019, 16(1), pp. 35-41.

5 Grigoryeva I.S., Meilikhova E.Z. *Physical quantities*. Moscow, Energoatomizdat, 1991, 223 p. [in Russian].

6 Sokolov, B.Y., Sharipov, M.Z. Magneto-optical properties of the iron garnet Tb_3 Fe_5 O_{12} near the magnetic compensation temperature. *Physics of the Solid State*, 2014, Vol. 56, No. 5, pp. 975 – 979.

7 Bukharaev A.A., Zvezdin A.K., Pyatakov A.P., Fetisov Yu.K. Straintronics: a new trend in micro- and nanoelectronics and materials science. *Phys. Usp.*, 2018, Vol. 61, Issue 12, pp. 1175 – 1212.

8 Pyatakov A.P., Zvezdin A.K. *Magnetoelectric and multiferroic media*. *Phys. Usp.*, 2012, Vol. 55, Issue 6, pp. 557 – 581.

9 Sokolov B.Yu., Talabov M.D., Sharipov M.Z. Domain structure of a thin single-crystal plate of terbium ferrite garnet near the point of magnetic compensation. *Physics of the Solid State*. 2013, Vol. 55, No.2, pp.278 – 283.

10 Bogdanov A.N., Yablonsky D.A. On the theory of the domain structure of ferrimagnets. *FTT.* 1980, Vol. 22, No. 3, pp.680 – 687. [in Russian].

11 Baryakhtar V.G., Bogdanov A.N., Yablonsky D.A. The domain structure of ferrites in the vicinity of the compensation temperature. *FTT.* 1986, Vol. 28, No. 1, pp. 87 – 94. [in Russian]

12 Shavrov V.G., Sheglov V.I. *Ferromagnitniy rezonans v usloviyah orientatsionnogo perehoda.* Moscow, Fizmatlit, 2018, 468 p. [in Russian].

Article accepted for publication 22.11.2019

.

DOI 10.31489/2019No2/26-30

UDC 620.13.40

EXPERIMENTAL STUDY OF CHANGES IN THE STRUCTURE OF POLYMER COMPOSITE MATERIAL BY COMPUTATIONAL X-RAY TOMOGRAPHY

Yurov V.M.[1], Goncharenko V.I.[2, 3], Vasiliev S.L.[2], Dmitriev S.A.[2], Yurgenson S.A.[2]

[1] E.A. Buketov Karaganda State University, Karaganda, Kazakhstan, exciton@list.ru
[2] Moscow Aviation Institute (National Research University), Moscow, Russia, fvo@mai.ru
[3] Institute of Control Sciences. V.A. Trapeznikova, RAS, Moscow, Russia, fvo@mai.ru

In article on the basis of the method of computing x-ray tomography the technique of assessing changes in the state structure of polymeric composite material under the dead load. The results of the analysis of structure changes for carbon fiber samples at the setting stage of loading are presented. Offered exploratory procedure allows to fracture propagation under the force action and to analyze the material changes depending on the presence and load levels. In addition, quantitative parameters are introduced to compare the tendency of the material to accumulate damage in various technological processes. The results of the test research show that the proposed method allows for high accuracy to analyze the behavior of the material under load and identify typical trends for the type of material and laying.

Keywords: composite material, X-ray computer tomography, nondestructive testing, aviation structure.

Introduction

At this moment in time production engineering of elements and item of equipment of composite material (CM) are developing ahead of schedule in almost all industrialized countries. Feature of CM is that they are not monolithic material, such as metals. KM is a structure which created in the process of manufacturing a product [1-3]. There is a problem of an objective assessment of quality of KM, possibility of application of various physical methods for control of their quality. Computational and analytical methods of research do not always allow obtain a complete picture of all the effects arising during servicing in polymer composite materials (PCM) [4, 5]. Conformance assessment of materials, blank part, and final production can be carried out using a variety of laboratory and industrial equipment. One of the methods of flaw detection and analysis of size dimensions of the product is the method of computational X-ray tomography [5].

Manufacturing computational X-ray tomography (CXT) is a highly effective method of nondestructive radiation control, combining the capabilities of X–ray radiation and digital technology, which allows obtain flat sections and three-dimensional images of controlled products. On-hand status of such equipment at the “Production planning and quality control” department of the Moscow aviation Institute (national research University) allows to carry out some work on the conformity assessment of military products [6, 7].

The proposed work is at the junction of several areas – the development of methods of application of high-energy tomography in the mechanics of structurally inhomogeneous materials and technological design [8-16]. Within these areas are suggested to develop perspective methods of research of new materials, correct methods of designing products from polymeric composite materials and to develop methods for computational and analytical evaluation of the product behavior during operation based on process defects.

The paper [7] describes the method of using CXT in solving problems of research the state of the structure of the PCM under load. The main data obtained in this work are related to the assessment of crack development in the material and measurements based on computer modeling of its contribution to the reduction of the sample strength. At the same time, the research method proposed in this paper allows not only to assess the crack development under force action, but also to analyze the material changes depending on the presence and level of loading. Quantitative parameters are introduced to compare the tendency of the material to accumulate damage in various technological processes.

1. Experimental procedure

For a measurement of change in the power action stand, allowing to apply to the samples uniaxial force action directly on the desktop of the X-ray tomography, had been engineered and made. At the figure 1 we can see diagram of the research using this stand. The initial fixed parameters are the characteristics of the sample and its mechanical properties, which are used to select the loading steps (drawing up the plan of the experiment).

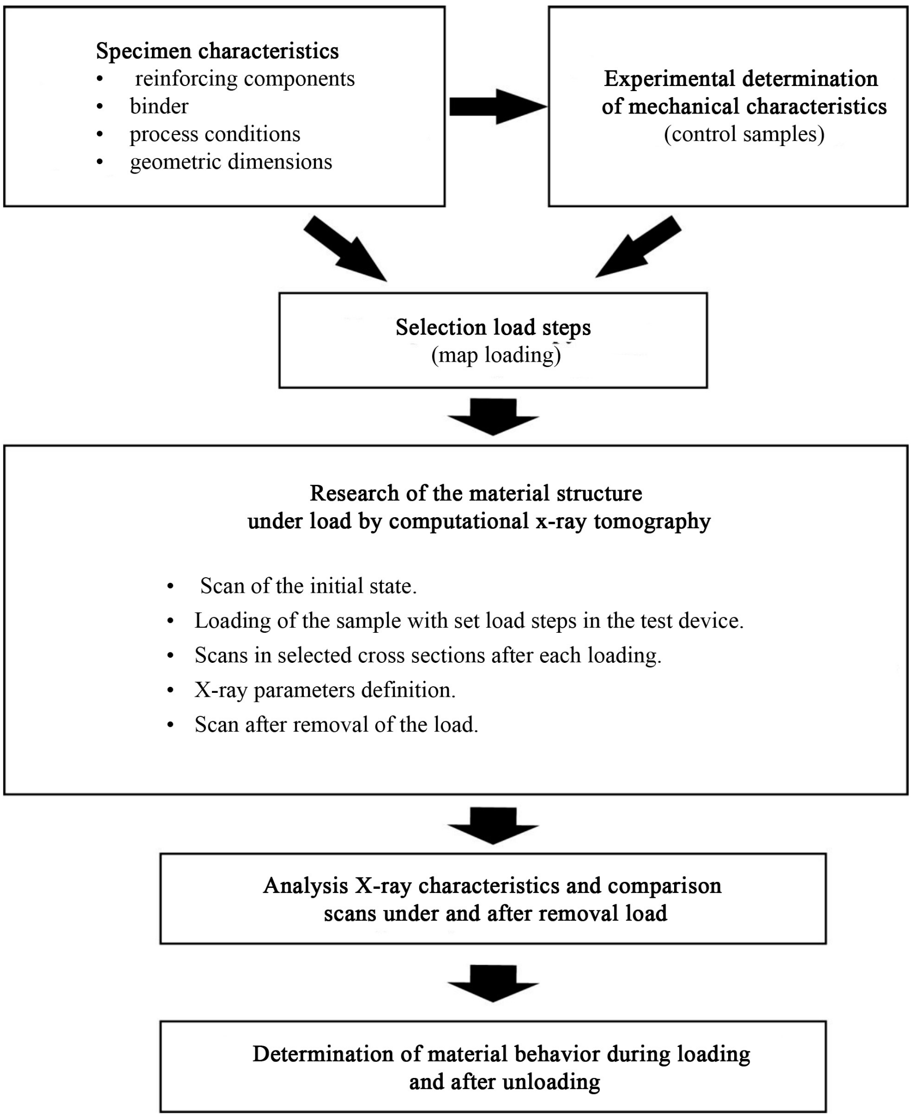

Fig.1. Study design

Test operation is determining the basic state of the material-the tomographic parameters that are considered to be the starting point for a this sample (selected technology, installation and types of binder and filler). And then step-by-step loading is performed for the selected load levels. At

.

every step the state of the material is fixed and tomographic parameters are determined, which are compared with the base state, which allows to evaluate the changes occurring in the material. Growth of density anomalies associated with both loosening of the material and its local compaction. The maximum value of the linear attenuation coefficient (LAC) is monitored to track the compaction of individual sections.

At every step of increasing the load, the following actions are performed:

– Each test sample is installed in a stand for force interaction on the sample. Initial strain measurement and preliminary scanning of all selected sections are carried out;

– A load is applied to the sample, the value of which corresponds to the first step of loading, deformations in the sample are measured and scanning is carried out;

– The sample is unloaded (complete removal of extension force) and immediately carried out deformation measurement and scanning;

– After a lapse of time after removal of load carried out repeating deformation measurement;

– Unloading and further loading of the sample is carried out in accordance with the plan of the experiment;

– Then the sample is loaded to the level of the second step and the test procedure is repeated.

– Number of steps of increasing the load are repeating while sample do not be destroyed (or reaching the limit to fit the force) or before deformations appear in the sample, indicating a complete loss of load-bearing capacity (expected for samples with oblique-angle reinforcement scheme) [10].

As tomographic parameters the criteria of correlation between the state of the structure of the sample material and the reconstructed scanning results are accepted:

1. The average value attenuation coefficient be a descriptor of structural density in the i-th scanned section after the j-th loading (j=0 - before loading) and is directly proportional to the increase in the number of secondary damage per unit area of the section;

2. Maximum and minimum value of LAC, which characterize growth process of individual defects and local compaction in the material structure;

3. Root-mean-square deviation (RMS) of the value of LAC in the scanned section characterizes the amplitude of the absolute deviation of the LCO from the most probable value, the increase in the absolute value of the LCO confirms the increase in the number of secondary damages per unit area.

2. Results of the experiment and their discussion

As test pattern applied specimen series UP-3 (with typical laying 0 / ±45/90) of carbon tape UOL-300-1 (TU 1916-167-05763346-96 production LLC "Argon") and the binder EPS-I-108 (TU 2225-047-17411121-2012 production LLC "Superplast"), obtained by impregnation and molding under a double vacuum bag. Research was being conducted in the 40 sections of the operating space with step for 5 millimeters for debugging parameters of scanning and analysis of the frequency of occurrence of values. In appropriate cases thickener or defect of anyone type can be input into researching space of specimen.

The research of the sample was carried out at four levels of tensile load – 5 %, 20 %, 30 %, 40 % from the destructive load, as well as its further full unloading. As a result, the graphs of the deviation of the controlled parameters from the initial state of the sample were obtained, presented in figure 2. Analysis of the change in the cross-sectional area of the sample was not carried out because of its minor fluctuations – sectional area was not more than 0.5 %, which may be caused by the heterogeneity of the sample surface. Based on the results for the selected installation and types of materials, the following conclusions are made:

- When applying up to 30 % of the breaking load the sample structure changes with a small step and does not undergo significant changes. There is an ordering of the structure of the material, as evidenced by a decrease in the deviation of the maximum values of the LAC and slight fluctuations in the deviation of the minimum value, which shows a variable growth of the primary defect. Growth deviations RMS in this case is associated with the most fluctuations in minimum values of LAC compared to the maximum, which indicates the early growth of the primary defect that causes the seal adjacent layers (decreases deviation of the average value of LAC);

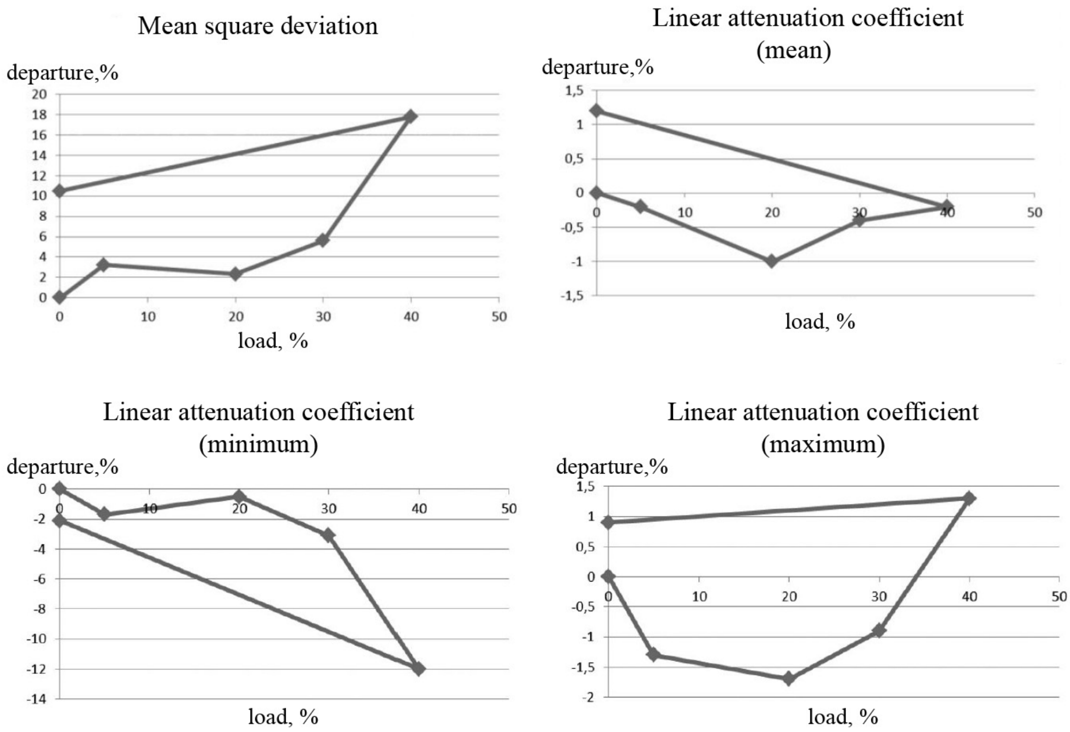

Fig. 2. Deviation of controlled parameters from the initial state depending on the applied load.

- When applying up to 40 % of the breaking load is reached, a significant change in the state of the structure of the material is observed. The increase in the deviation of the RMS value from the initial value when 40 % of the destructive load is reached is 2 times higher than the same indicator at 30 % of the destructive load. This is caused by a significant increase in the primary defect (the minimum value of LAC increases by 3 times compared to 30 % of the breaking load), which leads to compaction of the surrounding material. This conclusion is confirmed by the behavior of the average value of Loco, which is 40 % of the destructive load almost corresponds to the initial state of the sample, while the growth of RMS. After unloading of the sample, residual variation are observed, which are characterized by a local compaction of the sample structure, significant in comparison with the loaded state. The General behavior of the material structure after unloading is characterized by an increase in density variations in the sample (the deviation of the RMS from the initial state is 10 %) and a slight compaction of the material structure (the average value of the LAC increased by 1 %), which may mean a decrease in the number of primary defects in the sample. According to the results of the test research on this sample, the following conclusions can be made:

– for this placing and material characteristic considerable increase mainstream defect after reaching a certain load (in this case it was 30% of the destructive load);

– when the load is applied, the growth of the local primary defect occurs, while smaller defects are closed, and the structure of the material becomes less loose;

– after unloading the sample, there is a general compaction of the material structure, but at the same time there is a disclosure of the mainstream defect [12], which in the case of flaw detection after removing the load has a much smaller geometric dimensions compared to the loaded state.

Conclusion

The suggested procedure shows that the proposed technique helps high accuracy carry out an analysis of the material response when load is applied, and identify trends specific to the type of material and styling in question. Comparison of the initial, loaded, and unloaded state of the sample indicates the need for such a study for different types of materials in order to identify the characteristic trends in the main cracks.

The increase mainstream defect and less the influence of local defects on the structure of the material was obtained for this placing and material characteristic. At the same time local defects on the structure of the material must be research same the mainstream defect. The volume of porosity and moisture saturation may be changed in real structure by comparison with elementary samples was researched in the certification tests. The local changes of structure material was had on the low load, that mean that real volume of porosity (therefore and moisture saturation) can be higher and mechanical characteristics low than design value. The possibility of numerical evaluation of the processes of changing the structure of the composite material allows us to clarify the existing results and methods of finite element calculation. The methods of damage summation processes in CM can be improve with the experimental data sufficiency.

REFERENCES

1 Mikhailin Yu.A. *Structural polymer composite materials*, 2nd edition. Moscow, 2008, 822 p.

2 Goncharenko V.I., Oleshko V.S. Calculations of Tool Hardness in the Aviation Industry. *Russian Engineering Research.* 2017, Vol. 37, No. 6, pp. 554–556. DOI: 10.3103/S1068798X17060119.

3 Goncharenko V.I., Oleshko V.S. Determining the surface energy of tools in the aviation industry. *Russian Engineering Research*. 2017 Vol. 37, No. 7, pp. 628–630. DOI: 10.3103/S1068798X17070127.

4 Lurie S.A., Dudchenko A. *Introduction to the mechanics of nanocomposites*. Moscow, 2010, 160 p.

5 Klyuev V.V., Sosin F.R., Kovalev A.V. *Non-destructive testing and diagnostics*. Weinberg and others. 2nd edition. Moscow, Engineering, 2003, 656 p.

6 Boicov B.V., Vasilyev S.L., Hromachev A.G., Jurgenson S.A. Non-destructive testing methods used for structures made of advanced composite materials. *Labor of MAI: Electronic Journal*. 27.12.2011. Issue 49.

7 Vasilyev S.L., Artemyev A.V., Jurgenson S.A. Analysis of the impact of static load on the structure of polymer composite material by computational x-ray tomography. *Proceedings of the X Intern. Conference on nonequilibrium processes in nozzles and jets*, Alushta, May 25-31 2014. Moscow, 2014, pp. 543-545.

8 Nikishkov Y., Airoldi L., Makeev A. Measurement of Voids in Composites by X-Ray Computed Tomography. *Composites Science and Technology*, 2013, 89, pp. 89-97.

9 Fuji T., Zako M. *Fracture mechanics of composite materials*. Moscow, Mir, 1982, 232p.

10 Brautman L., Krok R. *Composite materials. Fracture and fatigue*. Moscow, 1978. Vol. 5, 483 p.

11 Potrakhov N.N., Anoshkin A.N., Zuiko V.Yu. and others. Computational and experimental evaluation of the strength of the composite frame segment using the method of in-situ X-ray inspection. *Bulletin of the Perm national research Polytechnic University. Mechanics*. 2017, No. 1, pp.118 – 133.

12 Na W.J., Ahn H.C., Park K.M., Kang H.M., Yu W.R. In-situ damage monitoring of textile composites using x-ray computed tomography. *Proceedings of the ECCM15: 15th European conference on composite materials.* Italy, Venice, 2012, pp. 229 – 236.

13 Withers P.J., Preuss M. Fatigue and Damage in Structural Materials Studied by X-Ray Tomography. *Annual Reviews*. 2012, Vol. 42, p. 81–103. DOI: 10.1146/annurev-matsci-070511-15511.

14 Brault R., Germaneau A., Dupré C., Doumalin P., Mistou S., Fazzini M. In-situ Analysis of Laminated Composite Materials by X-ray Micro-Computed Tomography and Digital Volume Correlation. *Experimental Mechanics*. 2013, Vol. 53, No. 7, p. 1143–1151. DOI: 10.1007/s11340-013-9730-9.

15 Yurov V.M., Oleshko V.S. The impact of the environment on the contact potential difference of metal machine parts. *Eurasian Physical Technical Journal*. 2019. Vol. 16, No. 1 (31). pp. 99–108.

16 Oleshko V.S. Optimal Number of Duralumin Samples in Determining the Surface Energy. *Russian Engineering Research*. 2019, Vol. 39, No. 3, pp. 272–275. https://doi.org/10.3103/S1068798X19030183.

Article accepted for publication 22.11.2019

DOI 10.31489/2019No2/31-35
UDC 620.13.40

X-RAY COMPUTED TOMOGRAPHY-BASED ANALYSIS OF IMPACT DAMAGE PROPAGATION IN COMPOSITE MATERIALS

Yurov V.M.[1], Goncharenko V.I.[2, 3], Vasiliev S.L.[2], Dmitriev S.A.[2], Yurgenson S.A.[2]

[1] E.A. Buketov Karaganda State University, Karaganda, Kazakhstan, exciton@list.ru
[2] Moscow Aviation Institute (National Research University), Moscow, Russia, fvo@mai.ru
[3] Institute of Control Sciences. V.A. Trapeznikova, RAS, Moscow, Russia, fvo@mai.ru

A composite structure impact damage propagation evaluation procedure using linear detector-equipped X-ray computed tomography scanner has been put forward. An impact damaged carbon-fiber samples research has been carried out to evaluate testing capabilities of internal delamination through X-ray computed tomography using linear detector. A special emphasis of the research has been laid on advanced composites. It is linked to the use of the composites for high-load structural elements and necessity of adjusting manufacturing procedures. The procedure helps simplify linear detector tomography analysis of delamination and verify mobile inspection methods data. Besides, the procedure may be used for developing composite structure repair methods. The article includes an example of tomographic image of impact-damaged samples linear attenuation coefficient distribution.

Keywords: *X-ray tomography, polymer composite materials, aircraft structure, nondestructive methods.*

Introduction

X-ray computed tomography is now the most promising non-destructive method involving borescope inspection of the most critical structural elements dedicated to aerospace industry. Rich tomographic data obtained through the method taking into account spatial position of cross-sections being monitored includes not only bright images but also hundreds of thousands material properties measures with precise spatial reference of each tomographic image element.

Aircraft engineering requires a vast employment of non-destructive methods for every life-cycle stage. It is related to high stresses in structural elements which result in minimal weight of a structure. The highest requirements for finished product non-destructive level are applied to structures created through purpose-oriented manufacturing procedures which influence a material structure. Such procedures include casting, welding, composite product production and so on [1-4].

Among the most precise methods of structure condition evaluation is X-ray computed tomography procedure which helps to a high precision (up to 50 microns) reveal internal discontinuities.

The main parameters of X-ray computed tomography evaluation are based on linear attenuation coefficient analysis, the value of which is dependent on a material density. The coefficient has been applied as the basis for developing a number of parameters to evaluate structure condition [5].

1. Experimental procedure

A traditional application of X-ray tomography is searching for internal defects which appear at various stages of a product life cycle. This method is mostly used in manufacturing for casting, welding, composite production and additive technologies. As far as operation is concerned the method is applied for polymeric composites since they feature developing internal damages.

In the context of works performed at MAI (National Research University) Production Planning and Quality Control department the following primary applications of X-ray computed tomography method dedicated to aircraft engineering have been highlighted:

1) Design stage:

– Developing new behavior models of polymeric composites at static and fatigue loading;

– Evaluating influence of processing factors on polymeric composite structure in regular areas and areas of concern of structures being designed;

– Studying a process of accumulation and propagation of damages with layer-by-layer analysis.

2) Developing manufacturing procedures:

– Adjusting parameter of purpose-oriented manufacturing procedures;

– Defining defect standards acceptable for operation and repair;

– Verifying and detailing (developing methods) capabilities of other non-destructive methods for a certain structure.

3) Structural elements manufacturing stage:

– Selective or overall evaluation of quality of composite products and their elements;

– Verification of non-destructive methods dedicated to composite products in industrial manufacturing.

4) Operational stage:

– Evaluating change of polymeric composite structure in high-load units and elements during operation;

– Verification of non-destructive methods for polymeric composite products being operated.

The emphasis in the context of the research methods development is laid on polymeric composite structures which have a number of dedicated damage propagation testing procedures [6, 7]. It is linked to the use of the composites for high-load structural elements and necessity of adjusting manufacturing procedures.

One of the most dangerous types of polymeric composite operational damages is an impact damage which results in heavy internal delamination. Aircraft structures have requirements as to internal delamination area depending on its detection time through visual or instrumental methods. Each structure may have individual requirements depending on applied testing methods and compulsory inspection periods [8-13].

Ultrasonic and thermal (vacuum) methods are most spread for evaluating internal delamination area. To obtain more detailed data received through these methods it is purposeful to verify them during adjusting inspection methods. The analysis of internal delamination testing capabilities using linear detector X-ray computed tomography involved a research dedicated to 30 and 50 Nm impact-damaged carbon-fiber samples (Figure 1).

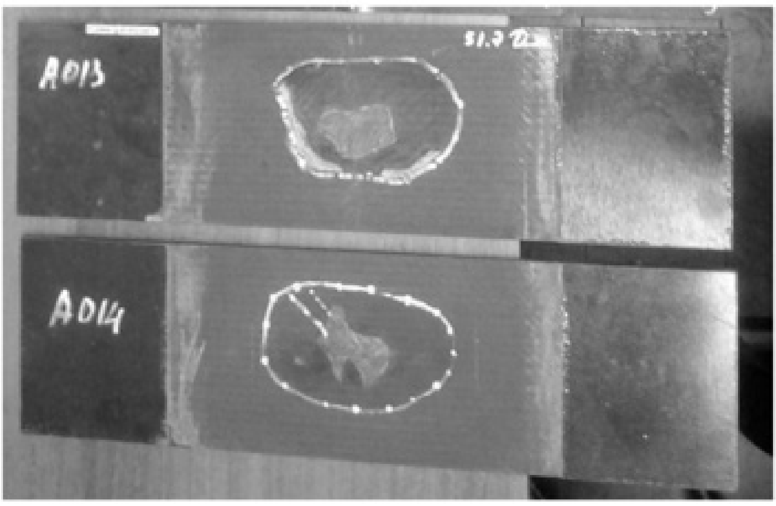

Fig. 1. Samples inspected. General view.

2. Results of the experiment and their discussion

The testing method includes the following stages:

– Layer-by-layer scanning of faulty samples;

– Breakdown of plane sections into areas, which involve an area-averaged analysis of linear attenuation coefficient and its mean square deviation;

– Generation of plane charts of coefficients distribution and analysis of internal defects area.

The necessity of such approach is caused by computed tomography limitations which include inclination of linear attenuation coefficient diagram at two area interface. Thus, it makes composite structure delamination analysis more complicated. You can see an example of impact-damaged samples tomographic image in Figures 2.

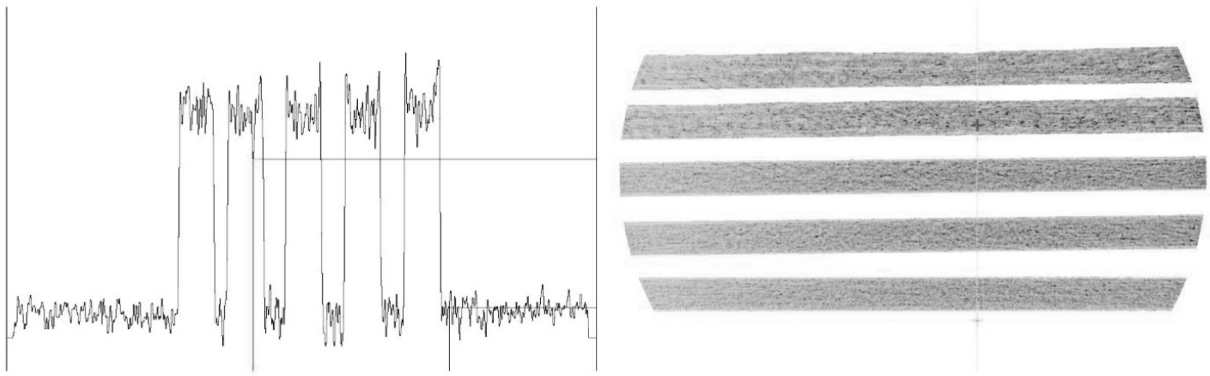

Fig. 2. Tomographic image and linear attenuation coefficient distribution diagram of impact-damaged samples

Plane distribution charts for impact damage points are shown in figures 3 and 4. The dimension of inspected area is 100×100 mm.

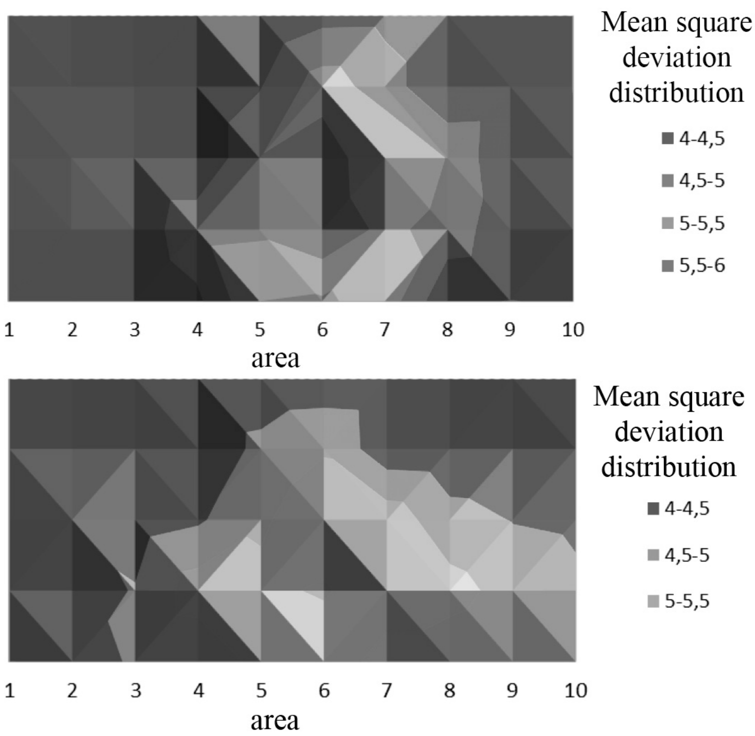

Fig. 3. Mean square deviation distribution chart in impact damage area.

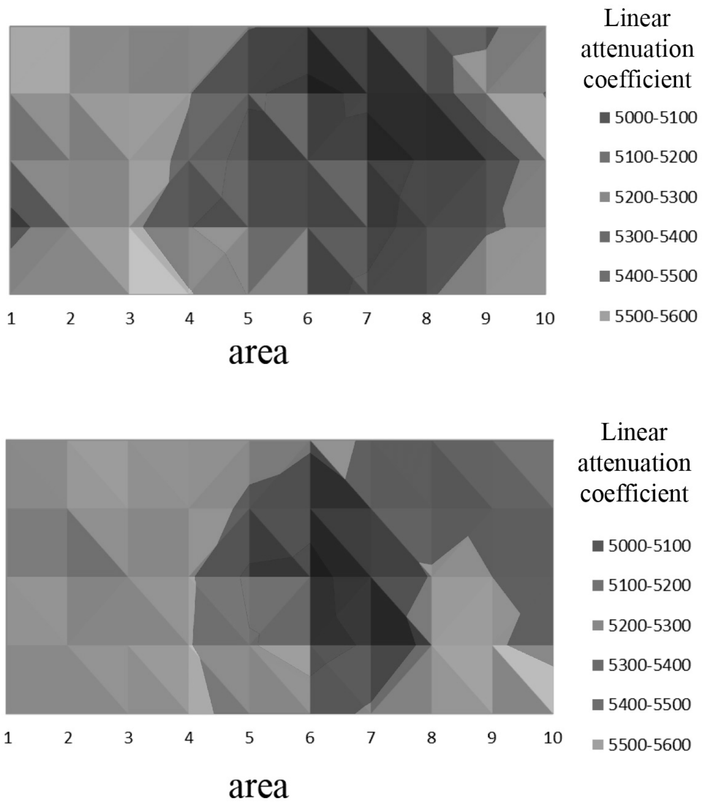

Fig. 4. Linear attenuation coefficient distribution in impact damage area.

Conclusion

As you can see from the charts there is an apparent difference between the impact damage distribution areas for various impact levels. Besides, one can observe that delamination area and distribution may be evaluated through linear attenuation coefficient data, meanwhile mean square deviation chart may be used to evaluate delamination expansion. The averaged characteristics is allowed comparison of different types of materials and thicknesses of structures under the impact of different energies.

The construction of flat maps of the propagation of defects under impact is peculiarity of the proposed method. This map are useful for the finite elements method analysis of CM with averaged mechanical characteristics. It are allowed residual strength of the material and compared results of real tests with FEM results. This method make allowance all defects in structure unlike ultrasonic methods (ultrasonic methods have shading of next to each other defects).

The suggested procedure helps simplify delamination analysis using linear detector tomography scanner and verify mobile inspection methods data. In addition to this the procedure may be applied for developing composite structure repair methods.

REFERENCES

1 Kluiev V.V., Sosin F.R., Kovalev A.V., Weinberg E.I. et al. *Nerazrushaiuschii control I diagnostika*, 2-nd edition. Moscow, Mashinostroenie, 2003, 656 p. [in Russian]

2 Weinberg E.I., Weinberg I.A. Computed Tomography Scanners for Non-Destructive Testing and Quantity-related Diagnostics of Aerospace Products. *Dvigatel*. 2008, No. 2, pp. 19 – 23. [in Russian]

3 Goncharenko V.I., Oleshko V.S. Calculations of Tool Hardness in the Aviation Industry. *Russian*

Engineering Research. 2017, Vol.37, No.6, pp. 554–556. DOI: 10.3103/S1068798X17060119.

4 Goncharenko V.I., Oleshko V.S. Determining the surface energy of tools in the aviation industry. *Engineering Research.* 2017, Vol.37, No.7, pp. 628–630. DOI: 10.3103/S1068798X17070127.

5 Boitsov B.V., Vasiliev S.L., Gromashev A.G., Yurgenson S.A. Metody nerazrushaiuschego kontrolya, primeniaemie dlya konstruktsiy iz perspektivnikh kompozitsionnikh materialov. *MAI, Electronic Journal*. 27.12.2011. Release No 49. Available at: http://www.mai.ru/science/trudy/. [in Russian]

6 Vasiliev S.L., Artemiev A.V., Yurgenson S.A. Analiz metodom vichislitelnoi rentgenovskoi tomografii vozdeistviaa staticheskoi nagruzki na strukturu polimernogo kompozitsionnogo materiala. *Proceedings of 10th International Conference on Non-Equilibrium Processes in Nozzles and Streams* (NPNJ 2014), May 25-31, 2014, Alushta. M.: MAI, 2014. pp. 543-545. [in Russian]

7 Vasiliev S.L., Artemiev A.V., Bakulin V.N., Yurgenson S.A. Kontrol obraztov metodom vichislitelnoi rentgenovskoi tomografii pod nagruzkoi. *Russian Journal of Nondestructive Testing*, 2016, No.5. pp. 63-73.

8 Advisory Circular № 20-107B Composite aircraft structure, USA, FAA, 2009. Available at: www.faa.gov/documentLibrary/media/Advisory_Circular/AC20-107B.pdf.

9 Mikulik Z., Kelly D.W., Prusty B.G., Thomson R.S. Prediction of flange debonding in composite stiffened panels using an analytical crack tip element-based methodology. *Composite Structures*. 2008, Vol.85, No. 3, pp. 233 – 244. DOI:10.1016/j.compstruct. 2007.10.027.

10 Nishino T., Hirokane D., Nakamae K. X-ray diffraction studies of the environmental deterioration of a transversely loaded carbon-fiber-reinforced composite. *Composites Science and Technology*. 2001, Vol.61, No.16, pp. 2455 – 2459. DOI:10.1016/S0266-3538(01)00174-9.

11 DeKalbermatten T., Jäggi R., FLüeler P., Kausch H.H., Davies P. Microfocus radiography studies during model interlaminar fracture tests on composites. *Journal of Materials Science Letters*. 1992, Vol.11, No.9, pp. 543 – 546.

12 Yurov V.M., Oleshko V.S. The impact of the environment on the contact potential difference of metal machine parts. *Eurasian Physical Technical Journal*. 2019, Vol.16, No.1 (31), pp. 99 – 108.

13 Oleshko V.S. Optimal Number of Duralumin Samples in Determining the Surface Energy. *Russian Engineering Research*, 2019, Vol. 39, No. 3, pp. 272–275. https://doi.org/10.3103/ S1068798X19030183.

Article accepted for publication 22.11.2019

DOI 10.31489/2019No2/36-42

UDC: 538.971: 621.039.64

PLASMA INSTALLATION FOR RESEARCH OF PLASMA-SURFACE INTERACTION

Rakhadilov B.K.[1], Skakov M.[1], Tulenbergenov T.[1], Zhurerova L.[2,*], Kurbanbekov Sh.[3]

[1]Institute of Atomic Energy of Kazakh National Nuclear Center, Kurchatov, Kazakhstan

[2]S. Amanzholov East Kazakhstan state university, Ust-Kamenogorsk, Kazakhstan, leila_uka@mail.ru

[3]Khoja Akhmet Yassawi International Kazakh-Turkish University, Turkestan, Kazakhstan

This work describes some of the features of the developed plasma setup for studying surface-plasma interactions. Results of the study of the interaction of tungsten and beryllium with plasma are presented. This facility is intended for testing materials and equipment of the Kazakhstan Materials Science Tokomak and for conducting a study of plasma-surface interactions. The main elements of a plasma installation are an electron beam gun, a plasma-beam discharge chamber, a vacuum interaction chamber, a cooled target device, an electromagnetic system consisting of electromagnetic coils, a lock device for quick changing and moving diagnostic tools or irradiated samples without depressurization of the installation. Experiments to study changes in the structure of tungsten and beryllium during plasma exposure have shown that after irradiation, the surface is subjected to erosion and pores form on the surface.

Keywords: plasma, plasma installation, tungsten, beryllium, irradiation.

Introduction

Recently in our country work is underway in to create the Kazakhstan Material-science of Tokomak (KMT) in the National Nuclear Center of the Republic of Kazakhstan, which will be used for research to substantiate the design and safety of a thermonuclear energy reactor [1]. As is known, the solution to the problem of creating reactors of controlled thermonuclear fusion is largely determined by the choice of structural materials for the most critical reactor assemblies (the first wall, its protection and the diverter). They experience a powerful impact of irradiation with neutrons, alpha particles and protons, as well as thermal loads from the side of thermonuclear plasma. The choice of structural materials is based on the results of studying the processes occurring during the interaction of the plasma of a thermonuclear reactor (TNR) with structural elements facing it [2]. However, the complexity and multifactorial nature of the interaction of the KMT plasma with structural materials, as well as the high cost of full-scale tests on full-scale installations, determine the need for its experimental modeling using small specialized simulation installations. Among such facilities, linear simulators with electron-controlled plasma generation [3–7] have several advantages as devices that allow combining the effect of plasma with electron beams when tested with high heat flux. In this regard, a plasma unit was developed for testing materials and equipment of the KMT and for conducting a study of plasma-surface interactions.

The purpose of this work is to study and describe in detail some of the features of the developed plasma setup for studying surface-plasma interactions and experimental study of the interaction of tungsten and beryllium with plasma.

1. Parameters of plasma installation

The developed plasma beam installation (PBM) is universal and allows testing materials under the conditions of complex exposure to them of both the plasma flow and the powerful heat load created by the electron beam. The use of a plasma setup makes it possible to quickly obtainpreliminary experimental data on the behavior of materials under conditions of their interaction with plasma under high thermal load, which will make it possible to make corrections to the methodology of experimental studies on KMT [8, 9].

The main elements of a plasma installation are an electron-beam gun (EBG), a plasma-beam discharge chamber, a vacuum interaction chamber, a cooled target device, an electromagnetic system consisting of electromagnetic coils, a lock device for quick change and movement of diagnostic tools or irradiated samples without depressurization installation [10]. A general view of a simulation stand with a plasma-beam installation is shown in Figure 1.

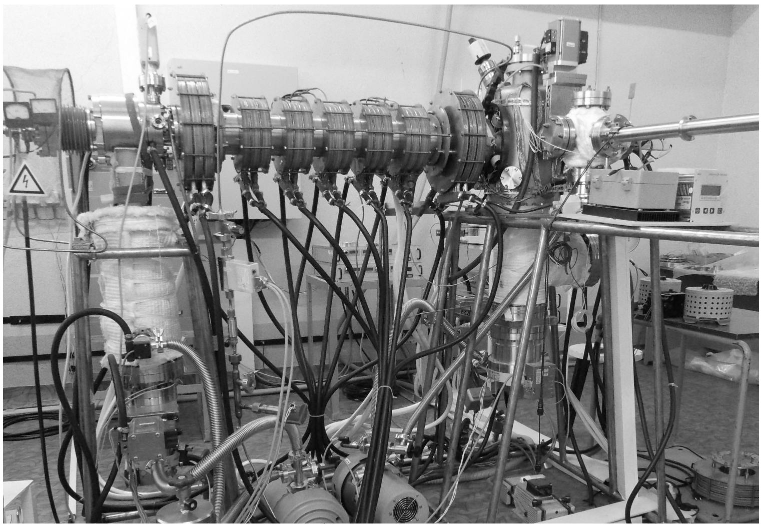

Fig.1. General view of the plasma installation.

A schematic representation of the installation is shown in Figure 2. The vacuum chamber includes a discharge chamber and an interaction chamber. In this case, the discharge chamber is made in the form of a narrow cylinder with a length of 0.9 m and a diameter of 0.2 m, and the interaction chamber is made in the form of a cylinder with a length of 0.5 m and a diameter of 0.4 m, located perpendicular to the discharge chamber. The cooled target device is a hollow cylinder with inlet and outlet tubes for cooling it with water. In this case, the plasma receiver is made so that it is possible to install the irradiated sample. The electron gun consists of a heated thermionic tungsten cylindrical cathode and a hollow anode. All gun assemblies are water-cooled, which ensures its operability, both in high-voltage vacuum mode and in low-pressure arc mode. The vacuum pumping system includes two fore vacuum and two turbo molecular pumps capable of providing a pressure of residual gases in the chamber at a level of $5 \cdot 10^{-8}$ Pa.

The performance of the pumping means may vary widely, depending on the gas-dynamic conditions of the experiments. The gas injection system consists of vacuum leaks, designed to ensure the gas inlet into the vacuum chamber with a stream size in a strictly specified small range, with the possibility of smooth adjustment. The leakage control is carried out by a personal computer, which ensures a stable flow of the working gas. The gateway device with a rod allows for translational-rotational movement for rapid change and movement of diagnostic tools or irradiated samples without depressurization of the installation. The plasma diagnostics system includes a quadruple mass spectrometry Langmuir probe. Warming up, control of parameters, diagnostic tools, as well as a complex of electric power sources of the electron gun, consisting of a direct heat block a voltage-regulated high-voltage unit for generating a primary beam of beam-plasma discharge, high-voltage unit for the controlled thermal testing without the beam-plasma discharge.

The installation management system includes computer programs for remote control of installation nodes. The recording of the current information and the display on the screen is

.

generated by means of the information and measurement system (power supply system, vacuum pumping, gas supply systems, gas, air, air and gas, air flow systems, vacuuming systems, gas flow systems, gas and air conditioning systems, vacuuming systems, gas flow systems and other applications.

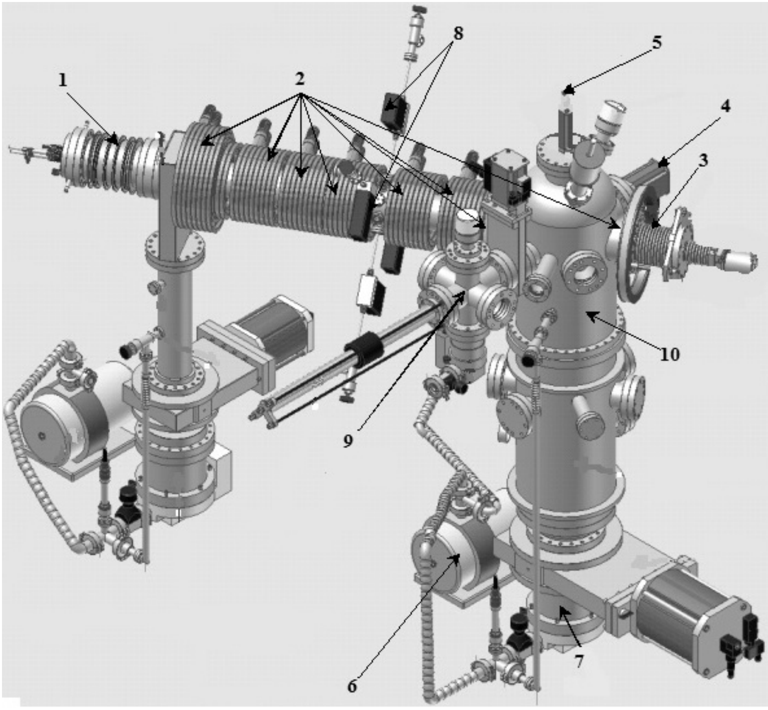

1- electron gun; 2 - electromagnetic coils; 3 – cooled plasma receiver; 4 - mass spectrometer; 5 - Langmuir probe; 6 - foreline pumps; 7 - turbo molecular pumps; 8 - gas pump system; 9 - sluice device for quick change and movement of diagnostic tools or irradiated samples; 10- vacuum chamber.
Fig.2. Schematic representation of a plasma installation.

The plasma installation provides the following plasma flow parameters: plasma flow diameter up to 30 mm; magnetic field strength generated on the axis of the installation of 0.1 T; magnetic field strength in the electron gun area of 0.2 T; the current in the plasma is 1 A; The plasma density in the beam is up to 10^{13} cm^{-3}, the electron plasma temperature is up to 30 eV.

The installation provides the following plasma flow parameters: the plasma flow diameter in front of the target is from 5 to 100 mm; the magnetic field strength generated on the EBG axis is 0.1 T; magnetic field strength in the electron gun area of 0.2 T; the current in the plasma is 1 A; The plasma density in the beam is up to $10^{13}cm^{-3}$, the electron plasma temperature is up to 100 eV.

Plasma installation works as follows. The electronic pad is formed by an axially symmetric electronic pad. The cathode of the gun is heated by electron bombardment from the heater thread. The power of the gun is regulated by the cathode heating power. The electronic probe is fed with the working gas supplied to the discharge zone, forming a plasma-beam discharge. Plasma shots are assembled using an electromagnetic system, which creates a longitudinal magnetic field in the discharge chamber. With a fall of the world the plasma discharge enters the sample of the test material installed in the plasma receiver, which is located in the interaction chamber. Figure 3a-b shows the process of irradiation with a tungsten plasma beam.

The plasma beam in the installation chamber is formed when the working gas is supplied to the chamber when the electron beam is tuned. Hydrogen, deuterium, helium, etc. are used as the working gas. To simulate the effect of plasma on materials in the plasma-beam discharge mode, it is sufficient to use from 2% to 30% of the maximum power of the electron gun. To obtain maximum power on the target without the development of breaks in the transport channel, the accelerating voltage should be increased and the beam current should be reduced.

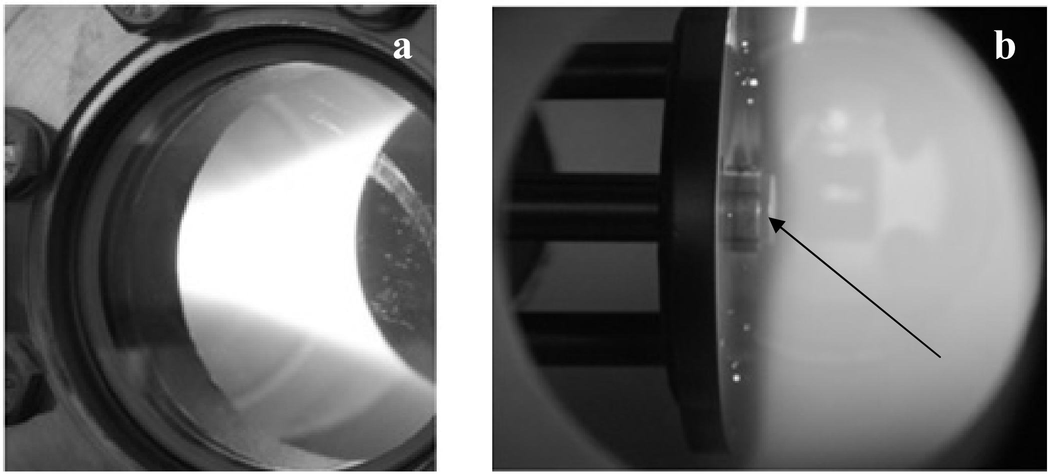

Fig.3. The process of irradiation with a tungsten plasma beam: a) - plasma beam ignition, b) - the arrow indicates the sample under the influence of plasma.

Recording of current information and display it on the display screen is generated by the information-measuring system. PBM is equipped with a system of remote control of PBM nodes with an information screen. To determine the parameters of the plasma flux in the PBM, a Langmuir probe is used. The method of probe diagnostics is based on measuring the current density of charged particles when an electrical conductor is placed in plasma, depending on its potential [11]. When testing materials for PBM, the control of the environment in the cavity of the interaction chamber was carried out using a CIS-100 quadruple mass spectrometer manufactured by Stanford Research Systems. Figure 1-2 shows the CIS-100 mass spectrometer externally. The analyzer of residual gases with a closed ion source (mass spectrometer) CIS100 was attached directly to the working chamber through valves. Unlike open gas source (RGA) residual gas analyzers, CIS devices are simultaneously connected to a high-vacuum turbo molecular pump, which ensures that the ionizer is at a pressure of 10^{-9} mm. hg art. [12].Performing the proposed installation [13] to study the interaction of plasma with the material allows obtaining the following benefits:

- high performance by reducing the time to replace the irradiated samples, as well as by remote control of the power supply system, vacuum pumping system, gas installation system;
- the presence in the design of the vacuum chamber of two turbo-molecular pumps, two flow heaters and two differential pumping diaphragms located in the vacuum chamber, which makes it possible to break the vacuum chamber into sections with different pressures, and also allows to obtain a working gas with the lowest residual gas from water vapor.

2. Experimental procedure

In this work, we studied the interaction of plasma with tungsten and beryllium using the developed plasma setup. Tungsten samples of 99.97% purity in the form of a cylinder 10 mm in diameter and 5 mm high, as well as TGP-56 beryllium samples of $10\times10\times5$ mm^3 in size, were cut on an EDM machine. Before irradiation, the samples were ground and polished. The samples were irradiated with a plasma beam in the helium, hydrogen and deuterium medium. During irradiation, the pressure in the chamber was 2×10^{-3} Torr. Table 1 shows the modes of irradiation of samples of tungsten and beryllium.

The research of the microstructure of the samples before and after irradiation was performed using a JSM-6390 scanning electron microscope.

.

Table 1. Modes of irradiation of samples.

Sample	Power of primary beam $W_{el.p.}$, W	Workinggas	Bias potential on target, B	Ion concentration, 10^{17} $м^{-3}$	Irradiationtime t, c
W	2500	hydrogen	-1200	$2{,}69\cdot 10^{17}$	3600
W	2500	hydrogen	-1600	$2{,}86\cdot 10^{17}$	3600
W	500	helium	-1000	$2{,}06\cdot 10^{17}$	21600
Be	1500	hydrogen	-1200	5,84	1800
Be	1500	deuterium	-1200	3,04	1800
Be	1500	helium	-1200	5,16	1800

3. Experimental results and discussion

3.1. The change in surface W when irradiated by a plasma beam

Figure 4 shows the SEM images of tungsten samples irradiated with hydrogen plasma at an accelerating potential of –1200 V and –1600 V. Images were taken at high magnifications. The topography of the irradiated surface indicates its strong erosion. It can be seen that as a result of irradiating tungsten with stationary plasma, etching pits in the size from 100 nm to 500 nm are formed in the grain body, as a result of sputtering of the surface caused by ion bombardment. In addition, microcracks and small pores are created in the volume of tungsten.

In particular, when irradiated with an accelerating potential of –1600 V, a large number of small pores with a size of 0.2 μm to 1.0 μm are created. The system of cracks and pores creates a transport path between the surface and the volume of the material, so you can expect deep penetration of ions into the volume of the metal. The reason for the occurrence of these structural disorders, apparently, are mechanical stresses in the tungsten lattice caused by implanted hydrogen.

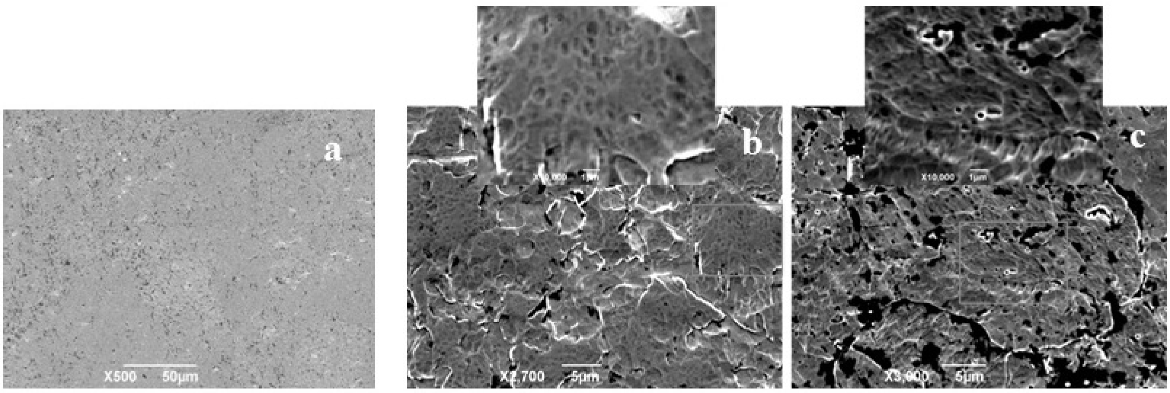

Fig.4. SEM-images of the surface of a tungsten sample before (a) and after irradiation with a plasma beam in a hydrogen medium at an accelerating potential of -1200 V (b) and -1600 V (c)

Figure 5 a-b show the SEM-image of a sample of tungsten irradiated with helium plasma, resulting in a large number of small pores ranging in size from 0.5 μm to 1.5 μm. As a result of irradiation of tungsten with stationary plasma along the grain boundaries, etching pits appear in the grain body. In addition, a large number of micro cracks are created in the volume of tungsten. It is assumed that they are directed from the surface into the depth of the metal, as well as the cause of the occurrence of these structural disorders are mechanical stresses in the tungsten lattice caused by implanted helium [14].

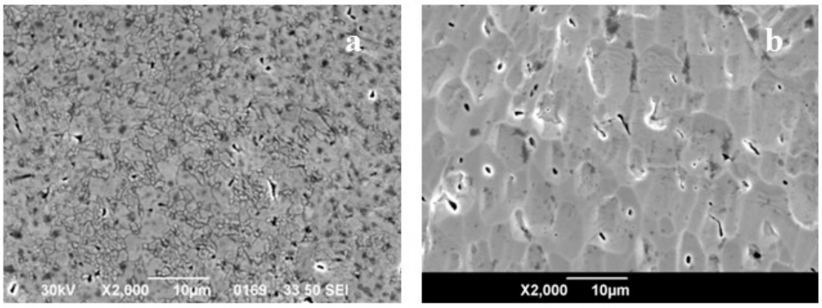

Fig.5. SEM image of a sample of tungsten irradiated with a helium plasma at an accelerating potential of -1200 V (a) and -1600 V (b)

3.2. Changes of Be surface variation upon plasma beam irradiation

Figure 6 shows SEM-images of the surface of beryllium samples before (Fig.6, a) and after irradiation in helium (Fig.6, b), hydrogen (Fig.6, c) and deuterium (Fig.6, d). Studies of the beryllium microstructure on a raster electron microscope showed that after irradiation a porous structure is formed. Pores of different bulk density are formed (Fig.6, a-d).

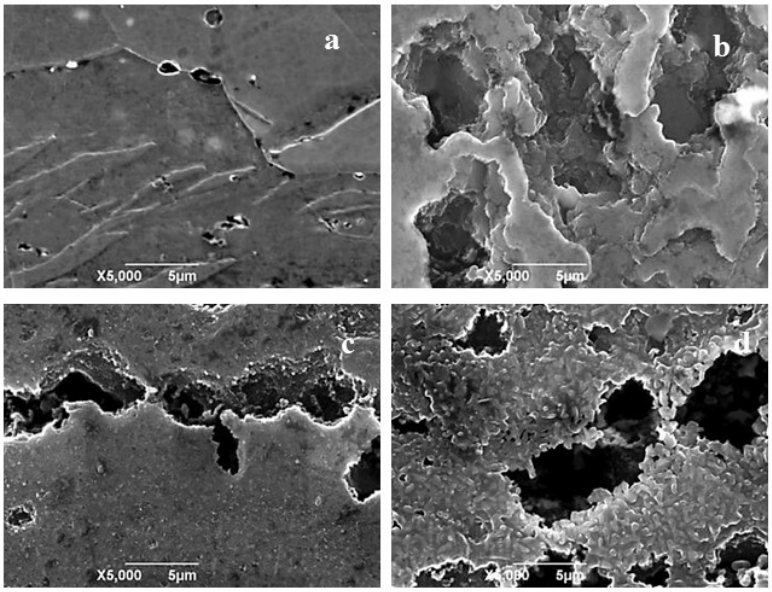

Fig.6. Surface modification of beryllium samples after irradiation.

A strong destruction of the structure is observed in the samples irradiated with hydrogen and helium plasma. At the same time, after irradiation with helium plasma, the surface of beryllium acquired a spongy structure, the reason for which is the appearance of large gas bubbles along which the main crack passes in the process of sample destruction. Spreading drops are visible on the surface. It can be assumed that these are products of erosion that have returned to the plasma sample during irradiation.

Conclusion

Thus, simulation facilities are very efficient, since they allow for the on-line testing of candidate materials from the NFR, replenishing the database on various aspects of plasma-surface interaction, testing the computational models and working out diagnostic methods in fairly well programmed conditions. The study of plasma-surface interactions with the help of simulation plasma systems allows us to substantiate the choice of materials for a thermonuclear energy reactor. At the same time, the installation developed by the author has a high productivity by reducing the time for changing the irradiated samples, as well as by remote control of the power supply system, the vacuum pumping system, and the gas supply system of the installation.

Experiments conducted to study changes in the structure of tungsten and berylliums during plasma irradiation have shown that pores are formed on the surface after irradiation. Moreover, after irradiation with helium plasma, etching pits are formed on the surface of tungsten. And on the surface of beryllium, droplet-like particles are formed, which are products of erosion. They were formed by sputtering the surface with helium ions.

Acknowledgment

This work was supported by grant of the Committee of Science, Ministry of Education and Science of the Republic of Kazakhstan.

REFERENCES

1 Pitts R.A., Carpentier S., Escourbiac F., Hirai T., Komarov V., LisgoS., et al.A full tungsten diverter for ITER: physics issues and design status. *J. Nucl. Mater.*2013, Vol.438, pp. 48 – 56.

2 PhilippsV.Tungsten as material for plasma-facing components in fusion devices.*Ibid*, 2011, Vol.415, pp.2 – 9.

3 Shimada M., Pitts R., Loarte A., Campbell D.J., Sugihara M., Mukhovatov V., Kukushkin A., Chuyanov V. ITER research plan of plasma–wall interaction. *Ibid*, 2009, Vol.390-391, pp. 282 – 285.

4 Ueda Y., Coenen J.W., Temmerman G. De, Doerner R.P., Linke J., Philipps V., Tsitrone E. Research status and issues of tungsten plasma facing materials for ITER and beyond. *Fusion Eng. Des.,* 2014, Vol.89, pp. 901–906.

5 Federici G., Skinner C. H., Brooks J. N., et al. Plasma-material interactions in current tokamaks and their implications for next step fusion reactors. *Nucl. Fusion*, 2001, Vol.41, pp. 1967 – 2137.

6 Tobita K., Nishio S., Enoeda M., et al. Design study of fusion DEMO plant at JAERI.*Fusion Eng.*, 2006, Vol.81, pp. 1151 – 1158.

7 Suchugov D. Yu., Shapovalov G. V., Chektybaev B. Zh., Skakov M. K., et al. The numerical code TOKSCEN for modeling plasma evolution in Tokomaks. *Nuclear Fusion,* 2015, No. 55, pp. 1 – 5.

8 Kurnaev V., Kolodeshnikov A., Tulenbergenov T., Sokolov I. Investigation of plasma–surface interaction at plasma beam facilities. *Journal of Nuclear Materials*, 2015, Vol.463, pp. 228 – 232.

9 Rakhadilov B. K.,Skakov M.K., TulenbergenovT.R., WielebaW.K. Change the tungsten surface when irradiated by plasma beam. *Bulletin of the Karaganda University. Physics Series*.2016, No. 3, pp. 40-44. [in Russian].

10 Kulsartov T.V., Tazhibaeva I.L., Gordienko YU.N., ZaurbekovaZh.A., Koyanbaev E.T., Kukushkin I.M., Kenzhin E.A., Mukanova A.O., Dyusambaev D.S., Shajmerdenov A.A., Chekushina L.V. Detritiation of different irradiated beryllium grades using high-temperature degassing method. *VANT. Ser. Termoyadernyjsintez,* 2014, No. 2, pp. 27 – 37. [in Russian].

11 Rahadilov B.K., Skakov M.K., Tulenbergenov T.R. Tungsten surface erosion by hydrogen plasma irradiation. *Key Engineering Materials*, 2017, Vol. 736, pp. 46 – 51.

12 Tulenbergenov T., Skakov M., Kolodeshnikov A., Zuev V., Rakhadilov B., Sokolov I., Ganovichev D.,Miniyazov A., Bukina O. Interaction between nitrogen plasma and tungsten. *Nuclear Materials and Energy*. 2017, No. 13, pp. 63 – 67.

13 Skakov M.K., Rakhadilov B.K., Tulenbergenov T.R. Installation for modeling the interaction of plasma with candidate materials of a fusion reactor. *Patent of the RK for utility model*, No. 2221, Bull.11, publ. 15.06.2017.

14 Tulenbergenov T.R., Kulsartov T.V., Sokolov I.A., Rakhadilov B.K., Ganovichev D.A., Miniyazov A.J., Sitnikov A.A. Studies on gas release from pre-saturated samples on a plasma beam installation. *Physical Sciences and Technology*, 2017, Vol. 4, No. 2, pp. 9 – 14.

Article accepted for publication 25.10.2019

DOI 10.31489/2019No2/43-47

UDC 621.9.048.7; 691.175.5.8

IMPACT RESEARCH OF ELECTRON BEAM PROCESSING ON THE STRUCTURE AND PROPERTIES OF PA6 POLYAMIDE

Rakhadilov B.K[1]., Sagdoldina Zh.B.[1], Ocheredko I.A.[1], Kombaev K.K.[2], Khassenov A.K.[3]

[1]S. Amanzholov East Kazakhstan State University, Ust-Kamenogorsk, Kazakhstan, sagdoldina@mail.ru

[2]D. Serikbayev East Kazakhstan State Technical University, Ust-Kamenogorsk, Kazakhstan

[3]E.A. Buketov Karaganda State University, Karaganda, Kazakhstan

In this work we studied the impact of electron irradiation with energy of 1.3 MeV on the structure and properties of PA6 polyamide. Irradiation doses ranged from 50 to 500 kGy. The results of research presented that irradiation with small doses of PA6 polymer is able to increase the mechanical characteristics, while irradiation with large doses significantly reduces them. Wear resistance decreases under irradiation conditions from 350 kGy, and the hardness of the samples varies slightly. The polymer structure was studied by X-ray diffractometry and IR spectroscopy. Electron irradiation at an energy of 1.3 MeV did not lead to a change in the crystalline form of the PA6 polymer, but caused partial crystalline damage. The peak intensity of the α-phase after electron irradiation increases compared with the unirradiated sample. It may be due to an increase in the crystallinity of the polymer.

Keywords: electron irradiation, polyamide, wear resistance, hardness, structure.

Introduction

Development of modern science and technology is unthinkable without polymeric materials using. Expanding the scope of application of polymeric materials required the creation on its basis of new materials with a given set of properties capable of processing into products using high-performance methods. The great interest in radiation methods is due to the fact that their use in industry instead of traditional methods of material modification (such as chemical modification methods using solvents and a long processing time, etc.) leads to significant savings resources, energy, increasing production efficiency, significant reducing the environmentally harmful effects of production.An important circumstance is also that in a number of cases, electron-beam processing allows one to obtain structural-phase states of materials that are not realized with traditional processing methods [1]. Intermediate formations appear under irradiation with beams of charged particles in polymers which high reactive - free radicals, ions, excited molecules. They are sources of further chemical transformations, leading to changes in the chemical structure, and consequently the properties of polymers.

In particular, transverse intermolecular and intramolecular bonds are formed under the activity of radiation in polymers - bond breaking processes occur in the main chain and side groups, grafting reactions, oxidation, etc. vinyl and vinylidene and vinylidene groups appears decompose and formation, as well as isomerization, cyclization [2].For example, the structuring (crosslinking) of molecules increases the mechanical strength and heat resistance of polyethylene under the radiation modification of polyethylene. Irradiated wires and cables with polyethylene insulation can be operated at higher temperatures (current loads) [3].

In work [4] was presented that the mechanical characteristics are closely related to the modification of the structure formed after electron irradiation. An increase in the wear resistance of polymeric materials is associated with the creation of a large number of cross-links upon irradiation with an electron beam. The results obtained in work [5] confirmed that crosslinking at significant doses prevails over depolymerization, even if irradiation was performed in air. In this regards the

.

aim of this work is to study the impact of electron irradiation on the structure and properties of PA6 polyamide.

1. Materials and methods of research

Electron beam irradiation of the samples was carried out on an ELV-4 industrial electron accelerator. Electron irradiation mode: beam energy 1.3 MeV, amperage beam 12 mA, conveyor speed 3.5 m/min and radiation doses of 50 and 150 kGy. The samples were ground and polished before irradiation. Provisions of samples for research in the form of a circle with a thickness of 3 mm were cut from a rod of polymers (rod diameter 30 mm). The morphology of the polymer samples was studied using a JSM-6490 scanning electron microscope and Solver HV atomic force microscope. X-ray diffraction studies of polymer samples were performed on an X'PertPRO diffractometer. The diffraction patterns were recorded using CuKα radiation (λ=2,2897A^0) at a voltage of 40 kV and a current of 30 mA. FTIR-801 Simex Fourier-IR spectrometer was used to research the changes in the chemical composition of the polymers. Samples were studied at a wavelength of (450–4700) cm^{-1}, resolution 1 cm^{-1}, t=25C^0.

The hardness of the polymer samples was measured on a TK-2M tool in accordance with GOST 4670-91. The diameter of the ball is 1.58 mm under the pressure of 100 kgf. Tribological sliding friction tests were carried out on a THT-S-BE-0000 tribometer with using the standard ball-disk technique (ASTM G 133-95 and ASTM G 99). A ball with a diameter of 6.0 mm was used as a counterbodyfrom a certified material– Al_2O_3. The experimentwas carried outunder the pressure of 10 N and a linear velocity of 10.5 cm /s with a wear radius of 5 mm where the friction path was 63.1m. The wear resistance of PA6 polymer before and after electron irradiation was characterized by the amount of wear.

2. Results and discussion

Research of the surface morphology of the PA6polymer which carried out by atomic force microscopy presented that the irradiated surface has a larger surface irregularities (Fig.1.). Since the main effect of medium-energy electron beams on materials is their heating [6], so the most probable reason for the observed change in the surface morphology is the melting of the surface layer with subsequent solidification in a time comparable to the pulse duration. The irregularity of the irradiated surface layers increases with increasing in the radiation dose.

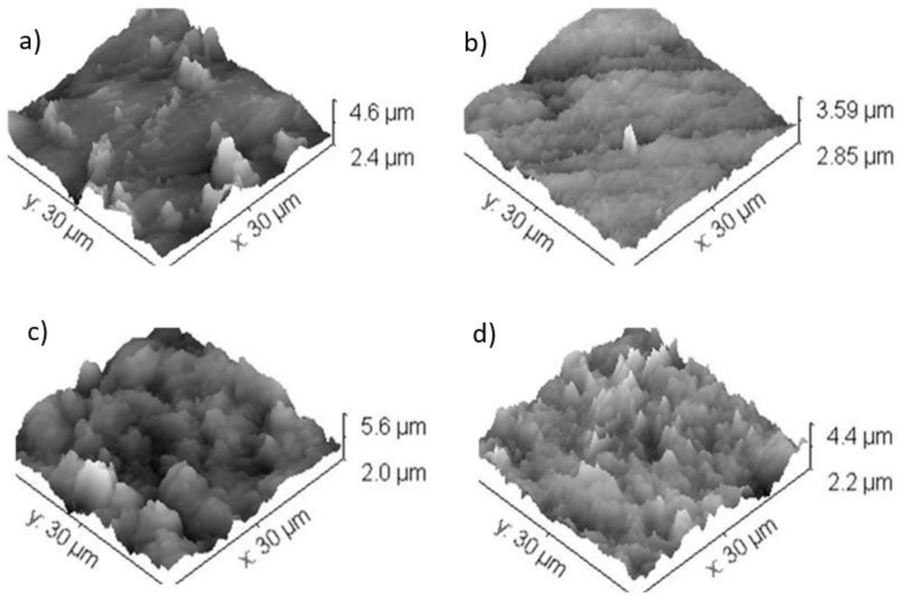

Fig.1. Surface topography of PA6 polymer samples a) initial; b) 150 kGy; c) 200 kGy; d) 500 kGy

We have studied changes in the structure of the PA6 polymer after electron irradiation with a dose of 200 and 500 kGy. Fig.2presents the results of an x-ray phase analysis of PA6 samples. The diffraction pattern of PA6 polyamide shows two diffraction peaks at 2θ=20.5˚and 23.5˚, which are a distinctive feature of the α-phase of PA6 [7-9]. This explains the crystalline form of polyamide PA6. The peak intensity of α phase increases compared with the unirradiated sample after electron irradiation and this may be due to increasing in the crystallinity of the material. Perhaps the irradiation process accelerated the crosslinking rate of free radicals and restrained pyrolysis and recombination, which lead to increasing in crystallinity.

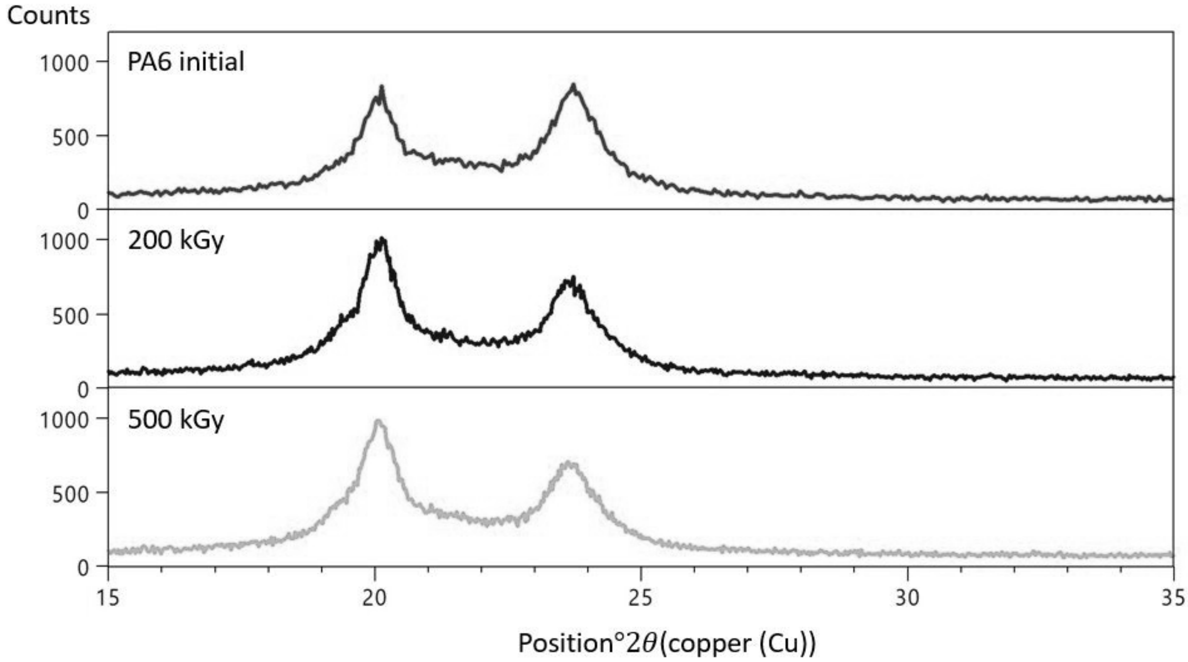

Fig.2. Diffractogram of PA6 samples

Fig.3 shows the infrared spectra of unirradiated and irradiated PA6 samples. The characteristic peaks of the PA6 vibrational frequency are at the level of 3579.4 (NH stretching), 2934.8 (CH_2 stretching), 1585.1 (C = O stretching, amide I), 1398.7 (NH bending vibration) and 776.28 cm^{-1}(bending vibration NH) [10]. Irradiation did not lead to a change in the crystalline form of the PA6 polymer, but caused partial crystalline defect.

Fig.4presents the surface hardness values of samples of PA6 polymers before and after electron irradiation. Based on the analysis of the obtained results on the determination of hardness, it was found that the hardness largely depends on the radiation dose. The highest hardness value is observed after irradiation with a dose of 50 kGy and 100 kGy. Decreasing in hardness is observed at high doses of radiation. Presumably, this is due to its destruction. The results of hardness measurements show that electronic irradiation of the PA6 polymer with small doses can increase the mechanical characteristics, while irradiation with large doses reduces them.

Fig.5shows the amount of wear (μm^3) of PA6 polymer samples after experiment of a “ball-disk” scheme. It can be seen that a decrease in the amount of wear is observed after irradiation with a dose of 50to 250 kGy and then at 300 kGy there is an increase in the amount of wear compared to the initial one. A decrease in the wear resistance of the samples with an increase in the radiation dose is probably due to the expansion of the polymer chain upon the absorption of electrons with the formation of crystalline defects [11].

.

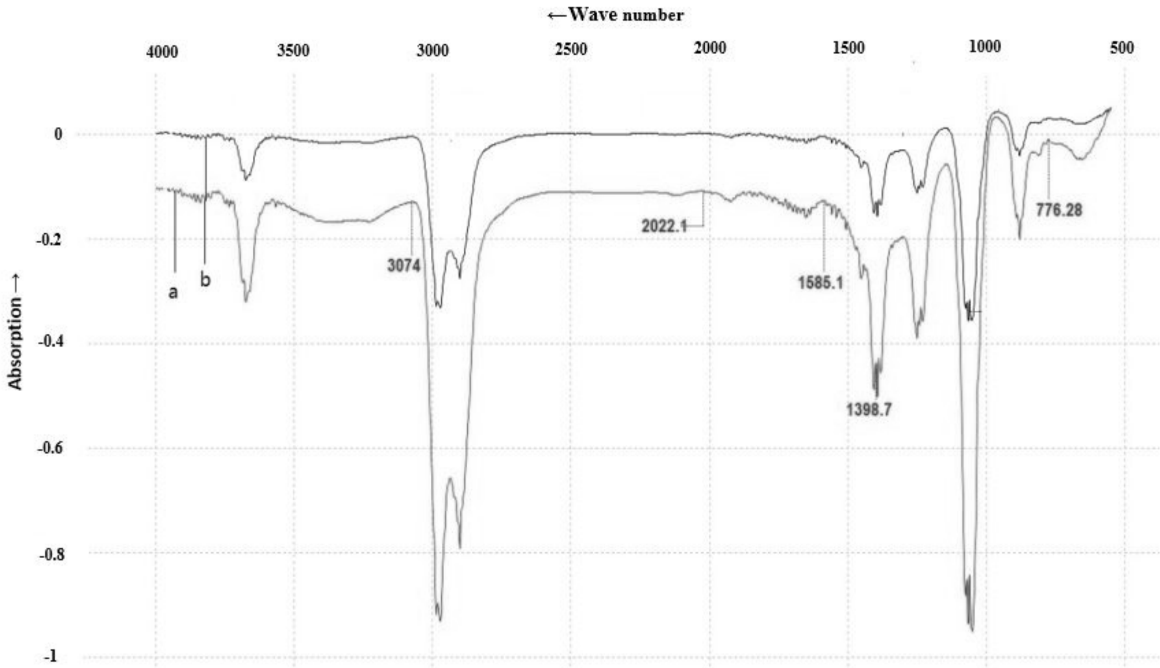

Fig.3. IR spectra of unirradiated (a) and irradiated (b, 150 kGy) PA6 samples.

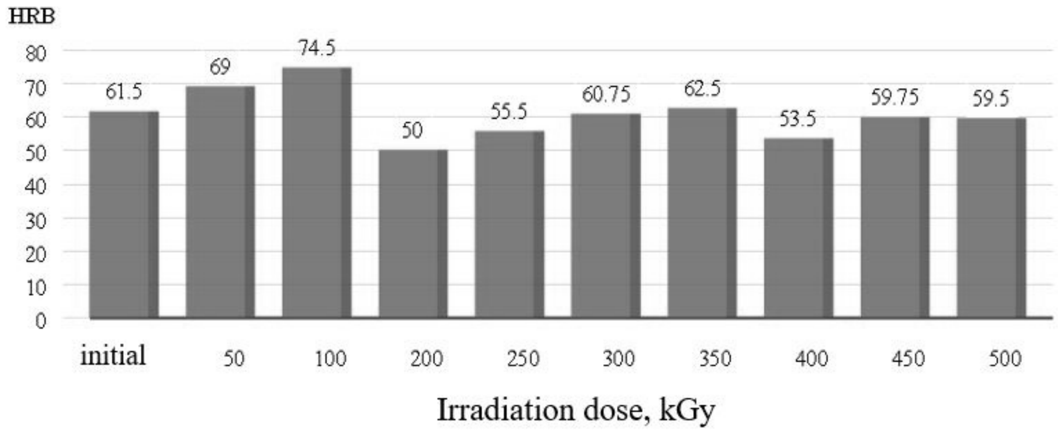

Fig.4. Rockwell hardness of PA6 samples before and after electron irradiation.

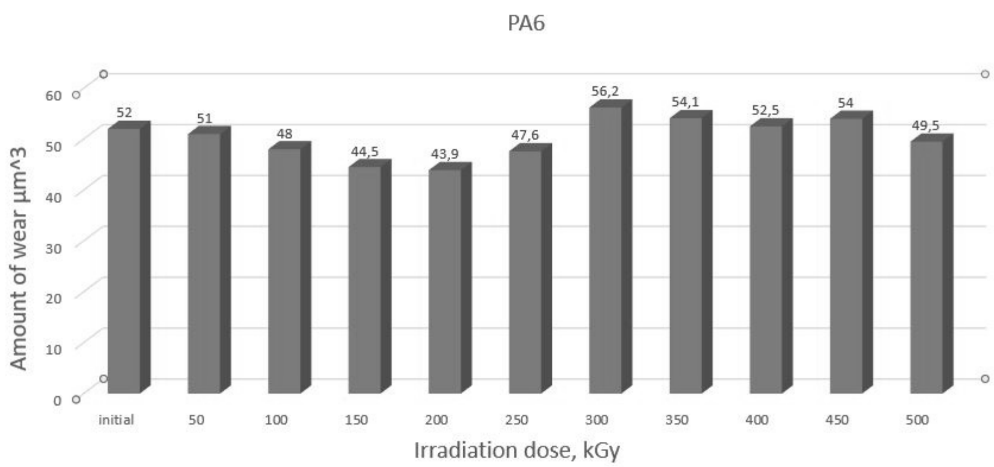

Fig.5. The amount of wear of samples PA6 before and after electron irradiation.

Conclusion

Based on the obtained experimental data and their analysis, it can be stated that irradiation with small doses of PA6 polymer can increase the mechanical characteristics, while irradiation with large doses significantly reduces them. Wear resistance decreases under irradiation conditions from 350kGy at an energy of 1.3 MeV. The hardness of the samples varies slightly. However, the characteristic dependence of surface properties on the dose of electron irradiation is difficult to establish on the basis of the results of structural studies, since insignificant changes cannot be a characteristic feature.

It was determined that the irregularity of the irradiated surface layers increaseswith increasing in the irradiation dose. However, in this case, a direct dependence of the micro-roughness of the irradiated surface layers with the amount of wear and the wear coefficient is not observed. This indicates that an increase in the wear resistance (decrease in the amount of wear) of the polymer materials studied after irradiation is not associated with the geometry of the surface, but is associated with structural changes. Conducted research have shown the use of electron beam processing with an energy of 1.3 MeV for PA6 polymers is possible at relatively low doses of electron irradiation (up to 300 kGy).

Acknowledgment

This work was financially supported by the Science Committee of the Ministry of Education and Science of the Republic of Kazakhstan under the Grant Financing for Scientific Research program (Project code - AR05134982)

REFERENCES

1 Raghu S., Archana K., Sharanappa C., Ganesh S., Devendrappa H. The physical and chemical properties of gamma ray irradiated polymer electrolyte films. *Journal of Non-Crystalline Solids*. 2015, Vol.426, pp.55 – 62.

2 Pikaev A.K. Novye razrabotki radiatsionnoi tehnologii v Rossii. *Himia vysokih energii*, 1999, Vol.32, pp. 3 – 11. [in Russian].

3 Sarada I., Ahmad A., Bakar A., et al. Influence of gamma irradiation on polymerization of pyrrole and glucose oxidase immobilization onto poly (pyrrole)/poly(vinyl alchohol) matrix. *Applied Surface Science*, 2017, Vol.400, pp. 118-128.

4 Visco A.M., Torrisi L., Campo N., et al. Mechanical Performance of Electron-Beam-Irradiated UHMWPE in Vacuum and in Air. *J Biomed Mater Res Part B: Appl. Biomater*, 2009, 89B, pp. 55 – 64.

5 Slouf M., Synkova H., Baldrian J., Marek A., et al. Structural changes of UHMWPE after e-beam irradiation and thermal treatment. *J Biomed Mater Res Part B: Appl.Biomater*, 2008, 85B, pp.240 – 251.

6 Shifeng Zhu, Meiwu Shi, Meifang Zhu Effects of Electron-Beam Irradiation Crosslinking on PA6 Fibers. *Fibers and Polymers*, 2013, Vol.14, No.4, pp.525 – 529.

7 Shifeng Zhu, Meiwu Shi, Meifang Zhu. Effects of Electron-Beam Irradiation Crosslinking on PA6 Fibers. *Fibers and Polymers.* 2013, Vol.14, No.4, pp.525 – 529.

8 Nalwa H.S. *Ferroelectric Polymers.* Marcel Dekker, New York, 1995, pp.283 – 286.

9 SibiliaJ.P.*A Guide to Material Characterization and Chemical Analysis.* VCH Publishers, New York, 1996, pp.148 – 150.

10 Sengupta R., Bandyopadhyay A., Sabharwal S., Chaki T.K. Polyamide-6,6/in situ silica hybrid nanocomposites by sol-gel technique: synthesis, characterization and properties. *Polymer,* 2005, Vol.46, No.10, pp.3343 – 3354.

11 Makuuchi K., Cheng S. *Radiation Processing of Polymer Materials and Its Industrial Applications*, John Wiley & Sons, Inc., New Jersey (2012).

Article accepted for publication 25.10.2019

.

DOI 10.31489/2019No2/48-54

UDC 532.529

INVESTIGATION OF TWO PHASE FLOW MOTION WITH SMALL-SIZE GAS BUBBLES

Vasenin I.M., Narimanov R.K., Perchatkina E.V., Shrager L.A.

Tomsk State University, Tomsk, Russian Federation, ring_0@mail.ru

The motion of a two-phase gas-liquid jet with small-size bubbles in an ozonizer has been calculated. The mathematical model used in the calculations, unlike the model of interpenetrating continuums for a two-phase medium, does not contain small parameters for derivatives. By virtue of the consideration of the medium compressibility and the dependence of the density on the concentration of bubbles, this model automatically takes into account the processes causing free convection in the gravity field in the presence of the heterogeneous concentration of bubbles. Parametric studies based on the proposed model have been conducted. The efficiency of this approach has been shown. The acceleration of the floating of a gas jet due to its involvement in the motion of the carrier medium has been confirmed. The parameters of the process of dissolution of ozone in the contact tank have been determined, the efficiency of the location of dispersants has been evaluated.

Keywords**:** two-phase flow, gas-liquid medium, small-size bubbles, water ozonation.

Introduction

The movement of gas-liquid mixtures is ubiquitous in nature, and in a variety of technological processes. One of the urgent technological processes of increasing interest is the disinfection of water in water supply systems by its ozonation [1-3]. If we analyze the use of ozone for water treatment, then two main stages can be identified. At the first stage, ozone was used mainly at the final stage of water purification as an effective disinfectant, which gives transparency to the water, deprives of odor, increases the content of dissolved oxygen, etc.

The second stage is connected with the research results of the last ten years, when they began to work out various options for the use of ozone and at the intermediate and initial stages of water purification. With multi-stage ozonation technology with combined cleaning methods, it will be possible to maximize the removal of various types of contaminants. However, it is necessary to optimize the entire technological process, first of all, with respect to the level of ozone and other reagents at each stage.

The equations of water-air mixtures are periodically considered in the scientific literature in various issues. However, it is authors' opinion that the flow of such mixtures in the field of gravity with the combined effect of free and forced convection needs further investigating. The relevance of the development of gas-liquid mixture models is undeniable. Vasenin et al. [4-5] proposed a physical and mathematical model of the motion of a two-phase mixture with small particles.

This work aimed at the calculation of a two-phase flow of water and small-size bubbles in relation to the problems similar to the problem of ozonation of water in contact tanks.

1. Physical task description

The movement of bubbles in a body of water is considered as the convective movement of small particles with a density much lower than the density of water. The physical basis of this convection is very simple. By means of the Archimedes buoyant force a lighter mixture containing a larger amount of gas floats in a heavier fluid in the same way as light warm air floats in a cold environment. The mathematical model for small-size bubbles is simpler than the equations of two-phase fluid flow with arbitrary size bubbles and allows us to significantly simplify the problem. The following assumptions were used:

– The movement of each bubble can be considered as the movement of a spherical particle. To satisfy this requirement the bubbles, floating up in water under the action of Archimedes buoyant force, should have a size smaller than $2-3\times10^{-3}\,m$.

– The temperature of the bubbles moving in water is equal to the ambient temperature. The estimates [6] show that for air bubbles with a diameter less than $2.5\cdot10^{-3}\,m$ the relaxation time of the air and water temperature difference does not exceed 0.1 *s*. Since the time of small-size bubble staying in the water mass of a contact tank is $\sim 20s$, the temperature difference between bubbles and water can be neglected.

– The third requirement for small-size bubbles is as follows. The transient time of the velocity of bubbles floating up in water should be negligible compared with the characteristic time of their motion in the whole region.

Implying these conditions, the convective flow with small-size bubbles is described by the mathematical model of convective flow with small particles that differ in density from the carrier medium. The mathematical model of convective flow with small particles is described in [4] in application to the case of a "water-solid particle" mixture. However, the presence of dissolving gas bubbles of variable volume in liquid allows us to consider the gas-liquid mixture as a compressible medium. A detailed description of the derivation of these relations and the validity of the assumptions used are presented in [5]. Based on these assumptions, the equations of motion are derived

$$\frac{\partial(\bar{u})}{\partial t}+\bar{U}\nabla\bar{u}+\frac{1}{\bar{\rho}_l+\bar{\rho}_s}\frac{\partial\bar{p}}{\partial\bar{x}}=\frac{1}{Re}\Delta\bar{u}+\frac{1}{Fr}\frac{|\bar{g}|}{\bar{g}}$$

$$\frac{\partial(\bar{v})}{\partial t}+\bar{U}\nabla\bar{v}+\frac{1}{\bar{\rho}_l+\bar{\rho}_s}\frac{\partial\bar{p}}{\partial y}=\frac{1}{Re}\Delta\bar{v}+\frac{1}{Fr}\frac{|\bar{g}|}{\bar{g}}$$

$$\frac{\partial(\bar{w})}{\partial t}+\bar{U}\nabla\bar{w}+\frac{1}{\bar{\rho}_l+\bar{\rho}_s}\frac{\partial\bar{p}}{\partial\bar{z}}=\frac{1}{Re}\Delta\bar{w}+\frac{1}{Fr}\frac{|\bar{g}|}{\bar{g}},$$

where p, U, u, v, w, ρs, ρl, Re, Fr, g - pressure, velocity vector, velocity components, density of air, density of medium, Reynolds number, and Froude number and a gravity vector, respectively.

$$P\left[\frac{1}{\rho}-\frac{z}{\rho^*\left(1+\frac{P}{k}\right)}\right]=\bar{R}T.$$

The equation of state

According to the estimation of the motion parameters in the ozonizer, the temperature of the mixture is constant and equal to the temperature of inflow water.

$$T=T_0$$

To close the system of equations, it is necessary to add the equation of conservation of mass of a two-phase mixture

$$\frac{\partial(\bar{\rho}_l+\bar{\rho}_s)}{\partial t}+\nabla(\bar{\rho}_l+\bar{\rho}_s)=0\ ,$$

and the equation of bubbles mass conservation

.

$$\frac{\partial \overline{\rho}_s}{\partial t} + \nabla \overline{\rho}_s = 0$$

The presented equations for given initial and boundary conditions make it possible to calculate the parameters of a two-phase flow in a contact tank, time and the trajectory of the movement of the bubbles filled with an ozone-air mixture.

2. Determination of dependence of the ozone dissolution

Though, we need another formula to calculate the dissolution of ozone in the bubbles. The mass concentration of ozone in bubbles m_{o3} obeys the conservation law.

$$\frac{d(V \cdot m_{o3})}{dt} = -q \tag{1}$$

where $\frac{d}{dt}$ – time derivative along the bubble trajectory; V – its volume; q – ozone flow into water through its surface.

We assume that the flow q is proportional to a bubble surface σ and to the difference in the concentrations of ozone in a bubble and in surrounding water

$$q = \alpha\sigma\left(m_{o3} - m_{o30}\right), \tag{2}$$

where m_{o30} – ozone concentration in water.

Substituting (2) in (1) we obtain

$$\frac{d\left(V \cdot m_{o3}\right)}{dt} = -\alpha\sigma\left(m_{o3} - m_{o30}\right). \tag{3}$$

When rising to the surface of the reactor, the volume of the bubble grows, and therefore the value V cannot be taken out of the sign of derivative. To simplify (3), we suppose water is not saturated with ozone, so we can assume $m_{o30} = 0$. Introducing the mass of ozone in the bubble $M_{o3} = m_{o3}V$, from (3) we derive the equation

$$\frac{dM_{o3}}{dt} = -\frac{\alpha\sigma}{V} M_{o3} \tag{4}$$

The following equality holds for a spherical bubble $\frac{\sigma}{V} = \frac{3}{2D}$, where D – bubble diameter. Therefore, equation (4) can be rewritten as

$$\frac{dM_{o3}}{dt} = -\frac{3\alpha}{2D} M_{o3} \tag{5}$$

In the case of constant D and α, this equation has a solution

$$M_{o3} = C\exp\left(-\frac{t}{T^*}\right),$$

where $T^* = 2D/\alpha$ – characteristic time during which the mass of ozone in a bubble changes e times.

Equation (5) was used in the mathematical model described above to calculate the ozone concentration along the trajectories of bubbles. In this case, the variability of bubble diameters D has been considered. The coefficient α was chosen so that for bubbles with an initial diameter of D_0=1.5 10^{-3} *m* in the conditions of the experimental contact tanks of the Eastern water station in

Moscow an ozone absorption coefficient of 90% was achieved. Following this approach, the coefficient $\alpha = 0.00018\,m/s$ was found. For the bubbles with a diameter of D_0=1.5 10^{-3} m and $\alpha = 0.00018\,m/s$, the characteristic time is T * ≈ 8.3 s. This result is consistent with the time of dissolution of the same air bubble in air-saturated water, which, according to [7], is 7.7 *s*. A slightly longer dissolution time of ozone may be described by its larger molecular weight, which reduces the diffusion coefficient.

3. Numerical simulation

3.1 Calculation of the movement of a single gas-liquid jet

Based on the proposed model, the parametric studies were carried out. They include parametric studies of the effect of the initial bubble density and inlet flow on the bubbles rate at which they reach the upper boundary of the cylindrical region. The region is a vertical axisymmetric cylinder; a gas jet is introduced on the cylinder axis. The height and the radius of the cylinder is 10 cm, the width of the jet is equal to 1/6 of the radius. The initial distribution of the bubbles volume concentration in the inlet is determined by a Gaussian probability function so that at the distance of a jet radius from the centerline their concentration is 1% of the maximum value on the axis. The reliability of calculations is confirmed by the investigation of grid convergence for the bubble sizes varying from 10 μm to 100 μm at a given initial concentration of the jet. Resizing of a bubble during its floating is neglected.

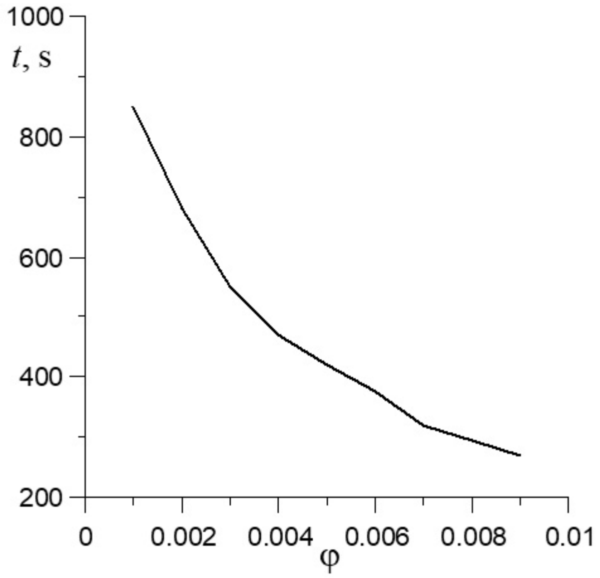

Fig.1. Effect of the introduced relative gas density on the time of reaching the upper boundary

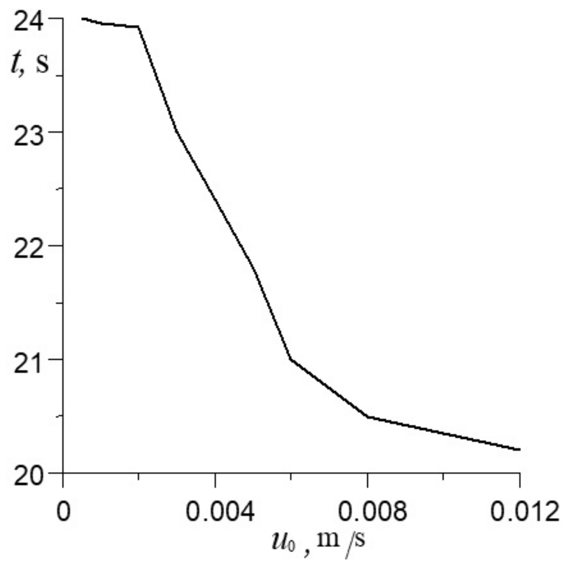

Fig.2. Dependence of the rise time on the perturbation velocity

Figure 1 shows the effect of the relative density of introduced gas φ on the time of reaching the upper boundary; here a particle diameter is 10 μm. When calculating the gas velocity, it is necessary to set a low initial injection velocity, which is parallel to the axis. The value of the velocity u_0, which does not alter the calculation results, was determined during parametric studies of the dependence of the floating time on the perturbation velocity at the diameter of 100 μm.

The result is presented in Figure 2. Figure 3 demonstrates the effect of a gas bubble diameter on its floating time at the fixed volume concentration of bubbles in a gas stream.

.

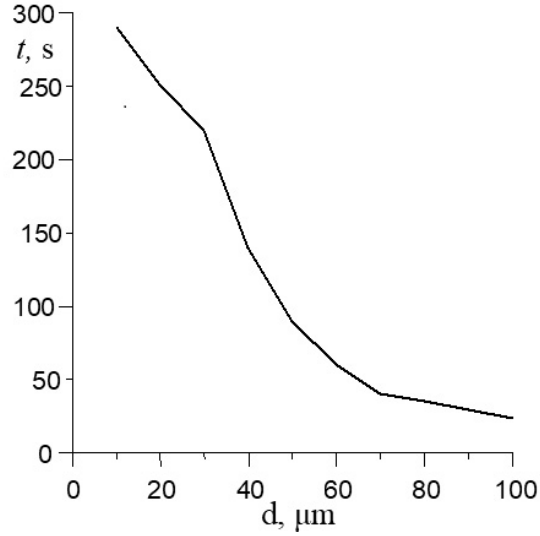

Fig.3. The effect of the diameter of a gas bubble on its ascent time

3.2. Parametric studies of ozone dissolution in a contact tank

Preliminary numerical investigations of the process of ozone dissolution in water have been carried out with the following purposes:

1) to validate the proposed mathematical model;

2) To find the ways to optimize and to improve the efficiency of ozonation;

3) To select the diffusion coefficient of ozone for bubbles in a body of water, ensuring the consistency of theory and experimental data.

The calculation of the flow of a two-phase mixture has been carried out for a section of the tank with a horizontal cross-sectional area of 1.6 m×1.6 m, since there is symmetry in the arrangement of dispersants in the contact tank. At the bottom of the section there are 25 dispersants with a diameter of 0.2 *m*. Water is delivered or drained between the dispersants. In this section water rate through 1 m^2 and the volume of the ozone-air mixture through dispersants are equal to the same parameters in the contact tank.

The axis of the coordinate system is directed from the surface of the tank toward the bottom. On the surface of the tank the atmospheric pressure is set. At the lateral boundaries of the computational domain, symmetry conditions are specified. The calculations showed that the jet stream of the ozone-air mixture will remain throughout the calculations until the establishment of the process. Figure 4 shows the calculation results of a single jet of ozone-air mixture flowing into the counter flow of water from a dispersant, which is 0.6 *m* in diameter.

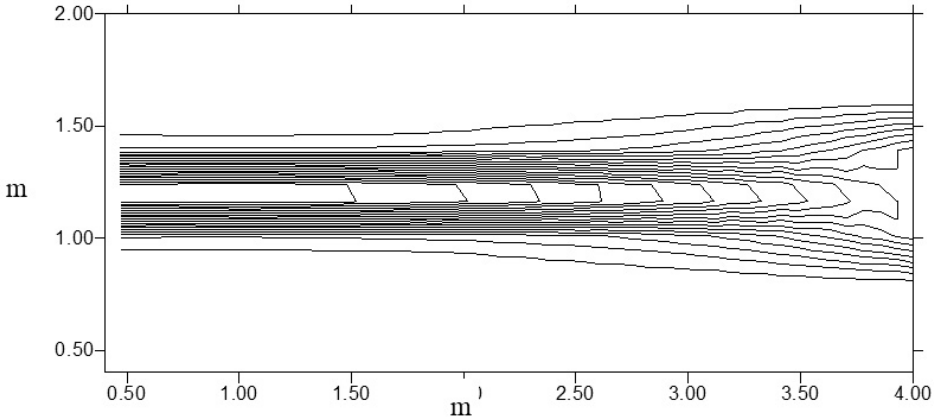

Fig.4. Separate stream flowing into the oncoming water stream.

The lighter ozone-air mixture floats up in the surrounding water in the field of gravity. The diameter of the jet decreases, because of its acceleration. Outside the jet water flow is directed toward the bottom. Its speed is 0.02 *m/s*. The rate of the rising water-air mixture is directed to the surface and reaches 0.08 *m/s*. This speed is added to the speed of bubbles and reduces their time in water. For this reason, the fraction of insoluble ozone in the stream increases. Figure 5 shows the results of calculations of the fraction of insoluble ozone in the cross section of the water-air stream. In the center of the jet near the surface of the water, this fraction is 0.1 and is maximum for a given level.

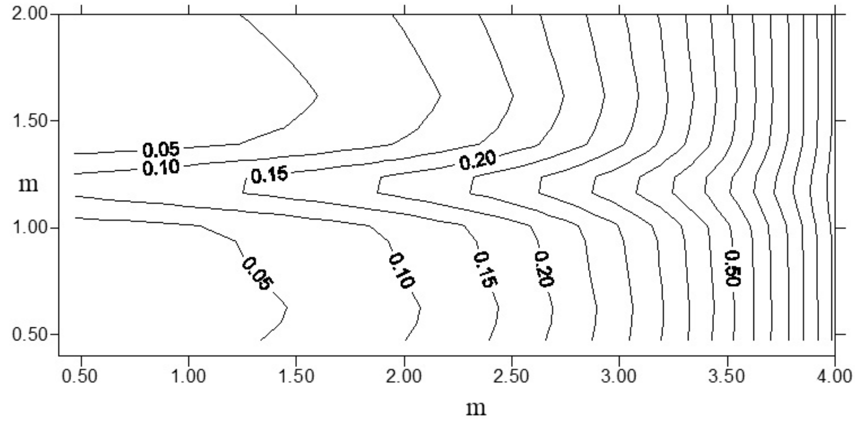

Fig.5. Contours of ozone concentration.

Figure 6 qualitatively shows the concentration of ozone on the surface of the tank for the pool section containing 25 dispersants. The figure shows that at the locations of the water-air mixture rising to the surface of the water, the fraction of insoluble ozone exceeds 10%. At the same time, between the jets this fraction is close to zero. Obviously, a decrease in the efficiency of ozone dissolution in jets is connected with an increase in the rising bubble rate, which leads to a reduction of the time of ozonation.

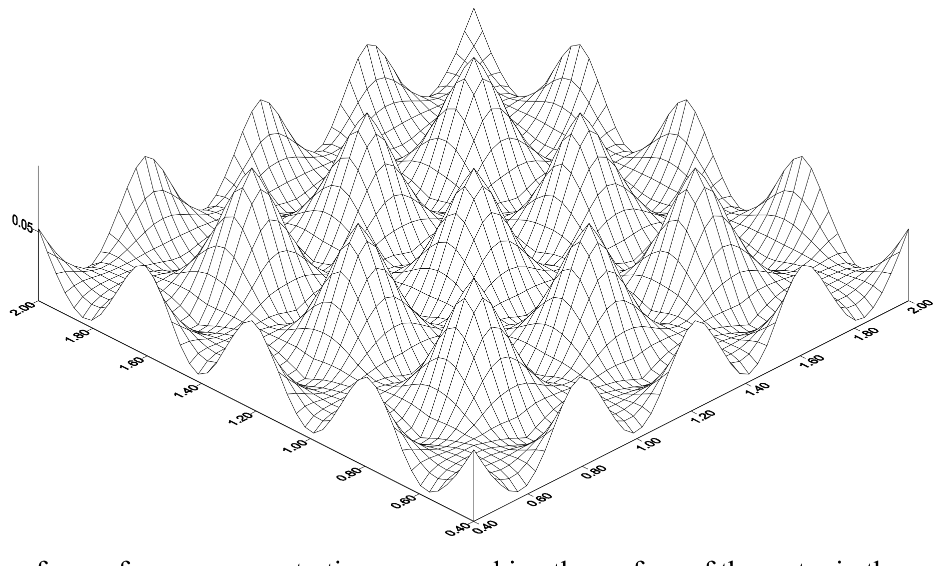

Fig.6. Isosurfaces of ozone concentration upon reaching the surface of the water in the contact tank.

Contact tanks with discretely located dispersants proved to be insufficiently effective. To compare the results we made the calculations, in which the sources of water and the ozone-air mixture were located continuously throughout the bottom of the pool. Figure 7 demonstrates the dependence of the levels of the relative fraction of insoluble ozone on the distance to the water surface for the case of continuously located sources.

.

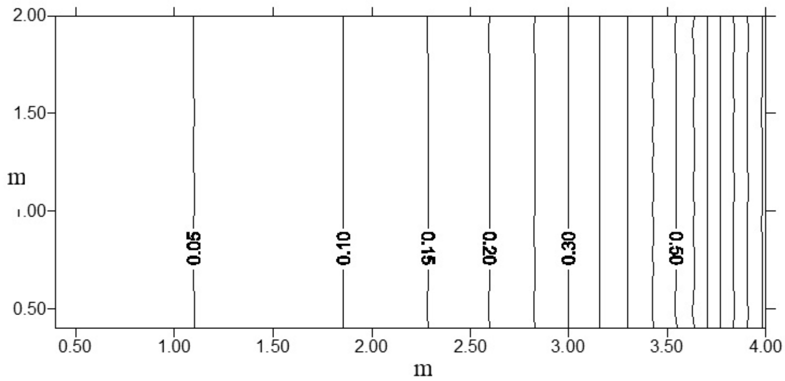

Fig.7. Degree of ozonation in the contact tank with uniform input ozone-air mixture.

The fraction of insoluble ozone on the surface is 2%, which indicates a noticeable (compared to 10%) increase in efficiency compared to the discrete location of sources.

Conclusion

The mathematical model used in the calculations, unlike the model of interpenetrating continuums for a two-phase medium, does not contain small parameters for derivatives and is much simpler from the point of view of numerical solution. By virtue of the consideration of the medium compressibility and the dependence of the density on the concentration of bubbles, this model automatically takes into account the processes causing free convection in the gravity field in the presence of the heterogeneous concentration of bubbles. This kind of convection, when the supply of gas mixture is not uniform in space, significantly affects the duration of stay of the bubbles in the reactor and, consequently, the completeness of the reactions that occur. An additional advantage of the proposed mathematical model is its analogy with compressible gas models. Going forward this analogy makes it possible to use well-developed numerical schemes for solving equations of gas dynamics. Parametric numerical studies, conducted according to the proposed model, have proved the efficiency of this approach. The acceleration of the floating of a gas jet due to its involvement in the motion of the carrier medium is confirmed. To determine the parameters of the ozone dissolution process during ozonation of water in contact tanks the preliminary numerical investigations have been carried out. The effectiveness of the location of the sources of ozone-air mixture at the bottom of the tanks has been evaluated.

Acknowledgements

The work was partially supported by the Ministry of Science and Higher Education of the Russian Federation (State Task No. 9.9625.2017/8.9).

REFERENCES

1 Kozhinov V.F., Kozhinov I.V. *Water ozonation.* M.: Stroiizdat, 1974, 496 p. [in Russian]

2 Orlov V.A. *Water ozonation.* - M.: Stroiizdat, 1984, 88 p. [in Russian]

3 Dankverts P.V. *Gas-liquid reactions.* M.: Himia, 1973. [in Russian]

4 Vasenin I.M., Dyachenko N.N., Elkin K.E., Narimanov R.K. Mathematical Modeling of Two-Phase Convective Flows with Fine Particles. *Journal of Applied Mechanics and Technical Physics,* 2004, No 6, pp. 788-793.

5 Vasenin I M, Narimanov R.K., Shrager L.A., Perchatkina E.V. Modeling of a two-phase flow of liquid with small-size gas bubbles. *Eurasian Physical Technical Journal.* 2019, Vol.16, No. 1(31), 2019, pp. 129-137.

6 Parkin B.R., Gilmor, F.R., Broud G.L. *Shock waves in water with air bubbles*. In the coll. *Underwater and underground explosions*. Moscow, Mir, 1974, pp. 152-258.[in Russian]

7 Epstein, P. S. and Plesset, M. S. *On the Stability of Gas Bubbles in Liquid-Gas Solutions.* Journal of Chemical Physics. 1950, 18 (11). pp. 1505-1509.

Article accepted for publication 09.12.2019

DOI 10.31489/2019No2/55-62
UDC 627.521.1

ON THE CREATION OF SMALL WIND POWER PLANTS IN KAZAKHSTAN

Baishagirov Kh.Zh., Omarov B.M.

Sh. Ualikhanov Kokshetau State University, Kokshetau, Kazakhstan, bayshagir@mail.ru

The article deals with the data on renewable energy sources in the Republic of Kazakhstan, in particular, on the creation of wind power plants. Here with, there are noted design features of the created small wind power plants. There are identified three stages that arise when creating small wind power plants, as well as a brief description of the corresponding types of work. The role of composite materials in creating new products in mechanical engineering is shown. There are described design features of a composite wind power plant with a diffuser in details. Results of analytical studies and graphs of the air velocity changes inside the diffuser are presented. There are described main points of the manufacturing technology of fiberglass fairings.

Keywords: wind power plant, composite material, fairing, diffuser, construction, generator.

Introduction

In recent years, there are actual the issues of using clean and sustainable energy, that is the sphere of mass application of high technology, a catalyst for "wide" social and economic development. It also provides a higher life quality and the transition of the whole society to a new technological structure, which is the subject of fundamental conceptual research [1]. This approach provides for the coordinated implementation of the national initiatives «Green Bridge», «Green Growth», and the Global Energy and Environmental Strategy. It considers the decisions of the UN Conference on Sustainable Development in the fields of energy, ecology, and economy, when national interests and characteristics are taken into account.

In Kazakhstan there is a Concept for the country's transition to a green economy that was approved by the President of Kazakhstan6 years ago. Herewith, there are given the desired indicators of the share of electricity from renewable energy sources. (RES): 3% in 2020, 10% – 2030, 50% – 2050. Wind power is an essential factor in achieving these goals. According to the Ministry of Energy of the Republic of Kazakhstan, the operation of wind power plants (WPP) with a total capacity of less than 230 MW began in 2010.This year there are already 15 functioning objects of wind power plants, and by the end of the year it is planned to put into operation three more objects [2].

In September 2019, there were announced the results of the tender for the selection of wind power plants projects [3], where the winners were the firms with an auction price of 19.27 − 19.33tg / kW (excluding VAT). This is a breakthrough step forward for our country, because these figures are already comparable to coal energy tariffs. However, these parameters are related to the energy sector as a whole, including large wind power plants. This article deals with the creation of small wind power plants (SWPP), for them the development indicators have not been determined in the country yet.

1. Small wind power plants of Kazakhstan

Nowadays, the use of electricity in agriculture of the Republic of Kazakhstan remains at an insufficient level in comparison with the developed countries − it is 7-10 times less in our country. This represents approximately 1% of total energy consumption. All this is due to the fact that centralized energy supply does not cover a large number of individual consumers and therefore does

.

not meet modern requirements. The reason for this situation is that the transmission of power lines by traditional methods is not economically attractive in remote and inaccessible places with a low population density. To improve the situation here, one can use autonomous sources of electricity. These include energy machines developed at the initiative of domestic specialists, in accordance with the goals and objectives of "Green Energy".

The scientists of the Republic of Kazakhstan have designed several types of SWPP with both vertical and horizontal axes of rotation. The first group includes the inventions of academician of NAS RK Yershin Sh.A., the academician of NEA RK Bolotov A.V., doctor of technical sciences Buktukov S.N., the academician of NAS RK Otelbayev M.O. and candidate of Physics and Mathematics Kunakbayev T.O. The second group includes the prototypes of doctor of technical sciences Kambarov M.N., doctor of technical sciences Baishagirov Kh.Zh., candidate of Physics and Mathematics Zhilkashinova E.M., and others. Standing apart, there is a model of the WPP, by doctor of technical sciences Kussaiynov K.K. and his students that works on the basis of the Magnus effect. Here the axis of rotation may not have a fixed direction [4, 5].

Thus, there are created a number of original SWPP in our country that differ from foreign plants both in terms of design and technical parameters. For instance, Bidarrieus wind turbine by academician Sh.A. Yershin combines two modes: Darrieus and Bidarrieus. It has a vertically axial rotor with two coaxial shafts that rotate independently in different directions [6]. Vertical-axis wind turbine by academician A. Bolotov (VWT) generates energy thanks to modules rotating in opposite directions. Thus, achieves a synergistic effect in combination with solar panels [7]. Original and sufficiently equipped with devices wind power plants by N. Buktukov can be as a light house in steppe remote areas. With increasing wind velocity, the rotor can change its shape due to the compression of the rotating blades [8].

Compact multistory model of a wind power station (CMWS) is being developed in al Farabi KazNU under the guidance of doctor of Physics and Mathematics T.O. Kunakbayev and academician of NAS RK M. Otelbayev. CMWS – a multistory construction, where there are situated various types of wind turbines on its floors. It has several advantages over conventional wind power plants located at the height of one floor on the ground. The advantages of CMWS – it is the stable use of wind energy, which has an increased velocity in the air passages between floors. There is also realized land saving of the territory given for the SWPP [9].

In National scientific laboratory at S. Amanzholov East Kazakhstan State University candidate of Physics and Mathematics A.M. Zhilkashinova put into operation the sail SWPP. This plant's wind wheel quickly adjusts to the direction of the air flow and has a low breaking moment [10]. Among compact SWPP one cannot emobile composite wind power plant with diffuser (WPPD), created under the guidance of doctor of technical sciences Kh.Zh. Baishagirov in the laboratory of Sh. Ualikhanov Kokshetau State University.

2. Stages of SWPP creating and composite materials.

To assess the completeness of plans and work on the creation of SWPP in the country, one should mind the "laws" of modern engineering. According to them, the whole process of creating machines consists of three large stages: 1 – obtaining the first prototype with the implementation of a new theoretical idea («know-how»); 2 – creation of prototypes of machines and drive into a competitive level; 3 – mass production. Such stages are usually implemented by various relevant organizations and specialists.

For instance, stage 1 is usually conducted in universities and research institutes of an academic or applied orientation. Here dominate the specialists in physics, mechanics, mathematics, etc. For the implementation of stage 2, there work design and industry research institutes, various design bureaus(DB), enterprises and R&D institutions involved in the implementation of the results of fundamental and applied science. The main backbone of such organizations is made up of scientists, designers - planners, engineer - technologists, etc.

The tasks of stage 3 are solved at factories and engineering enterprises. The work is carried out in various kinds of DB, experimental and other workshops of enterprises by engineers, technologists, adjusters, production innovators, etc. For instance, in the early 80s in Karaganda there were more than 20 research institutes serving industry enterprises (stage 2). In the same years "Vetroen" plant produced SWPP and the wind pumps “Romashka” for rural workers (stage 3).

Most of the domestic SWPP designers practically did not move beyond the first stage. The reason for this, apparently, is that in the country there are practically no enterprises where is implemented the entire chain of work from the idea to the serial production of modern high-tech products. Indeed, it is difficult to indicate the enterprises of machine, aircraft or shipbuilding, where the specialists in hydromechanics, strength, energy, design, technology of modern materials, electronics work together. But to create SWPP one need just such a team of specialists.

Among SWPP of the country only the wind power plant with diffuser (WPPD) is created from composites, moreover, the development moved to the second stage. Therefore, at present, after the model prototype, there is being created a technical prototype of the energy machine. It will serve as the basis for the creation of a pilot industrial prototype with the goal of moving to the third stage of small-scale or mass production. Here the fundamental issue is the development of the technology of composite materials and their products.

The rapid growth of global wind energy is directly related to the development of composite materials technologies, the most common one is fiberglass. In recent decades, composite materials (CM) are widely used in other areas of modern technology, where their high specific strength and stiffness are favorably used in constructions. In the science and practice of CM, there are developed new trends and approaches [11], caused by the desire to create multifunctional structures and expand the sphere of their application by using components with lower cost.

Composites arose as a natural reaction to the needs of modern technology. Composites, strictly speaking, are not materials in the classical sense, i.e. ready product, for example, in metallurgy, with predetermined and practically unchanged properties during processing. They constitute an extensive group of materials created from semi-finished products together with design, i.e. as a whole the properties of composites and the structure are technologically formed simultaneously during its manufacture. Therefore, when creating structures from CM, design issues (in the traditional sense), rational reinforcement and process development are three sides of a single problem and cannot be considered in isolation that is allowed when creating a construction from metals. Thus, the effective use of CM requires from the developers to solve the three-pronged problem at a time: problems of the mechanics of a composite body, micromechanics, and manufacturing technology.

Chronologically, the mechanics of CM first dealt with models of a homogeneous (quasi - homogeneous) anisotropic body, then CM were presented as anisotropic bodies with homogeneous layers, and a higher level of modeling are, for example, options when each layer itself has heterogeneity at the structural level. It is quite consistent that such a sequential staging of the research is observed in the development and creation of such essential products from CM as the working blade of an aircraft engine compressor or the blade of a wind power plant.

3. Wind power plant with diffuser

In view of the foregoing, for the model prototype of the WPPD, there was used the technology of layer-by-layer manufacturing of composite parts, its stress-strain state was studied earlier. This technology can significantly increase the service life of the products, the cost of maintaining the plant and generally increases the efficiency of using the wind engine. There are various wind power plants with a diffuser (USA, Japan, etc.), but, as a rule, they are stationary. In contrast, our WPPD is portable. Its mobility is ensured by the fact that it has got light weight. Here with, installation and dismantling of the WPPD can be carried out by 2-3 workers in a couple of hours without lifting devices. During the IUE “Astana EXPO - 2017. Future Energy” there was hosted the international forum“ Integration of Science and Business ”, organized by the National Center for State Scientific and Technical Expertise (NSSTE) together with the Ministry of Education and Science of the Republic of Kazakhstan. In the report “Energy of Kazakhstan: Yesterday, Today, and Tomorrow”, the President of the Scientific Center for Scientific and Technical Information singled out the project on the development of a model prototype of composite WPPD among the four best achievements of Kazakhstan innovators in the field of green technologies [12].

In this energy machine, the nodes are created from composite materials using appropriate technologies. A distinctive feature of the design is the use of a diffuser, as indicated in Figure 1.It turns with its narrow part in the wind and increases the velocity of the air flow in the wind wheel area. Also, the diffuser protects the generator from external undesirable effects (moisture, birds, sun rays, dust, etc.) [13].

WPPD consists of the following parts: a wind wheel with three-blades, generator, fairings of the generator; diffuser – wind direction indicator with sectors in the amount of 12 pieces, 4 stainless steel hoops; spars (pylons);strong ring; support tower with extensions; rotary device (at the top of the tower) with rectifier; channel support beam.

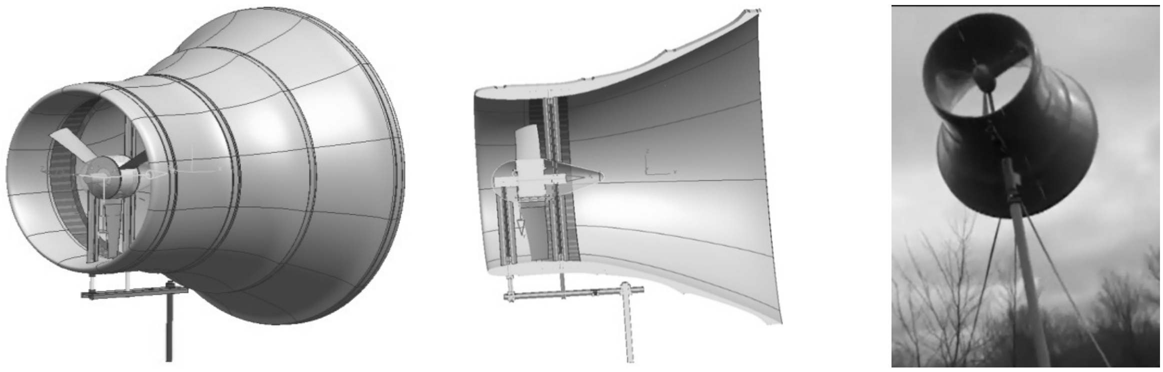

a) b) c)

Fig.1. Wind power plant with diffuser (ВЭУД): a – 3D model of a wind wheel and a diffuser, b – longitudinal section of a 3D model of a wind wheel and a diffuser, c – WPPD – 4 (4th prototype).

WPPD parameters: weight - 95 kg, tower height - 4 m, project capacity– 1kWt, temperature regime from minus 50 ° C to plus 80 ° C, 20 years of operating life, generates current at a wind velocity of 4-25 m/s. Using resource-saving technology for processing composite materials, the main components and diffuser were made of fiberglass, due to which there is increased the operating mode of the plant and the geography of its location [14; 99]. One can distinguish the high mobility of WPPD, ease of maintenance, increased serviceability, resistance to the effects of various manifestations of the climate, safety at the widest range of use, silent-running operation, low metal consumption, attractive design, lack of radio interference, etc. WPPD pays off in 4-5 months when used together with the "Vodoley-3" pump to supply drinking water from a well.

4. Modeling of the longitudinal velocity of the air flow inside the diffuser

The output characteristics obtained during field tests of the WPPD based on the PMGV3 electric generator prove its effectiveness. Therefore, there is carried out a cycle of work to create the corresponding nodes from composites for a technical prototype. This requires a preliminary mathematical justification of the effectiveness of the shapes of the diffuser and fairings. To obtain the simplest analytical dependence of the flow velocity distribution along the axis of the diffuser, we use the mass conservation equation. It is based on the equation of continuity of the one-dimensional motion of an ideal compressible gas in a pipe of variable cross section, which has the form [15]:

$$\rho VS = const, \quad (1)$$

where ρ – gas density, kg/m^3; V – gas velocity, m/s; S – cross-sectional area, m^2 .

Differentiating equation (1) with respect to x, we divide it by ρVS. If we take into account that we are considering the one-dimensional motion of an incompressible fluid, i.e. our conditions are close to normal ($\rho = 1$), then the equation will take the form:

$$\frac{1}{S} * \frac{dS}{dx} + \frac{1}{V} * \frac{dV}{dx} = 0 \quad (2)$$

The functions V and S vary with x, therefore, setting one of them based on empirical considerations, the other can be calculated from the differential equation (2). It is advisable to set the distribution $S = S(x)$, that is, the dependence of the cross-sectional area of the diffuser on the longitudinal coordinate along its axis. Since the inner surface of the diffuser is obtained by rotation of the curve forming $y = y(x)$, in sections we get circles with a radius equal to the ordinate of the points of this curve. Therefore, the area of the current section will be

$$S(x) = \pi y^2(x)$$

If we consider the longitudinal section of the WPPD, then we can describe the generating line of the diffuser through the function$y = a + bx^2$. Transforming and substituting in relation (2) we obtain a differential equation with separable variables. Integrating it and using the well-known experimental relation, we obtain:

$$V = \frac{1{,}27a^2V_\infty}{(a + bx^2)^2}$$

For the real sizes of our WPPD we use the numbers a= 0.5 and b=0.35. Then we get the values $V_{in} = 1.12\ V_\infty$, $V_{max} = 1.27\ V_\infty$ и $V_{out} = 0.32\ V_\infty$, corresponding to the distribution of air velocity inside the diffuser as shown in Figure 2.These calculations are made for the diffuser without considering the area of the wind wheel.

Figure 2 was obtained for the first prototype and is presented here for a qualitative comparison with the new calculated parameters. Since the above mentioned calculations were carried out without considering the wind wheel, it is necessary to divide the WPPD into 4 zones, as shown in Figure 3.Each zone has its own formula for calculating the air flow velocity.

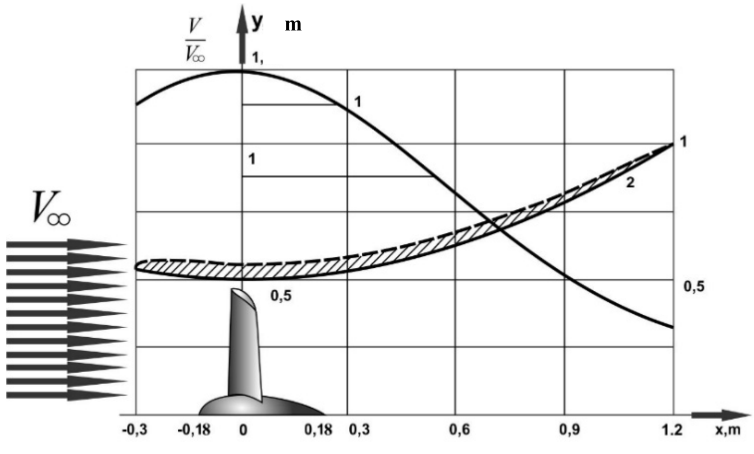

Fig.2. Velocity distribution and the profile of a diffuser with a quadratic generating line.

.

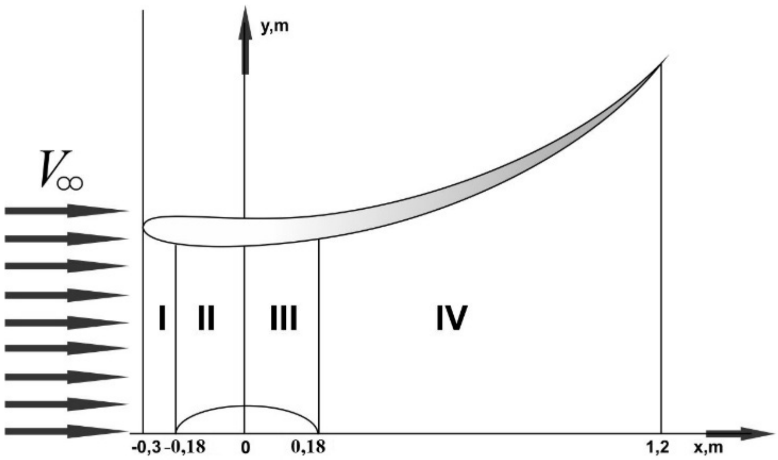

Fig.3. Dividing of the WPPD cross-section into zones.

In zones II and III the airflow is influenced by the shapes of the surfaces of the fairings and the diffuser, and in zones I and IV – only the diffuser. Generating lines of fairings can be described through the functions $y^2 = 2px+x_0$ and $y^2 = -2\,px+x_0$. As a result of solving the problem by dividing into zones, we obtain the following expressions for the air velocity:

for zone I and IV: $V = \frac{0{,}32V_\infty}{(a+bx^2)^2}$;

for zone II: $V = \frac{0{,}32V_\infty}{(a+bx^2)^2-(2px+x_0)^2}$;

for zone III: $V = \frac{0{,}32V_\infty}{(a+bx^2)^2-(-2px+x_0)^2}$.

As a result of the calculations, we obtain:

$V_{in}= 1.1V_\infty$, $V_{max}= 1.27V_\infty$, $V_{out}= 0.32V_\infty$.

Using the previously obtained theoretical results on the shapes of the diffuser and fairings, one should begin the technological part of the work with the manufacture of a new fairing.

5. Manufacturing technique of the fairings

To determine the amount of structural material - fiberglass, there has been solved the problem of calculating the surface area of fairings rotation. There were obtained numerical values of the volumes of the material considering the differences in shapes, sizes, and also the thickness of the layers in the structure of the product. The manufacturing technology of nodes also depends on the strength requirements for the product being created. For instance, when manufacturing the blades, there is required the use of a thermal press, which will give the material a high density, and hence appropriate strength. It is possible to use a simple press - without heating then the formed fiberglass structure will be less durable. Since the rear fairing does not carry a significant load, here one can do without the press and other expensive equipment. For this reason, on its example, we consider the entire process of manufacturing such a node. First, a series of preliminary works is carried out to determine the shape of the master models. Then, using hand-made patterns, there was created a series of components on a lathe with a copier. Further processing of components consists of grinding and varnishing processes in several layers manually. The obtained products are shown in Figure 4. Layers of fairings are made with the hand lay-up method: the lower layers are made of isotropic glass mat, and the upper layers are made of fiberglass T-23 and T-11 with ordered fiber orientation. These surface layers of fiberglass will be subjected to directional effects of external force factors; therefore, the material with anisotropic strength properties was selected as the upper layer.

Fig.4. The components and corresponding fiberglass fairings.

The creation of such structural elements as reinforced layers will enable to compose convenient algorithms for digitalization of calculations based on their regularity. This enables to provide the strength and rigidity of the fairings in the subsequent stages of creating experimental prototypes. Besides, such algorithms and programs are created to automate production in the future.

Conclusion

All types of SWPP developed in Kazakhstan are eligible for implementation, as each of them has its own consumer sector or region of effective use. Thus, sail SWPP and WPPD may be of interest to individual consumers who need an easy-to-use 1-2 kW power sources. For consumers of energy of 3-15 kW there are created Bidarrieus SWPP, VWT. If one need a more powerful power station, then you can choose CMWS. Here we note that all 4 types of the latest SWPPs work regardless of the wind direction. This is their advantage; the disadvantages include the relatively large material consumption of these energy machines in comparison with the WPPD or a sail wind power turbine. The advantage of domestic developments is that they are applicable almost anywhere in the country territory. This cannot be said about any single foreign wind power plant.

The existing scientific potential of the country is a significant reserve in order to speed up the creation of domestic SWWP. Here one can make a breakthrough in attracting investment and developing technology both in the country and in the regions. For the SWPP production in the Republic of Kazakhstan there are elements of a legal framework and other opportunities that require investment of resources and efforts.

Our experience enables to identify those difficulties and problems that hinder the quick bringing of theoretical development (ideas) to the release of final products at the factory:

1. Lack of motives for manufacturers to support R&D.
2. The lack of the SWPP market and the lack of qualified specialists.
3. Undeveloped scientific, technical and technological base for the creation of wind power plants.

Most recently, there has been appeared serious progress in this direction in the country. To realize the Concept for the country's transition to the Green Economy and achieve the relevant indicators for the development of small wind energy, we recommend the following:

1. In the regions of our country, one should create R&D laboratories, technological areas and technology parks connected with the creation of nodes for SWPP, including from perspective composite materials (fiberglass).
2. To work out issues of personnel training and technology transfer.

.

3. To organize activities on the formation of market elements in the field of renewable energy.
4. To create in Kazakhstan a coordinating structure for the development of SWPP.

Thus, in our country there has been created a wide range of the most diverse designs and types of prototypes and models of SWPP - thanks to the enthusiasm and long-term efforts of physicists, mechanics and other scientists. Now it is necessary to complete the final stage of these samples to a high competitive level in order to enter their production.

Acknowledgements

This research was conducted in the framework of grant financing for the Committee of Science of the Ministry of Education and Science of the Republic of Kazakhstan under the project AP05135906 "Creating a technical prototype of a composite wind power plant with a diffuser".

REFERENCES

1 Abykayev N.A., Kuznetsov O.L., Berturganov N.S., Spitsyn A.T., Zeynullin A.A., Sheulin A.S. On the concept of sustainable energy development in Kazakhstan till 2050. *The Journal of Kazakhstan National Academy of Natural Sciences*. 2013, No. 2, pp. 5 - 34. [in Russian]

2 Garkava Ye. Wind power in Kazakhstan: yesterday, today, tomorrow: 2019. Available at: www.eenergy. media/2019/06/17/ vetroenergetika-kazahstana-vchera-segodnya-zavtra/

3 Ilyas B.N. JSC "KAZAKHSTAN OPERATOR OF THE ELECTRIC ENERGY AND POWER MARKET". - Results of the auction for the selection of SES projects held on September 24, 2019 with the total installed capacity of 30 MW. 2019. Available at: www.korem.kz/rus/press-centr/novosti_kompanii /?cid= 0&rid=8608

4 Kusaiynov K., Sakipova S.E., Tanasheva N.K., et al. *Wind generator based on the Magnus effect*. Patent RK No. 30462. Published 15.10.2015, 3 p.

5 Tanasheva N.K., Shrager E.R., Sakipova S.E., Dussembayeva A.N., Nurgaliyeva Zh.G., Karsybekov R.A. study of the aerodynamic characteristics of the wind generator based on the Magnus effect. *Bulletin of the Karaganda University. Physics Series.* 2017, No. 3, pp. 60 – 64.

6 Yershina A.K., Yershin Sh.A., Yershin Ch. Sh. Vertical-axial composite rotary wind turbine (options). Patent No. 20748. Published 16.02.2009. – Available at: www. kzpatents.com/0-pp20748-vertikal-no-osevaya-sostavnaya-vetroturbina-karuselnogo-tipa-varianty.html

7 Bolotov A.V., Bolotov S.A. Wind power unit and wind power plant. Patent No.12233. Published 16.08.2004, 10 p.

8 Bukukov N.S., Zhakyp A.K., Bukukov B. Zh., Moldabayeva G. Zh. Buktukov wind power plant 6 (options). Patent No. 27817. Published 18.12.2013, 10 p.

9 Kunakbayev T., Otelbayev M. On the determination of the minimum possible distance between three rotating carousel-type wind turbines. *Abstract of the International Conference "Computational and Informational Technologies in Science, Engineering and Education*". 2015, pp. 210 – 211.

10 Sabiyev S.Ye., Zhilkashinova A.M., Ocheredko I.A., Tuyakbayev B.T. Wind generator "Breeze". Patent No.29296. Published 15.12.2014, 3 p.

11 Brautman L., Krok R., Noton B., Keider K. *Composite materials. Volume 3: The use of composite materials in technology*. 1978, 512 p. [in Russian]

12 Ibrayev A. Power industry in Kazakhstan: yesterday, today, tomorrow. Astana, 2017, 12 p. [in Russian]

13 Bayshagirov Kh. Zh. A method for testing a small wind power plant installed on a movable stand. Patent RK No. 30566. Published 16.11.2015, 4 p.

14 Yershina A.K. et al. Analysis of development of wind power apparatus in Kazakhstan**.** ***Eurasian*** *phys. tech. j., 2016, Vol. 1*3, No. 2(26), pp. 98 – 106.

15 Povkh I.L. Technical hydromechanics. 2nd edition with additions. Leningrad, Mechanical Engineering. 1976, 504 p. [in Russian]

Article accepted for publication 09.12.2019

DOI 10.31489/2019No2/63-67

UDC: 621.311.24

SOME DESIGN FEATURES OF THE CAROUSEL TYPE WIND TURBINE BIDARRIEUS

Yershina A.K.[1], Sakipova S.E. [2], Manatbayev R.K.[3]

[1]Kazakh National Women's Teacher Training University, Almaty, Kazakhstan, ainakul.yershina@gmail.com

[2]E.A. Buketov Karaganda State University, Karaganda, Kazakhstan

[3]al-Farabi Kazakh National University, Almaty, Kazakhstan

The article presents the results of studies to improve the vertical-axis Darrieus type wind turbine with two coaxially located rotating shafts. Some design features of the symmetrical NACA-0021 airfoil are discussed. Both moving blades streamlined area scheme is shown. The brief description of the laboratory models of the carousel type wind turbine with HBI-rotor is given. It is shown that placement of a vertical-axis wind turbine at a certain height, above the surface boundary layer, can provide opportunities to further improve its effectiveness.

Keywords: wind turbine, NACA airfoil, Darrieus, Bidarrieus, HBI-rotor, surface boundary layer

Introduction

At present in economically developed and developing countries promising is the use of local renewable energy sources. In many countries, wind power has become the backbone of their strategies for phasing out fossil and nuclear energy. According to the official statistical report World Wind Energy Association on June 4, 2019 the total capacity of all wind turbines installed worldwide by the end of 2018 reached 597 Gigawatt [1, 2]. Now all wind turbines installed by end of 2018 can cover close to 6% of the global electricity demand.

The Republic of Kazakhstan is one of the richest countries of the world in terms of renewable resources, evaluated to over 1000 billion kWh/year [3-5]. Now in Kazakhstan the use of wind energy is significant increases because it is most affordable and relatively cheap in implementation. The relevance and need of the development of wind energy is due to also the fact that Kazakhstan has voluntary commitments to reduce greenhouse gas emissions on 15% by 2020 and on 25% by 2050. It is also due to the worn-out equipment of existing thermal power plants and to large volume of their harmful emissions into the atmosphere.

For the successful development of wind energy the government support and thorough study of the potential of wind energy are required. Research in this direction using modern technology is still relevant [3]. In general, according to experts, the potential for wind energy, which can be realized, is 10 times higher than in Kazakhstan's electricity demand. Nevertheless, until now, the total capacity of all existing wind farms in Kazakhstan is only 1% of the total electricity generation. This is due to several reasons, one of which is the low efficiency of existing wind plants.

Despite the wide variety of operating wind turbines of various manufacturers and well-known companies, the creation of highly efficient wind power units (WPU) operating in a wide range of wind speeds remains an urgent problem. This problem can be solved by developing methods for improving existing wind turbines. A basic design of HBI-rotor and an operation principle of the Bidarrieus-2 wind turbine were discussed [6-8]. Let's consider some design features of this carousel type wind turbine.

1. The symmetrical NACA – 0021 airfoil

Now the propeller-type wind turbines with installed capacity up to several megawatts are widely used. On the basis of many years of experience, the technology of creating a high-power WPU of a propeller-type wind turbine has been mastered [8, 9]. But practice shows that the higher the capacity of wind farms, the wider the lifeless territory in these regions (birds, fauna, including the population, leave these places). Also, the gyroscopic effect of a propeller wind turbine can lead to emergency situations [9]. More preferable are the carousel type Darrieus wind turbines, which have the symmetrical wing form NACA and operate on the lifting power of the blades [6, 9-13].

The overall dimensions of such devices are much less at the same values of the installed power. The material consumption and space occupied by these devices is much less than the propeller ones. At the wind turbine Darrieus the flow is uninterrupted, and as a result, its work is almost noiseless. Darrieus apparatus has the advantages over propeller wind turbines, because a symmetrical airfoil of NACA provide continuous flow of operating blades with wind stream and so the turbulence level of wind turbine decreases, Fig.1.

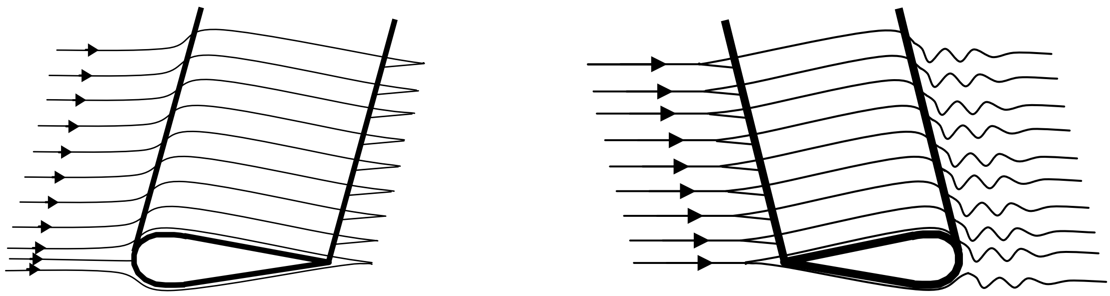

a) b)

Fig.1. The flow pattern of the symmetrical NACA – 0021 airfoil: a) - continuously under frontal direction of the wind flow; b) - tear-off flow under wind flow from blade tail side

The drag force of the NACA-0021 airfoil ξ_{xf} under φ =0 (Fig.1a) is small and equals:

$$\xi_{xf} = C_{xf}\rho\frac{U^2}{2},$$

where C_{xf} = 0.0028 is the drag coefficient.

Resistance of the same profile NACA-0021 to the wind flow directed to its trailing edge (turned towards) is an order of magnitude higher due to the separation flow (Fig. 1b):

$$\xi_{xb} = C_{xb}\rho\frac{U^2}{2},$$

where C_{xb} = 0.16.

According to previous static wind tunnel measurements of different tubercle configurations, the validation test for the optimum combination of and for NACA0021 was performed on an H-Darrieus wind turbine at various Reynolds numbers [11]. It was demonstrated experimentally that this blade could significantly increase the turbine self-starting capability at the expense of slightly lower peak power output, which was consistent with the numerical studies performed in [12].

These blades are very promising candidates for the future application in the low wind environment. Researchers continue to investigate blade profiles to Darrieus type wind turbine application [10, 11], but the results remain in conclusive and sometimes conflicting. The traditional symmetrical NACA series with large thickness still presents a simple but effective choice of blade geometry achieving a good compromise between good starting performance and adequate peak power operation.

Schematically streamlined areas of the blades are shown in Figure 2. It can be seen that the total streamlined area is obtained is almost 2 times larger than in a conventional Darrieus wind turbine. As a result, the amount of wind energy used by wind turbines with an HBI rotor should increase by 2 times [6, 7, 13].

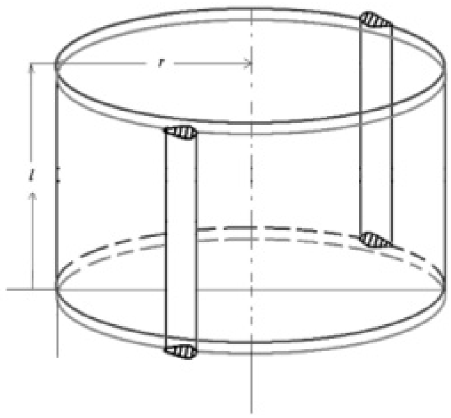

Fig. 2. Scheme streamlined areas of both working blades of the HBI rotor.

2. Testing models of the wind turbine HBI-rotor

A working laboratory and experimental version of the 5 kW kW HBI rotor wind turbine was designed and manufactured by research team of professor Sh.A. Yershin (photo in Fig. 3 a,b). Bidarrieus wind turbines with HBI rotor has two diametrically opposed blades, which are NACA wing profiles symmetrical with respect to the chord.

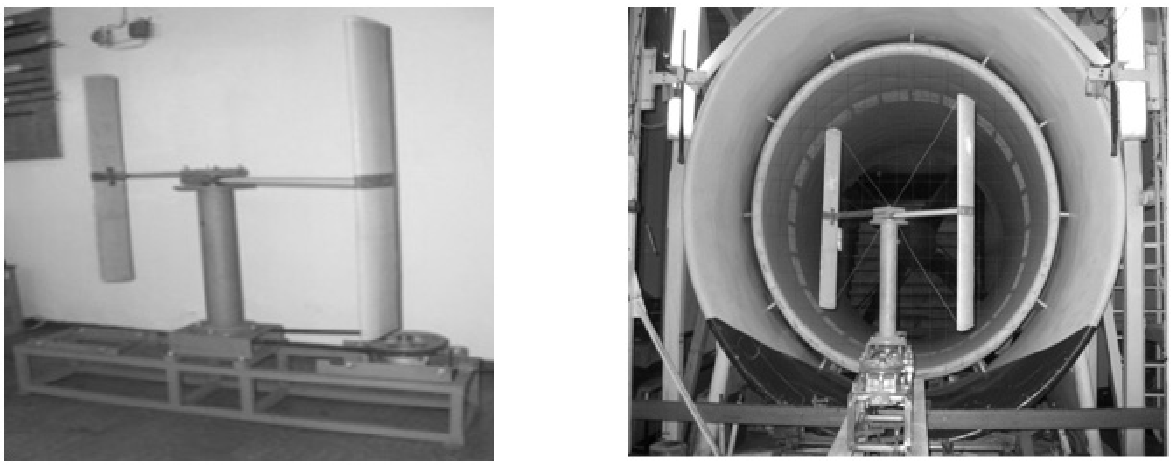

a) b)

Fig.3. Active laboratory model of wind turbines HBI-rotor:
a) main view; b) its location in the working section of the wind tunnel.

The experimental version of the Bidarrieus wind turbine of the HBI rotor has next dimensions: diameter of the wind turbine - 4 m, height - 5 m. Symmetrical blades NACA-0021, 2 m long and a chord of 0.5 m were used. The central shaft is connected by a half-span with one blade, the outer shaft with a half-span with the second blade which are located at an angle of 180° to each other. This position is determined using a special lock. The autonomy of the rotation of the shafts is provided by ball bearings separating them. An energy generator allows you to increase the total energy, get equipment. The energy generated by the two electric generators is summed up than usual [14, 15].

.

Tests of the developed semi-industrial Bidarrieus wind turbine with a 5 kW HBI-rotor showed the need for its placement at a certain height [15]. The fact is, outside the surface boundary layer where wind speeds are 2-2.5 times higher than the average wind speed in the surface boundary layer. Due to the cubic dependence of the wind turbine power on wind speed, the location of the wind turbine outside the surface boundary layer (20-30 m) will lead to a several-fold increase in the power of the wind turbine.

Therefore, the wind turbine should be installed at a height of 30 meters with the help of a light tripod above the surface boundary layer (Fig. 4). The tripod (1) is assembled from several I-beams, and for the strength of the structure, the tripod is fastened with several hoops (2).

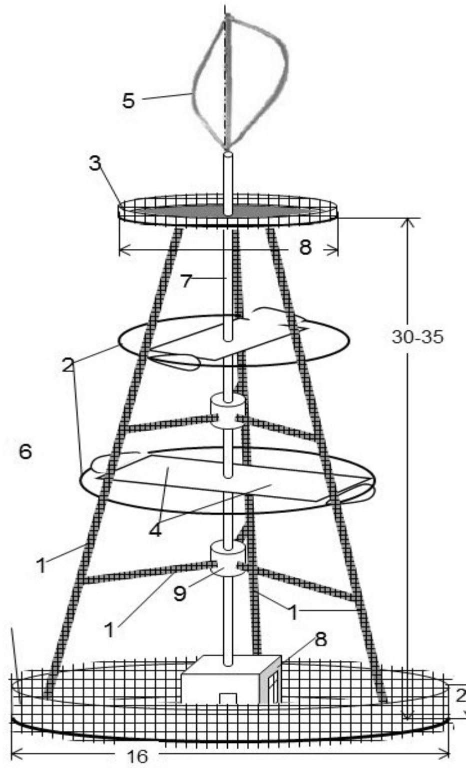

Fig. 4. Wind turbine with a vertical axis of rotation of the troposkino system (Darrieus with curved blades): 1 - tripod, 2 - hoops, 3 - mounting pad, 4 - NACA horizontal wing blades for stranding the wind turbines, 5 - wind turbines, 6 - guards for installation and batteries, 7 - rotation shaft, 8 – block for electric generator and batteries, 9 – bearings

Thus, there is reason to believe that the proposed option of a wind turbine with a capacity of 5kW will allow obtain an output power of up to 40-50 kW. At the same time, the economic performance of the construction is unlikely to affect the cost of the device. Unfortunately, due to force majeure circumstances, it has not yet been possible to conduct laboratory and field tests of these units.

Despite its geometrical simplicity, the aerodynamics of the Darrieus type wind turbine is complicated involving highly unsteady flow passing through its rotor [12]. The unsteadiness is caused mainly by the large variations of the blade angle of attack during the rotor operation. High rotor solidity (turbines with more than two blades) additionally contributes to the unsteadiness of the flow passing through the turbine by increasing the angle of attack fluctuations [14]. Wind turbines should provide stability for the extraction of wind energy. The use of brake pads, which automatically regulate the rotation of the shaft, up to its complete stop at drilling wind speeds, is supposed.

Conclusion

The vertical axis carousel type wind turbine Bidarrieus with HBI-rotor is one of the most promising wind energy converters for locations where there are rapid variations of wind direction, such as in the built environment. The most challenging considerations when employing one of these usually small machines are to ensure that they self-start and to maintain and improve their efficiency. However, due to the turbine's rotation about a vertical axis, the aerodynamics of the turbine are more complex than a comparable horizontal axis wind turbine and our knowledge and understanding of these turbines falls remains far from complete.

This carousel type two-rotor wind turbine Bidarrieus-2 has a low rotation speed. This allows it to work at high velocities of wind and the operating terms will not be limited practically. All this makes it important and necessary to carry out full-scale tests of these WPUs in order to ensure their industrial production in the future.

REFERENCES

1 World Renewables 2019. Global Status Report. https://www.ren21.net/reports/global-statusreport/

2 World Renewables 2018 Global Status Report (GSR). World Wind Energy Association, June 4, 2018. Available at: http://wwindea.org/11961-2/

3 Karatayev M., Hall S., Kalyuzhnova Y., Clarke M. Renewable Energy Technology Uptake in Kazakhstan: Policy Drivers and Barriers in a Transitional Economy. *Renewable and Sustainable Energy Reviews*. 2016, Vol. 66, pp. 120 – 136.

4 Mukhamediyev I.R., Mustakayev R., et al. Multi-criteria spatial decision making system for renewable energy development support in Kazakhstan. *IEEE Access.* 2019, Vol. 7, pp. 122275-122288.

5 Yershina A.K., Nursadykova Zh.K., Borybaeva M.A. Analysis of development wind power apparatus in Kazakhstan**.** *Eurasian phys. tech. j.* 2016, Vol. 13, Issue 2(26), pp. 99 – 106.

6 Yershina A.K., Manatbayev R.K., Sakipova S.E., Kalasov N.B. Improving the efficiency of wind turbine. *Proceeding of the 2nd Intern. Scient. Conf. "Alternative Energy Sources, Materials & Technologies (AESMT'19)*, Sofia, Bulfaria. 2019, Vol. 1, pp. 89 – 90.

7 Yershin Sh., Yershina A.K. About High efficiency of two-rotor wind power unit Bidarrieus-2. *Eurasian phys. tech. j.* 2019, Vol. 16, Issue 1(31), pp. 82 – 87.

8 Kayan V.P., Kochin V.A., Lebid O.G. Studying the Performance of Vertical Axis Wind Turbine (VAWT) Models with Blade Control Mechanism. Intern. *Journal of Fluid Mechanics Research*, 2009, Vol.36, Issue 2, pp. 154 – 165.

9 Bezrukikh P.P. *Ispol'zovanie energii vetra.(Wind power use)*. Moscow, 2008, 196 p. [in Russian]

10 Hashem I., Mohamed M.H. Aerodynamic performance enhancements of H-rotor Darrieus wind turbine. *Energy*, 2018, Issue 142, pp. 531 – 545.

11 Ma N., Lei H., Han Z., et al. Airfoil optimization to improve power performance of a high-solidity vertical axis wind turbine at a moderate tip speed ratio. *Energy*, 2018, Issue 150, pp. 236 – 252.

12 Longhuan Du, Ingram, Grant Dominy R. A review of H-Darrieus wind turbine aerodynamic research. *Journal of Mechanical Engineering Science*. 2019, Vol. 233, Issue (23-24), pp.7590-7616.

13 Yershina A.K., Yershin Sh.A., Yershin Ch.Sh., Manatbayev R.K. Wind motor. Kazakhstan Republic Patent No. 31662, 2016, Bulletin 15, 3 p. [in Russian]

14 Sungjun Joo, Heungsoap Choi, Juhee Lee. Aerodynamic characteristics of two-bladed H-Darrieus at various solidities and rotating speeds. *Energy.* 2015, Vol. 90, Issue P1, pp. 439 – 451.

15 Yershina A.K., Yershin Ch.Sh. Progressive innovations in applying of wind energy. *Journal of Intern. Scientific Publications: Materials, Methods & Technologies*. 2013, Vol. 7, Part 3, pp. 4 – 12.

Article accepted for publication 22.11.2019

DOI 10.31489/2019No2/68-73

UDC 662.642.2

IMPROVING FUEL PROPERTIES USING THE FGX-12 CRUSHING AND SCREENING COMPLEX

Shaimerdenova K.M., Shunkeyev T.A., Ospanova D.A.

E.A. Buketov Karaganda State University, Karaganda, Republic of Kazakhstan, gulzhan.0106@mail.ru

The method of improving the quality of coal by using a combined dry enrichment machine was considered. The description of combined dry enrichment machine, intended to process the run-of-mine coal from the Sarykol deposit of the Maikubensky lignite basin, was given. A coal concentrate, middlings and other enrichment products which were received as a result of processing, are accumulated in the warehouse. The main aim of the enrichment machine is to improve the qualitative characteristics of brown coal and, first of all, is an increase of coal calorific value (heat of combustion) and a reduction in ash content. As a result of enrichment, the shelf life of coal increases from 3 to 6 months.

***Keywords*:** coal processing, enrichment, increase of calorific value, brown coal.

Introduction

The competence of the Sarykol surface coal mine is 3.0 million tons of coal per year, and is provided by industrial reserves and by productivity, quantity and layout of mining equipment. But, as following from the current situation on the brown coal market of the Maikubensky lignite basin, the need for run-of-mine coal from the Sarykol deposit does not currently exceed 0.7-1.0 million tons of coal per year. Taking into account marketing research of the brown coal consumption market and the possible prospects for the energy complex development in the Republic of Kazakhstan, was proposed a variant of improving the consumer properties of coal by dry enrichment. The enrichment of the mined fuel makes it possible to improve the quality characteristics of the final product and, accordingly, expand market outlets within the country and also beyond its borders.

Studies and recommendations for the enrichment of coals in the Maikubensky lignite basin included traditional enrichment methods in heavy medium, as well as the wet enrichment method. But for enrichment in heavy medium, additional materials such as zinc chloride and bromoform are needed, as well as magnetite weighting agent, which undoubtedly entails additional financial costs for the purchase and delivery of the required raw materials. After enrichment of the first lot of coal, magnetite becomes off-specification. To extract magnetite for reuse, off-specification suspension is regenerated, which also leads to additional energy costs and loss of time. In case of the wet enrichment method, a large amount of water is required, as well as apolar reagents: kerosene, diesel fuel, oil refining intermediates, which are additional costs and are rest on the final cost of product. But since there are no ponds nearby, there is a shortage of industrial water at the surface coal mine. In addition, the increased sludge formation and high soak ability of Maikubensky coals make both methods absolutely not working in this particular case. In other words, if we compare all three methods of coal enrichment, then only dry enrichment can be called the most economical, compact and efficient method [1].

For these purposes, a combined dry enrichment machine of the type FGX-12 manufactured by the PRC was purchased. The modern layout and implementation of foreign equipment has significantly reduced energy consumption and harmful effects on the environment. The possibility of separation in the air makes the entire process as simple as possible. There is no need to build capital-intensive buildings; it is enough to complete the installation in the open air. In order not to raise the rock mass, the combined dry enrichment machine can be installed in surface coal mine [2].

1. Technological scheme and basic equipment

In crushing and screening complex the enrichment process is carried out due to a self-produced medium (fine particles of coal enriched). The accuracy of the enrichment process and the productivity of given separators is much higher than that of traditional dry enrichment separators.

Moreover, this method is characterized by:
- the simplicity of enrichment schemes, low capital costs;
- the lack of need for water and obtaining dry products;
- the low final cost of the processing process and low energy consumption.

Effective dust removal meets the requirements of environmental protection. There is high yield of marketable coals. No sludge compared to wet enrichment methods. Fine coal particles are collected by dust collecting devices. The operating practice shows reliable work, lack of easily damaged parts. The technological scheme of the crushing and screening complex (CSC) is shown in Fig. 1 [3].

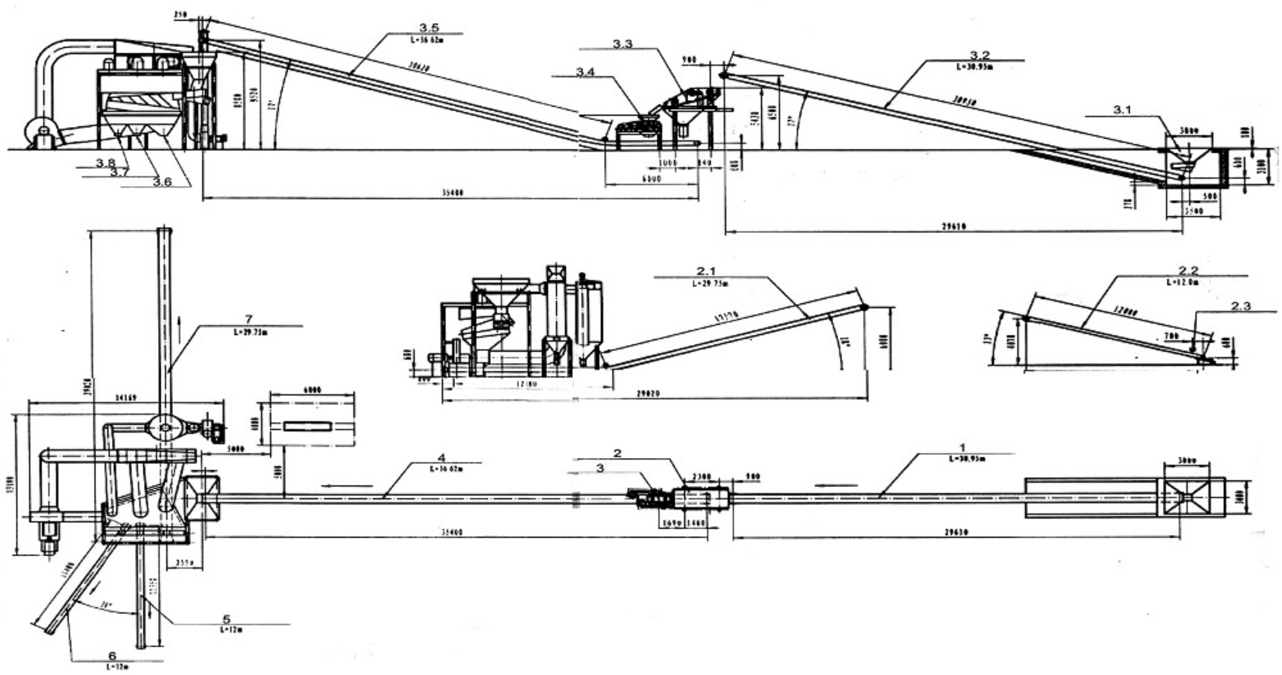

Fig.1. Crushing and screening complex (CSC):
1 - belt for screening Ш - 800 mm; 2 - screening SZD 1536 diameter - 80 mm; 3 - crusher 2PGF6550; 4 - belt for FGX Ш-800 mm; 5 - belt for middling Ш-500 mm; 6 - tape for solid Ш-500 mm; 7- tape for concentrate Ш-800 mm; 2.1- tape for concentrate Ш-800 mm; 2.2 - tape for solid (middling); 2.3-place of the fall of solid (middling); 3.1-receiving hopper and feeder; 3.2 - belt for screen Ш - 800 mm; 3.3 - screen SZD 1536 diameter - 80 mm; 3.4 - crusher 2PGF6550; 3.5-belt for FGX Ш-800 mm; 3.6- concentrate yield; 3.7 - middling yield; 3.8-solid yield.

The combined dry enrichment machine includes the following component parts:
- combined dry enrichment machine FGX-12;
- a funnel of the coal receiving device with a feeder;
- belt conveyor of run-of-mine coal;
- vibrating grit;
- roll crusher;
- belt conveyor for feeding sorted coal to a combined dry enrichment machine;

- belt conveyors for feeding enrichment products to accumulative warehouses;
- control cabin;
- control cabinet, cable products, bridge frame, fastenings.

The appearance of the combined dry enrichment machine of the type FGX-12 is shown in Fig.2 [4].

Fig.2. Combined dry enrichment machine of the type FGX-12 (main view)

Technical characteristics of the combined dry enrichment machine are shown in table 1.

Table 1. Technical characteristics of CDEM

Model	FGX-12
Coarseness of coal enriched	0 - 80 mm
External humidity	0 - 9 %
Performance	120 per hour
Coefficient of efficiency	More than 90 %
Total power	410 kVt
Dimensions (L×W×H)	15.0×13.0×10.0m

The processing and loading complex is a group of structures and installations, united by the technological process. The operation of the pneumatic concentration plant (separator of dry enrichment FGX-12) is based on the dry enrichment method. The performance of the concentration plant is 120 m^3 / hour. The performance of the main fan is 24-30.4 m^3 / s.

The outlet air pressure is 6.540-6.440 kPa. The separator has its own aspiration system, eliminating fugitive emissions of coal dust. For processing, coal from a receiving warehouse is supplied with a bulldozer or a loader to the horizontal part of the over loader. The over loader, lifting the coal to a height of 6.5 m, feeds it for processing to screening. From under the screen (to prevent over milling and excessive utilization of the FGX-12 unit), fines of the 0-13 mm class are fed by a belt conveyor to the coal fines warehouse. Coal from the screen, class 13-300 mm, is fed to the crusher and then, after crushing to class 50-60 mm, by a belt conveyor into the receiving hopper of the FGX-12 dry concentration plant.

From the FGX-12 dry concentration plant, the products obtained are transported: concentrate - delivered to the concentrate warehouse by a belt conveyor, warehouse formation, shipment by truck or excavator to dump trucks; middling - it is delivered to the middling warehouse by a belt conveyor, the formation of the warehouse, and shipment is carried out by a loader or excavator to dump trucks; solid - it is delivered to the solid warehouse by two belt conveyors, the formation of the warehouse, and shipment is carried out by a loader or excavator to dump trucks [5].

The technological scheme of processing run-of-mine coal on a combined dry enrichment machine includes the following operations:

- preliminary screening of small fractions (0-80 mm) on a vibrating grit;
- crushing of material with a particle size of 80-200 mm in a roll crusher;
- enrichment of run-of-mine coal.

Stationary belt conveyors with a belt width of 800 mm are used to transport material from the unit to the unit. Technological equipment is characterized by:

- increased productivity due to new construction solutions;
- high reliability and safety in operation.

The list and technical characteristics of the main technological equipment are given in Table 2 [6].

Table 2. Technical characteristics of the main technological equipment

No	Name	Technical characteristic	Quantity
1.	Coal funnel with feeder	$V = 5\ m^3$	1
2.	Round vibrating grit	The surface area is 5.4 m^2, the number of layers is 1, the vibration frequency is 850 times / min, the amplitude of one vibration is 3.5 mm, and the maximum size of the feedstock is 200 mm.	1
3.	Roll crusher	The dimensions of the slugging rolls: diameter - 650 mm, length - 600 mm, grain size of the starting material - 80-200 mm, grain size of the product - 0-80 mm, productivity - 80 t / h.	1
4.	Combined dry enrichment machine FGX-12	The working surface area is 12 m^2, the size of the enriched coal is 0-80 mm, the productivity is 80 t / h, the enrichment efficiency is 90%.	1
5.	Belt conveyor of run-of-mine coal with supporting structures, platforms, ladders, loading and unloading trays	Belt width - 800 mm, conveyor length - 30.95 m, feed fineness - 0-200 mm, belt speed - 1.4 m / s, installation angle - 17 *	1
6.	Belt conveyor for feed to the dry enrichment machine with supporting structures, platforms, ladders, loading and unloading trays	Belt width - 800 mm, conveyor length - 36.62 m, feed fineness - 0-80 mm, belt speed - 1.4 m / s, installation angle - 17 *	1
7.	Belt conveyor of concentrate with supporting structures, platforms, ladders, loading and unloading trays	Belt width - 800 mm, conveyor length - 29.75 m, feed fineness - 0-80 mm, belt speed - 1.4 m / s, installation angle - 17 *	1
8.	Belt conveyor of waste and middlings with supporting structures, platforms, ladders, loading and unloading trays	Belt width - 500 mm, conveyor length - 12.00 m, feed fineness - 0-80 mm, belt speed - 1.4 m / s, installation angle - 17 *	2

.

2. The principle of operation of the combined dry enrichment machine and the actual productivity of the equipment

Run-of-mine coal of a fraction of 0-200 mm enters a coal receiving funnel with a feeder and at a certain speed starts moving up the conveyor belt towards the grit. Getting on a vibrating grit , coal of a fraction of 0-80 mm is immediately sifted and sent to enrichment on the next conveyor belt, and the remaining coal of a fraction of 80-200 mm goes to a roll crusher, where coal is crushed to a fraction of 0-80 mm and also, then sent for enrichment. Getting into the dry processing unit, coal is laid out on a vibrating grit, which is at a slope of 30 degrees. Compressors are installed under the grit. After the enriched coal got on grit, the process of enrichment of coal begins due to the action of a two-phase medium (from small particles in the initial coal and air) with a relatively higher specific gravity. Strong vibration and constant ascending air streams increase the looseness of the entire mass and exfoliate the material by density. Strong air currents lift small particles of dust up, which are then sent to the dust collector. Also, due to air flows, the process of exfoliation of the rock and clay from coal occurs, which leads to an improvement in coal performance.

The broken rock and clay, under the influence of vibration and air currents, begins to move up the vibrating grit and, moving along the unloading side, falls onto a conveyor belt intended for waste. Ultimately, on vibrating grit remains 0-80 mm fraction coal, purified from fine dust, rock and clay. Refined coal is enriched, as its quality characteristics are significantly improved [3-4]. The CDEM workflow is shown in Figure 3, [7].

In the period from 2016 to 2019, 509.76 thousand tons of run-of-mine coals were processed on a combined dry enrichment machine, of which 146.88 thousand tons of enriched coal and 362.88 thousand tons of middlings. A coal prepared for enrichment has the following basic characteristics: heat of combustion (calorific value) - 3500 kcal / kg, ash content - 23.5%, moisture - 19.5%. Having passed all stages of dry enrichment, the product significantly improves its characteristics and already has the following parameters: heat of combustion (calorific value) - 4300 kcal / kg, ash content - 19%, moisture - 14.5%.

A comparative analysis of the improving the quality of coal by using a combined dry enrichment machine results is shown in Figure 4, [8]. The N is a change of the coal indicators. The N value is calculated as the ratio of the initial basic characteristics indicators to finished products indicators.

Fig.3. The CDEM workflow [7]

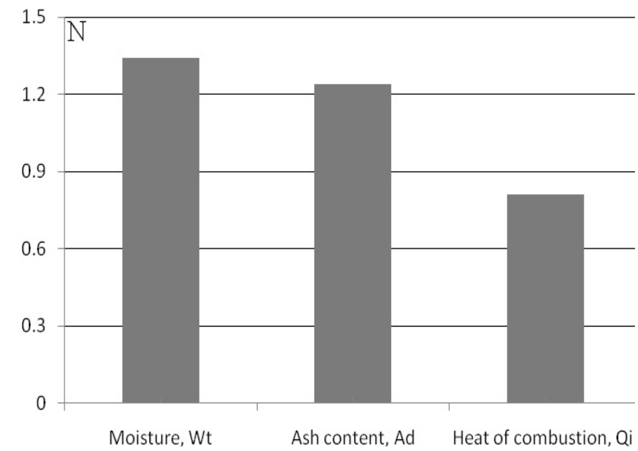

Fig.4. Comparative analysis of the results in the period from 2016 to 2019

Using this method, the moisture and ash content of coal decreased, as a result of which the heat of combustion of coal fuel from the Sarykol deposit increased.

Conclusion

Thus, the combined dry enrichment machine of the type FGX-12 is the most effective when working with brown coals, since none of the other methods of coal enrichment showed such an improvement in the characteristics of coal.

Coal processing reduces ash content and significantly increases the power output of the station, reduces harmful emissions into the environment. The quality of the burned coal affects the power of the station, and the chemical composition of the ash affects the operational parameters of the furnace. The process of coal enrichment, which is based on the use of various physical forces, changes the characteristics of run-of-mine coal in the direction that most meets the requirements of the market.

There is a trend in the world when coal consumers for energy purposes tighten requirements for coal producers to reduce coal moisture, its ash content and lower sulfur content. So, there are Government programs to reduce the ash content of mined coal, which involves not only a significant increase in calorific value of fuel, but also allows to solve environmental problems associated with reducing emissions of pollutants into the environment by more than 2 times.

REFERENCES

1 Yong X. et al. *FGX – 12 Installation and operating instructions for Sheng Zhou Engineering Plant*. 2016, 213 p.

2 Rybtsov K.N., Dzyubenko A.L. *Project for the construction and operation of a combined dry enrichment machine*. LLP "Karagandagiproshakht and K". 2016, 217p. [in Russian]

3 Fuel enrichment technologies. Available at: www.iqtec.pro/ru/projects-2/thermal-electric-stations/fuel-enrichment. 12/23/2019. [in Russian]

4 Usoltseva I. A., Peredery J. V., Krylenko R. I. Dry coal enrichment technology from the Korea Institute of Geo science and Mineral Resources (KIGAM). Available at: www.natd.gov.kz/wp-content/uploads/2015/08/Obzor-1.pdf. [in Russian]

5 Pulyaev V. The equipment for enrichment of coal. Available at: www.china-bridge.ru/oborudovanie-dlyaobogashheniya-uglya. 2/25/2019. [in Russian]

6 Technology of dry enrichment of coal from the company Osborn (South Africa). Electronic article. Available at: www.mining-media.ru/ru/article/obogach/684-tekhnologiy-sukhogo-obogashcheniya-uglya-ot-kompanii-osborn-yuar. 12/25/2019. [in Russian]

7 Stepanenko A.I. Dry enrichment - pneumatic separation complex “SEPAIR®”. Available at: www.gmexp.ru/netcat_files/340/531/4cea1ac90c68d791b 7c8e24172892507. 12/25/2019. [in Russian]

8 Shunkeev T.A., Shaimerdenova K.M., Imanasova N.V., Ospanova D.A., Rakhmankyzy A. Improving the quality of coal by using a combined dry enrichment machine. Proceeding of the 11th Intern. Scientific Conf. “Chaos and Structures in Nonlinear Systems. Theory and Experiment”. Karaganda, 2019, pp. 311 – 314.

Article accepted for publication 09.12.2019

.

DOI 10.31489/2019No2/74-77

UDC 621.7

STUDY OF THE RHEOLOGICAL PROPERTIES OF THE PLASTICIZER TO OBTAIN A COAL-WATER SLURRY

Tanasheva N.K.[1], Minkov L.L.[2], Tleubergenova A.Zh.[3], Sadenova K.K.[3]

[1] Institute of Applied Mathematics, Karaganda, Kazakhstan
[2]Tomsk State University, Tomsk, Russia
[3] E. A. Buketov Karaganda State University, Karaganda, Kazakhstan, shymkent.a7@mail.ru

The article presents the results of the study of the impact of plasticizers on the stability of coal-water suspensions obtained from Shubarkul coal slurries. As part of the task to determine the optimal reagent-plasticizer, an experimental installationwas developed. Fuel oil, gelatin, sodium humate were used as reagents-plasticizers. The process of enrichment of coal slurries of Shubarkul Deposit was studied; it is shown that the best results are obtained with the use of sodium humate. The use of sodium humate as a plasticizer makes it possible to create coal-water suspensions with a spatial network-like structure that do not delaminate for a long time.

Keywords: *electro-hydro-impulse installation, Shubarkul coal, coal-water fuel, plasticizer reagent, ultrasonic dispersant.*

Introduction

In the first half of the XXI century, it is to predict to increase the role of coal in the energy sector, due to its large reserves and depletion of oil and gas. At the same time, environmental problems arising from the use of coal fuel require the development and implementation of new economically and environmentally efficient coal technologies that will provide a significant environmental effect with the highest possible completeness of the use of the extracted fuel. Around many coal mining and coal processing enterprises, a large amount of extracted coal is accumulated in hydraulic dumps and sedimentation tanks, presented in the form of fine coal slurries, the transfer of which into a technologically acceptable fuel will not only improve the environmental situation in the regions, but also obtain a significant economic effect.

In this regard, it becomes relevant to use slurries in the form of coal-water suspensions (CWS), the development of effective processes for the production and application of which should be based on science-based processes of physical and physical-chemical effects on the source coal, taking into account the properties of its organic and mineral components [1]. CWS are mixtures of crushed coal with water. To give the suspension the properties of stability and the necessary fluidity, a small amount of reagent-plasticizer is introduced into the suspension. As a result, an artificial dispersion system is formed, representing a new type of fuel from coal – coal-water fuel (CWF).

The advantages of CWS as an ecological clean fuel are as follows:

- explosion prevention and fire safety in all technological operations (preparation, transportation, storage and use);
- absence of dust and pollution during storage and transportation; reduction of harmful emissions of nitrogen oxides, carbon and sulfur into the atmosphere during combustion.

In addition, CWS provide safety of technological properties during storage and transportation. At the same time, the decline in oil and gas production and the increase in their prices on the world and domestic markets in recent years have caused interest in CWF - a real alternative to liquid and gaseous organic type fuels.

The aim of this work is to study the rheological properties of reagents for stabilization of CWS. The object of study in this work is the coal of Shubarkul Deposit.

1. Experimental procedure

The essence of the processes of preparation of Shubarkul coal slurries for use in CWS consists in their electro-hydro-impulse (EHI) treatment and further enrichment by the method of ultrasonic (US) agglomeration (since other methods of enrichment are not acceptable due to the low selectivity of these processes during enrichment due to the fine state of coal particles). Electric discharges in the liquid, which are a source of shock waves, are used to grind particles of coal slurries from the Shubarkul Deposit and obtain finely ground fractions of specified sizes. Shock waves propagating in the medium of liquid-solid coal particles destroy and grind the treated coals to small fractions, necessary for obtaining coal-water fuel.

In order to select the most effective plasticizers for CWS prepared from coal slurries, the influence of the following plasticizers was studied: gelatin, fuel oil, sodium humate obtained from coal. These reagents meet the requirements for plasticizing reagents and are readily available. The effectiveness of these additives is due to their physical and chemical properties, the peculiarity of their structure, consisting of hydrocarbon, aromatic, carboxyl, hydroxyl and other groups [2].

For experimental works on obtaining CWF in the laboratory of physics of pulsed phenomena in heterogeneous media of the Department of Engineering Thermophysics named after professor Zh.S. Akylbayev, electrohydropulse installation with the ultrasonic flow disperser was collected (Fig.1).

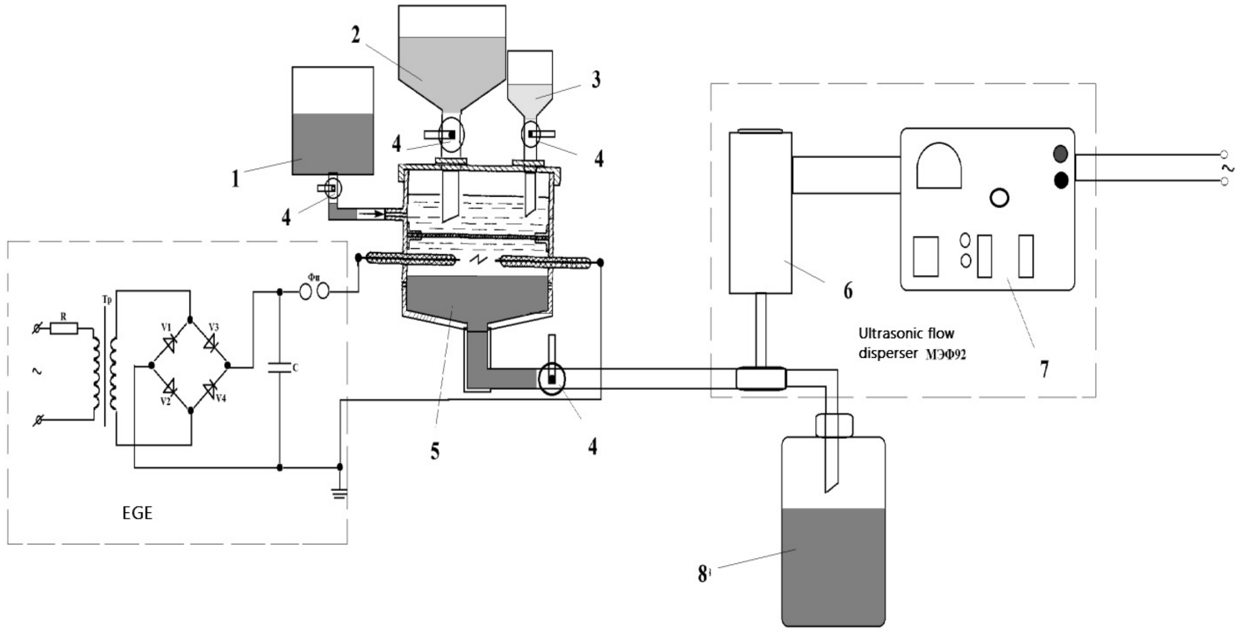

Fig.1. Schematic scheme of EHI installation with ultrasonic flow disperser:
1 – water tank, 2 - capacity for coal, 3 – tank for reagent - plasticizer, 4 – a valve for regulating ,
5 – working cell with two opposite electrodes, 6 – ultrasonic flow transducer, 7 – the control unit of the dispersant, 8 – tank with WCF.

To create electro-hydraulic shocks, a scheme that includes a power source with a capacitor as a storage of electrical energy, is assembled. The voltage on the capacitor rises to a value at which there is a spontaneous breakdown of the air forming gap, and all the energy stored in the capacitor instantly enters the working liquid gap, where it is released in the form of a brief electric pulse of high power. Further, the process is repeated at a given capacitance and voltage with a frequency depending on the power of the supply transformer and the electrical and physical characteristics of the medium in the inter electrode gap [3].

The EHI installation works as follows, the prepared coal slurries were sent to the working cell, where there was an underwater electrical explosion in the presence of a plasticizer. As a result of EHI treatment coal-water suspension sent to the enrichment installation, the principle of operation of which was based on the method of ultrasonic agglomeration. The ultrasonic dispersant consists of a flow transducer and a control unit. The dispersant performs the function of additional crushing, where a chemical bond is formed between resulting suspensions. The resulting fuel is drained into the tank.

2. Experimental results

As a result of the performed enrichment studies, graphical dependences were obtained, which are presented in Fig.2-4.

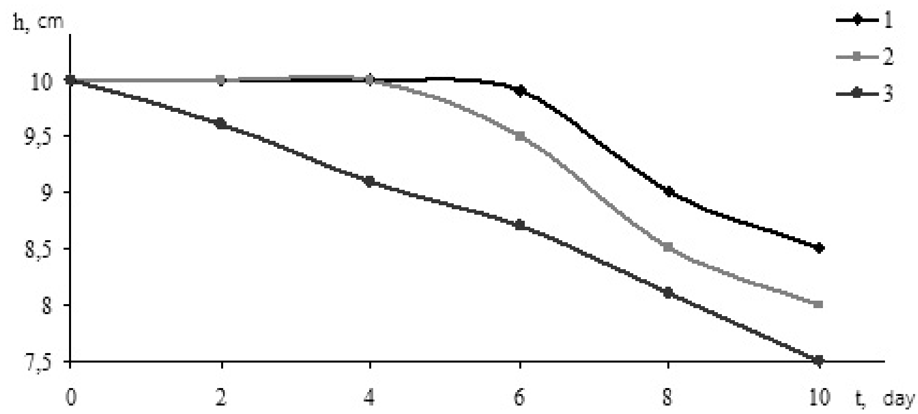

Fig.2. Dependence of the height of the dispersed phase layer on time
(suspensions with additives of fuel oil of various quantity):
1 – 1 % to weight of coal; 2 – 0.5 % to weight of coal; 3 – 2.0 % to weight of coal

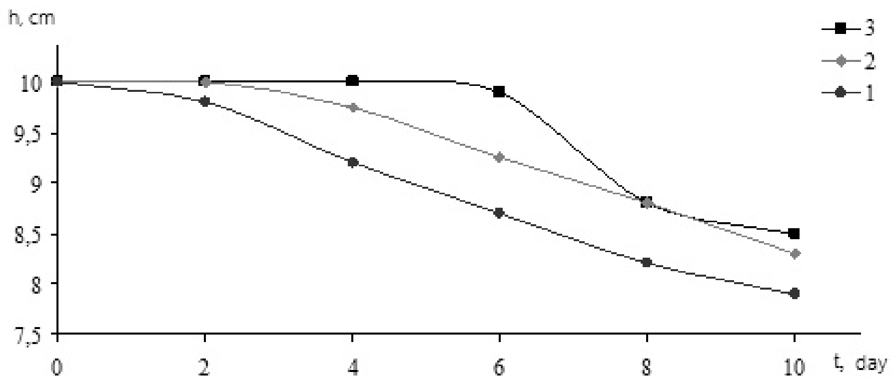

Fig.3. Dependence of the height of the dispersed phase layer on time
(suspensions with gelatin additives of various quantity):
1 – 0.5 % to weight of coal; 2 – 1.0 % to weight of coal; 3 – 2.0 % to weight of coal

Organic compounds and technology of metered addition of the found compounds to the mass of CWF are selected. The process of formation of spatial structure of CWS is investigated, their rheological properties are studied, it is established that stability of CWS, received on the basis of concentrates, is defined by physical and chemical properties of plasticizers. It should be noted that suspensions in the presence of additives have good fluidity. From the graph it can be seen that with the addition of fuel oil in the amount of 1%, the CWS had stability for a long time.

Suspensions with the addition of gelatin (Fig.3) from 2 % to weight of coal had stability for a long time, however, when the gelatin content is less than 1.0% to weight of Shubarkul coal, there is a noticeable decrease in the stability of suspensions.

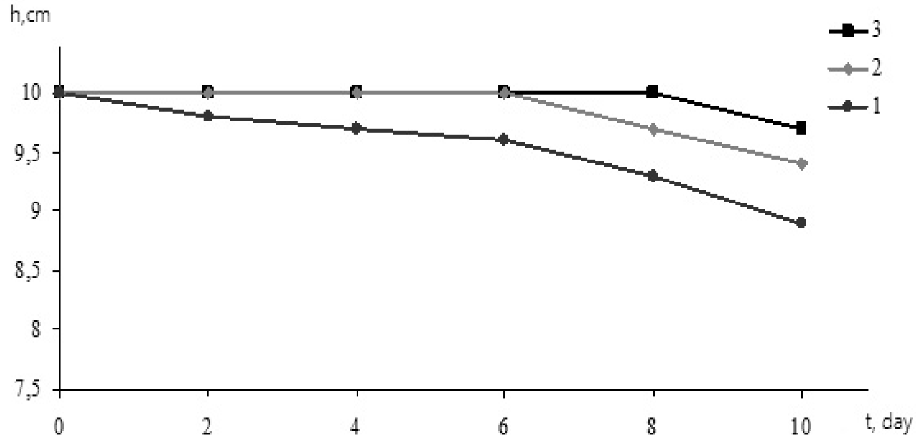

Fig.4. Dependence of the height of the dispersed phase layer on time (suspensions with various quantity of sodium humate additives):
1 – 0.5 % to weight of coal; 2 – 2.0 % to weight of coal; 3 – 1.0 % to weight of coal

Application as a stabilizer of humic preparation (Fig.4) (sodium humate) made it possible to obtain a stable CWS with stable and practically unchanged properties in time. The stability of CWS was maximal when using from 1% sodium humate to coal weight. After a very long storage, CWS were compacted to form loose sediments. When applying mechanical action (mixing) was the restoration of the original structure of the suspension.

Conclusion

Thus, on the basis of the results of the study, it was found that the addition of a stabilizer-sodium humate in the amount of 1% of the mass of coal-oil granules is due to the fact that at this rate, CWF has better stability. It is established that the stability of CWS obtained on the basis of coal-oil concentrates is determined by the physical and chemical properties of the reagents-plasticizers.

Acknowledgment
This work was financially supported by the RFBR project Mol_nr 19-38-50058

REFERENCES

1 Khodakov G.S. Suspension coal fuel (modern stage of research, technologies and industrial implementations). *Izvestiya Akademii Nauk. Energy*. 2000, No.2, pp.104 – 119. [in Russian]
2 Krapchin I.P. Economic efficiency of preparation and use of coal-water suspensions-environmentally friendly fuel for power plants. *Coal*. 2003, No.11, pp. 50 – 52.
3 Kussaiynov K., Tanasheva N.K., Tolynbekov A., Alpysova G., Tleubergenova A. The research of burning technology of water coal fuel got from Shubarkul coal. *Eurasian Physical Technical Journal*. 2014, Vol.11, No. 1(21), pp. 7 – 11.

Article accepted for publication 22.11.2019

DOI 10.31489/2019No2/78-82

UDC 621.891

POTENTIAL DIFFERENCE OF METAL MACHINE PARTS METHODOLOGY FOR DETERMINING THE PARAMETERS OF ADHESIONAL PROPERTIES OF MATERIALS ON THE SMC-2 FRICTION MACHINE

Kubich V.I.[1], Cherneta O.G.[2], Yurov V.M.[3]

[1] National University "Zaporizhzhya polytechnic", Zaporizhia, Ukraine, schmirung@gmail.com
[2]Dniprovsk State technical University, Kamenskoye, Ukraine, ocherneta@gmail.com
[3] E.A. Buketov Karaganda State University, Karaganda, Republic of Kazakhstan, exciton@list.ru

The paper develops the idea of the capabilities of a standard machine for testing materials for friction and wear SMC-2 to determine the parameters of the adhesive properties of materials. The results of experimental studies of tribological systems of materials "40X - steel 45", "12X2H4 - steel 45", "45XH2MФA - steel 45" are presented. The regularities of the change in the tangential strength of the molecular bond with increasing pressure in the contact, and the coefficients of its hardening during the interaction of the materials under consideration without lubrication are determined. It is shown that in order to reproduce the contact interaction of the operational surfaces of real friction units, it is possible to simulate their shear during deformation provided that full-size fragments placed in regular places of the SMC machine are used. In this case, the equipment of the SMC machine requires minor refinement, which allows us to simulate the shear rate of surfaces as well.

***Keywords*:** tribosystem, adhesion, hardness, coefficient of friction, wear, contact

Introduction

The study of the strength of the adhesive bond between the structural components of the surfaces of parts in tribological conjugations of various engineering objects always seems relevant, since the process of managing both bulk and surface physical and mechanical properties of materials with a wide range of applications is currently not completed. This is evidenced by the scientific results presented in [1-4] and other authors. Along with this, new adhesiometers are being developed and designs of earlier years of production are being improved [5].

Based on the fact that the contact interaction of metal surfaces during the transmission and transformation of movements is carried out with friction losses, which are determined by the molecular and mechanical components, the determination of the parameters of the latter seems to be an actual scientific and applied task. It is especially important to have numerical values of the parameters of adhesive properties directly for the metal surfaces of full-scale operational friction units of machines and mechanisms with reverse movement, i.e. in which there is a shift with a certain speed of movement, when the manifestation of the molecular (adhesive) component of the friction force manages to manifest itself.

The limited information on the manifestation of the parameters of the molecular component of friction — the shear strength of the adhesive bond τ_0 and the piezoelectric coefficient β of the molecular component for each particular study determines the use of either data previously obtained for similar materials, or the purposeful determination of parameters by modeling shear on small-sized samples in order to increase objectivity and accuracy evaluation of the result. The data obtained seem necessary, first of all, for the predictive assessment of the tribomechanical properties of material tribosystems using mathematical expressions that establish the relationship between the friction coefficient and parameters of the contact microgeometry, adhesion component, hardness, and load during the manifestation of elastic, plastic, elasto-plastic deformation of friction zones interactions.

Objective **-**introducing the capabilities of a standard machine for testing materials for friction and wear SMC-2 to determine the parameters of the adhesive properties of materials.

1. Research methodology

It is proposed to determine the parameters of the molecular component in accordance with the method of work on the OT-1 adhesio-meter [6] and on a device using a spherical indenter [1], which involve measuring the friction moment Mt during shear — a violation of the frictional bond of spherical surfaces to flat surfaces of samples (plates) and the radius (diameter) of the projection of the print R0 (d).

However, the simulation of the frictional bond violation will be carried out when shifted from the disk relative to the block, made, for example, in the form of a triangle with a cylindrical outer surface, with the corresponding loads (Fig. 1a) with the corresponding modification of the lower shaft drive.

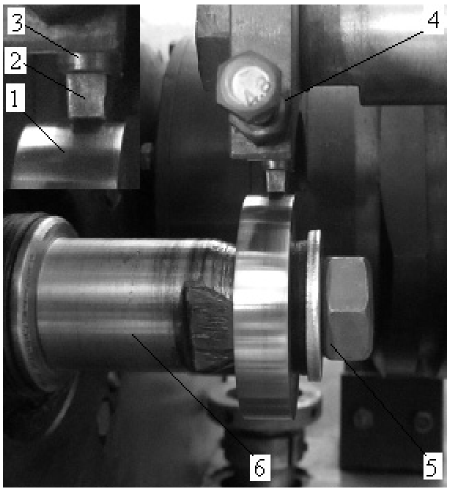

a)

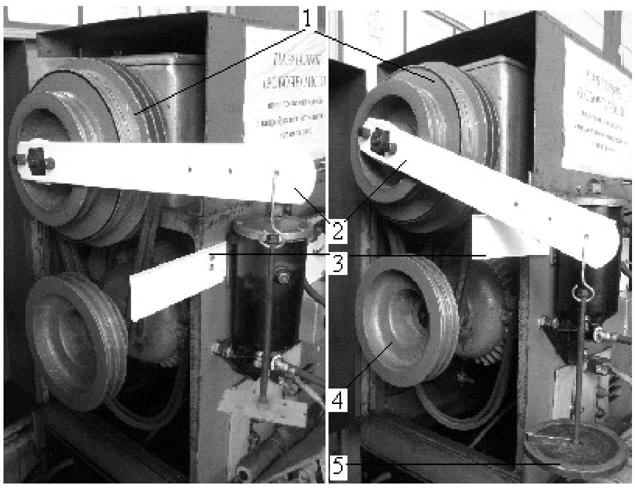

b)

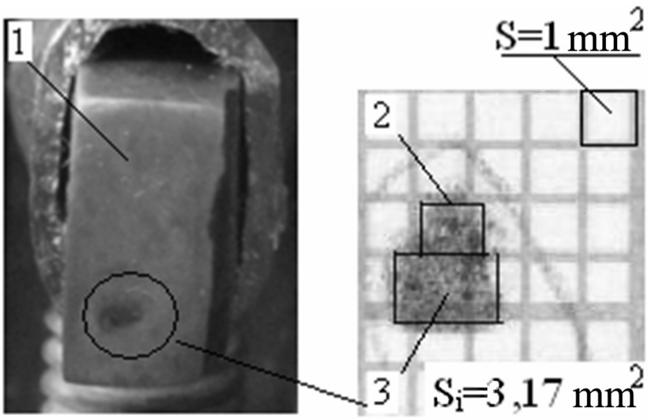

c)

Fig. 1. Methodological support for measuring resistance to displacement during shear: a - contact of model samples: 1 - disk; 2 - block; 3 - additional pad holder; 4 - screws securing the additional holder; 5 - details of the mounting of the disk; 6 - the lower shaft of the friction machine SMC-2; b - angular load drive of the lower shaft: 1 - upper pulley; 2 - cargo lever; 3 - limiter of the stroke of the lever of goods; 4 - lower pulley; 5 - cargo; in - the imprint of the contact, N = 280H: 1 - block; 2,3 - perimeters of the calculated areas; c - test sample of material in the mandrel: 1 - fragment of the operating cam of the camshaft of an internal combustion engine; 2,3 - contours of the trace and imprint of wear during shear

.

Wherein: - the maximum shear moment is determined by the recorder on the field of the scale tape with a fixed rotation through the angle α with a certain load applied to the lower shaft (Fig. 1 b). The mass of the load will determine the shear rate; - the area of interaction of the friction surfaces is determined by the imprint on graph paper (Fig. 1 c).

2. Test procedure

To test the methodology, the following tribological material systems were used:
- "40X - steel 45";
- "12X2H4 - steel 45";
- “45XH2MFA - steel 45.

Contact interaction was modeled without lubricant. The following samples were used:

- for steel 45 in the form of a triangle (Fig. 1 c) with a cylindrical outer surface, 4 mm thick, which was fixed in the mandrel on the fixed shaft of the machine;
- for other metals in the form of a disk with a diameter of 50 mm and a thickness of 12 mm, which were mounted on the lower shaft of the machine and rotated.

The measurements were carried out in this sequence. Disks of appropriate materials were fixed on the lower shaft of the friction machine. The block was placed in an additional holder, fixed with screws in a standard holder, which was fixed on the upper shaft of the friction machine. Next, the block was pressed with the corresponding force to the disk using the loading screw of the friction machine. The load had values of 140N, 185N, 230N, 280N. Further, the disk was shifted from its place - it was rotated with the help of weights 5 (Fig. 1 b) by a fixed angle α. The time for angular displacement also determined the shear rate - t_1 = 0.43s and t_2 = 1s. The average linear displacement of the disk was l = 4.5 mm. In this case, the recorder in the tribogram recorded the temporary shear resistance by deviation from zero

$$\tau = \frac{M_m}{r \cdot S_b} \quad , \tag{1}$$

where M_t is the moment of friction during shear, N•m; r is the radius of the disk, m; S_b is the imprint area, mm^2.

3. Research results

A graphical approximation of the averaged data in the form of linear dependencies with inverse extrapolation of the shear resistance of displacements is shown in Fig. 2. Moreover, according to the parameters of the trend lines in Excel, their equations and the reliability of the R^2 approximation are determined, the results are shown in Table. 1.

Table 1. Parameters for approximating experimental data for tribological material systems

Parameter	«12X2H4 – steel 45»	« 45XH2MΦA – steel 45 »	« 40X – steel 45 »
Type of equation	$\tau = 0.36p - 13.44$	$\tau = 0.11p + 3.58$	$\tau = 0.28p - 10.27$
Approximation reliability, R^2	0.98	0.99	0.9
Piezoelectric coefficient , β	0.36	0.11	0.28
Tangential strength, τ_0, MPa	> 0 at p ≈37 МПа	3.58	> 0 at p ≈36 МПа

In accordance with the data shown in Fig. 1, the static friction coefficients (2) are analytically determined — the friction coefficients of the surfaces from which graphical dependencies are constructed (Fig. 3), reflecting the nature of its change.

$$\mu_0 = \tau / p. \tag{2}$$

An analysis of the results indicates the following.

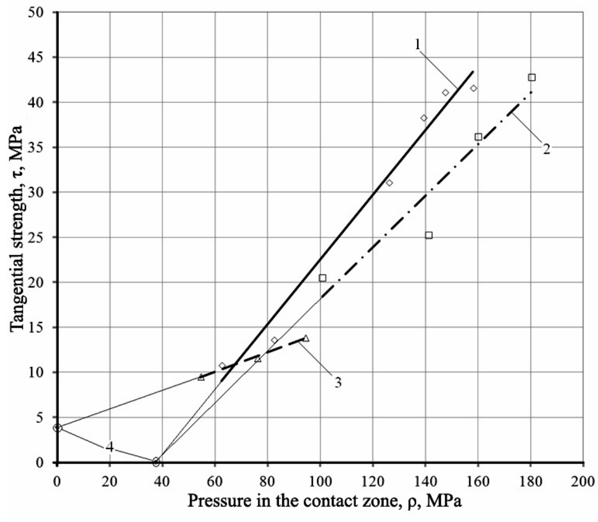

Fig. 2. The dependence of the tangential strength of the adhesive bond of steel 45 on pressure at a shear rate of 10.16 ± 0.8 mm/s: 1 - 12X2H4; 2 - 40X; 3 - 45XH2MFA; 4 - points of reverse extrapolation

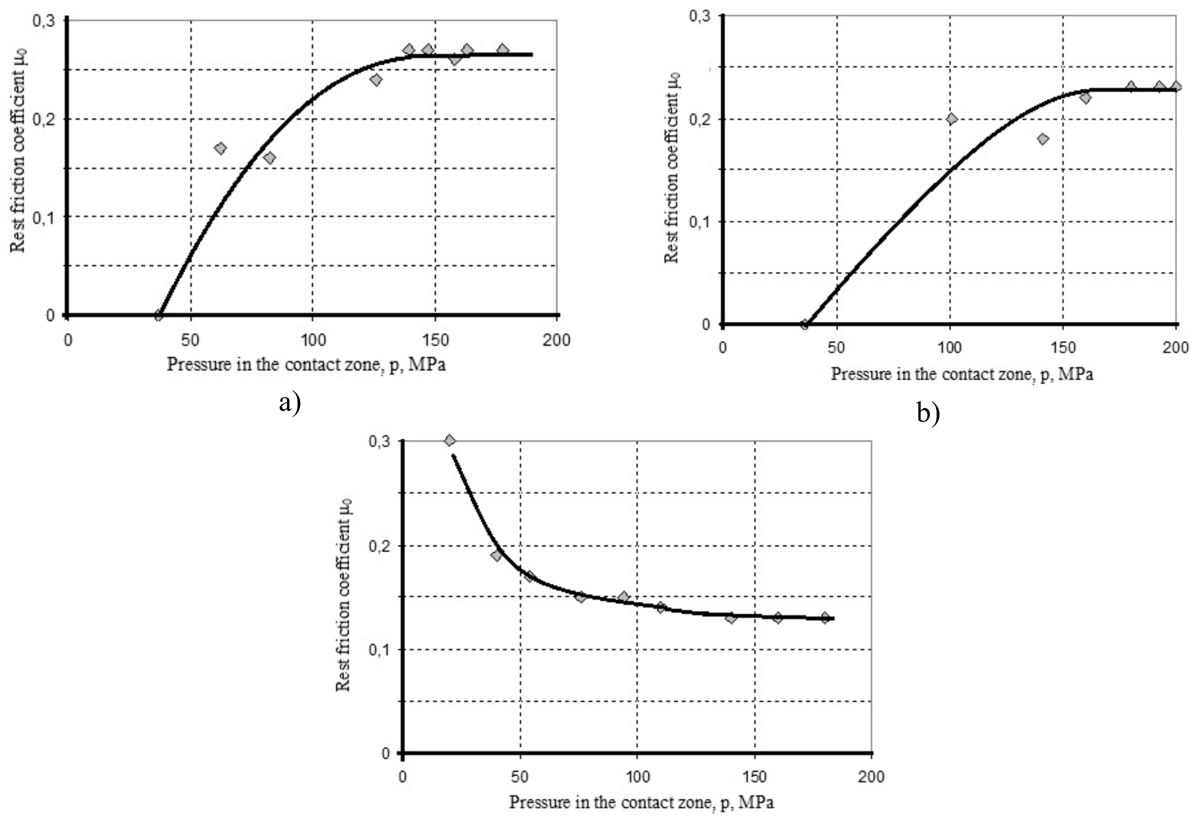

Fig. 3. Dependence of changes in the coefficient of static friction on contact pressure:
a - 1 - 12X2H4; b is 40X; c - 45XH2MFA

The steady-state value of the coefficient of friction manifests itself in the region of high contact pressures:

- for the material system "steel 45 - 12X2H4" $\mu 0 = 0.27$ at $p > 140$ MPa;
- for the material system "steel 45 - 40X" $\mu 0 = 0.23$ at $p > 160$ MPa;
- for the material system "steel 45 - 45XH2MFA" $\mu 0 = 0.13$ at $p > 130$ MPa.

Patterns of the nature of the change in the coefficient of friction of rest differ from each other. So for steels 12X2H4 and 40X, with an increase in contact pressure, the adhesion forces grow to a

.

certain value, and then stabilize. For steel 45XH2MFA, on the contrary, decrease with subsequent stabilization. Moreover, for 12X2H4 steel, the growth rate is higher than for 40X. This can be previously associated with the distribution densities of the microhardnesses of the phases, which are concentrated in the zone of formation of the contour contact areas and the manifestation of molecular interaction forces due to the degree of activation of the surface layers by shear loading.

An analysis of the obtained results indicates the realized possibility of experimentally determining the parameters of adhesive properties, for example, of the considered tribological metal systems. In this case, the numerical values of the parameters do not differ from similar results presented in [1]. Preliminarily obtained results indicate that there are modes of contact interaction with respect to the load, in which when calculating the coefficient of friction it is not advisable to take into account the molecular component, since it begins to appear only from a certain pressure in the contact.

Conclusion

The proposed approaches for modeling the shear resistance in the contact of small-sized samples depending on normal loading and shear rate with a slight modification of the equipment of the SMC-2 friction machine make it possible to determine the adhesion properties of materials.

The results of experimental studies are presented in accordance with which, on the example of tribological systems of materials “40X - steel 45”, “12X2H4 - steel 45”, “45XH2MΦA - steel 45” the ability to determine the parameters of their adhesive properties using the equipment of the friction machine SMTS-2 with little its completion.

The experimental values of the parameters of the molecular component of friction τ_0 and β obtained on full-scale samples of parts of engineering objects using the proposed approach allow us to obtain more accurate predicted values of the friction and wear characteristics of materials. For example, to determine the coefficient of friction depending on the type of contact and contact conditions (plastic, rough; elastic, rough; single elastic, run-in elastic, etc.), which is one of the parameters of the calculated estimate of the wear rate [7], the number of cycles to fracture of the material . And since the adhesive bond is formed taking into account the contact time, to a greater extent such information is advisable for mechanisms with reverse movement. The lack of objective data on the parameters of the molecular component of the friction force reduces the accuracy of the calculations, which is not excluded when the researchers use reference data obtained either for pure metals or for approximate mechanical properties for those considered in each case.

REFERENCES

1 Semenov V.I., Shuster L.Sh., Chertovskikh S.V., Raab G.I. Influence of the complex parameter of plastic frictional contact and material structure on the strength of adhesive bonds. *Friction and Wear*. 2005, Vol. 26, No. 1, pp. 74-79.

2 Dudikina V.V. Adhesion strength of nickel and zinc coatings with a copper base, electrodeposited under external stimulation by laser radiation. Science and transport progress. *Newsletter of the Dnipropetrovsk National University of Public Transport*, 2013, V.2(44). - P. 83-91

3 Nazarov V.G., Stolyarov V.P., Gagarin M.V. Durability of adhesive rubber-metal adhesion joints for surface fluorinated rubbers. *News of higher educational institutions. Problems of printing and publishing*. Moscow, MGUP named after Ivan Fedorov. 2013, No.3. - P.45-53

4 Kotomin S.V. Evaluation of the strength of the adhesive bond fiber - thermoplastic matrix by the loop method. *Engineering Journal: Science and Innovation,* 2015, No. 12. Available at http://engjournal.ru /catalog/msm/pmcm/1426.html

5 *Standard Test Method for Adhesion Coating Using Portable Adhesiometers*. Designation: D 4541 - 02. Available at: www. inspector.pro/wp-content/uploads/2016/01/ASTMD4541.pdf

6 Kragelsky I.V., Dobychin M.N., Kombalov V.S. *Bases of calculations for friction and wear*. Moscow, Mechanical Engineering. 1977, 526 p.

7 Diha O.V. *Calculation and experimental methods of control of processes of boundary lubrication of technical tribosystems.* Monograph.Khmelnitsky, KhNU, 2018, 197 p.

Article accepted for publication 22.11.2019

DOI 10.31489/2019No2/83-88

UDC 535.37; 535.47; 537.635; 543.544.2; 539.194; 541.18

OPTICAL SYSTEMS FOR REMOVAL OF POLARIZATION SPECTRA

Astanov S.Kh., Kasimova G.K., Sharipov M.Z.

Bukhara Engineering-Technological Institute, Bukhara, Uzbekistan, s.h.ostonov@rambler.ru

In the article optical systems are presented that are developed by the authors and have been used for many years to remove the polarization properties of anisotropic molecules. Both systems are designed for visible and close to ultraviolet spectral regions. In this case, the double Fresnel parallelepiped plays the role of an achromatic quarter of the wave plate. They are used in the Jasco-20 dichrograph after the Pockels cell. As a result, the sensitivity of the device increases from $\theta \cong 10^{-3} degree \cdot cm^{-1}$ *to* $10^{-5} degree \cdot cm^{-1}$ *of the value of the differences in optical density.*

Keywords: *optical systems, anisotropic molecules, polarization, ultraviolet spectral area, quarter wave plate, sensitivity, optical density.*

Introduction

Polarization spectra provide information on the orientation of the molecules of dissolved substances, and also these spectra are more informative with respect to electronic spectra [1]. The photophysical and photochemical properties and processes occurring in solutions of vitamin preparations were studied in [2-6]. Molecules of plant origin have such characteristics that determine their photostability and thermal stability, these characteristics are a guarantee of their use in pharmaceuticals and medicine. In [7–9], the results of a research on the study of photochemical processes occurring in solutions Some medications are water-soluble, which allows them to be prepared on the basis of various drugs used in pharmaceuticals [10, 11] in the form of their concentrated aqueous solutions [12, 13].

The creation of new drugs based on plant pigments requires further research on their self-assembly. The identification of the conditions for the formation of self-assembly of molecules is one of the urgent problems of pharmaceuticals, as a result of which it becomes possible to test drugs [14, 15]. The determination of the structure of self-assembled molecules allows their targeted usage in medicine [16, 17]. Carrying out these studies allows us to identify the relationship of anisotropic - optical spectra with the structure of self-aggregates. These research methods are highly sensitive in detecting the delicate details of optical transitions.

1. The spectral-optical method to polarization measurement

The first optical system includes a mirror system. The scheme of the mirror system is shown in Fig. 1, which contains a bi-mirror 1 with an angle of 270^0 between its working faces a and b, bi-mirrors 2 and 3 with an angle of 90^0 between their own working faces c, d, e, and g-d. We will consider the polarization transformation in successive reflections in the system. Let a light beam be incident on the input face of the system in the general case of an arbitrary ellipticity of polarization.

We denote by E_p and E_s the components of the electric field of the incident light lying in the plane of incidence and perpendicular to it, respectively. After reflection from the face *a*, the ellipticity of light changes - the components of the electric field become equal to E_p^I and E_s^I. The incidence planes for the faces *a* and *c* are mutually perpendicular, therefore the S-component on the face *a* is the P-component on the face *c*. Similarly, P-component on a face *a* is P-component on *c*. Such a transformation of the components of the electric vector is described by the matrix y = (*G*-*b*).

.

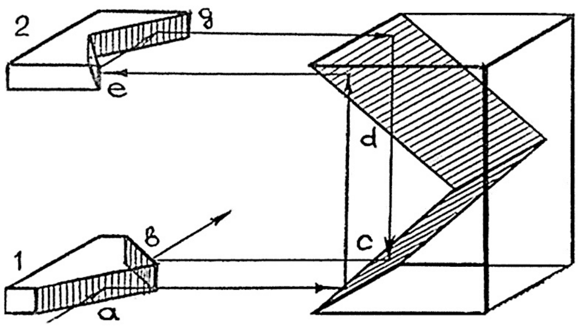

Fig. 1. Mirror system for spectral-optical polarization measurements**.**

After successive reflection from the faces *a* and *c*, the resulting vector of the electric field $\vec{E}'$ equal to

$$\vec{E}' = A\vec{E}, \quad (1)$$

where $\vec{E}$ –the electric vector of the light wave incident on the system, A – the transformation matrix.

In matrix A it is taken into account that the changes in the phases δ_p and δ_s, δ_s and δ_p of the oscillations of *p* and *s* components of the electric field of the light wave upon reflection from the faces a and c, are pairwise identical due to the equality of the angles of incidence of light on the faces. It follows from the form of matrix A that successive reflection from the faces of a and from the system of bi-mirrors introduces the same phase shifts ($\delta_p+\delta_s$) into both components of E_p and E_s. The ellipticity of the light does not change here, and the axis of the polarization ellipse rotates by 90^0. Successive reflections of the light beam from the faces *d* and *l* restore its initial state of polarization, since this reflection is identical to the reflection from the faces *a* and *c*. Further reflection of light from the faces *d, g, c*, and *b* does not change the state of polarization of the light wave due to the symmetry of the mirror system relative to the bisector plane of the bi-mirrors 1 and 2. The ellipticities of the light beams entering and between the faces *c-d* and *d-c* are equal. This device is used: as a universal prefix to a variety of optical and spectral devices for measuring optical activity, circular and linear dichroism. In this case, it is necessary to get rid of the scattered light, since it is possible to increase the optical path length without significant changes in the dimensions of the devices and without violating the initial polarization of the measuring light beam; as a reflecting system similar to multi-way ditches for increasing the optical density of discharged gas mixtures, vapors, and solutions. In addition, this optical device allows measurements of optical anisotropy in substances whose anisotropy is induced by the Earth's gravitational and magnetic fields, allows to isolate and identify these effects, which is achieved by placing the studied samples in different optical channels of the mirror system, since it is possible to ensure reciprocal passage of light beams with the same polarization

2. Fresnel double parallelepiped

The spectrum-polarimeter *Spektropol*-1, in which the compensation method of measuring the optical rotation of the plane of polarization of light is applied, has a sensitivity of $2\cdot10^{-3}$ – $8\cdot10^{-2}$ angular degrees [19]. Another method for measuring the linear dichroism of weakly oriented systems was implemented by us in serial circular dichrographs. The fundamental possibility of measuring linear dichroism with help of serial dichrographs, in which the electro-optical method for measuring circular dichroism was used, have been predicted in a number of works [18, 19]. One of these possibilities can be realized on Jasko-20, using an optical prefix - Fresnel double parallelepiped designed for the visible and near ultraviolet spectral area [19].

Figure 2 shows the optical scheme of the Fresnel double parallelepiped, a device that plays in our measurements the role of an achromatic quarter-wave plate and zero dichrograph lines, which we use to measure the linear dichroism of weakly oriented anisotropic and gyro anisotropic systems.

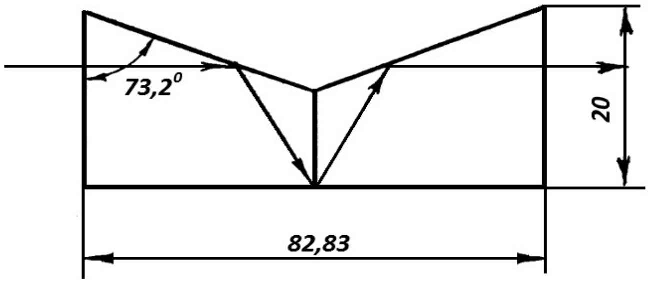

Fig.2. Fresnel double parallelepiped.

Figure 3 shows the data on the measurement of linear dichroism of the same linear dichroic sample using Spektropol-1spectropolarimeters and a Jasko-20 circular dichrograph according to the methods described above. As an anisotropic linear-dichroic object, a polymer film of polymethyl-methacrylate containing rhodamine 6G and its base, stretched uniaxially 4 times, was chosen. Both dyes in the polymer film are in an aggregated state and are easily oriented when stretched. Curves 1 and 2 were recorded on Spektropol-1 and Jasko-20 spectro-polari-meters, respectively, on the scales of these instruments: φ and θ. Nearby on the vertical axes are marked, the scale according to linear dichroism recalculated according to the above formulas.

The linear dichroism spectra were measured on a spectropolarimeter when the film was oriented with its axis of extension at an angle of 45^0 to the polarization vector of the light incident on it. The linear dichroism spectra were measured on a circular dichrograph when the film was oriented with its axis of extension at an angle of 0^0 to the linear polarization vector converted by a Fresnel double parallelepiped from a circular rhodamine 6G and its base, stretched 4 times. Film thickness is 0.3 mm.

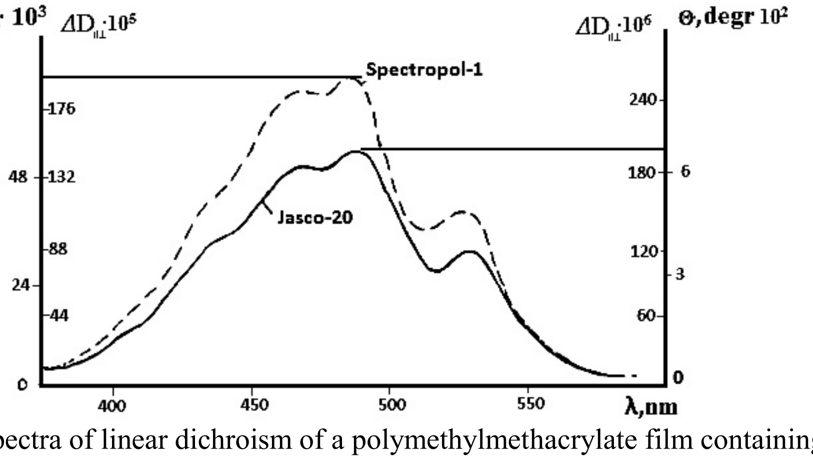

Fig. 3. Spectra of linear dichroism of a polymethylmethacrylate film containing.

The positions of the films in both cases corresponded to the maximum amplitudes of the bands of the recorded curves. In this case, there is good correspondence between the two spectra of linear dichroism. So, at the maximum of both curves $\lambda^{\varphi}_{\max}$= 490nm, the amplitudes recorded on Spektropol - 1 and Jasko-20 are respectively $2.03\cdot10^{-3}$ and $2.04\cdot10^{-3}$ units of difference optical density. As the electro-optical element in a serial Jasko-20 dichrograph, a Pockels cell with a KDP crystal (KH_2PO_4) is used [20].

.

In practice, the measure of circular dichroism is the ellipticity value, determined by the ratio of the minor and major axes of the ellipse and equal for small θ;

$$tq\,\theta \approx \theta = tq\,\frac{\pi}{\lambda}(X_L - X_R)\cdot l \approx 33C\cdot l(\varepsilon_l - \varepsilon_R), \tag{2}$$

where x_L, x_R, ε_L, ε_R – are absorption coefficients and molar extinction coefficients of a substance for light with a wavelength λ polarized in a circle to the left (L) and to the right (R); C- concentration of optically active substance; *l* - the thickness of the sample.

It is known that

$$\Delta\varepsilon = \varepsilon_l - \varepsilon_R = \frac{1}{Cl}\log_{10} {}^{I_R}\!/_{L_L}, \tag{3}$$

where I_R, I_L- the intensities of the light, transmitted through the sample, polarized in a circle to the right and left.

By virtue of this

$$\theta = 33\cdot\log_{10} {}^{I_R}\!/_{I_L} = 33\cdot\log_{10}\frac{1 + I_2/21}{1 - I_2/21}, \tag{4}$$

where $I_1 = \frac{1}{2}(I_R + I_L), I_2 = I_R - I_L$ a-priory.

As $\frac{I_R - I_L}{I_R + I_L} = \frac{I_2}{2I_1} \leq \mathrm{I}$ (for small optical activity), so

$$log_{10}\frac{1+{}^{I_2}\!/_{2I_1}}{1-{}^{I_2}\!/_{2I_1}} \approx log_{10}\frac{e+{}^{I_2}\!/_{2I_1}}{e-{}^{I_2}\!/_{2I_1}} = \frac{I_2}{I_1}\cdot log_{10}e \tag{5}$$

hence,

$$\theta = 33\cdot\frac{I_2}{I_1}\cdot log_{10}e \tag{6}$$

That is, the ellipticity value (in degrees) is proportional to the ratio of intensities I_2, I_1, which are recorded [21] by the Jasko-20 dichrograph photoelectric system. In the transition from circular to linear dichroism, it is convenient to use the formula for θ in another form:

$$\theta_{CD} = 28{,}6\frac{I_R - I_L}{I_R + I_L}. \tag{7}$$

When circular light polarization is incident on a Fresnel double parallelepiped, it is converted to linearly polarized light, and, for R and L, circular polarizations are orthogonal. Consequently, the Jasko-20 dichrograph, which measures θ_{KD} in degrees, is equipped with an optical prefix in the form of a double Fresnel parallelepiped, located after the Pockels cell in front of the sample, and measures linear dichroism

$$\theta_{LD} = 28{,}6\cdot\left|\frac{I_\perp - I_\parallel}{I_\perp + I_\parallel}\right| \tag{8}$$

where I_I, I_{II} - intensities of linearly polarized light transmitted through the sample and incident on the dichrograph photodetector:

$$\frac{I_\perp - I_\parallel}{I_\perp + I_\parallel} = \frac{10^{-D_\perp} - 10^{-D_\parallel}}{10^{-D_\perp} + 10^{-D_\parallel}} = \frac{e^{-D_\perp log_e 10} - e^{-D_\parallel log_e 10}}{e^{-D_\perp log_e 10} + e^{-D_\parallel log_e 10}} =$$

$$= th\left[(D_\perp - D_\parallel)log_e {}^{10}\!/_{2}\right] \approx \frac{(D_\perp - D_\parallel)\cdot log_e 10}{2} \tag{9}$$

(for small argument values). Thus, the dichroism measured by the dichrograph

$$\Delta D_{\perp,\parallel} = D_\perp - D_\parallel = \frac{\theta_{LD}}{32{,}98} \tag{10}$$

at the maximum sensitivity of the dichrograph

$$\theta_{CD} = 10^{-3} degr \cdot sm^{-1} \quad (11)$$

corresponds to its linear dichroism sensitivity

$$\Delta D_{\perp,\parallel} \cong 3 \cdot 10^{-5} \quad (12)$$

values of difference optical density.

The Spektropol-1spectropolarimeter allows measurements in the spectral area 200 - 610 nm, and the Jasko-20 dichrograph - in the spectral area 200-700 nm. The zero line of the spectrum of the polarimeter (through the air) has an ideal rectilinear character, while the zero line of a linear dichrograph based on the Jasko-20 is not quite ideal: the deviation of this line from the straight line in the spectral areas 200-320 and 640-700 nm, apparently, is associated with the imperfection of the Pockels cell of the dichrograph, which gives in these spectral areas values as in the circular polarization of light. As a result of this, after the light transmits through the Fresnel double parallelepiped, it acquires a polarization close to linear, with a very large ellipticity. Thus, if a linear dichroic sample has a small linear birefringence, it is preferable to measure the linear dichroism on the spectrum of a Spektropol-1polarimeter. In all other cases, especially when the sample is gyro-anisotropic and has significant optical activity, it is convenient to use Jasko-20.

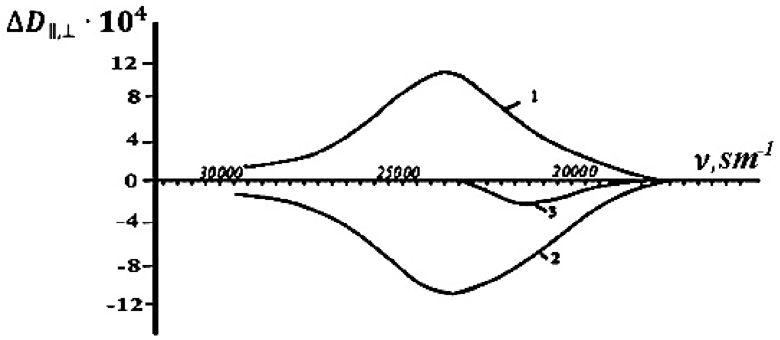

Fig. 4. The spectra of linear dichroism of tartrazine associates under the conditions of the hydrodynamic flow of its solution at an angle between the flow velocity vector and the transmitted light polarization vector + 45 ° (1) and –45 ° (2). Curve 3 is the difference between spectra 1 and 2. C = 2 · 10^{-4}M. *l* = 0.1 cm.

As an example, we studied solutions of tartrazine in a laminar hydrodynamic flow. It was found that they show significant linear dichroism, its value at the maximum of the absorption band at ν=23500 cm^{-1}makes$\Delta D_{\parallel,\perp}=10^{-3}$units of dichroic optical density.

Figure 4 shows the spectrum of linear dichroism of tartrazine associates oriented in the hydrodynamic flow of a binary mixture of a water-dioxane solution, obtained from the corresponding spectrum of the non-gyrotropic rotation of the plane of polarization at an angle between the flow velocity vector and the polarization vector, transmitting perpendicular to the linearly polarized light flow equal to +45° C (curve 1), and the linear dichroism spectrum of the same solution, recorded at an angle of -45° C (true linear dichroism spectrum) (curve 2). Just at these angles of orientation of the flow velocity vector relative to the polarization vector of transmitted light the maximum amplitudes of the main bands are observed in the corresponding non-gyrotropic rotation spectra of the plane of polarization, which is a necessary condition for recording the linear dichroism curves $\Delta D_{\parallel,\perp}$= (λ) on the spectropolarimeter [22] .

The algebraic sum of spectral curves 1 and 2 gives a curve 3, from which, by applying the decomposition into Lorentzian contours, it is possible to distinguish two different amplitude bands of linear dichroism. The positions of maxima and FWHM of which corresponds to that position of the maxima and half-widths of the absorption bands associated tartrazine, which confirms the correctness of measurements and calculations. The fact that tartrazine associates show linear dichroism, being easily oriented in a laminar hydrodynamic flow, indicates a strong anisotropy of dye microcrystals having a needle (rod-like) shape.

.

Conclusion

The results show that both in concentrated aqueous solutions and in binary mixtures of solvents, the association of food dyes shows itself as a result of combining the molecules of the studied compounds directly between themselves. In this case, the structures of the combined molecules are determined by the use of optical systems, obtaining spectra of linear dichroism. In these cases the sensitivity of the device increases by about two orders of magnitude

REFERENCES

1 Kasimova G.K., Astanov S., Kurtaliev E.N., Nizomov N. Structure of self-assembled riboflavin molecules in solutions. *Journal of Molecular Structure*. 2019, Vol.1185, pp. 107 – 111.

2 Astanov S.Kh., Sharipov M.Z., Fayzullaev A.R., Kurtaliev E.N., Nizomov N. Spectroscopic study of photo and thermal destruction of riboflavin. *Journal of Molecular Structure*. 2014, Vol.1071, pp.133–138.

3 Astanov S.Kh., Shamsiev R.Kh., Fayzullaev A.R. Food dyes (methods for stabilizing). Tashkent, *Development of science and technology*, 2014, pp.60 – 74.

4 Ahmad I., Ahmed S., Sheraz M.A., Vaid F. Effect of borate buffer on the photolysis of riboflavin in aqueous solution. *J. Photochem. Photobiol. B: Biology*. 2008, Vol. 93, pp. 82—87.

5 Ahmad I., Sheraz M.A., Ahmed S., Kazi S.H., Mirza T., Aminuddin M. Stabilizing effect of citrate buffer on the photolysis of riboflavin in aqueous solution. *Res. Pharma Sci*., 2011. Vol. 1, pp. 11—15.

6 Astanov S.Kh., Sharipov M.Z., Fayzullaev A.R., Kurtaliev E.N., Nizomov N. Thermal Destruction of Riboflavin in Different Aggregate States. *Journal of Applied Spectroscopy* 2014. Vol. 81(1), pp. 37 – 42.

7 Ahmad I., Fasihullah Q., Vaid F.H.M. A study of simultaneous photolysis and photoaddition reacti-ons of riboflavin in aqueous solution. *J. Photochem and Photobiol. B: Biology* 2004, Vol. 75, pp. 13 – 20.

8 Ahmad I., Fasihullah Q., Vaid F.H.M. Effect of phosphate buffer on photodegradation reactions of riboflavin in aqueous solution. *J. Photochem and Photobiol. B: Biology* 2005, Vol. 78, pp. 229 – 234.

9 Sheraz M.A., Kazi S.H., Ahmed S., Anwar Z., Ahmad I. Photo, thermal and chemical degradation of riboflavin. *Beilstein Journal of organic chemistry*. 2014, Vol.10, pp.1999 – 2012.

10 Ching-Yi Wu, Yu-Chie Chen. Riboflavin immobilized Fe3O4 magnetic nanoparticles carried with n-butylidenephthalide as targeting-based anticancer agents. *Artificial cells, nanomedicine, and biotechnology*. 2019, Vol. 47, No. 1, 210–220.

11 Astanov S.Kh., Kosimova G.K., Turdiev M.R. Spectroscopic displays of self-assembly of tartrazine food dye. *Journal Development of science and technology*. 2017, No.3, pp. 93.

12 Kubo Y., Yahata Sh., Miki S., Akanuma Sh., et al. Blood-to-retina transport of riboflavin via RFVTs at the inner blood-retinal barrier. *Drug Metabolism and Pharmacokinetics*. 2017. Vol. 32(1), pp. 92 – 99.

13 Lebedev-Stepanov P.V., Kadushnikov R.M., Molchanov S.P., Ivanov A.A., Mitrokhin V.P., et al. Self-assembly of nanoparticles in the microvolume of colloidal solution: Physics, modeling, and experiment. *Nanotechnologies in Russia*. 2013, Vol. 8, Issue 3–4, pp. 137 – 162.

14 Williamson G., Edmondson D. E. NMR spectral analysis of the ribityl side chain of riboflavin and its ring-substituted analogs. *Methods in Enzymology*. 1986, Vol.122, pp. 240 – 248.

15 Astanov S.Kh., Sharipov M.Z., Kasimova G.K. Hipochromic effect in riboflavin solutions. *Eurasian Physical Technical Journa*l, 2019, Vol.16, No.1(31), pp. 12 – 17.

16 Brzezinska E., Mielczarek C., Pajak W. Analysis of acid-base properties of riboflavin calculated via semi-empirical methods. *Acta Poloniae Pharmaceutic*a. 2008, Vol. 65 (1), pp. 59 – 63.

17 Klaumünzer B., Kröner D., Saalfrank P. (TD-)DFT Calculation of Vibrational and Vibronic Spectra of Riboflavin in Solution. *J. Phys. Chem. B.* 2010, Vol. 114 (33), pp. 10826 – 10834.

18 Wellus L., Legrand M., Grosjean M. *Optical circular dichroism*. Moscow, Astanov S.H., Kasimova G.K., Sharipov M.Z. *Theoretical and experimental aspects of the application of polarization spectra in the study of photonics of self-aggregated molecules*. Monograph. Tashkent. 2019, pp. 53-59.

19 Lebedev-Stepanov P.V., Kadushnikov R.M., et al. Simulation of self-assembly of micro- and nanoparticles in an evaporating microdrop of solution. *Russian nanotechnologies*. 2011, Vol. 6, Issue 1–2, pp 79–87.

20 P.J.Keller, Q.L.Van. A.Bacher, H.G. Floss. Biosynthesis of riboflavin: C-NMR techniques for the analysis of multiply C-labeled riboflavins. *Tetrahedron*. 1983, Vol. 39, No. 21, pp. 3471 – 3481.

21 Astanov S.Kh., Prishchepov A.S., Niyazkhanova B.E. Spectral-optical properties of indigo carmine and tartrazine associates in solutions. *Journal of Applied spectr*. 1990, Vol. 53, No. 5, pp. 800 – 806.

Article accepted for publication 22.11.2019

DOI 10.31489/2019No2/89-93

UDC 621.548

EFFECTS OF ELECTROHYDROIMPULSE DISCHARGES ON THE CRUSHING OF THE NATURAL MINERAL QUARTZ

Bulkairova G.A.[1], Stoev M.[2], Khassenov A.K.[1], Karabekova D.Zh.[1], Nurgaliyeva Zh.G.[1], Kipshakov M.S.[1]

[1]E.A. Buketov Karaganda State University, Karaganda, Kazakhstan, gulden2111@mail.ru
[2] Neofit Rila University, South-West, Blagoevgrad, Bulgaria

Electro-hydro-impulse (high-current discharge in water) also belongs to the technologies using strong impulse currents. With a powerful pulsed electric discharge between the electrodes placed in the liquid, an electro-hydraulic effect occurs. To study the influence of electro-hydro-pulse shock waves were designed and assembled the experimental setup. The dependences of the degree of grinding of natural mineral quartz on the electro-technical parameters of the discharges are given. The optimal conditions for the most intensive grinding of natural mineral quartz using electro-hydro-pulse treatment are determined.

Keywords: natural mineral quartz, electro-hydraulic effect, underwater electric discharge, degree of grinding.

Introduction

The growing consumption of fuel, ferrous, non-ferrous and rare metals, non-metallic materials, which are the basis for the development of modern industry, requires an increase in the volume of extraction and enrichment of minerals. Together with non-metal ore, construction materials and mining and chemical raw materials, the volume of mining and processing of minerals in the world is several billion tons per year.

Processing of most of the mined rock mass means crushing and grinding it as a preparatory process for direct enrichment. These processes are very expensive operations and reach 50%, and in some cases 70% of all costs in the processing plants. Of great importance for subsequent technological operations is the quality of crushing and grinding, which involves obtaining a product of a given size without re-grinding with maximum release of mineral grains from the waste rock with minimal damage. The requirements of increasing the number of processed rocks and ores while improving the quality indicators of processing (increasing the degree of extraction) pose very urgent problems aimed at streamlining and reducing the cost of crushing and grinding processes.

Rocks are mostly materials that break down brittle under normal conditions. In this regard, when conducting studies of physical processes occurring during the destruction, the most suitable model materials are brittle crystals. Quartz is a part of many igneous and metamorphic rocks: granite, porphyry, gneiss. The total content of quartz in igneous rocks is approximately 12%. The hardness of quartz is 7 units on the Mohs scale. Melting point is 1710°C.

The Republic of Kazakhstan has large reserves of quartz-containing raw materials, but most of it is used in the production of simple building materials, and only a small part-high-tech industries.

Quartz-one of the most common minerals, which is more or less pure silica SiO_2 (46.7% - Si; 53.3% - O_2). Practically, quartz crystals rarely approach this composition, as they usually contain various impurities: bubbles of gases and liquids, sometimes ingrown mica leaves. Quartz is one of the most common minerals, which is more or less pure silicic acid. Practically, quartz crystals rarely approach this composition, as they usually contain various impurities: bubbles of gases and liquids, sometimes ingrown mica leaves.

.

This article presents the results of the study of the influence of electro-hydro-impulsive shock waves on the crushing and grinding of the natural mineral quartz. Electro-hydro-impulse (high-current discharge in water) also belongs to the technologies using strong pulse currents. With a powerful pulsed electric discharge between the electrodes placed in the liquid, there is an electro-hydraulic Yutkin effect, which consists in the fact that the rapid release of energy in the discharge channel increases the pressure in it, and its further expansion leads to a shock wave and fluid flows [1]. The shock wave is a density jump in the liquid that propagates from the discharge channel at a speed exceeding the sound (in water more than 1500 m/s). Pressure at the shock wave front in the liquid can reach tens of kilobars. The impact of this pressure on the treated object can cause structural restructuring of the object material (crushing brittle materials, deformation, hardening of the surface, etc.). Fluid flows propagating at a speed of $10^2 \div 10^3$m/s transmit kinetic energy to the object being processed, causing, like a shock wave, its mechanical changes [2]. Mechanical manifestations of pulsed discharge in a liquid are called electro-hydraulic effect, and installations using this effect are called electro-hydraulic. As a working medium in such installations, as a rule, process water, kerosene, oils are used [3, 4].

1. Experimental technique

To study the effect of electro-hydro-impulsive shock waves on the crushing and grinding of the quartz mineral, an experimental unit was developed and assembled in the Laboratory of Electro-hydro-dynamics of the Engineering Thermophysics Department named after professor Zh.S. Akylbayev of the E.A. Buketov Karaganda State University.

Electro-hydraulic devices for crushing unlike mechanical crushers do not have moving parts, are made of conventional structural steel, and their body practically does not wear out during operation. During operation, these devices do not form dust, occupy a relatively small production area and allow them to combine the processes of crushing, mixing and flotation of materials [4].

The installation consists of the following units: pulse voltage generator, capacitor and protection system, control panel and electrode system. Figure 1 shows the working part of the installation, which consists of a cylindrical body 1, working electrodes 2, cover 3, caprolan washer 4 and caprolan sleeve 5.

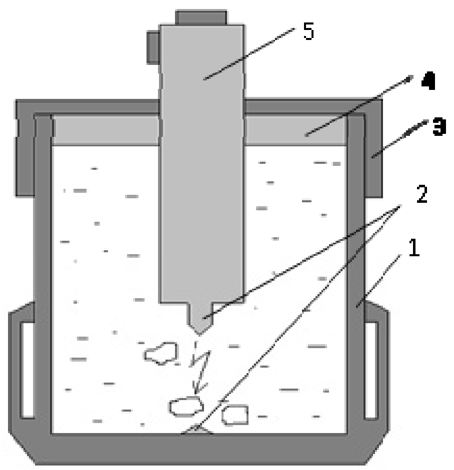

Fig.1. Working part of the experimental plant for crushing quartz mineral.

In the working part of the experimental installation, a linear system of electrodes is installed. The positive electrode is located vertically, and the negative electrode is the bottom of the cylindrical metal chamber. To obtain high pressures at the shock wave front, crushing and grinding solid fractions, an electric discharge is carried out in an aqueous solution of the mineral quartz [5].

The rapid release of energy generates a strong mechanical action applied to the macroscopic volumes of the medium and individual surfaces that have fallen into the discharge zone, at the same time, the rate of energy release is much faster than the rate of transmission of its perturbation to the environment. After the beginning of the breakdown occurs for some time, the so-called stage of formation of the discharge, which is characterized by a certain increase in current with a simultaneous decline in voltage and culminating in the formation of a highly conductive electric channel. The energy accumulated by the capacitor Bank is introduced into the formed zone. Under the action of high pressure, the discharge channel expands, the macroscopic volumes of the medium receive relatively high velocities, which are directed in all directions along radii originating approximately from the Central part of the discharge gap. Under the influence of high pressure, the liquid is compressed, the area of this compression ends with a moving shock wave front, where the pressure and all other parameters of the liquid medium are changed by a pressure jump. The energy of the heated plasma is transferred directly to the environment. Electrohydraulic crushing devices unlike mechanical crushers do not have moving parts, are made of conventional structural steel, and their body practically does not wear out during operation. During operation, these devices do not form dust, occupy a relatively small production area and allow them to combine the processes of crushing, mixing and flotation of materials. The liquid, having received acceleration from the discharge channel expanding at high speed, moves from it in all directions, forming in the place where the discharge was a significant cavity in volume (cavitation) causing the first (main) hydraulic shock. The development of a spark discharge in time occurs by successive «germination» of streamers in the inter-electrode interval. A growing streamer, as a rule, consists not of one, but of many channels with numerous branches from them.

Under the influence of electric pulse action in the treated medium there are hydrodynamic fluid flows and acoustic wave, and as a result of local pressure reduction in the liquid cavitation occurs. In this case, the cavitation bubble, moving with the flow of liquid to the area with a higher pressure, closes and emits a shock wave. After the collapse of the bubbles, micro-shocks of cumulative jets will form. The mixture, having received acceleration from the discharge channel expanding at high speed, moves from it in all directions. At the beginning of the process, the discharge channel increases with the maximum speed, at the end of the current flow, the cavity of the discharge channel continues to expand due to the inertia of the medium, reaches the largest size and then begins to shrink. The temperature and pressure in it during the expansion of the cavity fall, and increase during compression, i.e., there are damping pulsations of the cavity [6]. After a series of discharges, the natural mineral quartz is destroyed, the processing products are extracted and the cycle is repeated (figure 2).

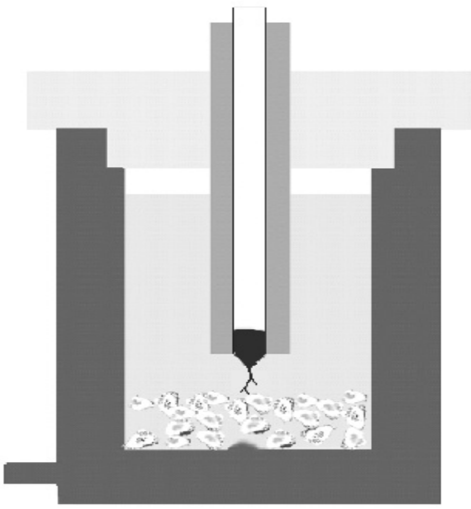

Fig.2. The process of crushing the mineral quartz.

.

In experiments, the degree of quartz grinding was studied, which was determined by the number of particles of a certain diameter, where; K - the fraction of the specified value of the total volume, C-the capacity of the capacitor Bank, d_0, d - the diameters of the fractions of the initial and final product after electro-hydro-impulse processing (figure 3).

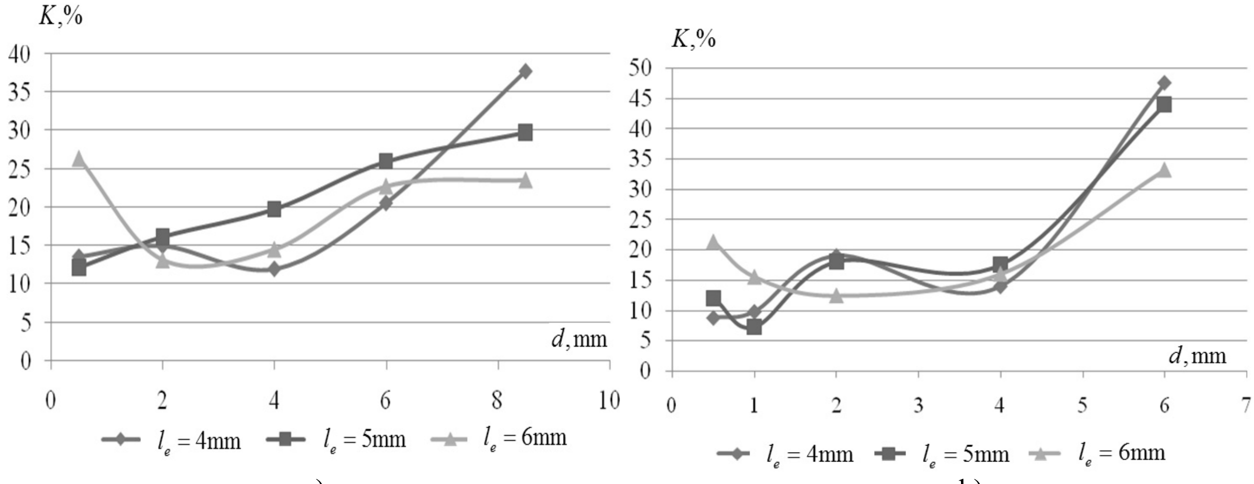

Fig.3. Graphs of the dependence of the degree of quartz grinding on the diameter of the final product fractions: a) C=0.75 mkF, d_0=10mm; b) C=0.5 mkF, d_0=7mm.

In figure 3, at the initial fraction with a diameter of d_0=10 mm and the length of the inter electrode distance of the working electrodes, the degree of grinding of small particles is 13.6%, and at the degree of small particles increases to 37.8%. When the diameter of the fractions d_0=7mm and C=0.5 mkF (figure 3, b) we see that small particles with a diameter d>1 mm are crushed most intensively. At the length of the inter electrode distance of the working electrodes, the degree of grinding is 8.8%, and at the degree of grinding was 21.3%. The obtained experimental data show that when grinding the natural mineral quartz, the most optimal diameter of the fractions is d0=7mm, and the optimal value of the capacitance of capacitor banks is C=0.5 mkF.

Figure 4 shows the results of tests performed at different discharge energy values on the W switching device.

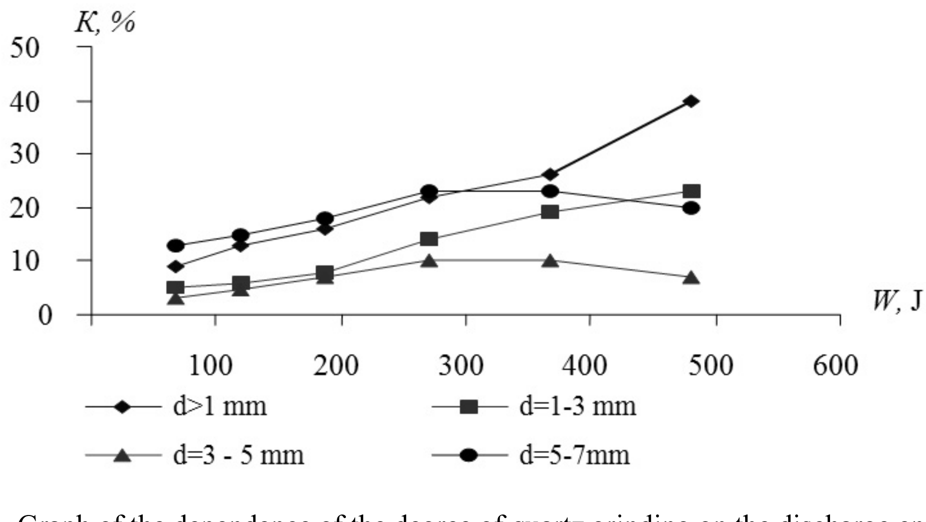

Fig.4. Graph of the dependence of the degree of quartz grinding on the discharge energy (C=0.5 mkF, d_0 =7 mm)

Conclusion

Analysis of the research results allows us to conclude that the degree of grinding of the quartz mineral (d>1 mm and d=1-2 mm) increases with increasing specific energy introduced into the discharge channel. The results obtained show that the spark gives energy through the surface of the shock wave propagation, therefore, the denser the material surrounds the discharge zone (the more crushed it is), the more rational and complete the energy allocated by the discharge channel is spent. In this regard, the electrohydraulic method of crushing into large fractions is less profitable compared to existing methods of crushing and, conversely, with an increase in the degree of grinding, electrohydraulic crushing becomes the most profitable method [2, 181 p.].

The analysis of the research results allows us to conclude that the degree of grinding of the quartz mineral increases with the increase in the specific energy introduced into the discharge channel, which is explained by the fact that the processed ore first forms a network of micro cracks on the path of the shock wave, which creates a continuous stress state.

The developed method of electrohydraulic treatment of water suspensions of minerals allows quickly and with minimal costs to obtain a powder (mixture) with certain sizes of solid fractions, change its structure and characteristics, and on its basis to create new materials with specified properties, as well as simultaneously improve sanitary and hygienic working conditions and significantly reduce environmental pollution [7].

REFERENCES

1 Kulinich V.V., Sagunov V.G., Uzhkenov B.S. and others. D*eposits of mining raw materials of Kazakhstan*. Handbook. Almaty: 2000, Vol.1, 372 p. [in Russian]

2 Yutkin L.A. *Electrohydraulic effect and its application in industry.* Leningrad, Mashinostroenie, 1986, 253 p. [in Russian]

3 Semkin B. V., Usov A. F., Kurets V.I. *Fundamentals of electrical impulse destruction of materials*. – Apatity: Publ. KNTS RAS, 1995, 189 p. [in Russian]

4 Kussaiynov K., Nussupbekov B.R., Bulkairova G.A., Omarova G.S. Electrohydroimpulse destruction of quartz mineral. *Bulletin of the Karaganda University. Physics Series.* 2004, No. 4 (36), pp. 73 – 75. [in Russian].

5 Bulkairova G.A., Shaiymerdenova G.M., Oktyabr A. Research microstructure and element composition of the mineral quartz deposit of Nadyrbay treat an electro-hydraulic method. *Bulletin of the Karaganda University. Physics Series.* 2015, No. 1 (77), pp. 66 – 71.

6 Kussaiynov K., Nussupbekov B.R. Shaimerdenova K.M., Bulkairova G. A., Khassenov A.K. Progressive methods of enrichment and complex processing of natural and technogenic mineral raw materials: *Proceedings of the international meeting*, Karaganda, 2015, pp. 129-132. [in Russian]

7 Bulkairova G.A., Nussupbekov B.R., Toktabolat G.G. Research of lectrohydraulic destruction of mineral quartz. *Bulletin of the Karaganda University. Physics Series.* 2018, No. 1 (89), pp. 81 – 87.

Article accepted for publication 09.12.2019

.

DOI 10.31489/2019No2/94-100

UDC: 621.516.7

MATHEMATICAL MODEL OF MULTI-MOTOR PLATE CONVEYOR TRACTION BODY WITH FREQUENCY-CONTROLLED ELECTRIC DRIVE

Breido I.V.[1], Kaverin V.V.[1], Kelisbekov A.K.[1], Daniyarov N.A.[2], Akhmetbekova A.M.[3]

[1]Karaganda State Technical University, APP Department, Karaganda, Kazakhstan, akelisbekov@mail.ru
[2]Kazakhmys Corporation LLP, Karaganda, Kazakhstan
[3]O.A. Baikonyrov Zhezkazgan University, Zhezkazgan, Kazakhstan

In the course of operation of chain conveyors emergency situations are possible. The reasons for this can be the intensity of the moving parts wear, increasing the pitch of the traction chains hinges, which leads to occurrence of shock loads in the traction body and failure of individual elements of the conveyor. Upon reaching a certain limiting increase in the pitch of the traction unit, further operation of the chain transmission cannot be possible due to significant decreasing the safety factor of the chains, violation of the ease of movement, or violation of the engagement of the chain joints with sprockets and cams of the intermediate drives. In the considered works dealing with studying the operating modes of plate conveyors, methods of solving the problem of distribution of loads between the master and slave drives in a multi-motor plate conveyor by means of a frequency-controlled electric drive are not considered.

Keywords: traction body, plate conveyor, frequency-controlled electric drive, load distribution, mathematical model.

Introduction

The operational experience of multi-drive plate conveyors shows that their high efficiency is possible provided that the conveyors are equipped with systems and tools for automatic distributing the total load of the conveyor between its drives, controlling the speed of the bearing belt, eliminating equalizing forces in the traction chain of the conveyor, automatic starting the multi-drive conveyor taking into account elastic-viscous properties of the traction-bearing belt and a number of other factors [1-4]. At present the intensity of developing new deposits is increasing, which leads to increasing the cargo flows. High complexity of the rock and ore delivery necessitates searching for various ways of improving the operation of open-cast plate conveyors (one of which is automation of the technological process of the conveyor operation). With the reloading-free transportation scheme, due to the presence of a two-drive system in the conveyor, it is necessary to solve the problem of automatic distribution of the total load in the traction body of the conveyor between the master and slave drives.

The distribution of load between electric drives of chain conveyors, in particular plate conveyors, was studied by such scientists as: Andrienko P.D., Babokin G.I., Bernshtein A.Ya., Blum O.O., Averbukh A.M., Borisov B.O., Brykhta P., Kachi V., Tezing X., Geiler L.B., Goykhman M.E., Hiller A.M., Saginov A.S., Daniyarov A.N., Akashev Z.T., Breido I.V., Shevchenko V.I., Yeshchin Ye.K. The analysis of works by the above scientists shows that in the course of operation of the multi-drive plate conveyor, in the traction, in addition to the calculated forces (pre-tension, static and dynamic components of resistance to movement), additional equalizing forces take place. It is clear that the reasons for their occurrence are various, but the main ones should be considered changing the conveyor loading mode, changing the values of the geometric parameters of drive parts during operation, the effect of external climatic conditions on the value of the coefficient of basic resistance to movement. In addition to the main factors, there can be minor ones that are manifested only in certain operating modes, with a particular electric drive system. They are nonequivalence of the pitch of the traction chain links, the static error of the speed control system of the rotors of the motors of the master and slave electric drives [5-7].

In the course of operation of chain conveyors, emergency situations are possible, the causes of which can be the intensity of the moving parts wear, increasing the pitch of the traction chains hinges, which leads to the occurrence of shock loads in the traction body and failure of individual elements of the conveyor [7]. Shock loads, periodically repeated and caused by wear and extension of the traction chain lead to surge currents in the power part of the electric drive power supply, which subsequently leads to overheating of the electric motor. Upon reaching a certain limiting increase in the pitch of the traction unit, further operation of the chain transmission cannot be possible due to a significant decrease in the safety factor of the chains, violation of the ease of movement or disturbance of engagement of the chain joints with sprockets and cams of the intermediate drives, which leads to frequent failures in the course of operation of the conveyor traction body [8]. The progress achieved in the development of power semiconductor technology, the creation of high-quality and powerful frequency converters using PWM modulation, the introduction of high-speed and high-discharge industrial controllers made it possible to use frequency-controlled AC drives for plate conveyors based on commercially available asynchronous motors for the mining industry [9-15].

It should be noted that in the presented works dealing with studying and modernizing plate conveyor operating modes, methods of solving the problem of load distribution between the master and slave drives in a multi-motor plate conveyor by means of a frequency-controlled electric drive are not considered. Based on the foregoing, it is relevant to solve the problem of load distribution between the master and slave drives. The objective of this work is to develop mathematical models that describe dynamic processes of the traction body and methods of load distribution between the master and slave electric drives of a multi-motor plate conveyor by means of a frequency-controlled electric drive, taking into account elastic properties of the traction body of the plate conveyor. The moments of the master and slave frequency-controlled electric drives are taken as the input parameters of the model.

Objective of the work: developing mathematical models describing the dynamic processes of the traction body operation and methods of load distribution between the master and slave electric drives of a multi-motor plate conveyor by means of a frequency-controlled electric drive, taking into account elastic properties of the traction body.

1. Analysis of previously developed methods of solving the problem

In work [1] it was noted that the most acceptable method of control providing the reduction of equalizing forces in the traction chain to minimum values is a combined one. The mismatch of the rotation angles of the shafts of the drive chain sprockets is controlled, and at the same time, the elastic elongations of the traction body on each span are compensated by working out the force difference between the actual tension value at the end point of the inter-drive section and its value corresponding to this load mode. The disadvantage of this method is that it is difficult to achieve the accuracy of matching the rotation angles of the drive sprockets due to the difference in the calculated geometric parameters of the structures of the electric drive and traction body parts and components and the actual ones.

In the work by Dr. Engineering, Professor I.V. Breido there was studied the automatic load distribution system in the course of industrial tests of the SPM-128P face conveyor with a thyristor electric drive, by stabilizing the speed on the master drive and the load moment on the slave drive [2]. During the test, the ratio between the load current of the master drive and the load current of the slave drive was 2:1. In this method there were used adjustable DC electric drives with sequential excitation motors, which do not allow providing the required dynamic characteristics to compensate for the elastic elongations of the traction body of the plate conveyor.

.

In the article by G. Babokin it was proposed to perform load balancing between the head and end electric drives of the conveyor by separate control of frequency converters supplying asynchronous motors (AM) of the head and end drives [8]. When considering the electric drive, the law of frequency control was adopted with maintaining a constant flow of the AM; active resistance of the AM stator was not taken into account in this version, and the load of the AM within the working area of mechanical characteristics was considered. Under the difference between the parameters of the head and end drives, their mechanical characteristics come from one point on the frequency axis and have different slopes to the moment axis. The load distribution between the drives is proportional to the rigidity of the mechanical characteristics. To equalize the loads of the head and end drives, it is proposed to control simultaneously the rotational speeds of both drives (AM): for the mechanical characteristic having a higher rigidity, down from the rated one, and for the one with a lower rigidity, up from the rated one until the AM moments are equal (1:1). The use of the variable frequency drive allows damping dynamic loads in a higher frequency region, which is typical for plate conveyors. The disadvantage of this method is the equal predetermined ratio of traction moments of the master and slave drives, which does not take into account the different loads acting on the working and idle branches of the traction body.

Thus, to ensure constant conveyor performance with variable load per unit of length of the traction body, as well as to distribute loads between the master and slave drives, it is necessary to equip plate conveyors with frequency-controlled electric drives. Among the commercially available electric motors in the CIS countries with an independent cooling system that provides high torque characteristics in a wide speed range, there are known the FCAMs series [16].

2. Results of mathematical modeling of the traction body of the plate conveyor

Having reached the rated speed of movement of traction body (1), the conveyor begins to be loaded with ore from hopper (2) (Fig. 1). When the traction body is fully loaded with the load (3)of mass *m*, head master electric drive (4) starts working to move the loaded upper branch (6) of the traction body, end slave electric drive (5) of the lower branch (7), respectively.

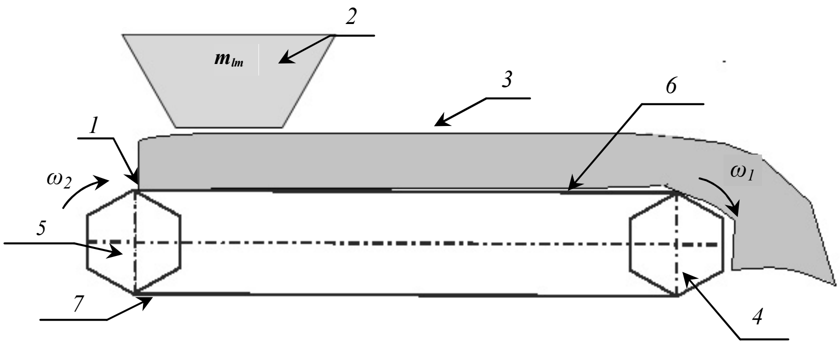

Fig.1. Diagram of loading a multi-motor plate conveyor with ore

The elements of the traction body of the multi-drive conveyor (MDC) possess elasticity, rigidity, inertiathe values of which must be taken into account when developing a mathematical model that describes the dynamic processes that occur in various units of the MDC in the course of its operation. To solve the problems of dynamics, the studied MDC units can be represented in the form of separate inertial elements interconnected by elastic bonds. For transient processes (starting, braking, speed change) it is necessary to take into account the effect of rotating and linearly moving parts of the traction body, electric drive, and the load mass. To do this, there is used the method of bringing all the moving masses to the shafts of the corresponding motors. The calculation formulas are compiled for the complete bringing to the motor shafts the moments of inertia of the rotating parts of the gearboxes, the moving traction body, and the load mass. The masses of the upper branch of the traction-carrying body, sprockets and rotating parts of the first gearbox are brought to the rotor of the driving motor, the masses of the lower branches of the traction body, sprockets and rotating parts of the second gearbox are brought to the rotor of the driven slave motor. Thus, the conveyor is replaced by a two-mass system connected by elastic links of the lower and upper branches. The diagram of a multi-motor plate conveyor with asynchronous frequency-controlled electric drives is presented in Figure 2.

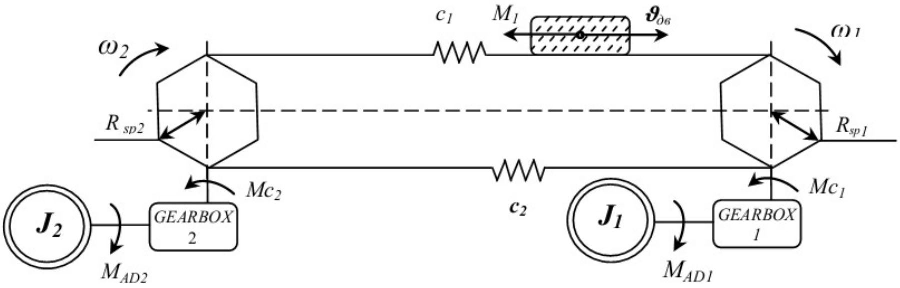

Fig.2. The diagram of a multi-motor plate conveyor with asynchronous frequency-controlled electric drives

The system of equations for the conveyor and the conditions under which the load is distributed between the electric drives (limiting unreasonable dynamic overloads in the traction body of the plate conveyor) is presented below:

$$J_{\Sigma 1}\frac{d\omega_1}{dt} = M_{AD1} - M_{c1} - M_{lm} - c_1\int(\omega_1-\omega_2)dt + c_2\int(\omega_2-\omega_1)dt \quad (1)$$

$$J_{\Sigma 2}\frac{d\omega_2}{dt} = M_{AD2} - M_{c2} - c_2\int(\omega_2-\omega_1)dt + c_1\int(\omega_1-\omega_2)dt \quad (2)$$

$$J_{\Sigma 1} = (J'_{red1} + J'_{red2})\frac{1}{i^2\eta_{r1}} + J_{AD1} = (m_{ub}+m_{lm})\frac{R_1^{\,2}}{2i_1^{\,2}\eta_{r1}} + J_{AD1} \quad (3)$$

$$J_{\Sigma 2} = J''_{red1}\frac{1}{i^2\eta_{r2}} + J_{AD2} = m_{lb}\frac{R_2^2}{2i_2^2\eta_{r2}} + J_{AD2} \quad (4)$$

$$c = dP/d\varepsilon, \quad \text{at} \quad [P_{\min}\langle P_{nom}\langle P_{\max} \quad (5)$$

$$M_i = 2M_{ki}S_{kn}(S_n/(S_n^2 + S_{kn}^2)), \quad \text{at} \quad [M_{\min}\langle M_{nom}\langle M_{\max}] \quad (6)$$

,

where:

M_{AD1} is the electromagnetic moment developed by the first master electric motor;

M_{c1} is the static moment reduced to the shaft of the first electric motor;

M_{AD2} is the electromagnetic moment developed by the second slave electric motor;

M_{c2} is the static moment reduced to the shaft of the second motor;

M_{lm} is the moment of resistance forces from the mass of the load transported;

ω_1, ω_2 are the angle speeds of rotation of the first and second electric motors, respectively;

$J_{\Sigma 1}$ is the inertia moment of the upper branch of the traction body taking into account the mass of the load transported reduced to the master electric motor;

$J_{\Sigma 2}$ is the inertia moment of the lower branch of the traction body taking into account the mass of the load transported reduced to the slave electric motor;

c_1, c_2 are the coefficients of rigidity of the upper and lower branches, respectively;

J'_{red1} are the reduced inertia moments of the traction body upper branch;

J'_{red2} are the reduced moments of the transported load mass inertia;

J''_{red1} are the reduced moments of the traction body lower branch mass inertia;

.

m_{ub} , m_{lm} are the masses of the upper branch and the load reduced to the radius of sprocket of the master drive;

m_{lm} is the mass of the lower branch reduced to the radius of sprocket of the slave drive;

i_1 , i_2 are the transfer ratios from the master and slave motors shafts to the corresponding gearboxes;

$P$is the conveyor traction body tension;

R_{sp1} , R_{sp2} are the radiuses of the master and slave drives sprockets;

M_i is the torque developed by the$n$-th drive;

M_{ki} is the critical moment developed by the$n$-th drive;

ε_i is the relative deformation of the traction body on the i-th drive.

This system of equations simulates the operation of a plate conveyor that is represented by a two-mass system with various inertial masses and moments of resistance. The inertia of the master drive is determined by the transported inertial masses of the master drive, the traction body, taking into account the parameters of the gearbox, as well as the flywheel masses of the asynchronous motor. The inertia of the slave drive is determined by the masses of the lower branch, the characteristics of the gearbox and the flywheel masses of the motor. The calculated resistance values of the master and slave drives must be determined taking into account the effect of external climatic conditions of operation.

It is known that the traction body rigidity directly depends on traction tension. From the first condition $c = dP / d\varepsilon$ for ensuring the limitation of traction efforts it follows that rigidity (the elastic modulus) of the upper branch of the traction body changes in the course of the conveyor operation depending on the degree of loading the working branch. In the mathematical model for describing the operation of the conveyor, the presented parameters: M_{c1}, M_{lm}, M_{c2}, $c_1\int(\omega_1 - \omega_2)dt$, $c_2\int(\omega_2 - \omega_1)dt$ are variable. So with the passage of time, they change depending on the characteristics of individual operating modes, the effect of external technological operating conditions and other factors.

In the course of the conveyor operation, increasing the critical slip of the induction motor and rigidity (the elastic modulus) of the traction body leads to a more uniform load distribution between the drives. The electromagnetic moment of the induction motor is developed by the interaction of the current in the rotor winding with the rotating magnetic field of the stator. The electromagnetic moment is inversely proportional to the frequency of the current supply network:

$$M_{AD} = N / \omega = (N \times p)/(2\pi f) \tag{7}$$

The moment of resistance forces from the mass of the transported load acting on the upper branch of the traction body is determined by the following expression:

$$M_{lm} = cg/(q_{tb} + q_n), \tag{8}$$

where:

c is rigidity (elasticity) of the traction body;

g is acceleration of gravity;

q_{tb} is the linear mass of the traction body;

q_n is the mass per unit of length on the traction body.

In order to develop a simulation model of the traction body of a multi-motor plate conveyor with a frequency-controlled electric drive, it is necessary to bring differential equations (1-6) into relative units.After the corresponding transformations, there is obtained the system of equations of the conveyor transfer function:

$$T_1\frac{d\omega_1^*}{dt}=(M_{AD1}^*-M_{c1}^*-M_{lm}^*)-\frac{1}{T_1}\int(\omega_1^*-\omega_2^*)dt+\frac{1}{T_3}\int(\omega_2^*-\omega_1^*)dt \tag{9}$$

$$T_4\frac{d\omega_2^*}{dt}=(M_{AD2}^*-M_{c2}^*)-\frac{1}{T_3}\int(\omega_2^*-\omega_1^*)dt+\frac{1}{T_2}\int(\omega_1^*-\omega_2^*)dt \tag{10}$$

where:

$T_1=\dfrac{\omega_{n1}}{M_{n1}}J_{\Sigma1}$ is the time constant of the first master electric drive;

$T_2=\dfrac{M_{n1}}{\omega_{n1}c_1}$ is the time constant of the moment of elastic oscillations of the upper branch;

$T_3=\dfrac{M_{n2}}{\omega_{n2}c_2}$ is the time constant of elastic oscillations of the lower branch;

$T_4=\dfrac{\omega_{n2}}{M_{n2}}J_{\Sigma2}$ is the time constant of the second slave electric drive.

$$T_1=\frac{\omega_{n1}}{M_{n1}}J_{\Sigma1}=2.15s,\ T_2=\frac{M_{n1}}{\omega_{n1}c_1}=0.17s,\ T_3=\frac{M_{n2}}{\omega_{n2}c_2}=0.09s,\ T_4=\frac{\omega_{n2}}{M_{n2}}J_{\Sigma2}=1.43s$$

Table 1. Specifications and time constants of the conveyor electric drives and traction body

Type of asynchronous motor	Names of parameters								
	Rated power, kW	Rated/max. speed, rpm	Rated moment, Nm	Rated current, A	Rated voltage, V	Rated frequency, Hz	Rotor J, kg/m^2	Cos φ	$T_1$and T_4, respect.
Head master FCAM280S4	110	1450/ 4500	707	202	380	50	2.2	0.85	2.15
End slave FCAM225M4	55	1450/ 4500	356	105	380	50	0.5	0.86	1.43

Conclusion

In this work there is substantiated the relevance of theoretical studies of plate conveyors with the master and slave adjustable drives. An equivalent circuit for the traction body has been developed and justified taking into account the flywheel masses of the electric motor and the gear ratio of the gearbox.

The article presents the developed mathematical model in relative units that describes dynamic processes of the traction body of the plate conveyor. Based on this model, the transfer function has been constructed and the time constants of the dynamic moments and moments of elastic vibrational forces of the working and idle branches of the traction body have been calculated. The developed model can be used to synthesize a load distribution system in a frequency-controlled electric drive of a plate conveyor.

.

Based on the above-said, there has been proposed a method for ensuring load distribution between the master and slave adjustable drives of the plate conveyor, taking into account characteristics of its technical parameters and technological operating conditions.

REFERENCES

1 Saginov A.S., Daniyarov A.N., Akashev Z.T. *Fundamentals of design and calculation of career plate conveyors*. Alma-Ata, Nauka,1984, 28 p. [in Russian]

2 Breido I.V. *Control principles and methods for the synthesis of controlled electric drives of underground mining machines.* Almaty, Giga Trade, 2012, pp. 78-85. [in Russian]

3 Breido I.V., Daniyarov N.A., Kelisbekov A.K., Akhmetbekova A.M. Using Soft Start Method in Multi-Drive Plate Conveyor Operation. *University Proceedings Journal*, KSTU Publ. House, 2018, No.4, pp.124. [in Russian]

4 Breido I.V., Intykov T.S., Daniyarov N.A., Kelisbekov A.K., Semykina I.Yu. Mathematical model of apron conveyor controlled Electric drive in operation starting modes. *NEWS of the Academy of Sciences of the Republic of Kazakhstan*, 2019, Vol. 2, No. 434, pp. 232-237. doi.org/10.32014/2019.2518-170X.59.

5 Belenky D.M., Kuznetsov D.G. *Plate conveyors.* Moscow, Nedra Publishing House, 1971, 184 p. [in Russian]

6 Perten Yu.A., Volkov R.A., Gnutov A.N., Dyachkov V.K. *Conveyors.* Reference book. Leningrad Motorering, 1984, 76 p. [in Russian]

7 Tazabekov I.I., Daniyarov N.A., Balgabekov T.K. *Adjustable drives of main chain conveyors*. Monograph. Karaganda, Publishing house of KSTU, 2009, 163 p. [in Russian]

8 Babokin G.I. Twin motor electric conveyor with load balancing system. *Izvestiya TulGU. Technical science,* 2010, Issue 3, Part 2, pp. 7. [in Russian]

9 Pajchrowski, T. Comparison of control structures for direct drive with PMSM motor with variable inertia and load torque. *Przeglad Elektrotechniczny.* 2018, Vol. 94, No.5, pp. 133-138.

10 Breido I.V., SivyakovaG., & Gurushkin A. State and Prospects of Developing the Interconnected Multi-motor Semiconductor Electric Drives. *Industrial Motorering–Challenges for the Future*. 2013, pp. 311 – 330.

11 Breido I.V. The State and Prospects of Development of the Interconnected Multi-Motor Semiconductor Electric Drives. *Scientific Book.* 2013, Vol. 12, pp. 193-212.

12 Breido I., Kaverin V., Ivanov V. Telemetric Monitoring Insulation Condition of High Voltage Overhead Power Lines. *Proceedings of the 29th DAAAM International Symposium*. 2018. pp.0319-0328. doi:10.2507/29th.daaam.proceedings.046.

13 Štatkić S., Jeftenić I.B., Bebić M.Z., et al. Reliability assessment of the single motor drive of the belt conveyor on Drmno open-pit mine. *International Journal of Electrical Power and Energy Systems*, 2019, Vol. 113, pp. 393-402. doi: 10.1016/j.ijepes.2019.05.062

14 Windmann S., Niggemann O., Stichweh, H. Computation of energy efficient driving speeds in conveying systems. *At-Automatisierungstechnik.* 2018, Vol. 66 (4), pp. 308-319. doi: 10.1515/auto-2017-0094

15 Świder, J., Herbuś, K., Szewerda, K. Control of Selected Operational Parameters of the Scraper Conveyor to Improve Its Working Conditions. *Advances in Intelligent Systems and Computing*, 2019, 2019934, pp. 395 – 405. doi: 10.1007/978-3-030-15857-6_39

16 The catalog of FCAM. Research and Development Design and Technological Institute of Electrical Motorering of Russia. 2014, pp. 31 – 34. http://www.ruselprom.ru/upload/iblock/912/katalog_2014.pdf

Article accepted for publication 9.12.2019

DOI 10.31489/2019No2/101-104

UDC 531.226: 621.38

QUANTUM - CHEMICAL CALCULATION OF DESTRUCTION AND HYDROGENATION OF THE OIL ASPHALTEN UNDER INFLUENCE OF SHORT PULSE DISCHARGES

Satybaldin A.Zh., Karabekova D.Zh., Khassenov A.K., Aitpaeva Z.K., Seldygaev O.B.

E.A. Buketov Karaganda State University, Karaganda, Kazakhstan, satybaldin.1975@mail.ru

Last years the interest to energetically influence on material for the reason change their characteristic remains stabiles high. The calculation of the oil material's individual particularities show it is possible to change structure in necessary direction using shock influence without observable external energy expenses. As such influence, for controlling structure of material used electro-hydro-impulse influence on the oil. It is can be reached easy to increase of regulate nuclear structure using this effect. Results of properties study of the heavy oil from the Karazhanbas field, which was subjected to electro-hydro-pulse discharge for the purpose of demetallization, are presented.

Keywords: oil asphalten, polycyclic systems, quantum-chemical calculations, semi-empirical approximation PM3, electro-hydro-pulse processing.

Introduction

Oil asphalt is the most highly condensed, highly aromatized part of heavy oil. The average number of aromatic cycles is 4–7, cycloparaffinic 1–2. Alkyl substituents are short and medium $C_1 - C_6$. Identified heterocycles of oxygen, sulfur, nitrogen, sulfides, ketone, phenolic, alcohol, carboxylic acid groups, porphyrin and non-porphyrin complexes, as well as quinoid cycles and lactones are present in oil asphaltene. In [1], it was shown that polycyclic systems provide stabilization of unpaired electrons, the source of formation of which are broken bonds in the boundary atoms of condensed carbon. The concentration of paramagnetic centers in high viscosity oil (HVO) was previously determined in [1], the concentration of free radicals is 1.1×10^{17} spin/g, the EPR line width (ΔH = 0.43 Er). However, the EPR showed us only the total amount of free radicals in the HVO and did not allow us to identify them.

1. Statement of the problem

Quantum-chemical calculations of the ground state of the asphaltene molecule were carried out non-empirically in the limited version of the Hartree-Fock method (RHF method) in the 3-21G (d) basis with geometry optimization in the semi-empirical approximation PM3 (Gaussian 03 software package) [2]. The asphaltene molecule has an extremely complex structure. Figure 1 shows the structural formula of the petroleum asphaltene molecule.

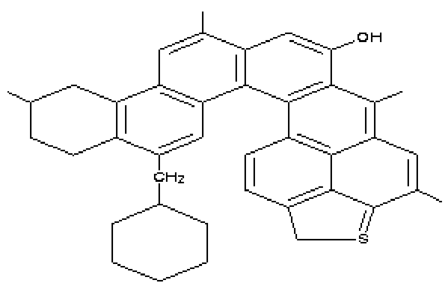

Fig. 1. The structural formula of the oil asphaltene molecule [1]

.

The spatial configuration of asphaltene includes aromatic, cyclic and heterocyclic rings and, as can be seen from Figure 2, the right and left parts of the molecule are oriented relative to each other at an angle of ~ 45-50 °. The numbering of atoms corresponds to the model for semi-empirical and non-empirical calculations. The optimized PM3 structure was used for calculations in the basis of 3-21G (d), because the presence of a sulfur atom in the molecule requires d-orbitals to be taken into account, which is possible in the framework of non-empirical calculations. Therefore, further discussion is carried out using the calculation data by the RHF/3-21G (d) method.

One of the further transformations of asphaltene is the hydrogenation of a molecule. Since the hydrogenation reaction is stepwise, for a preliminary study we considered the direct addition of a hydrogen radical (atom) to asphaltene. The hydrogen atom is an electrophilic reagent. Its attachment to the studied molecule should occur, apparently, to the unsaturated aromatic part of asphaltene.

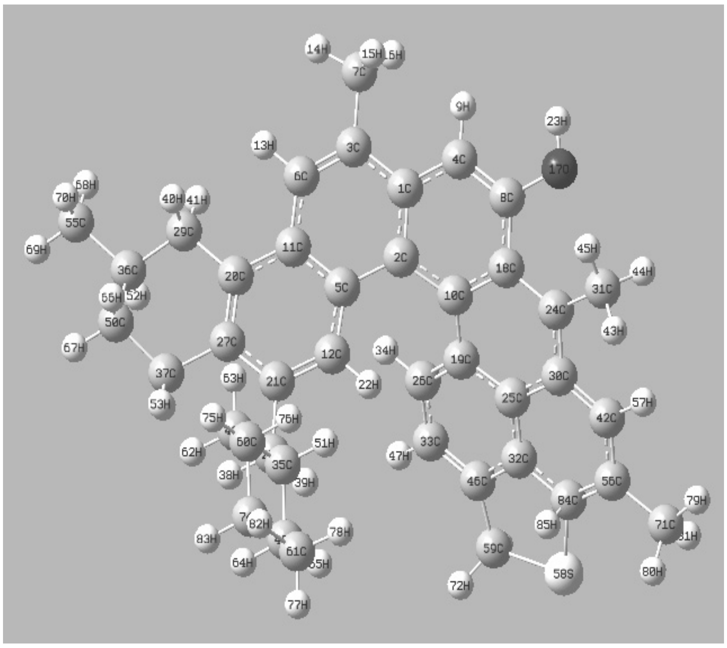

Fig.2. Mutual orientation of a part of a petroleum asphaltene molecule

To determine the direction of attack, the approximation of boundary orbitals was used. Figures 3 and 4 show the HOMO (upper occupied molecular orbital) and LUMO (lower unoccupied molecular orbital) asphaltene, respectively.

The orbital energy of the hydrogen radical is 0.11747 a.u. The LUMO energy of asphaltene is equal to 0.06663 a.u. A small difference in energies suggests the interaction of these orbitals. However, due to the smallness of the energy intervals, nearby orbitals can also interact with the attacking electrophile. Consequently, the number of atoms - centers of attack may be greater.

2. Discussion of experimental studies results.

We calculated the change in the energy of the system as the hydrogen atom approaches the C10 reaction center (selected taking into account the large weight coefficients of the molecular orbital) of the molecule with a step of 0.5 and 0.1 Å. The electronic configuration of the asphaltene - hydrogen radical system contains 313 electrons, of which, according to a non-empirical calculation, 157 electrons with alpha spin and 156 electrons with beta spin, which corresponds to 156 double and one once filled molecular orbitals, are shown in Figure 5.

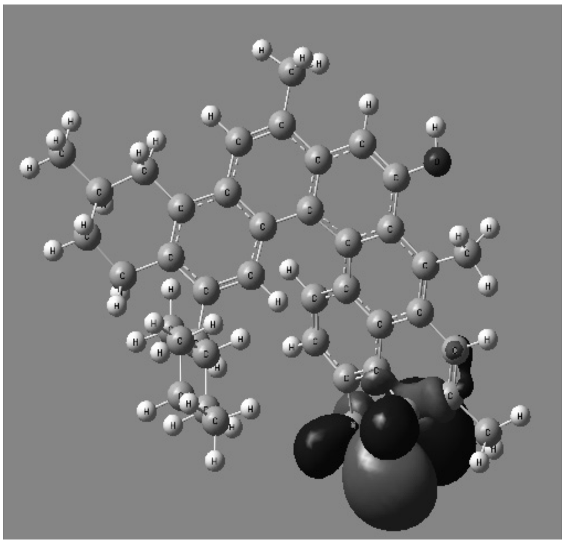

Fig.3. HOMO level of asphaltene

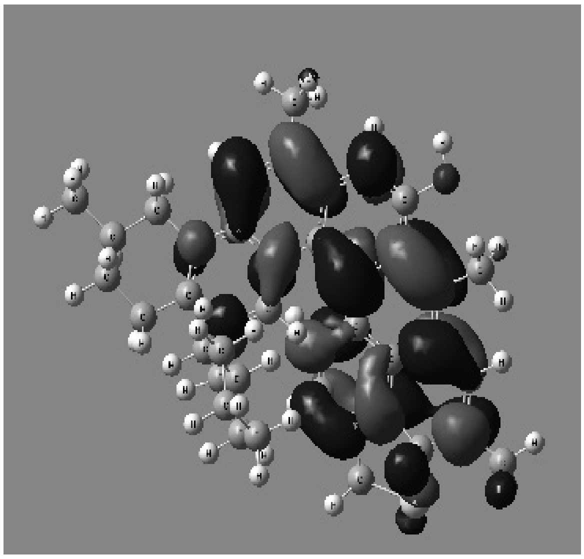

Fig.4. LUMO level of asphaltene

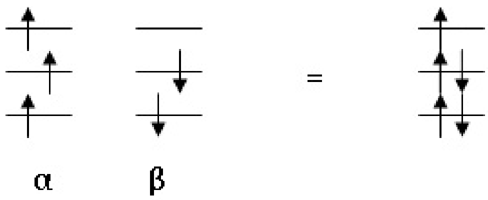

Fig.5. Schematically presented mechanism of filling with molecular orbitals in the calculations according to the ROHF method.

Due to the choice of the ROHF / 3-21G (d) calculation method, the problem of the purity of the spin state did not arise. The degree of purity of the spin state was estimated by the value of the square of the spin, which is 0.75 for the doublet. Figure 6 shows the surface profile of the potential energy E of the petroleum asphaltene hydrogenation reaction. From Figure 6 it is seen that the energy rises with a decrease in the distance between H and C10 to 1.4 Å, then drops and rises again. At 1.2 Å, a minimum is observed corresponding to the formation of a new oil radical.

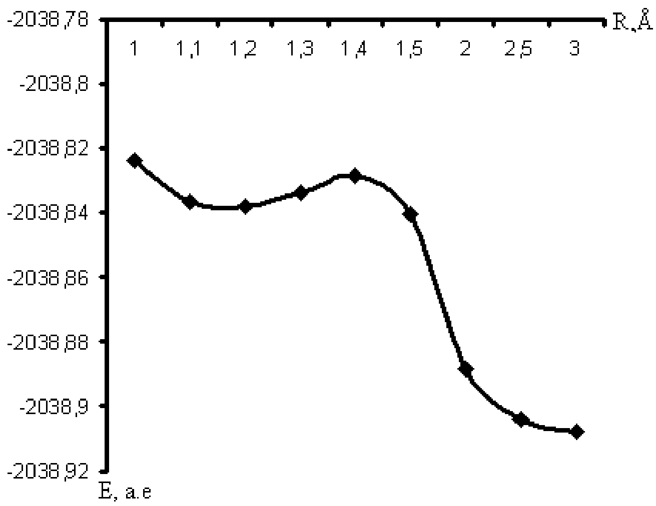

Fig.6. Surface profile of potential energy of petroleum asphaltene hydrogenation reaction.

Thus, the recombination of petroleum asphaltene with a hydrogen atom, which is a type 1 free radical, will obviously occur in places of excess spin density. When trying to quantum-chemical calculation of such a system, optimization of the geometry will lead to the opening of the heterocycle. Heavy oils, bitumen, oil residues differ from ordinary oils and oil products in the increased content of heavy metals (vanadium, nickel, iron, copper, molybdenum), sulfur, nitrogen, asphaltenes and resins [3]. Heavy metals (vanadium V, nickel Ni) adversely affect the quality of the target product and make it difficult to process, therefore demetallization of heavy oil residues and HVO is an important stage before their further processing [4]. The results of experiments with heavy oil from the Karazhanbas field, which was subjected to electrohydropulse discharge for the purpose of demetallization, are presented in Table 1.

Table 1. High viscosity oil demetallization of the Karazhanbas field, heavy oil is pre-processed using electrohydropulse discharge

Raw materials, products processed by high viscosity oil	Ni, g/t	V, g/t	The degree of demetallization of high viscosity oil, %		The degree of enrichment of the solid residue, %	
			Ni	V	Ni	V
HVO of Karazhanbas field	65-70	320				
Fraction of HVO under $T_{boiling}$> 300 ^{0}C	30	60	73	65		
Solid residue	480	650			4.3	3.8

Conclusion

The results of the HVO demetallization and the HVO fraction above 300° C (Table 1), are showed that the degree of demetallization for vanadium is 65%, for nickel 73%, the enrichment of the solid residue for vanadium increased by 3.8%, and for nickel 4.3%, respectively. The accumulation of heavy metals by a substance in the solid phase can occur due to complexation with chemical active groups (OH, COOH, SO_3, NH_2, etc.). Nickel and vanadium metals in the BBH of the Karazhanbas deposit are contained in porphyrin and non-porphyrin complexes, which form the basis of oil asphaltenes [5]. The above quantum chemical calculations confirm that the hydrogenation reaction of petroleum asphaltene and the demetallization process begin with an attack by a hydrogen atom (type 1 free radical) of a polyaromatic heterocycle that contains a sulfur, nitrogen or oxygen atom.

REFERENCES

1 Baikenov M.I. *Catalytic hydrogenation of coal and heavy oil*: Abstract. diss. dr . chem. sciences. - Almaty, 1999, 211 p. [in Russian]

2 Frisch M.J., Trucks G.W., Schlegel H.B. et al. *Encyclopedia of physical orcanic cemistri Gaussian 03,* Revision A.1, Gaussian Inc., Pittsburgh, 2003, 4372 p.

3 Jykova E.M., Sevostyanov V.P., Holkina T.V. Electro-hydraulic stabilization of polymer-containing cements. *University News, Series Chemistry and Chemical Technology*. 2008, Vol. 51, No. 11, pp. 110 – 113.

4 Cochevanov V.G., et al. *Spectrografic determination of cobalt, nickel, vanadium, chromium, titanium in silicate rocks and iron ore. Instruction No. 106-C.* Scientific Council on Analytical Methods (spectral methods). Moscow, 1971, 29 p. [in Russian]

5 Satybaldin A.Zh., Baykenov MI, Tanasheva NK, et al. Investigation of the influence of electrohydropulse shock waves on the rheological properties of oil sludge: on the surface of the Atasu-Alashankou oil pipeline. *Proceeding of the L VIII Intern. scientific and practical conf. "Technical sciences - from theory to practice"*. Novosibirsk, 2016, No. 25 (53), pp. 82 -89. [in Russian]

Article accepted for publication 4.12.2019

DOI 10.31489/2019No2/105-112

UDC 517.958+ 004.942+533.9

ON THE KERNEL PROPERTIES OF THE INTEGRAL EQUATION FOR THE MODEL WITH THE ESSENTIALLY LOADED HEAT EQUATION

Yesbayev A.N.[1], Yessenbayeva G.A.[2], Yessenbayeva G.A.[3], Ramazanov M.I.[2]

[1]L.N. Gumilyov Eurasian National University, Nur-Sultan, Kazakhstan

[2]E.A. Buketov Karaganda State University, Karaganda, Kazakhstan, esenbaevagulsima@mail.ru

[3] Karaganda Economic University of Kazpotrebsoyuz, Karaganda, Kazakhstan

Mathematical modeling of thermophysical processes in an electric arc of high-current disconnecting apparatuses leads to a boundary value problem for an essentially loaded heat conduction equation. Taking into account the transience of such phenomena, in some cases only a mathematical model is able to give adequate information about their dynamics. The mathematical model in the form of the boundary value problem is reduced to the Volterra integral equation of the second kind, as a result, we have that the solvability of the boundary value problem is equivalent to the solvability of the reduced integral equation. Thus, there is a need to study the reduced integral equation. The results of this study (various representations and properties of the kernel-forming function in general case and the types of the kernel of the integral equation in special cases) are presented in this article. The article is focused at physicists and engineers, as well as scientific researchers engaged in the practical applications of loaded differential equations.

Keywords: thermophysical processes, electric arc, loaded heat equation, boundary value problem, reduced integral equation, kernel of an integral equation.

Introduction

The modern trend in technology to use super-strong and super-weak currents in many electrical devices leads to the need to study phenomena outside the usual current range. When switching electrical devices or overvoltage an electric arc may appear in the circuit between the current-carrying parts [1]. To ignite the arc, you either need to overcome the breakdown voltage of the medium between the electrodes, or break the electrical circuit.

The occurrence of an electrical discharge in the form of an electric arc in an uncontrolled environment, as in the case of an arc flash, can lead to injury, fire, equipment damage, and other accidents. These are, first of all, contact switching devices used in power supply and electric drive: high-voltage switches, circuit breakers, magnetic starters, contactors, sectional insulators on the contact network of electrified railways and urban electric transport, etc.. When disconnecting the loads of the above mentioned devices or breaking the electrical circuit, an arc arises between the opening contacts [1].

Experimental studies of such phenomena are complex and burdensome due to their temporal short duration, therefore, in many cases, only a mathematical model can give necessary and adequate information about their dynamics [1]. During the burning of an electric arc a lot of heat is released, a burning temperature of the electric arc reaches values of more than 3000 degrees Celsius. In high-voltage circuits, the arc length reaches a meter or more. As a result, there is a danger of harming human health and damage to equipment, as well as damage to environment.

Thermo-physical processes in the electric arc of high-current disconnecting devices are described by the physical model, the mathematical interpretation of which is the studied problem (1) - (3) [1], [2]. The formulation of the boundary value problem (1) - (3) is as follows. In the domain $\Omega = \{(x,t): \quad x \in (0,\infty); \quad t \in (0,\infty)\}$ the essentially loaded heat equation is investigated

.

$$\frac{\partial u}{\partial t}-\frac{\partial^2 u}{\partial x^2}-\frac{1-2\beta}{x}\cdot\frac{\partial u}{\partial x}-\lambda\cdot\left.\frac{\partial^k u}{\partial x^k}\right|_{x=\bar{x}(t)}=f(x,t) \qquad (1)$$

where $u=u(x,t)$ is an unknown function. β, λ и k are numerical parameters, and $0<\beta<1$, $\lambda\in C$, $k=0,1,2...$ $\lambda\cdot\left.\frac{\partial^k u}{\partial x^k}\right|_{x=\bar{x}(t)}$ is a loaded summand, $f(x,t)$ is a known function defined in the domain Ω. The load point moves according to a given law $x=\bar{x}(t)$ for $t\in(0,\infty)$, and the initial condition

$$u(x,0)=g(x), \qquad (2)$$

a boundary condition

$$u(0,t)=h(t) \qquad (3)$$

are given. Functions $g(x)$ and $h(t)$ are given at $x\in(0,\infty)$ and $t\in(0,\infty)$ respectively.

The mathematical model in the form of the boundary value problem (1) - (3) is reduced to the Volterra integral equation of the second kind, as a result of which the solvability of the boundary value problem is equivalent to the solvability of the reduced integral equation.

1. Reduced integral equation

When finding solutions to the boundary value problem (1) - (3) for a essentially loaded differential parabolic equation, the necessity naturally arises to study the Volterra integral equation of the second kind of the following form

$$\mu(t)-\lambda\cdot\int_0^t K_k(t,\tau)\cdot\mu(\tau)\cdot d\tau=F(t), \qquad (4)$$

where $\lambda\in C$ is the numerical parameter of the equation, $F(t)$ is the known function defined on the interval $(0,\infty)$, $\mu(t)$ is the desired function. The kernel $K(t,\tau)$ of the integral equation (4) has the form

$$K(t,\tau)=\left.\frac{\partial^k Q(x,t-\tau)}{\partial x^k}\right|_{x=\bar{x}(t)}, \qquad (5)$$

where

$$Q(x,t-\tau)=\frac{x^\beta}{2(t-\tau)}\cdot\exp\left(-\frac{x^2}{4(t-\tau)}\right)\cdot P(x,t-\tau), \qquad (6)$$

$$P(x,t-\tau)=\int_0^\infty \xi^{1-\beta}\exp\left(-\frac{\xi^2}{4(t-\tau)}\right)\cdot I_\beta\left(\frac{\xi\cdot x}{2(t-\tau)}\right)\cdot d\xi, \qquad (7)$$

and $x=\bar{x}(t)$ is the given function with $t\in(0,\infty)$, k is the order of the loaded term ($k=0,1,2...$), $I_\beta(z)$ is the order of the loaded term.

2. Various representations of the kernel-forming function $Q(x,t-\tau)$ and special cases of the kernel $K(t,\tau)$

The function $Q(x,t-\tau)$ defines the kernel of the integral equation (4), and besides

$$Q(x,t-\tau)=K_0(x,t).$$

As it is known, a type (a form) and the properties of the kernel play an important role in the question of solvability of the integral equation and dictate the methods of investigation of the integral equation. We calculate the function $Q(x,t-\tau)$ in general form and the kernel $K(t,\tau)$ in special cases and present their various types (interpretations) that will be used to determine the properties of the kernel and in the further study of the original boundary value problem (1) - (3).

1) Taking into account that [3]

$$\int_0^\infty x^{\alpha-1}\exp\left(-px^r\right)\cdot I_\nu(cx)dx = \frac{c^\nu}{2^\nu r\cdot p^{\frac{\alpha+\nu}{r}}\,\Gamma(\nu+1)}\sum_{n=0}^\infty \frac{1}{n!(\nu+1)_n}\Gamma\left(\frac{2n+\alpha+\nu}{r}\right)\cdot\left(\frac{c}{2p^{\frac{1}{r}}}\right)^{2n},$$

when $\operatorname{Re} p,\ \operatorname{Re}(\alpha+\nu)>0\,; r>1$, where

$$(\nu+1)_0=1,\qquad (\nu+1)_n=(\nu+1)(\nu+2)\cdot\ldots\cdot(\nu+n),\ n=1,2,3,\ldots$$

are Pochhammer symbols, $\Gamma(z)$ is the gamma function, from (6) we receive the following representation for the function $Q(x,t-\tau)$

$$Q(x,t-\tau)=\left(\frac{x}{2}\right)^{2\beta}\frac{1}{\Gamma(\beta+1)(t-\tau)^\beta}\cdot\exp\left(-\frac{x^2}{4(t-\tau)}\right)\cdot\sum_{n=0}^\infty\frac{1}{(\beta+1)_n(t-\tau)^n}\cdot\left(\frac{x}{2}\right)^{2n}. \tag{8}$$

We calculate $K(t,\tau)$ (5) for $k=2$. To do this, we find $K(t,\tau)$ for $k=1$

$$K(t,\tau)\Big|_{\substack{k=1\\ x=\bar{x}(t)}}=K_1(t,\tau)=\frac{\bar{x}^{2\beta}}{2^{2\beta-1}\Gamma(\beta+1)(t-\tau)^\beta}\cdot\exp\left(-\frac{\bar{x}^2}{4(t-\tau)}\right)\times$$
$$\times\sum_{n=0}^\infty\frac{\bar{x}^{2n-1}}{2^{2n}(\beta+1)_n(t-\tau)^n}\cdot\left(\beta+n-\frac{\bar{x}^2}{4(t-\tau)}\right).$$

Further, we obtain $K(t,\tau)$ for $k=2$

$$K(t,\tau)\Big|_{\substack{k=2\\ x=\bar{x}(t)}}=K_2(t,\tau)=\frac{\bar{x}^{2\beta-1}}{2^{2\beta-2}\Gamma(\beta+1)(t-\tau)^\beta}\cdot\exp\left(-\frac{\bar{x}^2}{4(t-\tau)}\right)\cdot\sum_{n=0}^\infty\frac{\bar{x}^{2n-1}}{2^{2n}(\beta+1)_n(t-\tau)^n}\times$$
$$\times\left\{\frac{\bar{x}^4}{16(t-\tau)^2}-\left[2(\beta+n)+\frac{1}{2}\right]\cdot\frac{\bar{x}^2}{4(t-\tau)}+(\beta+n)\left(\beta+n-\frac{1}{2}\right)\right\}. \tag{9}$$

2) For the function $Q(x,t-\tau)$, another a relation can be obtained using the integral representation of the modified Bessel function [4]

$$I_\beta(z)=\frac{\left(\frac{z}{2}\right)^\beta}{\Gamma\left(\beta+\frac{1}{2}\right)\cdot\Gamma\left(\frac{1}{2}\right)}\cdot\int_{-1}^{1}\left(1-t^2\right)^{\beta-\frac{1}{2}}\cdot\exp(\pm zt)dt,\quad \operatorname{Re}\left(\beta+\frac{1}{2}\right)>0,$$

the equality [4]

$$\int_0^\infty x\cdot\exp\left(-\mu x^2-2\nu x\right)\cdot dx=\frac{1}{2\mu}-\frac{\nu}{2\mu}\cdot\sqrt{\frac{\pi}{\mu}}\cdot\exp\left(\frac{\nu^2}{\mu}\right)\cdot\left[1-\Phi\left(\frac{\nu}{\sqrt{\mu}}\right)\right]$$

when $|\arg\nu|<\dfrac{\pi}{2}$, $\operatorname{Re}\mu>0$; the relationship [5]

$$\int_0^a\left(a^\mu-x^\mu\right)^{p-1}dx=\mu^{-1}\cdot a^{\mu(p-1)+1}\cdot B\left(p,\frac{1}{\mu}\right),$$

where $a,\ \mu,\ \operatorname{Re}p>0$, and the ratio [3]

.

$$\int_0^a x^{\alpha-1}\left(a^2-x^2\right)^{p-1}\exp\left(c^2x^2\right)\cdot\begin{Bmatrix} erf(cx) \\ erfc(cx)\end{Bmatrix}dx=$$

$$=\pm\frac{a^{\alpha+2p-1}c}{\sqrt{\pi}}B\left(\frac{\alpha+1}{2},p\right)\cdot{}_2F_2\left(1,\frac{\alpha+1}{2};\frac{3}{2},p+\frac{\alpha+1}{2};a^2c^2\right)+$$

$$+\begin{Bmatrix} 0 \\ 1\end{Bmatrix}\frac{a^{\alpha+2p-2}}{2}B\left(\frac{\alpha}{2},p\right)\cdot{}_1F_1\left(\frac{\alpha}{2};\frac{\alpha}{2}+p;a^2c^2\right)$$

for $a,\ \operatorname{Re} p>0$; $\operatorname{Re}\alpha>-\frac{1\pm 1}{2}$, where

$$erf(z)=\frac{2}{\sqrt{\pi}}\int_0^z e^{-t^2}dt,$$

is the error function, moreover

$$erfc(z)=1-erf(z)=\frac{2}{\sqrt{\pi}}\int_z^\infty e^{-t^2}dt;$$

$B(z)$ is a beta function;

$$_pF_q\left(a_1,...,a_p;b_1,...b_q;z\right)=\sum_{k=0}^{\infty}\frac{\left(a_1\right)_k\cdot...\cdot\left(a_p\right)_k}{\left(b_1\right)_k\cdot...\cdot\left(b_p\right)_k}\cdot\frac{z^k}{k!} \tag{10}$$

is a generalized hyper-geometric function,

$$_1F_1\left(a;b;z\right)=\sum_{k=0}^{\infty}\frac{(a)_k}{(b)_k}\cdot\frac{z^k}{k!} \tag{11}$$

is the degenerate hyper-geometric function.

After using the above equalities, the relation (7) takes the form

$$P(x,t-\tau)=\frac{x^\beta(t-\tau)^{1-\beta}}{2^{2\beta-1}\Gamma(\beta+1)}\pm\frac{x^{\beta+2}}{2^{2\beta=1}\Gamma(\beta+2)(t-\tau)^\beta}\cdot{}_2F_2\left(1,\frac{3}{2};\frac{3}{2},\beta+2;\frac{x^2}{4(t-\tau)}\right). \tag{12}$$

Substituting (12) into (6), we obtain the following representation for the function $Q(x,t-\tau)$

$$Q(x,t-\tau)=\exp\left(-\frac{x^2}{4(t-\tau)}\right)\cdot\left[\frac{x^{2\beta}}{2^{2\beta}\Gamma(\beta+1)}\cdot\frac{1}{(t-\tau)^\beta}\pm\right.$$

$$\left.\pm\frac{x^{2\beta+2}}{2^{2\beta+2}\Gamma(\beta+2)}\cdot\frac{1}{(t-\tau)^{\beta+1}}\cdot{}_2F_2\left(1,\frac{3}{2};\frac{3}{2},\beta+2;\frac{x^2}{4(t-\tau)}\right)\right], \tag{13}$$

3) Using (10) to find the function ${}_2F_2\left(1,\frac{3}{2};\frac{3}{2},\beta+2;\frac{x^2}{4(t-\tau)}\right)$

$$_2F_2\left(1,\frac{3}{2};\frac{3}{2},\beta+2;\frac{x^2}{4(t-\tau)}\right)=\sum_{n=0}^{\infty}\frac{1}{(\beta+2)_n}\cdot\left(\frac{x^2}{4(t-\tau)}\right)^n$$

and substituting the obtained relation in (13), we obtain the representation for the function $Q(x,t-\tau)$ in the form

$$Q(x,t-\tau)=\exp\left(-\frac{x^2}{4(t-\tau)}\right)\cdot\left[\frac{x^{2\beta}}{2^{2\beta}\Gamma(\beta+1)}\cdot\frac{1}{(t-\tau)^\beta}\pm\right.$$

$$\left.\pm\frac{x^{2\beta+2}}{2^{2\beta+2}\Gamma(\beta+2)}\cdot\frac{1}{(t-\tau)^{\beta+1}}\cdot\sum_{n=0}^{\infty}\frac{1}{(\beta+2)_n}\cdot\left(\frac{x^2}{4(t-\tau)}\right)^n\right]. \tag{14}$$

Now we calculate $K(t,\tau)$ when $k=2$ using a sequential differentiation of (14).

$$K(t,\tau)\big|_{\substack{k=1\\ x=\bar{x}(t)}}=K_1(t,\tau)=\frac{\bar{x}^{2\beta}}{2^{2\beta-1}\cdot(t-\tau)^{\beta}}\cdot\exp\left(-\frac{\bar{x}^2}{4(t-\tau)}\right)\times$$

$$\times\left\{\frac{1}{\Gamma(\beta+1)}\left[\frac{\beta}{\bar{x}}-\frac{\bar{x}}{4(t-\tau)}\right]\pm\frac{1}{\Gamma(\beta+2)}\sum_{n=0}^{\infty}\frac{\bar{x}^{2n}}{2^{2n+2}(\beta+2)_n(t-\tau)^{n+1}}\left[(\beta+n+1)\bar{x}-\frac{\bar{x}^3}{4(t-\tau)}\right]\right\}.$$

For $Q(x,t-\tau)$ (13), (14) the kernel $K(t,\tau)$ when $k=2$ has the form

$$K(t,\tau)\big|_{\substack{k=2\\ x=\bar{x}(t)}}=K_2(t,\tau)=\frac{\bar{x}^{2\beta}}{2^{2\beta+1}\cdot(t-\tau)^{\beta+1}}\cdot\exp\left(-\frac{\bar{x}^2}{4(t-\tau)}\right)\times$$

$$\times\left\{\frac{1}{\Gamma(\beta+1)}\left[\frac{\bar{x}^2}{2(t-\tau)}-4\beta-1+\frac{4\beta(2\beta-1)(t-\tau)}{\bar{x}^2}\right]\pm\right.$$

$$\left.\pm\frac{1}{\Gamma(\beta+2)}\sum_{n=0}^{\infty}\frac{\bar{x}^{2n}}{2^{2n}(\beta+2)_n(t-\tau)^n}\left[\frac{\bar{x}^4}{8(t-\tau)^2}-\frac{4(n+\beta)+5}{4(t-\tau)}\bar{x}^2+(\beta+n+1)(2(\beta+n)+1)\right]\right\}. \quad (15)$$

4) If we use relation [3] to calculate function $P(x,t-\tau)$ (7),

$$\int_0^{\infty}x^{\alpha-1}\exp(-px^2)\cdot I_{\nu}(cx)\cdot dx=A_{\nu}^{\alpha}$$

when $\operatorname{Re}p$, $\operatorname{Re}(\alpha+\nu)>0$; $|\arg c|<\pi$, where

$$A_{\nu}^{\alpha}=2^{-\nu-1}c^{\nu}p^{-\frac{\alpha+\nu}{2}}\frac{\Gamma\left(\frac{\alpha+\nu}{2}\right)}{\Gamma(\nu+1)}\cdot{}_1F_1\left(\frac{\alpha+\nu}{2};\nu+1;\frac{c^2}{4p}\right),\quad A_{\nu}^{2-\nu}=\frac{(2p)^{\nu-1}}{c^{\nu}\Gamma(\nu)}\cdot\exp\left(\frac{c^2}{4p}\right)\cdot\gamma\left(\nu,\frac{c^2}{4p}\right),$$

$$\gamma(\nu,x)=\Gamma(\nu)-\Gamma(\nu,x)=\int_0^x t^{\nu-1}\cdot e^{-t}dt \quad (16)$$

is the lower incomplete gamma function,

$$\Gamma(\nu,x)=\int_x^{\infty}t^{\nu-1}\cdot e^{-t}dt$$

is the upper incomplete gamma function, then from representation (7) we obtain

$$P(x,t-\tau)=\frac{2(t-\tau)}{x^{\beta}\cdot\Gamma(\beta)}\cdot\exp\left(\frac{x^2}{4(t-\tau)}\right)\cdot\gamma\left(\beta,\frac{x^2}{4(t-\tau)}\right). \quad (17)$$

Substituting (17) into (6), we calculate $Q(x,t-\tau)$

$$Q(x,t-\tau)=\frac{1}{\Gamma(\beta)}\cdot\gamma\left(\beta,\frac{x^2}{4(t-\tau)}\right). \quad (18)$$

After calculations, we have

$$K(t,\tau)\big|_{\substack{k=1\\ x=\bar{x}(t)}}=K_1(t,\tau)=\frac{1}{\Gamma(\beta)\cdot 2^{2\beta-1}}\cdot\frac{\bar{x}^{2\beta-1}}{(t-\tau)^{\beta}}\cdot\exp\left(-\frac{\bar{x}^2}{4(t-\tau)}\right).$$

Next, we calculate the kernel $K(t,\tau)$ when $k=2$ for the integral equation (4) by making similar calculations,

.

$$K(t,\tau)\Big|_{\substack{k=2\\ x=\bar{x}(t)}} = \frac{\bar{x}^{2\beta-2}}{2^{2\beta-1}\Gamma(\beta)(t-\tau)^{\beta}} \cdot \exp\left(-\frac{\bar{x}^2}{4(t-\tau)}\right) \cdot \left[2\beta - 1 - \frac{\bar{x}^2}{2(t-\tau)}\right]. \tag{19}$$

5) Using (16), (18), the function $Q(x,t-\tau)$ can also be represented as

$$Q(x,t-\tau) = 1 - \frac{1}{\Gamma(\beta)} \cdot \Gamma\left(\beta, \frac{x^2}{4(t-\tau)}\right). \tag{20}$$

Obviously, the kernel $K(t,\tau)$ when $k=2$ has the form (19).

6) Taking into consideration the ratio [3]

$$\gamma(\nu,x) = \frac{z^{\nu}}{\nu} \cdot {}_1F_1(\nu;\nu+1;-z)$$

and relation (11), we transform the representation (18) to the form

$$Q(x,t-\tau) = \frac{1}{\Gamma(\beta)} \cdot \frac{x^2}{2^{2\beta}(t-\tau)^{\beta}} \cdot \sum_{n=0}^{\infty} \frac{(-1)}{(\beta+n)\cdot n!} \cdot \left(\frac{x^2}{4(t-\tau)}\right)^n. \tag{21}$$

Next we compute the kernel $K(t,\tau)$ under the condition $k=2$

$$K(t,\tau)\Big|_{\substack{k=2\\ x=\bar{x}(t)}} = \frac{1}{2^{2\beta-1}\Gamma(\beta)(t-\tau)^{\beta}} \cdot \sum_{n=0}^{\infty} \frac{(-1)^n \cdot (2n+1)(n+1)}{(\beta+n)\cdot n! \cdot (t-\tau)^n \cdot 2^{2n}} \cdot \bar{x}^{2n}. \tag{22}$$

7) Taking into account that [3]

$$\gamma(\nu+1,z) = \nu \cdot \gamma(\nu,z) - z^{\nu} e^{-z},$$

we obtain from (18) for the function $Q(x,t-\tau)$ a representation in the form [6]

$$Q(x,t-\tau) = \frac{1}{\Gamma(\beta)} \cdot \left[(\beta-1)\cdot\gamma\left(\beta-1, \frac{x^2}{4(t-\tau)}\right) - \left(\frac{x}{2}\right)^{2\beta-2} (t-\tau)^{1-\beta} \exp\left(-\frac{x^2}{4(t-\tau)}\right)\right]. \tag{23}$$

Since (23) is obtained from (18), the kernel $K(t,\tau)$ when $k=2$ has the form (19), as you can see by direct differentiation.

3. Properties of the kernel-forming function $Q(x,t-\tau)$

We list some properties of the function $Q(x,t-\tau)$, necessary for our research.

1) The function $Q(x,t-\tau)$, $0<\tau<t<\infty$, is continuous function.

2) The function $Q(x,t-\tau) \ge 0$, $0<\tau<t<\infty$ [1].

3) For function $Q(x,t-\tau)$, an estimate

$$Q(x,t-\tau) \le \frac{1}{\Gamma(\beta+1)} \cdot \left(\frac{x^2}{4(t-\tau)}\right)^{\beta}. \tag{24}$$

takes place. The estimate (24) can be obtained in two ways: from the representation (18) and from the representation (8) for the function $Q(x,t-\tau)$.

4) For the function $Q(x,t-\tau)$, there is an inequality

$$Q(x,t-\tau) < \frac{1}{\Gamma(\beta+1)(t-\tau)^{\beta}} \cdot \left(\frac{x}{2}\right)^{2\beta} \exp\left(-\frac{x^2}{4(t-\tau)}\right) \pm$$

$$\pm \frac{1}{\Gamma(\beta+2)(t-\tau)^{\beta+1}} \cdot \left(\frac{x}{2}\right)^{2\beta+2} \exp\left(-\frac{x^2}{4(t-\tau)}\right) \pm \frac{1}{\Gamma(\beta+2)(t-\tau)^{\beta+2}} \cdot \left(\frac{x}{2}\right)^{2\beta+4}. \tag{25}$$

This inequality (25) is received from the representation (14) of the function $Q(x,t-\tau)$.

5) The following integral representation

$$\int_0^t Q(x,t-\tau)d\tau = \frac{1}{\Gamma(\beta)} \cdot \left[t \cdot \gamma\left(\beta, \frac{x^2}{4t}\right) + \frac{x^2}{4} \cdot \Gamma\left(\beta - 1, \frac{x^2}{4t}\right)\right]. \quad (26)$$

holds for the function $Q(x,t-\tau)$. The relation (26) is derived from the representation (18) for the function $Q(x,t-\tau)$.

6) The function $Q(x,t-\tau)$ satisfies the following relation

$$\lim_{t\to 0} \int_0^t Q(x,t-\tau)d\tau = 0. \quad (27)$$

In fact, passing to the limit as $t \to 0$ in (26), we obtain the desired relation (27).

The required ratio (27) for the function $Q(x,t-\tau)$ can be obtained in a simpler way, for this purpose the limit $\lim_{t\to 0} \int_0^t Q(x,t-\tau)d\tau$ is calculated using the estimate (24) [7].

Here we have presented those interpretations (8), (13), (14), (18), (20), (21), (23), properties (24) - (27) functions $Q(x,t-\tau)$ in general case and types (9), (15), (19), (22) of the kernel $K(t,\tau)$ in particular cases, which are most convenient in studies of the integral equation (1), and, consequently, in further studies of the boundary value problem (1) – (3) for various specified values of parameters and for a specified law of motion $x = \bar{x}(t)$ of the load point.

Conclusion

1. For the boundary-value problem (1) - (3) where $\bar{x}(t) = t^{\omega}$, $\omega \in R$, in [1] solvability issues were determined and solutions were obtained in cases, when $k = 0$ and $k = 1$ for any values of ω, and when $k = 2$ for $\omega < \frac{1}{2}$.

It is known that the boundary-value problem is completely investigated if solvability issues are determined and solutions are obtained for any parameter values from the domain of their determination.

2. As we have shown in [1], the solvability of the boundary value problem (1) – (3) is equivalent to the solvability of integral equation (4). It was also shown in [1] that in case $k = 2$ for $\omega \geq \frac{1}{2}$, the integral equation (4) is a special Volterra integral equation, which requires a specific research. In the study of the special Volterra integral equation of the second kind, the following tasks are set: to investigate its solvability, and to investigate spectral questions for this special Volterra integral equation of the second kind [8], [9]. The shape and type of the kernel determine how to solve these problems.

3. In the general case, when solving mathematical models of applied problems that describe physical, mechanical, and other processes or phenomena, preference is given to obtaining an exact analytical solution in comparison with graphic, approximate, experimental, and other solutions.

Thus, before investigating the solvability issues and obtaining analytical solutions for the parameters $k = 2$ in the case $\omega \geq \frac{1}{2}$, as well as in the future for $k = 3, 4....$, when $\omega \in R$, due to the bulkiness of the kernel (2) of the integral equation (1), it is necessary to carry out mathematical calculations that simplify the further study of the boundary value problem (1) - (3).

These mathematical calculations, representing various representations and properties of the kernel-forming function $Q(x,t-\tau)$, are carried out in general case, and the kernel $K(x,t-\tau)$ is calculated in the special cases for further research to obtain an analytical solution of the boundary value problem (1) - (3) for the remaining parameter values.

.

M.I. Ramazanov [2] completely investigated boundary value problems for this essentially loaded heat equation in the special case $\beta = \frac{1}{2}$. In contrast to these previous studies on the theory of loaded differential equations, in this paper boundary value problem for the essentially loaded heat equation (1) is considered in an unlimited domain in the general case with $0 < \beta < 1$.

REFERENCES

1 Yesbaev A.N., Yessenbayeva G.A., Ramazanov M.I. Investigation of the model for the essentially loaded heat equation. *Eurasian Physical Technical Journal*. 2019, Vol. 16, No. 1(31), pp. 113 – 120.

2 Dzhenaliev M.T., Ramazanov M.I. *Loaded equations as perturbations of differential equations*. Almaty, Publishing house «Gylym», 2010, 334 p.

3 Prudnikov A.P., Brychkov Yu.A., Marychev O.I. *Integrals and series.* Vol. 2. Special functions, Moscow, Fizmatlit, 2003, 664 p.

4 Gradshtein I.S., Ryzhik I.M. *Tables of integrals, sums, series and products*. Moscow, 1963, 1108 p. [in Russian]

5 Prudnikov A.P., Brychkov Yu.A., Marychev O.I. *Integrals and series.* Vol. 1. *Elementary functions*, Moscow, Fizmatlit, 2002, 632 p.

6 Yesbayev A.N., Yessenbayeva G.A. On the integral equation of the boundary value problem for the essentially loaded differential heat operator. *Bulletin of Karaganda University. Mathematics Series*. 2016, No. 3(83), pp. 62 – 69.

7 Yesbayev A.N., Yessenbayeva G.A., Ramazanov M.I. The research of one boundary value problem for the loaded differential operator of heat conduction. *Bulletin of Karaganda University. Mathematics Series*. 2013, No. 3(71), pp. 35 – 42.

8 Polyanin A.D., Manzhirov A.V. *Spravochnik po integral'nym uravneniyam: Metody resheniya*. Moscow, Publishing House "Factorial Press», 2000, 384 p. [in Russian]

9 Polyanin A.D., Manzhirov A.V. *Spravochnik po integral'nym uravneniyam.* Moscow, Fizmatlit, 2003, 608 p. [in Russian]

Article accepted for publication 09.12.2019

SUMMARIES	ТҮСІНІКТЕМЕЛЕР	АННОТАЦИИ

Потапов А.А., Пахомов А.А., Потапов А.А. (кіші), Потапов В.А.
Марс бетінің оптикалық текстуралық кескіндерінің ағындарын робасты кепстральдік фракталды-топологиялық әдістермен өңдеу.
Жұмыста кескіндердің сапасы мен айқындылығын жоғарылату мақсатында оларды сандық өңдеу әдістерін қолдану нәтижелері берілген. Әдіс Маринер және Викинг американдық танымал серіктерімен жасалған Марсиандық кратерлердің суреттерін өңдеуде қолданылған. Өңделген суреттерді көзбен шолып талдауы бұрын белгісіз жаңа бөлшектерді анықтауға мүмкіндік берді. Суреттер Ғаламтордан алынды. Ұсынылған әдістер көп арналы дабылдарды берілгіштер матрицасымен өңдеуге қолдануға болады.

Потапов А.А., Пахомов А.А., Потапов А.А. (мл.), Потапов В.А.
Обработка робастными кепстральными фрактально - топологическими методами потоков оптических текстурных изображений поверхности Марса.
В работе представлены результаты применения методов цифровой обработки изображений с целью повышения их качества и разборчивости. Метод применен для обработки снимков Марсианских кратеров, сделанных известными американскими спутниками Маринер и Викинг. Визуальный анализ обработанных снимков позволяет выделить новые ранее неизвестные детали. Снимки получены из Интернета. Разработанные методы пригодны для обработки многоканальных сигналовматрицей датчиков.

Сенють В.Т., Витязь П.А., Валькович И.В., Хейфец М.Л., Колмаков А.Г.
Бордың кубтық нитридінің наноқұрылымды және микронды ұнтақтармен модификацияланған және жоғары температура мен жоғары қысымда өңделгеннен кейінгі өздігінен балқитын қоспаның құрылымы мен қасиеттерін зерттеу.
Жоғары қысымда және жоғары температурада кубтық BN (cBN) наноөлшемді және микрондық ұнтақтармен пісірілген ПГ-СР4 өздігінен балқитын қоспаның құрылымдық ерекшеліктері мен мкироқаттылығы зерттелген. Эксперименттер негізінде жоғары қысыммен және жоғары температурада өңдеу режимдері анықталған. Ең жоғары микроқаттылыққа ие материал қалыптасатын cBN наноқұрылымды қоспасының оптималды құрамы анықталды. Микрондық өлшемді cBN қоспаға ие материалдың микроқаттылығы наноқұрылымды cBN бар үлгілердің микроқаттылығы 1,5–2 есе төмен екендігі көрсетілген.

Сенють В.Т., Витязь П.А., Валькович И.В., Хейфец М.Л., Колмаков А.Г.
Изучение структуры и свойств самофлюсующегося сплава после модифицирования наноструктурным и микронным порошками кубического нитрида бора и обработки при высоком давлениии высокой температуре.
Исследованы структурные особенности и микротвердость спеченного при высоком давлении и высокой температуре с добавлением наноразмерных и микронных порошков кубического BN (cBN) самофлюсующего никелевого сплава ПГ-СР4. На основании экспериментов установлены режимы обработки под высоким давлением и высокой температуре. Определено оптимальное содержание добавки наноструктурногосBN, при которомформируется материал с наибольшей микротвердостью. Показано, что микротвердость материала с добавкой cBN микронного размера в 1.5–2 раза ниже, чем для образцов с таким же содержанием наноструктурного cBN.

Аймуханов А.К., Зейниденов А.К., Ильясов Б.Р., К., Завгородний А.В., Пазыл Б.М.
Кобальт фталоцианин қабықшасының фото-электрфизикалық қасиеттерін зерттеу.
Мақалада кобальт фталоцианинінің (CoPc) қатты қабықшадағы және нанолентадағы фото-электрофизикалық сипаттамаларын зерттеу нәтижелері ұсынылған. CoPc қатты қабықшасы тоқ өткізгіш беті бар төсеніштегі ITO (индий-қалайы оксиді) вакуумдағы термиялық булану әдісімен алынды. CoPc нанолeнталары TG-PVD әдісімен бу фазасынан тұндыру арқылы алынды. Вольтамперлік сипаттамаларды өлшеу (ВАС) потенциостат-гальваностат P20X көмегімен сызықтық өрістету режимінде жүргізілді. Көлік кинетикасын және тасымалдаушылардың рекомбинациясын зерттеу P45X импедансметрінде жүргізілген. Күн сәулесінің имитаторы ретінде 100мВт/см^2 тең зерттеу ақрқындылығына ие ксенон шамы қолданылды.

Аймуханов А.К., Зейниденов А.К., Ильясов Б.Р., К., Завгородний А.В., Пазл Б.М.
Исследование фото-электрофизических свойств пленки фталоцианина кобальта.
В статье представлены результаты исследования фото-электрофизических характеристик в твердой пленке и нанолентах фталоцианина кобальта (CoPc). Твердая пленка CoPc на подложке с токопроводящей поверхностью ITO (оксид индия-олова) была получена методом термического испарения в вакууме. Наноленты CoPc были

получены осаждением из паровой фазы методом TG-PVD. Измерения вольтамперных характеристик (ВАХ) проводились при помощи потенциостата-гальваностата P20X в режиме линейной развертки. Исследование кинетики транспорта и рекомбинации носителей проведены на импедансметре P45X. В качестве имитатора солнечного света использована ксеноновая лампа с интенсивностью изучения равной 100мВт/см^2.

Шарипов М.Ш., Хайитов Д.Э., Ризокулов М.Р., Исломов У.Н., Раупова И.Б.

Магнитті компенсация нүктесінің маңындағы тербий феррит-гранаттың домендік құрылымы және магниттік қасиеттері

Магнитооптикалық әдіспен $Tb_3Fe_5O_{12}$ феррит-гранатының жұқа монокристалды пластинасының домендік құрылымы бұл ферримагнетиктің магниттік компенсация T_c = 248,6 K нүктесіне жақын температуралық аймақта зерттелген. Үлгінің температурасының компенсация нүктесіне жақындағанда домендердің ені айтарлықтай өсетіні, $T = T_c$ кезде ақырғы болып қалатындығы көрсетілген. Температура мен сыртқы магнит өрісінің өзгеруі кезінде домендік құрылымының қайта құрылуын визуалды бақылау негізінде үлгінің көп домені және монодомды (біртекті магниттелген) күйлері арасындағы шекараны анықтайтын магниттік H-T-диаграмма тұрғызылған.

Шарипов М.Ш., Хайитов Д.Э., Ризокулов М.Р., Исломов У.Н., Раупова И.Б.

Доменная структура и магнитные свойства тербиевого феррита-граната в окрестности точки магнитной компенсации.

Магнитооптическим методом исследована доменная структура тонкой монокристаллической пластинки феррита-граната $Tb_3Fe_5O_{12}$ в температурной области вблизи точки магнитной компенсации этого ферримагнетика T_c = 248,6 K Показано, что при приближении температуры образца к точке компенсации ширина доменов существенно растет, оставаясь конечной при $T = T_c$. На основе визуальных наблюдений за перестройкой доменной структуры при изменении температуры и внешнего магнитного поля построена магнитная $H-T$-диаграмма, определяющая границу между многодоменным и монодоменным (однородно намагниченным) состояниями образца.

Юров В.М., Гончаренко В.И., Васильев С.Л., Дмитриев С.А., Юргенсон С.А.

Полимерлі композициялық материал құрылымының өзгеруін есептеуіш рентгендік томография әдісімен эксперименттік түрде зерттеу.

Мақалада есептеуіш рентгендік томография әдісін қолдану негізінде статикалық жүктеме әсер еткенде полимерлі композициялық материалдың құрылым күйінің өзгеруін бағалау әдістемесі ұсынылған. Жүктеменің бастапқы сатыларында көмірпластикалық үлгілер үшін құрылымның өзгеруін талдау нәтижелері келтірілген. Ұсынылған зерттеу әдістемесі күш әсері кезіндегі жарықшақтың дамуын бағалауға ғана емес, сонымен қатар жүктеменің болуы мен деңгейіне байланысты материалдағы өзгерістерді талдауға да мүмкіндік береді. Одан басқа, әр түрлі технологиялық үдерістер кезінде материалдың зақымданулардың жинақталуына бейімділігін салыстыруға мүмкіндік беретін сандық параметрлер енгізілді. Сынақ зерттеудің алынған нәтижелері ұсынылған әдістеме материалдың жүктемедегі тәртібін жоғары дәлдікпен талдау жүргізуге және материал мен төсеудің қарастырылып отырған түріне тән үрдістерді анықтауға мүмкіндік беретінін көрсетті.

Юров В.М., Гончаренко В.И., Васильев С.Л., Дмитриев С.А., Юргенсон С.А.

Экспериментальное исследование методом вычислительной рентгеновской томографии изменения структуры полимерного композиционного материала.

В статье на основе применения метода вычислительной рентгеновской томографии предложена методика оценки изменения состояния структуры полимерного композиционного материала при воздействии статической нагрузки. Представлены результаты анализа изменения структуры для углепластиковых образцов на начальных этапах нагружения. Предложенная методика исследования позволяет не только оценить развитие трещины при силовом воздействии, но и проанализировать изменения материала в зависимости от наличия и уровня нагружения. Кроме этого, введены количественные параметры, позволяющие сравнивать склонность материала к накоплению повреждений при различных технологических процессах. Полученные результаты тестового исследования показывают, что предложенная методика позволяет с высокой точностью проводить анализ поведения материала под нагрузкой и выявлять тенденции, характерные для рассматриваемого типа материала и укладки.

Юров В.М., Гончаренко В.И., Васильев С.Л., Дмитриев С.А., Юргенсон С.А.

Есептеуіш рентгендік томография әдісімен композициялық материалдардағы соққы зақымдарының таралуын талдау

Композициялық материалдардан жасалған конструкцияда сызықтық детекторы бар рентгендік есептеуіш томографты қолдануымен соққы зақымдалуын үлестіруді бағалау әдістемесі ұсынылған. Сызықты детекторды пайдалана отырып, есептеуіш рентгендік томография әдісімен ішкі қатпарларды бақылау мүмкіндігін талдау мақсатымен көмірпластиктен жасалған соққы зақымдары бар үлгілерді зерттеу бойынша эксперимент жүргізілді. Жүргізілген зерттеу аясында композициялық материалдардан жасалған конструкцияларға ерекше назар аударылды. Бұл конструкцияның жоғары жүктемеге ие элементтерінде осы материалдарды қолдануға және оларды дайындаудың технологиялық процестерін пысықтау қажеттігіне байланысты. Әзірленген әдістеме сызықтық детекторы бар томографтарды қолдану кезінде қатпарларды талдау рәсімін жеңілдетуге және бақылаудың мобильдік әдістерінің деректерін верификациялауға мүмкіндік береді. Одан басқа, әдістеме композициялық материалдардан жасалған конструкцияларды жөндеу әдістерін әзірлеу кезінде қолданылуы мүмкін. Соққы зақымдалуымен үлгілерді әлсіреудің сызықтық коэффициентінің таралу томограммасының мысалы ұсынылған.

Юров В.М., Гончаренко В.И., Васильев С.Л., Дмитриев С.А., Юргенсон С.А.
Анализ распространения ударных повреждений в композиционных материалах методом вычислительной рентгеновской томографии.
Предложена методика оценки распределения ударного повреждения в конструкции из композиционных материалов с использованием рентгеновского вычислительного томографа с линейным детектором. В интересах анализа возможности контроля внутренних расслоений методом вычислительной рентгеновской томографии с использованием линейного детектора был проведен эксперимент по исследованию образцов с ударными повреждениями энергиями из углепластика. Особое внимание в рамках проводимого исследования было сфокусировано на конструкциях из перспективных композиционных материалов. Связано это с применением данных материалов в высоконагруженных элементах конструкции и необходимостью отработки технологических процессов их изготовления. Разработанная методика позволяет упростить процедуру анализа расслоений при применении томографов с линейным детектором и верифицировать данные мобильных методов контроля. Кроме этого методика может применяться при разработке методов ремонта конструкций из композиционных материалов. Представлен пример томограммы распределения линейного коэффициента ослабления образцов с ударным повреждением.

Рахадилов Б., Скаков М., Туленбергенов Т., Журерова Л., Курбанбеков Ш.
Плазмалық беттік әсерлесуді зерттеуге арналған плазмалық қондырғы.
Ұсынылған мақалада вольфрам мен бериллийдің плазмамен әсерлесуін зерттеу нәтижесі келтірілген және құрастырылған плазмалық беттік әсерлесуді зерттеуге арналған қондырғының кейбір ерекшеліктері сипатталған. Аталған қондырғы Қазақстандық материалтану Токомагының жабдықтары мен материалдарына сынақ жүргізуге және плазмалық беттік әсерлесу тәжірибелерін жүзеге асыруға арналған. Плазмалық қондырғының басты элементтері - электрондық сәулелік зеңбірек, плазмалық шоғырлық разряд камерасы, әсерлесудің вакуумдық камерасы, нысаналық салқындату қондырғысы, электромагниттік катушкалардан құралған электрмагниттік жүйе, қондырғының саңылаусыздығын жоймай сәулеленетін үлгілерді немесе сынақ құралдарының орнын ауыстыруға және алмасытруға араналған шлюздік құрал болып есептеледі. Плазмалық әсер кезінде вольфрам мен бериллийдің құрылымының өзгеруін зерттеуге арналған тәжірибелер нәтижесі бойынша сәулеленуден кейін беттерде эрозияның салдарынан қуыстар пайда болатындығы анықталды.

Рахадилов Б., Скаков М., Туленбергенов Т., Журерова Л., Курбанбеков Ш.
Плазменная установка для исследования плазменно-поверхностных взаимодействии. В статье описаны некоторые особенности разработанной плазменной установки для исследования плазменно-поверхностных взаимодействии и представлены результаты исследования взаимодействие вольфрама и бериллия с плазмой. Данная установка предназначена для испытаний материалов и оборудования Казахстанского материаловедческого Токамака и для проведения исследовании плазменно-поверхностных взаимодействии. Основными элементами плазменной установки являются электронно-лучевая пушка, камера плазменно-пучкового разряда, вакуумная камера взаимодействия, охлаждаемое мишенное устройство, электромагнитную систему, состоящей из электромагнитных катушек, шлюзовое устройство для оперативной смены и перемещения средств диагностики или облучаемых образцов без разгерметизации установки. Проведенные эксперименты по исследованию изменений структуры вольфрама и бериллия при плазменном воздействии, показали, что после облучения поверхность подвергается к эрозию и на поверхности образуется поры.

Рахадилов Б.К., Сагдолдина Ж.Б. Очередько И.А, Комбаев К.К., Хасенов А.К.
РА6 полиамид құрылымы мен қасиеттеріне электронды-сәулелі өңдеудің әсерін зерттеу.
Бұл жұмыста 1,3 МэВ энергиясымен РА6 полиамидінің құрылымы мен қасиеттеріне электрондық сәулеленудің әсері зерттелді. Сәулелену дозалары 50-ден 500 кГр-ге дейін құрады. Зерттеу нәтижелері РА6 полимерінің шағын дозалары бар сәулелену механикалық сипаттамаларды арттыруға қабілетті екенін көрсетті, бұл ретте үлкен дозалармен сәулелену оларды едәуір төмендетеді. Тозуға төзімділігі 350 кГр-ден сәулелену режимінде төмендейді, ал үлгілердің қаттылығы шамалы өзгереді. Полимердің құрылымы рентгендік дифрактометрия және ИК-спектроскопия әдістерімен зерттелді. 1,3 МэВ энергия кезіндегі электрондық сәулелену РА6

полимерінің кристалдық пішінінің өзгеруіне әкелмеді, бірақ жартылай кристалдық зақым келтірді. Электронды сәулеленуден кейін α-фаза шыңының қарқындылығы сәулеленбеген үлгімен салыстырғанда артады, бұл материалдың кристалдылығының ұлғаюына байланысты болуы мүмкін.

Рахадилов Б.К., Сагдолдина Ж.Б. Очередько И.А, Комбаев К.К., Хасенов А.К.
Исследование влияния электронно-лучевой обработки на структуру и свойства полиамида РА6. В данной работе было изучено влияние электронного облучения с энергией 1,3 МэВ на структуры и свойства полиамида РА6. Дозы облучения составили от 50 до 500 кГр. Результаты исследования показали, что облучение с небольшими дозами полимера РА6 способно повышать механические характеристики, при этом облучение большими дозами значительно их снижает. Износостойкость снижается при режимах облучения от 350 кГр, а твердость образцов меняется незначительно. Структура полимера была изучена методами рентгеновской дифрактометрии и ИК-спектроскопии. Электронное облучение при энергии 1,3 МэВ не приводило к изменению кристаллическую форму полимера РА6, но вызвало частичное кристаллическое повреждение. После электронного облучения интенсивность пика α-фазы увеличивается по сравнению с необлученным образцом, это может быть связано с увеличением кристалличности материала.

Васенин И.М., Нариманов Р.К., Перчаткина Е.В., Шрагер Л.А.
Озонаторда кіші өлшемді газ көпіршіктерге ие екіфазалы ағын қозғалысын зерттеу.
Озонаторда кіші өлшемді газ көпіршіктерге ие екіфазалы газ-сұйықтық ағыстың қозғалыс етсептеулері жүргізілген. Өзара кіруші континуумдар екі фазалы ортаның моделімен салыстырғанда қолданылған математикалық модельде туындыларында кіші параметрлерге ие болмайды. Ортаның сығылуын және тығыздықтың көпіршіктердің концентрациясынан тәуелділігінің ескеру негізінде осы модельде ауырлық күші өрісінде көпіршіктердің концентрациясының біртекті емес болуы кезінде еркін конвекцияны шарттайтын процестер автоматты түрде есепке алынады. Ұсынылған модель негізінде параметрлік зерттеулер орындалған. Бұл әдіс-тәсілдің жұмысқа қабілеттілігі көрсетілді және көтергіш орталарды қозғалысқа тарту есебінен газ ағысының көбеюін үдетілуі расталды. Контактілі резервуарда озонды еріту процесінің параметрлері анықталды, диспергаторлардың орналасу жерінің тиімділігі бағаланды.

Васенин И.М., Нариманов Р.К., Перчаткина Е.В., Шрагер Л.А.
Исследование движения двухфазного потока с пузырьками газа малого размера в озонаторе
Выполнены расчеты движения двухфазной газожидкостной струи с пузырьками малого размера в озонаторе. Используемая математическая модель в отличие от модели двухфазной среды взаимопроникающих континуумов не содержит малых параметров при производных. Благодаря учету сжимаемости среды и зависимости плотности от концентрации пузырьков в этой модели автоматически учитываются процессы, обуславливающие свободную конвекцию в поле силы тяжести при наличии неоднородности концентрации пузырьков. Выполнены параметрические исследования на основе предложенной модели. Показана работоспособность данного подхода и подтверждено ускорение всплытия газовой струи за счет вовлечение в движение несущей сред. Определены параметры процесса растворения озона в контактном резервуаре, оценена эффективность месторасположения диспергаторов.

Байшагиров Х.Ж., Омаров Б.М.
Қазақстанда шағын жел энергетикалық құрылғыларды жасау туралы.
Мақалада Қазақстан Республикасында жаңартылатын энергия көздері туралы, атап айтқанда, жел энергетикалық құрылғылардың құрылымын құрастыру туралы мәліметтер келтірілген. Сонымен қатар құрастырылған шағын жел құрылғысының ерекшеліктері атап көрсетілген. Шағын жел құрылғыларын жасау кезіндегі үш кезең, сонымен бірге тиісті жұмыс түрлерінің қысқаша сипаттамасы бөліп көрсетілген. Машина жасаудағы жаңа өнім құру кезінде композициялық материалдардың рөлі көрсетілген. Диффузоры бар композициялық жел энергетикалық қондырғының құрылымдық ерекшеліктері егжей-тегжейлі сипатталған. Талдау зерттеулерінің нәтижелері, диффузор ішіндегі ауа ағынының жылдамдығын өзгеру графиктері келтірілген. Жұмыста шыны пластиктен ағызғыштарды жасау технологиясының негізгі сәттері баяндалған.

Байшагиров Х.Ж., Омаров Б.М.
О создании малых ветроэнергетических установок в казахстане
В статье приводятся данные о возобновляемых источниках энергии в Республике Казахстан, в частности, о разработках конструкций ветроэнергетических установок. При этом отмечены особенности конструкции создаваемых малых ветроустановок. Выделяются три этапа, возникающих при создании малых ветроустановок, а также краткая характеристика соответствующих видов работ. Показана роль композиционных материалов при создании новой продукции в машиностроении. Подробно описаны конструктивные особенности композиционной ветроэнергетической установки с диффузором. Приведены результаты аналитических исследований, графики изменения скорости воздушного потока внутри диффузора. В работе изложены

основные моменты технологии изготовления обтекателей из стеклопластика.

Ершина А.К., Сакипова С.Е., Манатбаев Р.К.
Бидарье карусель типті жел турбинасының конструкциясының ерекшеліктері.
Мақалада екі коаксиалды-орналасқан айналмалы біліктерінен құралатын Дарье типті вертикаль-өстік жел турбинасын жақсарту бойынша зерттеу нәтижелері берілген. НАСА аэродинамикалық профилінің кейбір конструкциялық қасиеттері талқыланады. Екі қалақшаны айналуы кезіндегі желдің орап ағу сұлбасы көрсетілген. HBI-роторы бар карусель типті жел турбинасының зертханалық үлгілерінің қысқаша сипаттамасы келтірілген. Вертикальді-өстік жел турбинасының қондырғысы жерге жақын шекаралық қабаттан жоғары орналасқан белгілі бір биіктікте оның тиімділігін жақсартуға мүмкіндік береді.

Ершина А.К., Сакипова С.Е., Манатбаев Р.К.
Особенности конструкции ветротурбины карусельного типа Бидарье.
В статье представлены результаты исследования по улучшению вертикально-осевой ветротурбины типа Дарье с двумя коаксиально-расположенными вращающимися валами. Обсуждаются некоторые конструкционные свойства аэродинамического профиля НАСА. Показана схема обтекания при вращении обоих лопастей. Приведено краткое описание лабораторных моделей ветротурбины карусельного типа с HBI-ротором. Показано, что установка ветрикально-осевой ветротурбины на определенной высоте, выше приземного пограничного слоя, также позволяет улучшить ее эффективность.

Шаймерденова К.М., Оспанова Д.А., Шункеев Т.А.
FGX-12 ұнтақтау-сұрыптау кешенін қолдана отырып, отынның қасиетін жақсарту
Бұл мақалада құрғақ байытудың құрамалы машинасын қолдану арқылы көмір сапасын арттыру әдісі қарастырылады. Майкөбе қоңыр көмір бассейнінің Сарыкөл кен орнының қатарындағы көмірді өңдеуге арналған құрғақ байытудың құрамалы машинасының сипаттамасы келтірілген. Қайта өңдеу нәтижесінде алынған көмір концентраты, өнеркәсіп өнімдері мен басқа да байыту өнімдері қоймада жинақталады. Байыту машинасының негізгі мақсаты қоңыр көмірдің сапалық сипаттамаларын жақсарту болып табылады, яғни бірінші кезекте бұл көмірдің калориялығын (жану жылуын) арттырып, күлділігін азайтады. Байыту нәтижесінде көмірді сақтау мерзімі 3 айдан 6 айға дейін өседі.

Шаймерденова К.М., Оспанова Д.А., Шункеев Т.А.
Улучшение свойства топлива с применением дробильно-сортировочного комплекса FGX-12
Рассмотрен метод повышения качества угля путем применения комбинированной машины сухого обогащения. Приведено описание комбинированной машины сухого обогащения, предназначенной для переработки рядового угля Сарыкольского месторождения Майкубенского буроугольного бассейна. Полученные в результате переработки угольный концентрат, промпродукты и другие продукты обогащения аккумулируются на складе. Основной целью обогатительной машины является улучшение качественных характеристик бурого угля и, в первую очередь, это повышение калорийности (теплоты сгорания) угля и понижение зольности. В результате обогащения увеличивается срок хранения угля с 3-х до 6 месяцев

Танашева Н.К., Миньков Л.Л., Тлеубергенова А.Ж., Саденова К.К.
Сулы-көмірлі суспензия алу үшін пластификатордың реологиялық қасиеттерін зерттеу.
Мақалада пластификаторлардың Шұбаркөл көмірінен алынған көмір сулы суспензияның тұрақтылығына әсерін зерттеу нәтижелері келтірілген. Оптималды реагент пластификаторды алуға байланысты қойылған міндеттер аясында тәжірибелік қондырғы құрастырылды. Реагент-пластификаторлар ретінде мазут, желатин және натрий гуматы қолданылды. Шұбаркөл кен орнының көмір қалдықтарын қайта өңдеу үрдісі зерттелді, ең жақсы нәтиже натрий гуматын қолданғанда алынды. Гумат натрийды пластификатор ретінде қолдану арқылы кеңістігі тор тәріздес құрылымы бар және ұзақ уақыт тұнбайтын көмір сулы суспензия алуға болады.

Танашева Н.К., Миньков Л.Л., Тлеубергенова А.Ж., Саденова К.К.
Исследование реологических свойств пластификатора для получения водоугольной суспензии.
В статье приведены результаты исследования воздействия пластификаторов на стабильность водоугольных суспензии полученных из шламов Шубаркульских углей. В рамках поставленной задачи по определению оптимального реагента-пластификатора, разработана экспериментальная установка. В качестве реагентов-пластификаторов были применены мазут, желатин, гумат натрия. Изучен процесс обогащения угольных шламов Шубаркульского месторождения, показано, что наилучшие результаты получены при использовании гумата натрия. Применение гумата натрия как пластификатора позволяет создать водоугольные суспензии с пространственной сетеобразной структурой, не расслаивающиеся в течение длительного времени.

Кубич В.И., Чернета О.Г., Юров В.М.
СМЦ-2 үйкеліс машинасында материалдардың адгезиялық қасиеттерінің параметрлерін анықтау әдістемесі.
Жұмыста материалдардың адгезиялық қасиеттерінің параметрлерін анықтау мақсатында тозуы мен үйкеліске материалдарды сынаудың СМЦ-2 стандартты машинасының мүмкіндіктері туралы түсініктер берілген. «40Х - болат 45», «12Х2Н4 - болат 45», «45ХН2МФА - болат 45» материалдарының трибологиялық жүйелерін эксперименттік түрде зерттеу нәтижелері келтірілген. Жанасудағы қысымның өсуімен молекулалық байланыстың тангенциалды беріктігінің өзгеру заңдылықтары және зерттелінетін материалдардың майлаусыз өзара әрекеттесуі кезінде оның беріктілік коэффициенттері анықталған. Нақты үйкеліс тораптарының эксплуатациялық беттерінің контактілі өзара әрекеттесуін қайта жаңғырту үшін СМЦ машинасының штаттық орындарында орналасқан табиғи фрагменттерді пайдалану шартымен олардың ығысуын модельдеуге болады. Бұл кезде СМЦ машинасының құрал-жабдығы шамалы өңдеуді талап етеді, бұл өз кезекте беттердің ығысу жылдамдығын модельдеуге мүмкіндік береді.

Кубич В.И., Чернета О.Г., Юров В.М.
Методика определения параметров адгезионных свойств материалов на машине трения СМЦ-2
В работе развивается представление о возможностях стандартной машины испытания материалов на трение и износ СМЦ-2 для определения параметров адгезионных свойств материалов. Приведены результаты экспериментальных исследований трибологических систем материалов «40Х - сталь 45», «12Х2Н4 - сталь 45», «45ХН2МФА - сталь 45». Определены закономерности изменения тангенциальной прочности молекулярной связи с ростом давления в контакте, и коэффициенты ее упрочнения при взаимодействии рассматриваемых материалов без смазки. Показано, что для воспроизведения контактного взаимодействия эксплуатационных поверхностей реальных узлов трения, возможно, моделировать их сдвиг при деформировании при условии использование натурных фрагментов, размещаемых в штатных местах машины СМЦ. При этом оборудование машины СМЦ требует незначительной доработки, что позволяет моделировать также и скорость сдвига поверхностей.

Астанов С.Х., Касимова Г.К., Шарипов М.З.
Поляризациялық спектрлерді тіркеп алуға арналған оптикалық жүйелер.
Көптеген жылдар бойы анизотропты молекулалардың поляризациялық қасиеттерін зерттеу үшін қолданылған оптикалық жүйелер келтірілген. Екі жүйе көзге көрінетін және ультракүлгін спектрлік аймағына жақын облыстарда жұмыс істейді. Френельдің қос параллелепипедтің рөлін толқындық пластинкасының ахроматикалық төрттен бірі атқарады. Олар Поккельс ұяшығынан кейін Jasco-20 дихрографында қолданылады. Нәтижесінде аспаптың сезгіштігі $\theta \cong 10^{-3}$град$\cdot$ см$^{-1}$ -ден $3\cdot 10^{-5}$ –ге дейін оптикалық тығыздықтар айырым шамасына артады.

Астанов С.Х., Касимова Г.К., Шарипов М.З.
Оптические системы для снятия поляризационных спектров.
Приведены оптические системы, которые разработаны авторами и в течение многих лет применялись для исследования поляризационных свойств анизотропных молекул. Обе системы рассчитаны на видимую и близко к ультрафиолетовой спектральные области. При этом двойной параллелепипед Френеля играет роль ахроматической четверть волновой пластинки. Они используются в дихрогрофе Jasco-20 после ячейки Покельса. В результате чего чувствительность прибора возрастает от $\theta \cong 10^{-3}$град$\cdot$ см$^{-1}$ до $3\cdot 10^{-5}$ величины разностей оптической плотности.

Булкаирова Г.А., Стоев М., Хасенов А.К., Карабекова Д.Ж., Нургалиева Ж.Г., Кипшаков М.С.
Электрогидроимпульсті разрядтардың табиғи кварц минералын ұсақтауға әсері.
Табиғи кварц минералын бөлшектеу және ұсақтаудың технологиялық процестеріндегі импульстік әсер ету көпкомпонентті сұйықтағы жоғары вольтты электр разрядтарын сызықты емес үлестірілген сипаттамалары бар жоғары қысымды пайдалануға негізделген. Сұйықтағы электр разряды көптеген отандық және шетелдік технологиялардағы негізгі әрекет етуші механизм болып табылады. Сұйықтағы электр разряды кезінде пайда болатын барлық күрделі құбылыстар кешенінен электр энергиясының соққы толқындары қысымының энергиясына тікелей айналуы қолданылады. Табиғи минералды кварцтың ұсақталу дәрежесінің разрядтардың электртехникалық параметрлерінен тәуелділігі келтірілген. Электрогидроимпульсті өңдеуді пайдалана отырып, табиғи минералды кварцтың ең қарқынды ұсақтаудың оптималды шарттары анықталды.

Булкаирова Г.А., Стоев М., Хасенов А.К., Карабекова Д.Ж., Нургалиева Ж.Г., Кипшаков М.С.
Влияния электрогидроимпульсных разрядов на дробление природного минерала кварца

Импульсное воздействие в технологических процессах дробления и измельчения природного минерала кварца основано на использовании высоких давлений, сопровождающих высоковольтные электрические разряды в многокомпонентной жидкости с нелинейно распределенными характеристиками. Электрический разряд в жидкости, является основным действующим механизмом во многих отечественных и зарубежных технологиях. Из всего сложного комплекса явлений, возникающих при электрическом разряде в жидкости, используется непосредственная трансформация электрической энергии в энергию давления ударных волн. Приведены зависимости степени измельчения природного минерального кварца от электротехнических параметров разрядов. Определены оптимальные условия наиболее интенсивного измельчения природного минерального кварца с использованием электрогидроимпульсной обработки.

Брейдо И.В., Каверин В.В., Келисбеков А.К., Данияров Н.А., Ахметбекова А.М.
Жиіліктік-реттелетін электр жетегімен көп қозғалтқышты пластиналы конвейердің тартқыш-тасымалдаушы органының математикалық моделі.
Тізбекті конвейерлердің жұмысы барысында авариялық жағдайлар болуы мүмкін. Қозғалатын бөліктердің тозу қарқындылығы, тартқыш шынжырлардың топсалары қадамының артуы себеп болуы мүмкін, бұл тартқыш органда соққы жүктемелерінің туындауына және конвейердің жеке элементтерінің істен шығуына әкеп соғады. Тартқыш орган қадамының кейбір шекті ұлғаюына жеткен кезде тізбекті берілістің одан әрі жұмысы қауіпті болуы, тізбектердің беріктілік қорының айтарлықтай азаюынан, жүрістің бірқалыпты бұзылуынан немесе аралық жетектердің жұлдызшалары мен жұдырықтары бар шынжыр топсалары ілінуінің бұзылу себептерімен байланысты. Пластиналы конвейерлерді пайдалану режимдерін зерттеуге және жаңғыртуға арналған жұмыстарда көп қозғалтқышты пластиналы конвейерде жиілік-реттелетін электр жетегі құралдарымен басшы және басқарылатын жетектер арасында жүктемелерді бөлу мәселесін шешу тәсілдері қарастырылмайды. Жұмыстың мақсаты тартқыш-тасымалдаушы орган жұмысының динамикалық процестерін және тартқыш-тасымалдаушы органның серпінді қасиеттерін ескере отырып, жиілік-реттелетін электр жетегі құралдарымен көп қозғалтқышты пластиналы конвейердің басшы және басқарылатын электр жетектері арасында жүктемелерді бөлу тәсілін сипаттайтын математикалық моделін әзірлеу.

Брейдо И.В., Каверин В.В., Келисбеков А.К., Данияров Н.А., Ахметбекова А.М.
Математическая модель тягово-несущего органа многодвигательного пластинчатого конвейера с частотно-регулируемым электроприводом.
В процессе работы цепных конвейеров, возможны аварийные ситуации. Причинами которых могут стать интенсивность износа движущихся частей, увеличение шага шарниров тяговых цепей, что приводит к возникновению ударных нагрузок в тяговом органе и выходу из строя отдельных элементов конвейера. При достижении некоторого предельного увеличения шага тягового органа дальнейшая работа цепной передачи может оказаться невозможной из-за значительного уменьшения запаса прочности цепей, нарушения плавности хода или нарушения зацепления шарниров цепи со звездочками и кулаками промежуточных приводов. В рассмотренных работах посвященных исследованию и модернизации режимов эксплуатации пластинчатых конвейеров не рассматриваются способы решения проблемы распределения нагрузок между ведущим и ведомым приводами в многодвигательном пластинчатом конвейере средствами частотно-регулируемого электропривода. Цель работы: Разработка математических моделей описывающих динамические процессы работы тягово-несущего органа и способа распределения нагрузок между ведущим и ведомым электроприводами многодвигательного пластинчатого конвейера средствами частотно-регулируемого электропривода с учетом упругих свойств тягово-несущего органа.

Сатыбалдин А.Ж., Карабекова Д.Ж., Хасенов А.К., Айтпаева З.К., Сельдюгаев О.Б.
Қысқа импульсті разрядтардың көмегімен мұнай асфальтенін деструкциялау мен гидрорлеудің кванттық-химиялық есебі.
Соңғы жылдары материалға энергетикалық әсер ету қызығушылығы олардың сипаттамасының өзгеруі себебіне байланысты тұрақты түрде жоғары болып қала беретіндігі сөзсіз. Мұнай материалының жеке ерекшеліктерін есептеу аса айтарлықтай сыртқы энергетикалық шығындарсыз соққы әсерінің көмегімен құрылымды қажетті бағытта өзгерту мүмкіндігін көрсетеді. Мұндай әсер ретінде, материал құрылымын басқару үшін ауыр мұнайға электрогидроимпульстік әсер қолданылады. Осы әсердің көмегімен реттелетін молекулалық құрылымды арттыруға оңай қол жеткізуге болады, сондай-ақ Қаражанбас кен орнының ауыр мұнайының деметиллизациясын зерттеу нәтижелері ұсынылған.

Сатыбалдин А.Ж., Карабекова Д.Ж., Хасенов А.К., Айтпаева З.К., Сельдюгаев О.Б.
Квантово-химический расчет разрушения и гидрогенации асфальта нефти под влиянием коротко-импульсного разряда

В последние годы интерес к энергетическому воздействию на материал с целью изменения их характеристик остается стабильно высоким. Расчет индивидуальных особенностей нефтяного материала показывает, что можно изменять структуру в нужном направлении, используя ударное воздействие без заметных затрат внешней энергии. В качестве такого влияния для контроля структуры материала использовали электро-гидроимпульсное воздействие на нефть. С помощью этого эффекта можно легко увеличить упорядоченность структуры ядра. Представлены результаты исследования свойств тяжелой нефти месторождения Каражанбас, подвергнутой электро-гидро-импульсному разряду с целью деметаллизации.

Есбаев А.Н, Есенбаева Г.А., Есенбаева Г.А., Рамазанов М.И.

Жылуөткізгіштіктің маңызды жүктелген теңдеуі бар модель үшін интегралды теңдеу ядросының қасиеттері туралы.

Жоғары тоқты ажырататын құрылғылардың электр доғасындағы жылуфизикалық процестерді математикалық модельдеу маңызды жүктелген жылуөткізгіштік теңдеуі үшін шекаралық есептерге әкеледі. Мұндай құбылыстардың жылдамдылығын ескере отырып, бірқатар жағдайларда математикалық модель олардың динамикасы туралы адекватты ақпарат бере алады. Шекаралық есеп түріндегі математикалық модель екінші түрдегі Вольтеррдің интегралдық теңдеуіне редукцияланады, соның нәтижесінде шекаралық есептің шешілуі редукцияланған интегралдық теңдеудің шешілуіне эквивалентті. Сонымен, редукцияланған интегралдық теңдеуді зерттеу қажеттілігі туындайды. Бұл зерттеудің нәтижелері (жалпы жағдайда ядро жасайтын функцияның әр түрлі көріністері мен қасиеттері және жеке жағдайларда интегралдық теңдеулер ядросының түрлері) осы мақалада берілген. Мақала физиктер мен инженерлерге, сондай-ақ жүктелген дифференциалдық теңдеулердің практикалық қосымшаларымен айналысатын ғылыми зерттеушілерге арналған.

Есбаев А.Н, Есенбаева Г.А., Есенбаева Г.А., Рамазанов М.И.

О свойствах ядра интегрального уравнения для модели с существенно нагруженным уравнением теплопроводности.

Математическое моделирование теплофизических процессов в электрической дуге сильноточных отключающих аппаратов приводит к краевой задаче для существенно нагруженного уравнения теплопроводности. Учитывая быстротечность таких явлений, в ряде случаев лишь математическая модель способна дать адекватную информацию об их динамике. Математическая модель в виде краевой задачи редуцируется к интегральному уравнению Вольтерра второго рода, в результате чего разрешимость краевой задачи эквивалентна разрешимости редуцированного интегрального уравнения. Таким образом, возникает необходимость исследования редуцированного интегрального уравнения. Результаты этого исследования (различные представления и свойства образующей ядро функции в общем случае и виды ядра интегрального уравнения в частных случаях) представлены в данной статье. Статья ориентирована на физиков и инженеров, а также на научных исследователей, занимающихся практическими приложениями нагруженных дифференциальных уравнений.

INFORMATION ABOUT AUTHORS | **АВТОРЛАР ТУРАЛЫ МӘЛІМЕТТЕР** | **СВЕДЕНИЯ ОБ АВТОРАХ**

Aimukhanov, A.K. – PhD, Professor, Physical-Technical Faculty, E.A. Buketov Karaganda State University, Karaganda, Kazakhstan

Aitpaeva, Z.K. - Candidate of chem. sciences, Associate Professor, Physical-Technical faculty, E.A. Buketov Karaganda State University, Karaganda, Kazakhstan

Akhmetbekova, A.M. - Candidate of technical sciences, Head of the Department "Electric power and labor protection", O. Baykonurov Zhezkazgan University

Astanov, S.Kh. – Doctor of phys.-math. sciences, Professor, Department of Physics, Bukhara Engineering-Technological Institute, Bukhara, Uzbekistan

Baishagirov, Kh.Zh. – Doctor of Technical Sciences, Professor, Academician of International Academy of Ecology Man and Nature Protection Sciences, Sh. Ualikhanov Kokshetau State University, Kokshetau, Kazakhstan

Breido, I.V. - Doctor of technical sciences, Professor, Head of the Department "Automation of production processes", Karaganda state technical university, Karaganda, Kazakhstan

Bulkairova,G.A. ¯ Master, Senior Lecturer, Physical-Technical Faculty, E.A. Buketov Karaganda State University, Karaganda, Kazakhstan

Cherneta, O. G. - Candidate of technical sciences, Associate Professor of the Department of Cars and Automotive Economy, Dneprov State Technical University, Zaporizhzhye, Ukraine

Daniyarov, N.A. - Doctor of technical sciences, Head of "Corporate University" of LLP "Corporation Kazakhmys", Karaganda, Kazakhstan

Dmitriev, S.A. – Senior lecturer of the Department of engine Design and design Moscow Aviation Institute (National Research University), Moscow, Russia

Goncharenko, V.I. – Doctor of Engineering Sciences, Research Officer, Director of the Military Institute, Moscow Aviation Institute (National Research University), Leading Researcher of the Laboratory of System Integration of the Control Means, Institute of Control Sciences. V.A. Trapeznikova RAS, Moscow, Russia

Hayitov, D.E. - Senior Lecturer, Department of Physic, Bukhara Engineering - Technological Institute, Bukhara, Uzbekistan

Ilyassov, B.R. - PhD, Physical-Technical Faculty, E.A. Buketov Karaganda State University, Karaganda, Kazakhstan

Islomov, U.N. - Senior Lecturer, Department of Physics, Bukhara Engineering - Technological Institute, Bukhara, Uzbekistan

Karabekova, D.Zh. - PhD, Docent, Physical-Technical Faculty, E.A. Buketov Karaganda State University, Karaganda, Kazakhstan

Kasimova, G.K. - Postgraduate student, Department of Physics, Bukhara Engineering - Technological Institute, Bukhara, Uzbekistan

Kaverin, V.V. - Candidate of technical sciences, Associate Professor, Department "Automation of production processes", Karaganda state technical university, Karaganda, Kazakhstan

Kelisbekov, A.K. – PhD student, Department "Automation of production processes", Karaganda state technical university, Karaganda, Kazakhstan

Khassenov, A.K. - PhD, Associate Professor, Physical-Technical Faculty, E.A. Buketov Karaganda State University, Karaganda, Kazakhstan

Kheyfetz, M.L. - Doctor of techn.sciences, Professor, Deputy Director General, «NPO Center» OJSC, National Academy of Sciences of Belarus, Minsk, Belarus

Kipshakov M.S. - Postgraduate student, Physical-Technical Faculty, E.A. Buketov Karaganda State University, Karaganda, Kazakhstan

Kolmakov, A.G. - Corresponding Member of RAS, Doctor of phys.-math. sciences, Professor, Head of laboratory, A.A. Baykov Institute of Metallurgy and Materials Science, Russian Academy of Sciences, Moscow, Russia

Kombaev, K.K. - Associate Professor, D. Serikbayev East Kazakhstan state technical university

Kubich, V.I. - Candidate of technical sciences, Associate Professor, Department of Cars, National University of Zaporizhzhya Polytechnic, Zaporizhzhye, Ukraine

Kurbanbekov, Sh. - PhD, Khoja AkhmetYassawi International Kazakh-Turkish University, Turkestan, Kazakhstan

Manatpaev R.K. - Candidate of phys.-math.sciences, Senior Lecturer, al-Farabi Kazakh National University, Almaty, Kazakhstan

Minkov, L.L. - Doctor of of phys.-math.sciences, Professor, Physics and Engineering Faculty, Tomsk State University, Tomsk, Russia

Narimanov, R.K. – Candidate of phys.-math.sciences, Assoc. Professor, Physics and Engineering Faculty, Tomsk State University, Tomsk, Russia

Nurgaliyeva, Zh.G. – Master student, Senior Lecturer, Physical-Technical Faculty, E.A. Buketov Karaganda State University, Karaganda, Kazakhstan

Ocheredko, I.A. - Engineer-designer of the Educational-Scientific and Production Site, S. Amanzholov East Kazakhstan State University

Omarov, B.M. – Master, Lecturer, Department of Physics and Mathematics, Sh. Ualikhanov Kokshetau State University, Kokshetau, Kazakhstan

Ospanova D.A. – Master, Senior Lecturer, Physical-Technical Faculty, E.A. Buketov Karaganda State University, Karaganda, Kazakhstan

Pakhomov, A.A. - Doctor of phys.-math. sciences, Senior Researcher, V.A. Kotelnikov Institute of Radio Engineering and Electronics, RAS, Moscow, Russia

Pazyl, B.M. – Master student, Physical-Technical Faculty, E.A. Buketov Karaganda State University, Karaganda, Kazakhstan

Perchatkina, E.V. - Postgraduate student, Physics and Engineering Faculty, Tomsk State University, Tomsk, Russia

Potapov V.A. - Engineer, V.A. Kotelnikov Institute of Radio Engineering and Electronics, RAS, Moscow, Russia

Potapov, A.A. – Doctor of phys.-math. sciences, Professor, Academician, Head of the Chinese-Russian laboratory of informational technologies and signals fractal processing of JNU-IREE RAS, JiNan University (JNU), Guangzhou, China, V.A. Kotelnikov Institute of Radio Engineering and Electronics, RAS, Moscow, Russia

Potapov, A.A. (Jr.) - Engineer, V.A. Kotelnikov Institute of Radio Engineering and Electronics, RAS, Moscow, Russia

Rakhadilov, B.K. - PhD, Head of the National Laboratory of Collective Use, S. Amanzholov East Kazakhstan State University

Ramazanov, M.I. - Doctor of phys.-math.sciences, Professor, E.A. Buketov Karaganda State University, Karaganda, Kazakhstan

Raupova, I.B. – Assistant, Department of Physics, Bukhara Engineering - Technological Institute, Bukhara, Uzbekistan

Rizoqulov, M.N. - Postgraduate Student, Department of Physics, Bukhara Engineering - Technological Institute, Bukhara, Uzbekistan

Sadenova, K.K. - Master, Senior Lecturer**,** Physical-Technical Faculty, E.A. Buketov Karaganda State University, Karaganda, Kazakhstan

Sagdoldina, Zh.B. - PhD, Head of the research centre «Surface engineering and tribology», S. Amanzholov East Kazakhstan State University

Sakipova, S.E. – Candidate of phys.-math.sciences, Professor, Physical-Technical Faculty, E.A. Buketov Karaganda State University, Karaganda, Kazakhstan

Satybaldin, A.Zh. – Candidate of chem. sciences, Associate Professor, Physical-Technical faculty, E.A. Buketov Karaganda State University, Karaganda, Kazakhstan

Seldygaev, O.B. – Candidate of chem. sciences, Physical-Technical faculty, E.A. Buketov Karaganda State University, Karaganda, Kazakhstan

Senyut, V.T. - Candidate of techn.sciences, Leading Researcher, Joint Institute of Mechanical Engineering of NAS of Belarus, Minsk, Belarus

Shaimerdenova K.M. - Candidate of technical sciences, Assoc. Professor, Head of the Engineering Thermophysics Department named after prof. Zh.S. Akylbayev, E.A. Buketov Karaganda State University, Karaganda, Kazakhstan

Sharipov, M.Z. - Doctor of phys.-math.sciences, Head of Physics Department, Bukhara Engineering - Technological Institute, Bukhara, Uzbekistan

Shrager, L.A. – Master, Head of the University Laboratory, Physics and Engineering Faculty, Tomsk State University, Tomsk, Russia

Shunkeyev T.A. - Postgraduate student, Physical-Technical Faculty, E.A. Buketov Karaganda State University, Karaganda, Kazakhstan

Skakov, M. - Doctor of phys.-math. sciences, Professor, Deputy Director General on Science of National Nuclear Center of the Republic of Kazakhstan

Stoev, M.- Doctor of engineering, PhD, Associate Professor, Neofit Rila University, South-West, Blagoevgrad, Bulgaria

Tanasheva, N.K. – PhD, Senior Researcher, Institute of Applied Mathematics, Ministry of Education and Science of Republic Kazakhstan, Karaganda, Kazakhstan

Tleubergenova, A.Zh. – Master, Lecturer, Physical-Technical Faculty, E.A. Buketov Karaganda State University, Karaganda, Kazakhstan

Tulenbergenov, T. - Engineer is laboratory of Thermophysic Reactor Systems, Institute of Atomic Energy, the National Nuclear Center of the Republic of Kazakhstan

Val`kovich, I. V – Researcher, Joint Institute of Mechanical Engineering of NAS of Belarus, Minsk, Belarus

Vasenin, I.M. - Doctor of of phys.-math.sciences, Professor, Physics and Engineering Faculty, Tomsk State University, Tomsk, Russia

Vasiliev, S.L. – Candidate of technical sciences, Associate Professor of Technological design and quality management Department Moscow Aviation Institute (National Research University), Moscow, Russia

Vityaz, P.A. – Academician of the NAS of Belarus, Doctor of techn. sciences, Professor, Head of Academy Staff of the National Academy of Sciences of Belarus, Presidium of the National Academy of Sciences of Belarus, Minsk, Belarus

Yershina, A.K. – Doctor of phys.-math.sciences, Professor, Kazakh National Women's Teacher Training University, Almaty, Kazakhstan

Yesbayev, A.N. - PhD student, L.N. Gumilyov Eurasian National University, Nur-Sultan, Kazakhstan

Yessenbayeva, G.A. - Candidate of phys.-math.sciences, Docent, E.A. Buketov Karaganda State University, Karaganda, Kazakhstan

Yessenbayeva, G.A. - Candidate of technical sciences, Doctor of Pedag. Sciences, Professor, Head of the Department of Merchandising and Certification, Karaganda Economic University of Kazpotrebsoyuz, Karaganda, Kazakhstan

Yurgenson, S.A. – Candidate of technical sciences, Researcher of the Department Technology of aircraft production Moscow Aviation Institute (National Research University), Moscow, Russia

Yurov, V.M. - Candidate of phys.-math.sciences, Professor, Director of the Scientific Research Center, E.A. Buketov Karaganda State University, Karaganda, Kazakhstan

Zavgorodniy, A.V. – PhD student, Physical-Technical Faculty, E.A. Buketov Karaganda State University, Karaganda, Kazakhstan

Zeinidenov, A.K. – PhD, Associate Professor, Dean of the Physical-Technical Faculty, E.A. Buketov Karaganda State University, Karaganda, Kazakhstan

Zhurerova, L. - PhD, Senior scientific associate, National scientific laboratory of collective use, S. Amanzholov East Kazakhstan state university

Eurasian Physical Technical Journal

ISSN 1811-1165 Key title: Eurasian physical technical journal (Print)
Abbreviated key title: Eurasian phys. tech. j. (Print)

ISSN 2413-2179 Key title: Eurasian physical technical journal (Online)
Abbreviated key title: Eurasian phys. tech. j. (Online)

"Eurasian Physical Technical Journal" (Eurasian phys. tech. j.) is a peer-reviewed open access international scientific journal publishing original research results on actual problems of Technical Physics, Energy, Engineering and other related fields.

Since 2004 "Eurasian phys. tech. j." is publishing in English. Periodicity is 2 issues per year.

E.A. Buketov Karaganda State University is the main organizer and financial sponsor of EAPhTJ. The efforts of the international highly qualified Editorial Board consisting prominent physicists from 12 countries allow provide EAPhTJ international level.

Since 2008 EAPhTJ has been included in the list of publications recommended by the Ministry of Science Education and Science of the Republic of Kazakhstan for the publication of the main results of the master's and PhD doctoral dissertations on the Physical and Mathematical sciences.

Based on the decision of the Content Selection & Advisory Board (CSAB) of May 8, 2019, the Eurasian Physical Technical Journal has been inducted into Scopus data base on three scientific areas: Energy, Materials Science, Engineering.

Publication Ethics and Malpractice Statement

Submission of an article to the Eurasian phys. tech. j. implies that the paper described has not been published previously, that it is not under consideration for publication elsewhere, that its publication is approved by all authors and tacitly or explicitly by the responsible authorities where the paper was carried out, and that, if accepted, it will not be published elsewhere in the same form, in English or in any other language, including electronically without the written consent of the copyright holder. In particular, translations into English of papers already published in another language are not accepted.

For information on Ethics in publishing and Ethical guidelines for journal publication see http://www.elsevier.com/publishingethics and http://www.elsevier.com/journal-authors/ethics.

The Eurasian phys. tech. j. follows the Code of Conduct of the Committee on Publication Ethics (COPE), and follows the COPE Flowcharts for Resolving Cases of Suspected Misconduct (http://publicationethics.org/files/u2/New_Code.pdf).

To verify originality, your article may be checked by the originality detection service Cross Check http://www.elsevier.com/editors/plagdetect.

Authors are responsible for the content of their publications. No other forms of scientific misconduct are allowed, such as plagiarism, falsification, fraudu-lent data, incorrect interpretation of other works, incorrect citations, etc. Authors are obliged to participate in peer review process and be ready to provide corrections, clarifications, retractions and apologies when needed. All authors of a paper should have significantly contributed to the research.

Reviewers should provide objective judgments and should point out relevant published works which are not yet cited. Reviewed articles should be treated confidentially. The reviewers will be chosen in such a way that there is no conflict of interests with respect to the research, the authors and/or the research funders.

Editors have complete responsibility and authority to reject or accept a paper, and they will only accept a paper when reasonably certain. They will preserve anonymity of reviewers and

promote publication of corrections, clarifications, retractions and apologies when needed.
The acceptance of a paper automatically implies the copyright transfer to the Eurasian phys. tech. j.
All submitted papers will the sent for reviewing to leading experts in the given area.
The Editorial Board of the Eurasian phys. tech. j. will monitor and safeguard publishing ethics.
The editors reserve the right to accept or reject manuscripts.

GUIDELINES FOR AUTHORS

Research articles, survey papers and short notes are accepted for exclusive publication in the «**Eurasian phys. tech. j.**» in English. The manuscripts and short notes must contain original results of investigation in the following scientific areas of Physics and Engineering:

ENERGY.
- **Thermophysics.**
- **Hydrodynamics.**

MATERIALS SCIENCE.

PHYSICS AND ASTRONOMY.

ENGINEERING:
- **Devices and methods of experiment.**
- **Modeling of the nonlinear physical - technical processes.**
- **Ecological Aspects of New Technologies.**

All publishing manuscripts and short notes must have been recommended by a member of the editor board or by the organization (University), where the work was performed. The author who submitted an article for publication will be considered as a corresponding author.

The paper, short note or review paper shall include an abstract of the contents, not exceeding 200 words and keywords (no more than 10). The abstract must not coincide with the introduction or conclusive part of the work and must not contain references, abbreviations and other unknown words.

All articles should have list of keywords or terms (3 to 10) for indexing purposes.

The text of a paper must not exceed 8-12 pages including tables, figures (no more than 6) and references. A short note must not exceed 4-5 pages including no more than 2 figures. A review paper must not be more than 20 pages (including no more than 10 figures).

The text should be divided on structural parts: **Introduction, Theoretical part, Experimental technique, Results and Discussion, Conclusion,** etc.

Printed copies shall be on good quality paper of International size A4. All texts must be printed in Microsoft Word. It is preferable to use the Times fonts. The text must be printed in 12 point letters, 1.0 intervals. There shall be a margin of 30 mm at the left-hand edge, of 15 mm at the fore edge, of 30 mm at the head of the page and of 30 mm at the tail. All pages must be numbered.

Acknowledgments may be shown at the end of the article text, before **REFERENCES**.

All references must be numbered in the text (for example, [1], [2-4]) and listed in numerical order.

Equations in your paper have to be written using the Microsoft Equation Editor or the MathType (http://www.mathtype.com) for (Insert | Object | Create New | Microsoft Equation or MathType Equation).

Tables must be inserted into the text.

Figures should be prepared in a digital form suitable for direct reproduction. Figures shall be submitted on the separate sheets and not included into the text.

The following files must be submitted via e-mail:
- Article text (*.doc);

- Figures (fig1.jpg, fig2.pcx);
- Figure captions (*.txt, *.doc).

The text file containing all Authors' names, organizations, postal code, postal address, telephone, fax, E-mail, scientific topic of the paper.

It is possible to use **rar** or **zip** compressors and to transmit the files as an attachment.

Title page (specimen)

UDC

TITLE

Smith J.H., Cooper H.J.

E.A. Buketov Karaganda State University, Karaganda, Kazakhstan, Universitetskaya Str. 28, Karaganda, 100028, Kazakhstan, email@for_correspondence.kz

Abstract: 5-6 sentences

Keywords:

Introduction

Article text. Article text. Article text. Article text. Article text. Article text. Article text. Article text. Article text. Article text Article text. Article text. Article text. Article text. Article text Article text. Article text. Article text. Article text. Article text Article text. Article text. Article text. Article text. Article text Article text. Article text. Article text. Article text. Article text…

References Format (specimen)

1 Nahar J., Wahedra M. Elastic scattering of positrons and electrons by argon. *Physical Rewiew A,* 2016, Vol. 35, No. 5, pp. 2051 – 2064.

2 Rivoalen H. Electrotubular heat exchanger in chemical industry. *Proceeding of the 12th International Congress on Electricity Applications.* Birmingham, 2017, pp. 29 – 39.

3 Conrad H., Muhlbauer A., Thomas R. *Elektrothermische Verfahrenstechnik*. Vulkan-Verlag, Essen Publ.House, 2008, 240 p.

The authors should represent References according to the requirements of international journals on physics, but should to consult preliminarily for standard abbrevi-ations of journal's names.

For more information on references guidelines for journal publication you see Harvard reference system: http://www.emeraldgrouppublishing.com/authors/guides/write/harvard.htm?part=2